Imperial College London
Department of Computing

Action selection in the rhythmic brain: The role of the basal ganglia and tremor.

Zafeirios Fountas

March 2016

Submitted in partial fulfilment of the requirements for the degree of
Doctor of Philosophy in Computing of Imperial College London
and the Diploma of Imperial College London

Declaration

I herewith certify that all material in this dissertation which is not my own work has been properly acknowledged.

Zafeirios Fountas

Abstract

Low-frequency oscillatory activity has been the target of extensive research both in cortical structures and in the basal ganglia (BG), due to numerous reports of associations with brain disorders and the normal functioning of the brain. Additionally, a plethora of evidence and theoretical work indicates that the BG might be the locus where conflicts between prospective actions are being resolved. Whereas a number of computational models of the BG investigate these phenomena, these models tend to focus on intrinsic oscillatory mechanisms, neglecting evidence that points to the cortex as the origin of this oscillatory behaviour.

In this thesis, we construct a detailed neural model of the complete BG circuit based on fine-tuned spiking neurons, with both electrical and chemical synapses as well as short-term plasticity between structures. To do so, we build a complete suite of computational tools for the design, optimization and simulation of spiking neural networks. Our model successfully reproduces firing and oscillatory behaviour found in both the healthy and Parkinsonian BG, and it was used to make a number of biologically-plausible predictions.

First, we investigate the influence of various cortical frequency bands on the intrinsic effective connectivity of the BG, as well as the role of the latter in regulating cortical behaviour. We found that, indeed, effective connectivity changes dramatically for different cortical frequency bands and phase offsets, which are able to modulate (or even block) information flow in the three major BG pathways. Our results indicate the existence of a multimodal gating mechanism at the level of the BG that can be entirely controlled by cortical oscillations, and provide evidence for the hypothesis of cortically-entrained but locally-generated subthalamic beta activity.

Next, we explore the relationship of wave properties of entrained cortical inputs, dopamine and the transient effectiveness of the BG, when viewed as an action selection device. We found that cortical frequency, phase, dopamine and the examined time scale, all have a very important impact on the ability of our model to select. Our simulations resulted in a canonical profile of selectivity, which we termed selectivity portraits. Taking together, our results suggest that the cortex is the structure that determines whether action selection will be performed and what strategy will be utilized while the role of the BG is to perform this selection. Some frequency ranges promote the exploitation of actions of whom the outcome is known, others promote the exploration of new actions with high uncertainty while the remaining frequencies simply deactivate selection.

Based on this behaviour, we propose a metaphor according to which, the basal ganglia can be viewed as the ”gearbox" of the cortex. Coalitions of rhythmic cortical areas are able to switch

between a repertoire of available BG modes which, in turn, change the course of information flow back to and within the cortex. In the same context, dopamine can be likened to the "control pedals" of action selection that either stop or initiate a decision. Finally, the frequency of active cortical areas that project to the BG acts as a gear lever, that instead of controlling the type and direction of thrust that the throttle provides to an automobile, it dictates the extent to which dopamine can trigger a decision, as well as what type of decision this will be.

Finally, we identify a selection cycle with a period of around 200 ms, which was used to assess the biological plausibility of the most popular architectures in cognitive science. Using extensions of the BG model, we further propose novel mechanisms that provide explanations for (1) the two distinctive dynamical behaviours of neurons in globus pallidus external, and (2) the generation of resting tremor in Parkinson's disease.

Our findings agree well with experimental observations, suggest new insights into the pathophysiology of specific BG disorders, provide new justifications for oscillatory phenomena related to decision making and reaffirm the role of the BG as the selection centre of the brain.

Acknowledgements

I would like to express my sincere gratitude to

- My thesis supervisor, Professor Murray Shanahan, for introducing me to the fascinating worlds of cognitive science, neurodynamics, brain-inspired artificial intelligence and philosophy of mind, and for giving me the opportunity to work with him on some of these fields. His patience, guidance and professionalism were proved fundamental for my growth as a scientist and allowed me to develop my own intuition.
- My colleagues in the Computational Neurodynamics Group and my co-workers including (with estimated graduation order) Pedro Martinez Mediano, Marta Garnelo, Kyriacos Nikiforou, Nat Dilokthanakul, Claudia Schulz, Anastasia Sylaidi, Filipe Peliz Pinto Teixeira, David Bhowmik, Richard Newcombe and Mark Wildie, for making my environment an inspiring, creative and enjoyable place to work, and for always being there to answer my preposterous questions. I will remember the office 444b in Huxley building as the best working enironment in my student life.
- The Department of Computing of Imperial College London for supporting financially the 2.5 last years of my PhD, via an EPSRC student grant. I am also deeply thankful to Google and EmployAbility for supporting my studies with a Google EMEA Scholarship for the academic year 2014-15, which also played a crucial role in the completion of my studies.
- Andreas Fidjeland and David Gamez, who also played a very important role on my introduction to the aforementioned fields, for giving me the opportunity to work on my MSc project, through which I acquired my initial enthusiasm for my PhD topic.
- Dr. Amani El-Kholy and Dr. Lloyd Kamara for their limitless support over the last 4 years, as well as Dr Mark Humphries and Prof. Peter Brown's group for their valuable feedback and discussions.
- Samantha Matsa, Nikitas Thomareis, Zacharias Fotos, Anastasia Sylaidi, Marily Nika, Stavros Rousis, Pinelopi Kivelou, Evangelos Stromatias, Dimitris Karagiannis, as well as friends in my home town Thessaloniki, who all contributed to this work in their own unique way and without their support it could have not been completed.

Last but foremost, I would like to deeply thank my dearest family for their never ending love, support and positivity throughout all the years of my life, including the four years of my PhD, including my parents Dimitrios Fountas and Christina Athanasiadou, my wonderful sister Antigoni

Maria Founta, and my beloved aunt Anastasia Founta. I would like to dedicate this work to my parents and especially my mother, who played a major role in my attraction to academia. I believe we all are the result of a unique trade-off between nature and nurture and I personally feel deeply grateful for both.

Contents

1 Introduction **15**

1.1 An introduction to biological action selection . . . 15

1.1.1 Behaviour . . . 15

1.1.2 Anatomy . . . 16

1.1.3 Computational models . . . 18

1.2 The unexplained relevance of oscillatory activity . . . 20

1.3 Objectives . . . 22

1.4 Achievements and structure of thesis . . . 22

2 Modelling tools **25**

2.1 Introduction . . . 25

2.1.1 NeMo spiking neural network simulator . . . 27

2.1.2 Brian simulator . . . 28

2.2 Brain studio . . . 29

2.2.1 Network topology and simulation structure . . . 30

2.2.2 The front-end: Designing experiments . . . 32

2.2.3 The back-end: Running experiments . . . 34

2.2.4 Extending brain studio . . . 36

2.2.5 Evaluation . . . 37

2.3 GPU-based fast parameter optimization for phenomenological neural models . . . 39

2.3.1 Introduction . . . 39

2.3.2 Methodology . . . 41

2.3.3 Evaluation . . . 48

2.3.4 Concluding Remarks . . . 55

3 A neural model of the basal ganglia circuitry **56**

3.1 The model . . . 56

3.1.1 Anatomy . . . 56

3.1.2 Mathematical models . . . 60

3.1.3 Neural parameter estimation . . . 65

3.1.4 Connectivity estimation . . . 71

3.2 Resulting behaviour . . . 75

4 The role of cortical oscillations in the basal ganglia function **78**

4.1 Introduction . . . 78

4.2 Results . . . 79
4.2.1 Dopaminergic modulation of intrinsically-induced beta oscillations in the GPe-STN loop . . . 79
4.2.2 Only low cortical frequencies can be maintained throughout the BG structure 83
4.2.3 Cortical frequency defines the effective connectivity of the BG pathways . 85
4.3 Discussion . . . 88
4.3.1 Beta activity is locally-generated but cortically-entrained in the Parkinsonian state . . . 88
4.3.2 Oscillations and the BG function . . . 91
4.3.3 The STN-GPe circuit . . . 94

5 The role of bursts and pauses of neurons in the globus pallidus externa 97
5.1 Introduction . . . 97
5.2 Modelling cortical input . . . 98
5.3 Results . . . 99
5.3.1 High-frequency GPe neurons produce pauses caused by over-excitation . . 99
5.3.2 Bursting and pauses in GPe can be modulated by STN depression 101
5.3.3 GPe bursts and pauses emerge in normal BG function and depend on cortical behaviour . . . 102
5.3.4 GPe silence can be caused by local neural accommodation in (post-) synaptic sites . . . 105
5.4 Discussion . . . 107
5.4.1 The role of GPe bursts and pauses in BG behaviour . . . 107
5.4.2 Is the silence of LFB neurons biologically plausible? . . . 109

6 Assessing selectivity in the basal ganglia 113
6.1 Introduction . . . 113
6.2 Metrics . . . 115
6.2.1 Selectivity . . . 115
6.2.2 Dependence . . . 117
6.3 A reduced version of the basal ganglia model . . . 118
6.4 Selectivity portraits . . . 119
6.4.1 The combination of dopamine concentration and cortical frequency defines BG effectiveness and exploration . . . 120
6.4.2 The BG can almost always select the most salient action transiently . . . 123
6.4.3 Cortical oscillations with low frequencies are required for selection change 124
6.4.4 Selectivity portraits are largely maintained in simplified versions of the BG model but not in the minimal model . . . 126

6.4.5 The effect of the phase offset between low-frequency cortical inputs on selectivity portraits . . . 128
6.4.6 Selecting the most salient input does not require coherence between competitor populations. . . . 130
6.5 Behavioural predictions . . . 130
6.5.1 Evidence for the existence of a long selection cycle that can be used for evidence accumulation . . . 130
6.5.2 Low-frequency oscillations facilitate the resolution of ambiguity . . . 138
6.6 Discussion . . . 139
6.6.1 The gear box metaphor . . . 139
6.6.2 Psychophysical studies . . . 140
6.6.3 Alpha and theta oscillations act as a BG mechanism to reset selection and explore alternative actions . . . 141
6.6.4 Cortical frequency is a better predictor of the exploration-exploitation trade-off than dopamine . . . 142

7 Two possible sources of Parkinsonian tremor 144
7.1 Introduction . . . 144
7.2 Methods . . . 145
7.2.1 The full cortico-BG loop . . . 145
7.2.2 The oscillator model . . . 147
7.2.3 Modelling deep brain stimulation . . . 148
7.3 The single-channelled model . . . 149
7.3.1 Experiment with coupled oscillators . . . 149
7.3.2 The thalamo-BG-cortical loop experiment . . . 152
7.4 The two-channelled model . . . 154

8 Conclusions and future directions 157
8.1 Summary of contributions . . . 157
8.2 Applications and future directions . . . 159
8.2.1 The BG model . . . 159
8.2.2 Action selection . . . 160
8.2.3 Cognitive architectures . . . 161
8.2.4 Parkinsonian tremor . . . 162

List of Tables

3.1 **Network parameters.** N_x represents the number of neurons in each nucleus x. S is a scaling factor that determines the number of microscopic channels within the complete BG. R_x represents the ratio of each type of neuron x within the corresponding nucleus, while P_{x-y} is probability of a neuron from the nucleus x to be connected to one in y. 59
3.2 **Neuron equations and synaptic input with dopamine.** 64
3.3 **GPe and SNr neuron parameters.** 66
3.4 **GPe and SNr neuron parameters.** 68
3.5 **STN neuron parameters.** 70
3.6 **Synaptic parameters.** 72

6.1 Neural parameters in the simplified basal ganglia model. 120

List of Figures

1.1 Brain circuits for voluntary and stimulus-driven actions . . . 17
1.2 Studies with computational models of the BG . . . 19

2.1 Hierarchical overview of the architecture of brain studio . . . 30
2.2 Nodes and edges in brain studio interface . . . 31
2.3 Graphical user interface of brain studio in simulation mode . . . 33
2.4 Performance of brain studio . . . 38
2.5 Optimization algorithm . . . 41
2.6 Parallel architecture of the optimization method . . . 47
2.7 Properties of the thalamocortical neuron model . . . 49
2.8 Neural avalanches . . . 52
2.9 Average execution time of the optimization method . . . 54

3.1 Architecture of the basal ganglia model . . . 57
3.2 Effect of short-term plasticity in synaptic conductances . . . 63
3.3 Properties of the tuned neurons of the basal ganglia . . . 67
3.4 Firing behaviour of the system . . . 76
3.5 Connectivity of the STN in the phasic mode. . . . 76

4.1 Frequency spectrum of STN-GPe loop without oscillatory input . . . 80
4.2 Firing patterns of the three types of STN neurons . . . 82
4.3 Cortical coherence throughout the basal ganglia . . . 84
4.4 Effective connectivity of the basal ganglia model . . . 87
4.5 Competition of STN-/GPe-mediated pathways triggered by cortical alpha . . . 95

5.1 Properties of GPe neurons . . . 100
5.2 Response of GPe neurons for random cortical input . . . 103
5.3 Accommodation in dendritic spikes using the Hodgkin-Huxley model . . . 106
5.4 Neural accommodation in GPe dendrites . . . 107
5.5 Pauses in GPe neurons. . . . 109

6.1 Metrics for distinctiveness and dependence. . . . 116
6.2 Simplified version of the basal ganglia model. . . . 119
6.3 Selectivity portraits of the basal ganglia model. . . . 121
6.4 Transient changes in selectivity. . . . 123
6.5 Inhibition of the SNr microscopic channels. . . . 125

6.6 Comparison of selectivity portraits of reduced versions of the BG model. 127
6.7 The ubiquitous effect of the phase offset φ at beta frequencies. 129
6.8 Cortical stimulation at two non-equal frequencies. 131
6.9 BG output during a two-choice task. 132
6.10 BG response for stimulus of varying duration. 133
6.11 BG response for stimulus of varying duration in non-neighbouring channels. . . . 134
6.12 Timing of action selection in popular cognitive architectures. 135
6.13 Ambiguity effects on BG selectivity. 139

7.1 Model architecture and visualization of the single-channelled hypothesis. 145
7.2 Behaviour of an phasic BG channel in PD realized with a network of coupled Kuramoto oscillators. 150
7.3 Oscillations in the full-loop model. 153
7.4 The phase offset between two channels could cause PD tremor. 155

Acronyms

BG Basal ganglia

RT Reaction time

SNN(s) Spiking neural network(s)

GUI Graphical user interface

API Application program interface

STDP Spike-timing-dependent plasticity

TCP/IP Transmission Control Protocol/Internet Protocol

STN Subthalamic nucleus

GP Globus pallidus

GPe Globus pallidus external

GPi Globus pallidus internal

SNr Substantia nigra pars reticulata

SNc Substantia nigra pars compacta

MSN Medium spiny-projection neuron

FSI Fast-spiking interneuron

DA Dopamine

PD Parkinson's disease

HD Huntington's disease

DBS Deep brain stimulation

RB Rebound bursting neuron of the subthalamic nucleus

LLRS Long-lasting rebound spiking neuron of the subthalamic nucleus

NR No-rebound neuron of the subthalamic nucleus

AHP After-hyperpolarization

ISI Inter-spike interval

EPSP Excitatory post-synaptic potential

IPSP Inhibitory post-synaptic potential

F-I Frequency-current

V-I Voltage-current

F-F Frequency-frequency

TE Transfer entropy

MEG Magnetoencephalography

1 Introduction

> *"This is your last chance. After this, there is no turning back. You take the blue pill-the story ends, you wake up in your bed and believe whatever you want to believe. You take the red pill—you stay in Wonderland, and I show you how deep the rabbit hole goes. Remember: all I'm offering is the truth. Nothing more."*
>
> – Morpheus, *The Matrix*

Action can be conceived as the relationship between brain-driven motor variables and their sensory consequences, which reflect the perceived impact of selected control policies on world dynamics. Biological organisms employ actions in their effort to survive in their surrounding environments while maximizing rewards under conditions of uncertainty and incomplete knowledge about the world. Decision making constitutes an essential skill that supports this competence, which is realized in a wide spectrum of contexts ranging from reflexive sensory driven activities (e.g. simple hand-reaching movements) to cognitively driven complex activities (e.g. learning how to ride a bicycle).

The ability to make decisions regarding what to do next is a fundamental cognitive feature and arguably one of the most substantial driving forces underlying the evolution of intelligence, which is often treated by contemporary views as a closed-loop relationship between perception and action.

But how is this mechanism of action selection realized in the brain? A plethora of evidence and theoretical work indicates that the basal ganglia (BG) might be a key locus where conflicts between prospective actions are resolved. However, a full understanding of the role of this structure in the behavioural, computational and neurobiological aspects of action selection remains, to date, an open challenge.

1.1 An introduction to biological action selection

1.1.1 Behaviour

In cognitive psychology, the topic of action selection is mainly studied via the measurement of reaction times (RT). The initial contributions in this study come from astronomers in the early 19th century, who tried to measure the individual differences in human errors when recording the time that it took for a star to cross a particular distance (Woodworth and Schlosberg 1954;

Jensen 2006). They termed this unique pattern the *personal equation*, whose parameters were measured via devices called chronographs.

In recent years, a variety of experimental choice tasks have been introduced in the field of mental chronometry, to study how well humans and animals select actions (Healy and Proctor 2003). In these tasks, RT are divided into various categories including simple RT, where the participant simply responds to a particular stimulus, choice RT, where tasks require unique responses for every stimulus class and Go/No-Go RT, where tasks require a response to a particular stimulus and response inhibition to others.

Another explicit measure of the effectiveness of action selection is the percentage of error choices in a series of tasks. Although there is a strong variation between tasks, the accuracy in responses is inherently linked to the time that was spent before selection (Wickelgren 1977). A person can choose to be more prone to errors and respond rapidly, or improve their accuracy at the expense of speed. This trade-off between these two qualities has been studied extensively and was used to assess optimality of decision making (Bogacz et al. 2006).

Furthermore, in the process of understanding how natural organisms select actions, a need to separate simple reflexes, object-oriented (stimulus driven) and voluntary actions emerged. Whereas the last two types require some kind of action selection, only the last is largely dependent on individual development and can be associated with the subjective experiences of 'agency' and 'intention' (Haggard 2005, 2008).

Finally, voluntary action selection also differs with respect to the tactic that is employed. The most prominent antithesis stems from the dilemma of selecting the action with the most predicted outcome, over the exploration of an alternative, less-safe choice. From what we know, there is no optimal solution to the problem of exploration versus exploitation that can be applied in all domains. Nevertheless, the fast manipulation of the trade-off between these two extremes is critical for behavioural flexibility in dynamic environments (Cohen et al. 2007).

1.1.2 Anatomy

In mammalian brains, nearly all information signals that represent actions converge on the primary motor cortex (M1), which is directly connected to muscles via the spinal cord (Haggard 2008). An exception to this rule are simple reflexes that are often purely spinal. Inputs to M1 can be broken down into two major pathways, depicted in Fig. 1.1. The first concerns signals that originate directly from the sensory cortex and involves only neighbouring cortical areas. Through this pathway, simple stimulus-driven actions can be quickly relayed to M1 without significant processing.

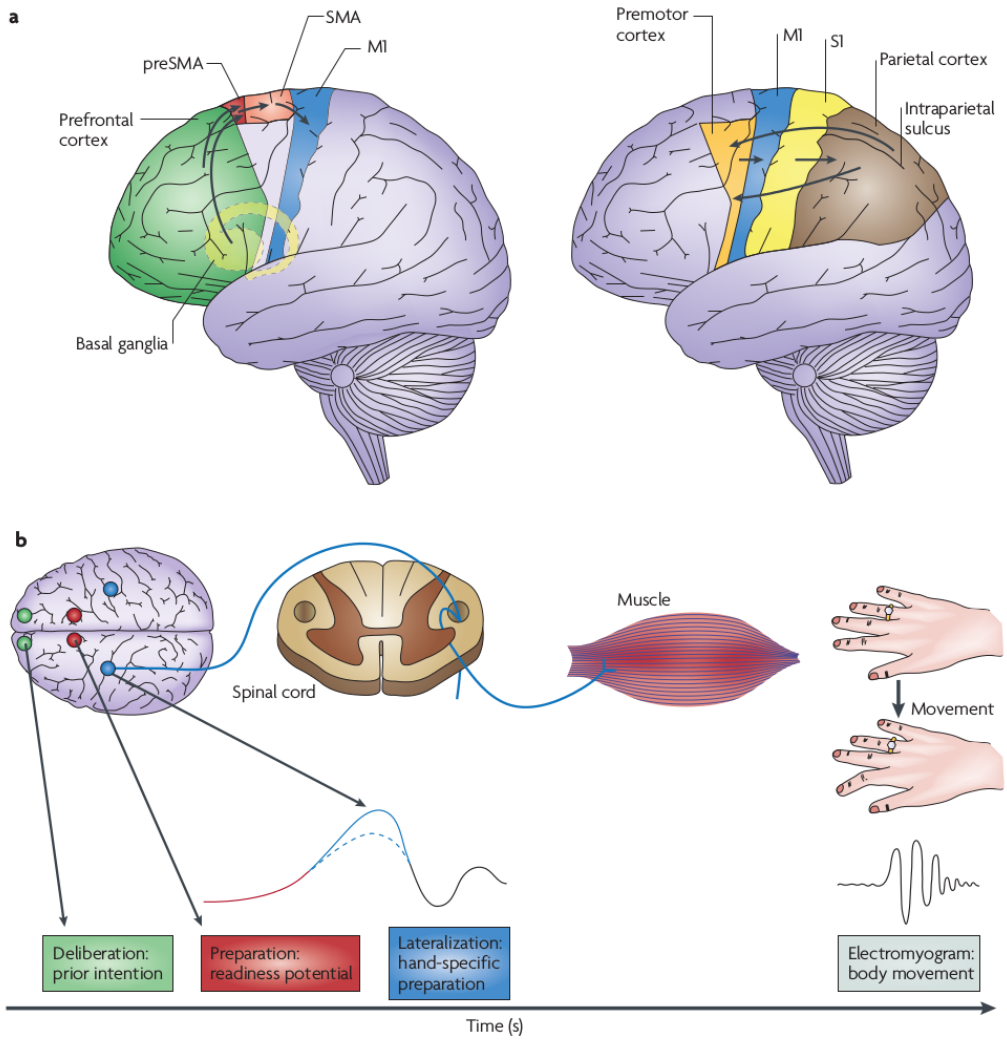

Figure 1.1: **Brain circuits for voluntary and stimulus-driven actions a:** The two main pathways that lead to the activation of the primary motor cortex (M1). In the top left panel, one key input reaches M1 from the supplementary motor area (SMA) and the preSMA, which in turn receives inputs from the basal ganglia and the prefrontal cortex. In a second cortical network (right panel), information from early sensory cortices (S1) is relayed to intermediate-level representations in the parietal cortex, and from there to the lateral part of the premotor cortex, which projects in turn to M1. This parietal–premotor circuit guides object-oriented actions, such as grasping, using current sensory input, but also contributes to some aspects of 'voluntary' behaviour. **b:** Brain activity preceding a voluntary action of the right hand. The frontopolar cortex (green) forms and deliberates long-range plans and intentions. The pre-supplementary motor area (red) begins the preparation of the action; together with other premotor areas, it generates the readiness potentials (red trace) and immediately before the action takes place, M1 (blue) becomes active. Finally, neural signals leave M1 for the spinal cord and the contralateral hand muscles. Figure and caption adopted from Haggard 2008, with permission.

On the other hand, a second pathway involves a wider range of structures including midbrain areas, prefrontal areas of the cortex and the pre-supplementary motor area (preSMA). This network is employed when a voluntary action is under consideration and plays a major role in "binding intention and action" (Haggard 2008). Thus, this is the network that features heavily in this thesis.

A key region of this pathway comprises a group of subcortical nuclei called the basal ganglia (BG). These highly interconnected structures show remarkable similarities, both anatomically and functionally, across vertebrate nervous systems (Stephenson-Jones et al. 2011). Both their physical location and their broad bidirectional connectivity with major cortical areas, the limbic system and the thalamus, place the BG in a key position to modulate the information flow between the cortex and the body. In addition, their strictly topographic organization on different scales suggests that through the BG, common modulatory operations are applied to functionally different channels of information flow.

The above features have led to the widely held hypothesis that the BG constitute a critical component for the action selection system of the vertebrate brain (Redgrave et al. 1999), a view that has recently gained strong support from experimental studies (Jin et al. 2014; Friend and Kravitz 2014).

1.1.3 Computational models

Numerous computational approaches have been proposed that try to capture various aspects of biological action selection, a number of which are mentioned above. In statistics and game theory, models tend to be abstract decision making techniques, at the algorithmic level, that aim at optimal performance and social interactions. For comparison of the optimality of biologically-inspired decision making algorithms see Bogacz et al. 2006 and for a wide range of natural action selection models see Seth et al. 2011.

Within the context of cognitive psychology and computational neuroscience, the emphasis is often given to less abstract implementations that can be used to explore aspects of physiology and cognition, including models of neural circuits. Although simple selection mechanisms can be realized using only a very small number of neural units, scaling these systems up to the size required for a realistic number of cognitive streams of information has proved to be surprisingly challenging. Gurney et al. 2001 argued that the scaling up problem can be solved by a combination of a feedforward selection pathway and a control pathway, both of which can be mapped to the exact internal circuit of the BG. Finally, Bogacz and Gurney 2007 showed that this circuit implements an asymptotically optimal decision mechanism which outperforms other

psychophysical approaches.

Basal ganglia models

Because of the aforementioned features of the BG, the last decade has seen a great deal of interest in producing mathematical models that capture the dynamics of their circuitry. In a review article, Frank 2011 begins the introduction by mentioning that "a Google Scholar search for articles mentioning both 'computational model' and 'basal ganglia' yields 2960 matches in the last twenty years, with 2550 of them appearing in the last decade alone, comprising more than a ten-fold increase." Indeed, this trend has continued since 2011 as shown in Fig. 1.2 with more than 1400 articles being published just during 2014.

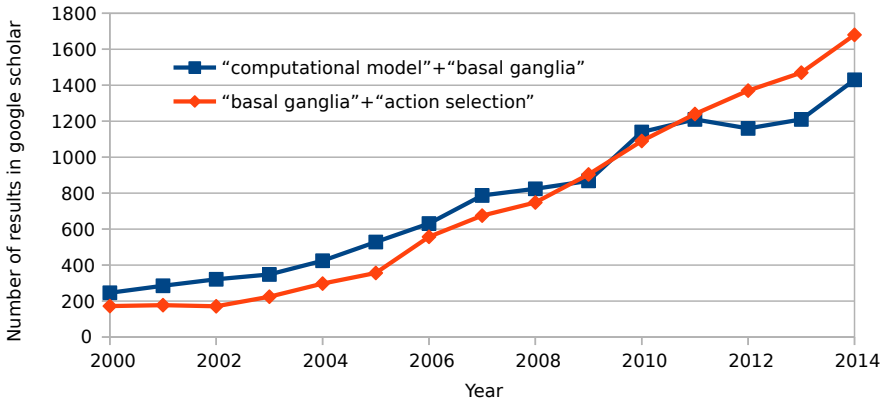

Figure 1.2: **Studies with computational models of the BG.** Number of results in a *scholar.google.com* search per year.

In addition, the same trend can be found in both theoretical and experimental studies that relate the BG with action selection. This is not surprising since the vast majority of computational studies of the BG aim to provide new insights in this direction. Due to this enormous number of models, naming all important contributions is impossible. Hence, this section is restricted to studies that played a major role in the development of the current thesis, either because of their novelty or relevance to the current approach.

In the former category, initial mathematical models of the BG that are based on the distinction of competing signals include Barto 1995; Beiser et al. 1997. Most prominently, Gurney et al. 2001 developed the first mathematical model which is based on the action selection hypothesis. This model was later used as the starting point for a complete implementation of the BG circuitry in Humphries et al. 2006 based on equations of spiking neurons. Finally, Bogacz and Gurney 2007 developed an algorithmic model that maps the BG anatomy to a sequential hypothesis test

which achieves optimal decision time, thus providing the first theoretical framework to explore the relationship between the BG and action selection.

The second category of BG models comprises neural approaches that have influenced the current thesis. The computational work of Gurney et al. 2001 was also used in Stewart et al. 2010, where the equations that represent each BG nucleus were directly mapped to spiking neurons through the neural engineering framework (Eliasmith and Anderson 2004). This model was then used to produce results regarding the neural correlates of cognitive cycles and to complete a fully working neural cognitive architecture.

In addition, more biologically plausible neural systems have been also proposed including studies that focus on decision making (Bahuguna et al. 2015), the effects of of synaptic plasticity (Lindahl et al. 2013), the anatomy of particular BG nuclei (Humphries et al. 2009) or the dynamics of the complete loop that involves the thalamus and the cortex (Tomkins et al. 2013). For a full review of other computational approaches see Helie et al. 2013; Schroll and Hamker 2013.

1.2 The unexplained relevance of oscillatory activity

Neural oscillations are ubiquitous in the brain and one of its most widely-studied phenomena (Buzsaki 2006). In the mammalian cortex, oscillations in low-frequency ranges (< 100 Hz) have been associated with numerous cognitive and motor functions, that range from feature binding (Eckhorn et al. 1988) and mental simulation (Brinkman et al. 2014) to movement preparation and execution (Leventhal et al. 2012). This activity has provided a fruitful framework to study neural computation which has given rise to theories on the control of communication between regions (Fries 2005, 2009) as well as memory formation and retrieval (Hanslmayr et al. 2012).

Additionally, low-frequency brain oscillations have been widely implicated in the process of decision making (Zhang et al. 2008; Siegel et al. 2011; Brinkman et al. 2014). Cortical rhythms mediate the processing of new information (Fries 2009), the dynamic formation of neural ensembles that represent different actions and the suppression of other task-irrelevant regions (Siegel et al. 2009; Buschman et al. 2012). They are also found to encode uncertainty and influence the exploration-exploitation trade-off (Cavanagh et al. 2011).

Apart from the cortex, rhythmic activity is also a prominent feature of sub-cortical structures such as the BG (Brittain and Brown 2014). Interestingly, experimental and theoretical studies have provided evidence suggesting that cortical oscillations in the same low-frequency bands that are related to decision making drive activity in the striatum and subthalamic nucleus (STN), the

input structures of the BG (Tseng et al. 2001; Mahon et al. 2006; Litvak et al. 2011; Kim and Kita 2013). Furthermore, it has been shown that those signals are not simply relayed through the BG pathways but they are rather subjected to a form of internal processing, depending on their initial frequency (Brittain and Brown 2014).

However, most of the knowledge that has been acquired so far does not come from studies on healthy humans, due to the inability of even the most current non-invasive recording techniques to reach sub-cortical structures. Instead, most studies are confined either to animal models or human patients undergoing deep brain stimulation (DBS), a common surgical treatment of BG diseases, which provides the opportunity to record the spiking activity of multiple structures simultaneously.

For this reason, and due to substantial modelling challenges, oscillations are largely neglected in current cognitive models, even in large-scale computational approaches with spiking neurons (Eliasmith et al. 2012), despite the aforementioned evidence of their importance.

Pathological implications

Low-frequency spontaneous activity in the BG is enhanced in neurodegenerative disorders that affect this region, including Parkinson's (PD) and Huntington's (HD) disease. These disorders are often accompanied by devastating motor symptoms, such as rigidity and tremor, as well as cognitive symptoms including impairments in decision making (Euteneuer et al. 2009) and episodic memory loss (Montoya et al. 2006) among others.

It has been shown that DBS can stop some of these symptoms and partly restore motor and cognitive function (Little et al. 2013; Nagel et al. 2015). In fact, these benefits are correlated with the reduction of abnormal oscillatory activity brought about by DBS when applied to the underlying brain structure (Kühn et al. 2006; Little and Brown 2014).

This effect, alongside the aspects of action selection discussed above, give rise to a number of questions. First, to what extend do the oscillatory effects of PD and DBS influence BG function? Second, is this activity generated within the BG circuit itself or is it driven by cortical regions? Finally, are Parkinsonian tremor and rigidity directly associated with action selection at the motor level?

1.3 Objectives

The central aim of this work is to narrow the gap between studies with genuine interest in action selection, the BG and cortical oscillations, relying solely on computational methods and available data from the literature, without the need for new animal experimentation. Our approach centres on the construction of a bottom-up model of the complete BG circuit, based on physiological studies which can provide the means for a direct comparison with existing behavioural data.

Recently, a number of computational tools have been proposed that allow the simulation of large-scale networks of biologically plausible spiking neurons in a feasible time scale (Fidjeland and Shanahan 2010; Brette and Goodman 2012). The employment of these tools fulfils the needs of the current approach since it enables the simulation of multiple BG parallel loops in full scale.

The next objective of this work is the investigation of whether this resulting neural model can provide new insights into the rhythmic-based BG pathology and, in particular, into the questions posed in the previous section.

Finally, our last objective is to release a user-friendly implementation of this novel framework and thus create a computational platform that other scientists can use to investigate the dynamical behaviour of the BG.

1.4 Achievements and structure of thesis

All aims described in section 1.3 were achieved within the context of this thesis. The remaining chapters provide a full description of this work, in the form of individual sub-projects and they are presented in chronological order. A brief overview of these results, following the structure of the thesis, is as follows.

Chapter 2 describes the overall methodology that is used in the rest of the thesis. Initially we developed Brain Studio, a spiking neural network editor and simulator that was designed to be general enough to cover the complete range of simulation needs of the current thesis. Then, we designed a novel technique to optimize biological realistic neuron models to behave like real cells in specific brain regions.

Using these tools, in Chapter 3, we built a new large-scale neural model of the BG circuit. This model was employed in Chapter 4, where we investigate the dynamical behaviour of the BG for different oscillatory inputs, and we demonstrate their internal effective connectivity.

Based on the same analysis, in Chapter 5 we observed a common phenomenon in the Globus Pallidus neurons that emerged from our model, although it was not considered in the design phase, and we investigated its consistency with real data. Using both the above BG model, as well as a more detailed simulation of these particular neurons, we identified a biologically plausible mechanism that might cause this effect in their biological counterparts.

Having established the desired level of biological plausibility in our simulations, chapter Chapter 6 is focused on behavioural results. In particular, we investigated the effectiveness of this circuit in selecting between salient signals and we report a number of predictions that arose from our simulations. Most notably, we present a novel hypothesis that views the BG as the "gearbox" of the cortex, a mechanism that provides various modes of signal selection on demand, and the existence of a selection cycle that re-evaluates the plausibility of current cognitive architectures.

Furthermore, based on the analysis in chapters 4 and 6, we identified two potential mechanisms for the generation of Parkinsonian tremor which are briefly presented in Chapter 7. Finally, in Chapter 8 we provide a more extensive summary of our findings as well as an overview of future directions for this research.

Relevant publications

Papers that have been already published:

- Z. Fountas, M. Shanahan, "GPU-based Fast Parameter Optimization for Phenomenological Spiking Neural Models", IEEE International Joint Conference on Neural Networks (IJCNN), Killarney, Ireland, 2015
- Z. Fountas, M. Shanahan, "Phase Offset Between Slow Oscillatory Cortical Inputs Influences Competition in a Model of the Basal Ganglia", IEEE International Joint Conference on Neural Networks (IJCNN), Beijing, China, 2014.
- Z. Fountas, M. Shanahan, "A cognitive neural architecture as a robot controller." In Biomimetic and Biohybrid Systems, pp. 371-373. Springer Berlin Heidelberg, 2013.

Papers submitted:

- Z. Fountas, M. Shanahan, "The Role of Cortical Oscillations in a Neural Model of the Basal Ganglia", submitted to the Journal of Computational Neuroscience

Papers in preparation:

- Z. Fountas, M. Shanahan, "The "gearbox" of the cortex: How cortical oscillations shape

selectivity in the basal ganglia.", to be submitted for journal publication.

- Z. Fountas, M. Shanahan, "The role of bursts and pauses of neurons in the globus pallidus external", to be submitted for journal publication.
- Z. Fountas, M. Shanahan, "Two plausible sources of Parkinsonian tremor.", to be submitted to conference proceedings.
- Z. Fountas, M. Shanahan, "Brain Studio: A practical high-performance tool to design and simulate spiking neural networks.", to be submitted to conference proceedings.

Finally, Brain Studio is currently being officially used within the TIMESTORM project, a three year EU-backed collaboration between six academic institutions across Europe (http://timestorm.eu). The latest version of its source code is available through (http://brain-studio.org).

2 Modelling tools

2.1 Introduction

The largest part of the methodology presented in this thesis regards the mathematical modelling of brain structures using networks of phenomenological spiking neurons. In this type of spiking neural networks (SNNs), the equations that model the membrane potential fluctuations of neural cells correspond to mathematical abstractions rather than modeling individual ionic mechanisms. The basic objective for the resulting models is to conform to the dynamical behaviour of their real counterparts. This can be used as a proof of their biological plausibility, before these models are employed to make new testable predictions. However, SNNs inherently entail some distinct functional attributes that need to be carefully considered and built upon, in order to achieve biologically meaningful simulations.

The rich dynamical behaviour of single cells in the brain can be clustered into distinct categories, all of which can be captured by phenomenological spiking neuron models (Izhikevich 2007a), and result in different group dynamics. In addition, this computational framework enables the investigation of known neural phenomena that have been considered important for our quest, such as oscillatory activity, plasticity and neuromodulation. Nonetheless, the great flexibility of these models is accompanied by a vast number of open parameters, often without physiological meaning, that make their employment a difficult challenge and create a need for optimization. The amount of the available computational resources is therefore critical for both the ability to simulate a realistic number of neuronal computational units, as well as for work which is prerequisite for the simulation.

For these reasons, a substantial number of methods and software systems have been recently proposed, that facilitate the design and simulation of SNNs. First, a number of software systems aims to the optimization of single spiking neurons in order to replicate recorded electrical traces of real cells. A review of these methods can be found in Geit et al. 2008. Despite their success, these tools have failed to establish a globally accepted methodology, since there is no single measure of “goodness" that accounts for all the desired features in the behaviour of a model neuron. For instance, some optimization tools focus on capturing the exact voltage trajectories and spike trains of biological neurons. The successful tuning of ionic-based models through this process, can result in valuable predictions on the structure of these cells. However, this is a difficult, and often impossible, task for simple phenomenological models, due to their limited state space. In contrast, these simple models can be tuned to produce the same type of dynamical

behaviour found in their real counterparts, without a significant computational cost.

Second, a wide variety of simulation environments are dedicated to the calculation of the action potential propagation and the membrane potential dynamics of SNNs. These tools are using typical numerical integration methods, with optimized performance for different research applications. One category of tools, a characteristic example of which is the software NEURON (Hines and Carnevale 1997), is focused on muli-compartmental neuron models and sub-cellular processes. The tool GENESIS (Bower and Beeman 2012) (and the follow-up tool Moose) extends this concept to small-scale neural networks. On the other hand, a number of tools, such as NeMo (Fidjeland and Shanahan 2010), Nengo 2.0 (Bekolay et al. 2013), NEST Kayraklioglu et al. 2015 and CARLsim 3.0 (Beyeler et al. 2015), aim at simulations of large-scale networks, by focusing on phenomenological, single-unit models of neurons, and thus reducing the level of biological detail. Finally, the tools Brian (Goodman and Brette 2008) and "Geppetto Simulation Engine" 2016 belong to a category where a compromise between flexibility and network size is intended.

From the network design perspective, a number of software simulators are supplemented by embedded graphical environments, that include Nengo, Geppetto and Spikestream (Gamez 2007). However, there is currently no implementation of a simulator-independent graphical user interface (GUI) that exhibits syntactic interoperability. Such an approach would be very beneficial for rapid prototyping, the cross-validation of simulation results and the reuse of existing model components. At a lower level, the vast majority of the above systems provide application programming interfaces (APIs) and can be used as libraries of general-purpose programming languages, such as C/C++ (NeMo and CARLsim 3.0) or Python (Brian, Nengo 2.0, NEST and Geppetto), while others provide their own scripting languages (NEURON and GENESIS). Unlike in the case of GUIs, the issue of compatibility that emerges from the plethora of available APIs can be addressed by the use of simulator-independent languages, such as PyNN (Davison et al. 2008) and neuroML (Cannon et al. 2014).

In conclusion, despite the major progress of recent years, there is still a considerable room for improvement of the above techniques and introduction of new approaches. This deficiency in the existing software tools is reflected in the requirements of this thesis, where flexibility, computational performance, and real-time visual monitoring are all crucial factors.

Therefore, our first aim here is to automate and speed-up the process of designing and testing large-scale SNNs, through a suite of new simulation tools. In particular, this suite should provide (1) a framework for the compact representation of modular SNNs, suitable for large-scale brain circuits and cognitive systems, (2) a generic and powerful simulator that allows the fast implementation, visualization and real-time adjustments of SNNs, and (3) a fast optimization

technique, which could be used in order to mimic the dynamical behaviour of specific neurons in the brain, using simple phenomenological models.

In the remaining sections of this chapter, we present a number of software systems that have been developed in order to address the above requirements. As the computational foundation of these systems, two well-known simulators have been selected and are presented below in more detail. These two simulators feature distinct strengths, namely speed and flexibility, which make them to complement one another.

2.1.1 NeMo spiking neural network simulator

NeMo is a high performance spiking neural network simulator which was originally developed in the Computational Neurodynamics lab by Fidjeland and Shanahan 2010, and has the form of a C++ library. NeMo takes advantage of the large number of CUDA-based graphics processing units (GPUs) of the NVidia graphics cards to provide a remarkably high memory bandwidth, and run parallel simulations with large number of neurons and synapses in real time. In a recent commercial of-the-shelf desktop computer, this system is able to simulate up to 500.000 Izhikevich neurons in real time, connected with 10.000 synapses each, under biologically plausible conditions that correspond to almost 5 billion spike events per second.

Although NeMo supports the development of custom neuron models, the default numerical integration of the neuronal differential equations is carried out using the Euler's method with a step size of 0.25 milliseconds (ms). Also, the conductance delays of the synapses have a precision of 1 ms, with a supported range from 1 to 64 ms. The default featured models include various forms of the phenomenological *integrate-and-fire* neurons including the *simple model* by Izhikevich 2003, as well as the analytical conductance-based model by Hodgkin and Huxley 1952. In addition, learning in NeMo is realized by means of spike-time dependent plasticity (STDP), a form of Hebbian learning, initially introduced by Song et al. 2000. Finally, NeMo can be used directly, as a C++ class library, but it also provides interfaces for the languages Python, Matlab, PyNN and pure C.

The key feature of NeMo is its performance in parallelizing the propagation of synaptic events in the network and distributing computation over the available resources (Brette and Goodman 2012). One of the major performance bottlenecks in GPU-based distributed applications is the time required for global memory access. In the case of SNN simulators, fetches of global memory chunks are required for each synaptic event at each timestep in order to calculate the effect of this event on the post-synaptic neuron. NeMo addresses this issue by clustering synapses that have the same source and delay, so as potential synaptic events can be fetched simultaneously.

Despite its speed improvements over other systems, NeMo is inadequate for a large number of applications, due to limitations in flexibility and the lack of visualization tools. The default version of NeMo provides a fixed and limited set of neural models and a single type of synapses. Any modification to the equations of these models, or implementation of new ones, constitutes a complicated procedure, which requires adjustments in the C++ source code and re-compilation of the system. In addition, NeMo features a low-level API where neurons and synapses can be only added individually, which can make the design of complicated experiments a laborious task. For these two reasons, the implementation of a simulation with NeMo often becomes more time consuming than using other approaches.

2.1.2 Brian simulator

Brian (Goodman and Brette 2008), and its more recent version Brian 2.0 (Stimberg et al. 2014), is a SNN simulator based in python, that focuses on high-flexibility and rapid prototyping. To achieve this, its API provides a concise syntax, compared to other python-based simulators, and the ability to write new equations for neurons and synapses in standard mathematical form. In addition, Brian features basic data recording, analysis, and plotting tools, and therefore it can support the complete process of designing and conducting a computational experiment based on SNNs.

The syntactic advantages of Brian can be partly attributed to the dynamic typing capabilities of python, according to which, objects are assigned a type at the runtime. Through this feature, the user can call the same methods to define entities in a network, using different types of attributes, and the system parses any given information transparently. Furthermore, neural populations or synapses with common characteristics can be grouped in single vectorised objects, and processed at once. Hence, scripts written in Brian become more readable, easy to learn and quickly extensible, while the simulated network models can incorporate a great deal of biological detail, compared to similar software systems.

Like NeMo, Brian is an open source project that can be developed and used in almost any platform. It only utilizes three standard python libraries, namely NumPy, Scientific Python (SciPy) and Pylab/Matplotlib, and it does not require local compilation of individual components. Finally, Brian interfaces with the language PyNN, and it can also be employed using its simulator-independent API.

On the negative side, a significant drawback of this framework is the compromise of computational efficiency, in both memory and time. Brian has been shown to be significantly slower in execution time than other approaches, in a comparison using different benchmark models

in Bekolay et al. 2013. Due to the expensive function call overhead, it is not well-suited for interactive, real-time simulations, such as the control of a robotic platform, or the real-time adjustments using a GUI. For instance, the former example would require a network update, in the order of milliseconds, every time that the sensors of the robot receive new stimulus. Additionally, as in the case of NeMo, Brian is designed for simulations of unit neurons, and the support for multi-compartmental models is limited, while currently there is no GUI implementation provided.

All things considered, the two simulators mentioned here address different issues of SNN computational modelling, and thus have little functional overlap. The employment of both systems, for the purposes of the current thesis, establishes a good trade-off between design and simulation performance.

2.2 Brain studio

The first software tool that was developed to address the issues described in the previous section is called Brain studio. This tool has the form of a spiking neural network editor and simulator which focuses on cognitive architectures and large-scale neural systems. Its main aim is to provide the first independent graphical environment that can be used with multiple SNN simulators simultaneously. With this approach, the user can integrate different existing models that might have been developed based on different syntax, or design a new model from scratch.

Brain studio consists of two individual software layers. A GUI can be used to design and monitor an experiment in a user-friendly manner, and a stand-alone back-end executes the required calculations. These two parts communicate over the network via the TCP/IP protocols (Fig. 2.1) and can be instantiated independently. The complete system is fully cross-platform and can run in either Windows-based, Unix-based or Macintosh computer systems.

One major advantage of tool is that it allows the live monitoring and adjustments of the designed networks during simulation. The final experiments are represented and archived using a simple XML-based model description format that includes any live adjustments. Hence, saved projects can be loaded directly by the back-end, and run without the need for visualization. In addition, its simulation engine is modular and can be easily extended to account for any low-level neural network simulator that provides a python application program interface (API), as well as new visualization techniques. These features make brain studio an advantageous platform for rapid prototyping and integration of existing network modules, written in different simulators.

In order to demonstrate this extensibility, and evaluate the speed of brain studio, NeMo simulator

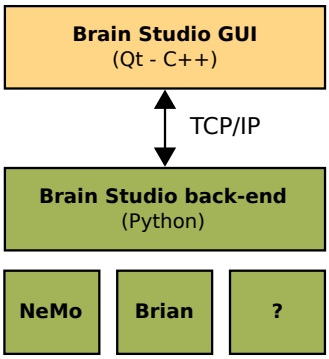

Figure 2.1: **Hierarchical overview of brain studio's architecture.** The *front-end* user interface communicates with the selected version of the *back-end* via a TCP/IP connection.

was integrated, and gave the ability to this system to simulate large-scale networks in near real-time. In the following sections, we give details regarding the structure of individual components of brain studio, as well as its resulting simulation performance. The latest version of its source code is available through (http://brain-studio.org).

2.2.1 Network topology and simulation structure

Network topologies in brain studio are internally represented using only two unordered lists of entities, that include *nodes* and *edges* (Fig. 2.2.A). A *node* can be any group of indexed computational units, such as equations of spiking neurons, rate-based neurons or random event generators, which share common characteristics and connectivity. It contains statistical information for the parameters and states of these units, as well as their number and basic graphical properties. Each parameter or state can be defined either as a single number, a random variable that follows a known distribution, or as a function of random variables.

In addition, a group of similar, directed connections between two nodes is described by an *edge*. As in the previous case, edges also contain statistical information that defines the pattern and the parameters of their underlying connections. The definition of a connectivity pattern requires its type and the indexes of the computational units in the source and the target nodes. Finally, the available types of patterns include *all-to-all*, *topographic* (one-to-one), and *sparse* connection groups (see Fig. 2.2.B).

In order for a complete experiment to be defined, a third list of entities is used that represents *actions* during the network simulation. Each action requires a timestamp and can refer to either the adjustment of a parameter in a single unit or a node in the network, the stimulation of a node, or the termination of the experiment.

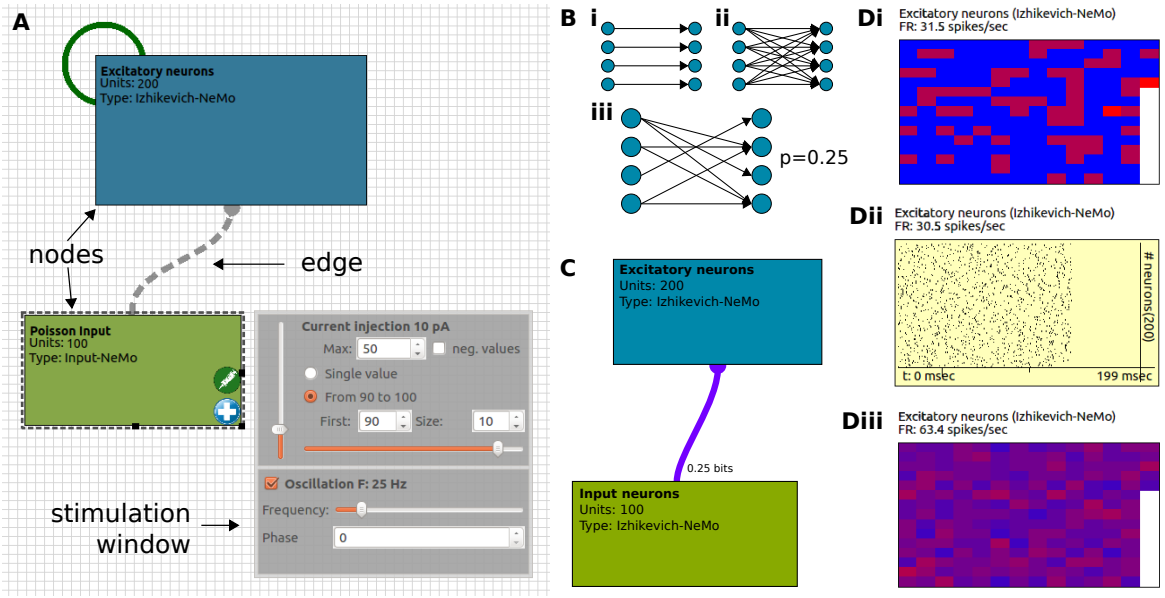

Figure 2.2: **Nodes and edges in brain studio interface. A:** Default representation of network topology. Dashed lines represent topographic and green lines plastic connections. **B:** Available connectivity patterns include **(i)** topographic **(ii)** all-to-all and **(iii)** sparse edges. **C:** Visualization of effective connectivity between two nodes. Connection colour: transfer entropy $\in [0, max]$ bits. Connection thickness: average synaptic weight. **D:** Visualizations of nodes: **(i)** Firing rates of individual neurons (using a cold to hot colour scale). **(ii)** Raster plot of neuron spikes over time. **(iii)** Membrane potentials of individual neurons.

Using this approach, all entities of an experiment can be represented internally using a compact and modular structure that includes only basic parameters and statistics. Brain studio is able to encode and save this structure in text files, using an XML-based format, under the extension '*.brn*'. Therefore, the user is provided with two options for the access and modification of experiments, either via the high-level graphical representation of the front-end, or directly via the automatically generated *brn* files. An example experiment that illustrates the format of these files, for a simple network with one node and one recurrent edge, is shown below.

```
<actions>
    <stimulate t="50" node="0" current="150" frequency="0"\>
    <stimulate t="350" node="0" current="100" frequency="90"\>
    <adjust t="650" node="0" parameter="sigma" value="7.0"\>
    <stop t="1000"\>
</actions>
<nodes>
    <Izhikevich-NeMo id="Excitatory" x="12" y="68" w="302" h="167" c="#357998">
        <version>0.001</version>
        <a>0.02</a>
        <b>0.2</b>
        <c>-65+15*RANDF()**2</c>
        <d>8-6*RANDF()**2</d>
```

```
14          <eval_for_each>False</eval_for_each>
15          <neurons>200</neurons>
16          <sigma>1</sigma>
17          <u>b*v</u>
18          <v>-65</v>
19      </Izhikevich-NeMo>
20  </nodes>
21  <edges>
22      <NeMoSynapticPathway-NeMo id="Excitatory-Excitatory">
23          <source>Excitatory</source>
24          <target>Excitatory</target>
25          <preFirst>0</preFirst>
26          <preLast>199</preLast>
27          <postFirst>0</postFirst>
28          <postLast>199</postLast>
29          <version>0.001</version>
30          <__connectivity>probability</__connectivity>
31          <__probability>0.1</__probability>
32          <delay>RANDI(1,60)</delay>
33          <plastic>False</plastic>
34          <weight>RANDF()</weight>
35      </NeMoSynapticPathway-NeMo>
36  </edges>
```

Finally, in case that a more advanced simulator is needed, brain studio has the ability to convert *brn* files either to the simulator-independent languages PyNN by Davison et al. 2008 and NeuroML 2.0 by Cannon et al. 2014, or to python code that is compatible with the brian simulator.

2.2.2 The front-end: Designing experiments

The first part of brain studio is a tool that aims to the high-level design and graphical representation of neural networks as well as the remote monitoring of their simulation. It is written in the programming language C++, based only on the cross-platform application framework Qt and the C++ standard library, providing high consistency and compatibility across systems. A real-time snapshot of this tool is shown in Fig. 2.3.

At each point of the design process the user can toggle between the default editor mode and the real-time simulation mode. When the simulation mode is selected, the current experiment is transferred to a connected instantiation of the back-end and a number of editing options are disabled. The back-end is then instructed to initialize the network by generating all the connections and allocating the necessary memory, and to finally start the simulation.

During the simulation mode, different types of two-dimensional plots can be used to visualize the activity within nodes. These include raster plots, local field potential and firing rate graphs, among other visualizations. Examples of these plots are shown in Fig. 2.2.D and Fig. 2.3.

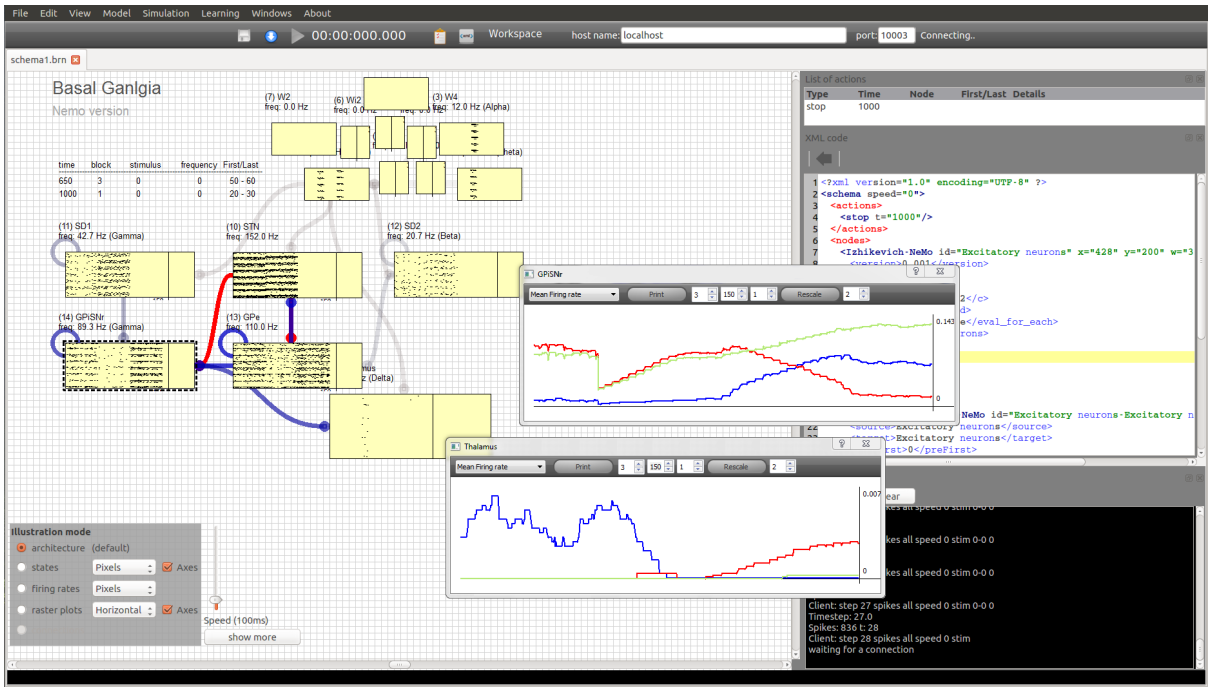

Figure 2.3: **Graphical user interface of brain studio in simulation mode.** A snapshot taken during a real-time simulation of a model of the basal ganglia. Left: Graphical representation of the experiment. Right: XML representation of the experiment.

Furthermore, a number of real-time visualizations are also available for the edges, that aim to highlight the dynamical properties of the simulation from the network perspective. The properties that are visualized include structural links, such as the absolute number of connections or connection weights, statistical dependencies (functional connectivity) and causal interactions (effective connectivity). An example is illustrated in Fig. 2.2.C, where the thickness of the line between two nodes represents the average weight of all individual connections and its colour represents information flow, calculated by means of transfer entropy.

The use of a programming language with low-level capabilities resulted in a reduced utilization of computer resources. In addition, since the necessary computation for the network simulation can be carried out remotely, on a separate device, brain studio front-end is able to perform analysis of the current state of the network in real-time, and thus enable visualizations of more advanced metrics, such as transfer entropy.

Finally, adjustments in existing nodes and edges are also supported in simulation mode. The system records any real-time changes, such as parameter tuning or stimulation, and updates the network accordingly. These changes can be saved as 'actions' with the time of each adjustment, relatively to the simulation, used as a timestamp.

2.2.3 The back-end: Running experiments

The back-end is the core component of brain studio, whose main role is to execute the simulation, independently from the user interface. Written in the programming language python, it is highly extensible and adjustable by the user, and it is designed to operate in both mobile robotic systems with limited resources, as well as in high-end workstations. Its two supported modes of operation include a *slave* mode, where the front-end has the complete control of the simulation, and a *master* mode, where brn-experiments are loaded and executed independently. When in the master mode, connection requests by the front-end are also accepted, which can either monitor or take control of the simulation.

The back-end also constitutes the only part of the system that holds information regarding the currently-supported mathematical models for nodes and edges. This information is retrieved by the front-end following the initial network handshake between the two. Hence, when a new neuron model is added to the brain studio, the front-end is updated automatically without the need of a new compilation. The list of the default available computational models that can be clustered in a node contains the following:

- *RateLayer-Python:* Equations for a simple rate-based neuron, implemented in python.
- *Input-NeMo:* An empty neuron unit, without dynamics, that can be forced to spike.
- *PoissonSource-NeMo:* A source that generates spikes according to a Poisson process.
- *Kuramoto-NeMo:* Delay-coupled Kuramoto oscillators, implemented in NeMo.
- *HH-NeMo:* Hodgkin-Huxley equations of neuron's ionic currents implemented in NeMo.
- *IF_ curr_ exp-NeMo:* Equations of the integrate-and-fire neuron model, with conductance-based synaptic input, implemented in NeMo.
- *QIF-NeMo:* Equations of the Quadratic integrate-and-fire neuron model, implemented in NeMo.
- *Izhikevich-NeMo:* Equations of the Izhikevich model, implemented in NeMo.
- *Izhikevich2007-NeMo:* Equations of the Izhikevich model, in the form where parameters have biophysiological meaning, implemented in NeMo.
- *Izhikevich2007_ TCR-NeMo:* Equations of thalamo-cortical relay neurons, based on the Izhikevich model, implemented in NeMo.
- *Izhikevich2007_ TI-NeMo:* Equations of thalamic interneurons, based on the Izhikevich model, implemented in NeMo.

- *IzhikevichRS-NeMo:* Equations of regular spiking neurons, based on the Izhikevich model, implemented in NeMo.

In addition, the list of the default instantiatable synaptic models that can be used as edges, along with their parameters, includes:

- *NeMoSynapticPathway-NeMo:* Synapses between groups of spiking neurons implemented in NeMo. Available parameters include weight, delay, and the existence of STDP.
- *RateToSpikeConverter-Python:* Equations that convert the current rate of a neuron to spiking input, with the same firing rate. The only available parameter is the weight of the connection.
- *SpikeToRateConverter-Python:* Equations that convert the current firing rate of a spiking neurons to rate-based input. Parameters include the window of the measured firing rate and a weight.

Finally, the list of the provided models of instantiatable nodes includes a number of extra, special cases that require further discussion. These cases regard the integration of brain-studio with external systems and demonstrate the extensibility of its core architecture. Here, a node represents an interface and the number of units it contains depends on the number of inputs and outputs supported. The currently supported nodes include:

- *Servomotor-output*: This single-unit node controls the speed of a servo motor, via pulse width modulation (PWM) on a digital port of the computational platform used. It can be used only as a connection target, and requires a SpikeToRateConverter. This node has been successfully tested on a raspberry pi computer.
- *Retina-input*: This node handles the raw input of a web camera, which transforms into spikes. The received image is initially down-sampled, and then the difference between frames is calculated for each pixel, and mapped into the firing rate of a corresponding neuron. This node can be used only as a connection source. The number of its units represents the available pixels.
- *Webots-Robot*: This node provides an interface with the 3D simulated environment of Webots, where a differentially-driven mobile robot is controlled. The communication is implemented as a second TCP/IP connection. This node can be used both as a source and a target of an edge, as it combines camera input and motor output.
- *UT2004*: This node provides an interface to control an virtual agent within the 3D environment of the video game Unreal Tournament 2004. It comprises 22 rate neurons that

are directly connected with either an input or an output of this simulated agent. The outputs include 13 neurons that encode exteroception, interoception and proprioception, while the inputs include 9 neurons that encode both motor sequences as well as single motor functions. For more details on the methodology used for this interface see Fountas 2011.

2.2.4 Extending brain studio

Brain studio can be extended in various ways. Three main categories of extensions are currently supported including new models for nodes, new models for edges and new visualizations. The updates in all cases can be carried out entirely by changing parts of the source code of the back-end in python. After an update has finished, the front-end can be automatically notified by the changes during the initial network handshake between the two parts, and the new extensions can be displayed.

Adding new nodes A node can be added to the existing collection, in case that either a new mathematical model, or a new interface with another software system is required. In brief outline, this process involves, first, the creation of a new python class that extends the base class *Node*, the specification of the required '*fields*' which can be used to configure the model, an output array, and finally the implementation of two methods for the model initialization and update. The required fields include any parameters or states of the simulated neurons that can be edited in the front-end, as well as any group attributes, such as the number of neurons. There is no limitation on the number of fields that can be defined, as long as they belong to one of the following supported types (bool, integer, float, integer list, float list or picklist). Using one of the aforementioned editing options, fields can be assigned a single value, a random variable or a function of random variables.

Since the only point of the interaction between the new class and the rest of the simulated network is through the input and output arrays, a new node can represent numerous types of different network components. In the case of a new mathematical model, the node can be either a group of instances of a specific neuron model with common characteristics, or a complete neural network. The second case is particularly useful when existing SNNs need to be integrated into a larger simulation. In both cases, calculations can be performed directly in python, or using another simulator such as NeMo or Brian.

In addition, the user can build general nodes that correspond to any models supported by a selected simulator. For instance, the class *NeuronGroup*() in Brian 2.0 simulator can support

any group of neurons, whose differential equations are written as a python multi-line string using Brian's syntactic rules. In this case, the fields of the node will contain the attributes of the constructor of this class, along with the parameters of the neuron model.

Finally, new nodes can be added when a new interface with an external system is required. Representative examples of this category comprise the special cases of nodes in the end of Section 2.2.3.

Adding new edges As in the case of nodes, a new edge can either represent a new type of connection, or an interface with an existing simulator, that can be used to instantiate any supported types of this simulator. The necessary steps consist of the creation of a new python class that extends the provided base class *Edge*, the specification of the required '*fields*' which can be used to configure the connection, and the implementation of two methods for the model initialization and update. However, the update function here can be neglected, if both the source and the target nodes of the new edge are using the same simulator as a back-end. In this case, brain studio can redirect the implementation of this connection to the underlying simulator.

Adding new visualizations This final type of extension concerns the development of new methods to visualize the behaviour of nodes and edges in the network. Initially, the type of plot that would better illustrate the desired network property needs to be defined. The front-end of brain studio features a wide range of supported types, which are implemented through the Qt library QCustomPlot by Eichhammer 2014. Then, the user can write python code that is executed at every timestep, and performs analysis on the state of the desired network component. The resulting information can be visualized by the front-end in real-time.

In addition, the source code of the front-end can be also altered and recompiled if better computational performance is required during the analysis, or the flexibility of the back-end is not enough. The implementation of this functionality of brain studio is still at a preliminary stage.

2.2.5 Evaluation

One of the key aims of brain studio is to maintain the low computational time that can be achieved with low-level software systems, when simulating large-scale SNNs or networks with other neural units. This would allow users to have a clear overview of the dynamical behaviour of the simulated network and apply changes in real time. Its performance in achieving this aim can be assessed by means of scalability tests, with respect to the size of the simulated network. Such an analysis can indicate how the resource utilization of both parts of the system grows

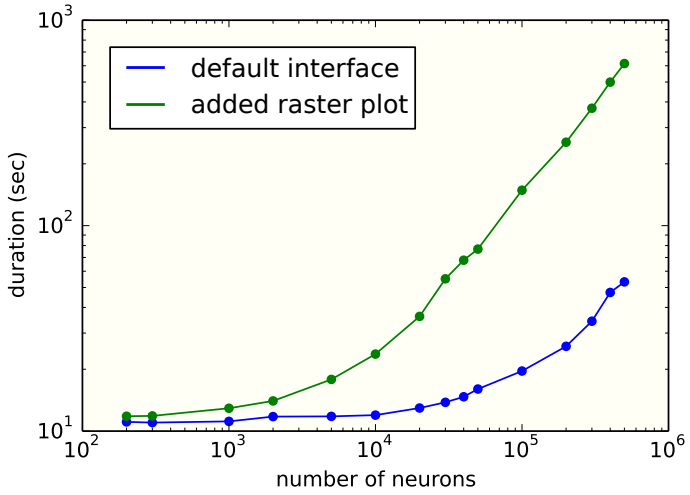

Figure 2.4: **Performance of brain studio in simulating large-scale networks.** Absolute time on the computational platform used for 1 second worth of simulated time, for networks of various sizes.

with increasing load and reveal potential bottlenecks.

For this purpose, we ran a series of test simulations, using a default biologically SNN architecture that comprises 80% excitatory Izhikevich spiking neurons and 20% inhibitory. Each neuron in the network formed synapses with each other neuron with likelihood 0.1, and the simulated time was set to 1 second. All excitatory neurons were stimulated with external injected current that allowed the network to have an average firing rate of 15 spikes/second. Thus, the only parameter of the simulation that remained free was the total number of neurons, which was used as an indication of the computational load of the simulation.

All simulations were executed on the same platform, which comprises an Intel i7-4790K 4.00GHz CPU, 16GB DDR3 2333MHz RAM and a single GeForce GT 730 GPU. The operating system was 64bit Ubuntu 14.04. The neurons of the network were defined using a NeMo-based node and NeMo was set to execute calculations using the CPU of the device. Both back- and front-end were initialized on the same platform.

Fig.2.4 illustrates that, under these conditions, the simulated SNN can scale up significantly, with a performance which is comparable to current low-level simulators. The addition of a full raster plot to the front-end, which updates in real-time during the simulation, slowed down the process by an acceptable order of magnitude (less than 3 times in most experiments), although the extra amount of information that this visualization requires to be transferred from the back-end to the front-end is significantly more (approximately 153 times).

Brain studio has now become an ongoing open source project with an increasing number of

users. Future improvements include the introduction of more advanced visualization tools, the development of a wider variety of models for nodes and edges, and the integration of other low-level neural simulations such as Brian.

2.3 GPU-based fast parameter optimization for phenomenological neural models

The last significant obstacle in using phenomenological models of spiking neurons for large-scale simulations is the approximation of the optimal parameters for a type of neuron, given the available experimental data. In this last section we illustrate a method for optimizing the parameters of such models, based on a combination of different frequency-current and voltage-current relations of a neuron as well as known physiological properties. We also present a python toolbox which uses the simulator NeMo and provides a fast GPU-based implementation of our method. As a benchmark, our toolbox was used to fit Izhikevich equations to neurological data obtained from a cat's thalamic relay cell. The resulting model was able to predict the firing patterns of known membrane potential traces of this neuron, although they were not explicitly defined during training. A further comparison between this neuron model and a previous approach, when both models are used in the simulation of a generic thalamic nucleus, revealed that the distribution of neuronal avalanches is significantly different and conforms better to power law-like distributions, thus increasing the likelihood of a critical regime and the biological plausibility of the simulation.

2.3.1 Introduction

Phenomenological models of spiking neurons can be very useful in computational neuroscience, since they provide a powerful way of capturing the dynamical behaviour of real cells and replicating their exact membrane potential traces with a reduced computational cost. For this reason, the popularity of this approach is continuously growing, especially in large-scale networks that include from real-time simulations of abstract models (Eliasmith et al. 2012; O'Connor et al. 2013; Gamez et al. 2013) to slower simulations of complete brain structures (Izhikevich and Edelman 2008; Humphries et al. 2010; Fountas and Shanahan 2014). However, since a large proportion of the parameters of these models do not have any biological meaning, their employment usually requires prior fine-tuning, to make them operate accurately in different regimes.

A number of different optimization methods have been proposed that may involve matching exact membrane potential trajectories in different stimulus conditions (Bhalla and Bower 1993),

spike trains (Rossant et al. 2011), approximation of the phase plane of a neuron (Achard and Schutter 2006), frequency-current (F-I) or voltage-current (V-I) relations (Hertäg et al. 2012) or a combination of the above (Friedrich et al. 2014) (for a review of these methods, see Geit et al. 2008). In addition, a variety of recently developed software tools, that aim to tune spiking neurons, provide implementations for many of the aforementioned methods at a certain computational cost. Examples of such software systems include the software tools Neurofitter (Geit et al. 2008) and Optimizer (Friedrich et al. 2014) as well as tools that work at the network level (Carlson et al. 2014).

Despite the wide range of available approaches, the literature still lacks a general methodology and, as a result, researchers often prefer to follow the safest but remarkably time-consuming solution of hand-tuning (Izhikevich 2007a; Prinz 2007; Booth 2014). Also, it is not yet clear which of the neuron features that have been used for optimization are more important to capture realistic dynamical behaviours at the network level (Li and Vu 2013).

In Hertäg et al. 2012, Hertag et al. showed that the process of fitting neuron models to frequency current (F-I) current clamp and sub-rheobase voltage-current (V-I) data constitutes a sufficient estimator of the firing patterns of a real neuron. Their method, however, based on analytical approximation of F-I/V-I curves, does not assess electrophysiological properties or statistical variations of a neuron, two important properties for large-scale simulations.

The purpose of this work is to build a robust automatic method for parameter optimization, able to overcome the problems posed by the previous approaches, as well as an implementation of this method that minimizes its significant computational cost. Our method, based on both global and local optimization algorithms, combines the ideas of F-I/V-I tuning with electrophysiological and statistical properties estimation. In addition, a new python toolbox provides a GPU-accelerated implementation of this method, based on Fidjeland and Shanahan 2010, able to complete the optimization process in a matter of minutes, requiring minimized user intervention.

To assess the performance of the proposed method, we examined to what extent it is able to improve a model of a cat's thalamocortical (TC) relay cell, previously fitted to membrane potential traces. The resulting model was a closer fit to the real cell properties than previous approaches. We found that it was able to reproduce firing patterns which are unique for TC neurons (Sherman and Guillery 2006) without any relevant training. Also the employment of this model as the building block of a general thalamic nucleus resulted in a more biologically plausible simulation than previous optimized neurons.

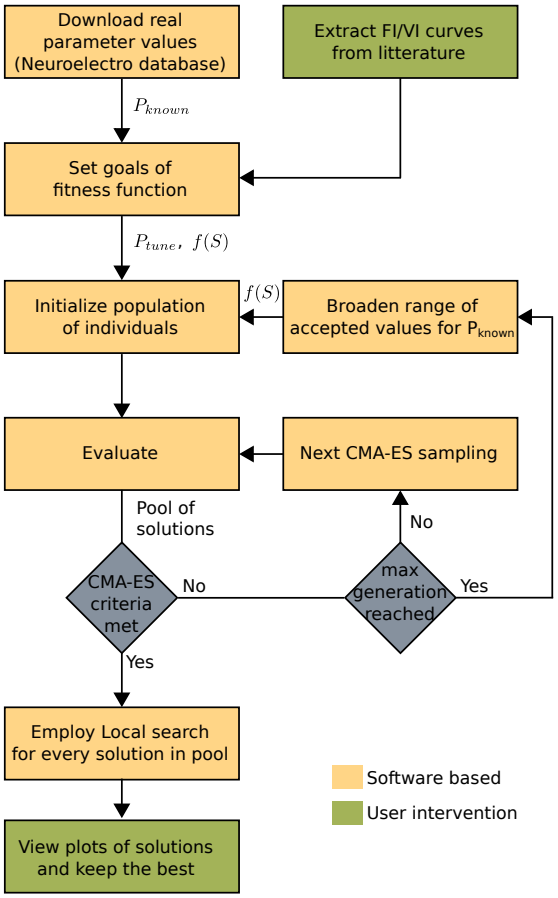

Figure 2.5: Overview of the method used to find the mean values of the parameter set for the targeted neuron. P_{known}: The parameters whose real values were found in NeuroElectro database. P_{tune}: The parameters that need to be tuned. $f(S)$: The fitness function.

2.3.2 Methodology

Neuron models

Our methodology can be applied to any phenomenological neuron model. The default selection in our toolbox is the Izhikevich (Izhikevich 2003) simple model which is shown to have the simplest possible form that is able to reproduce the majority of the computational properties of brain cells and have indistinguishable behaviour of *in vitro* and *in vivo* recordings (Izhikevich

2007a). The membrane potential v of this model is governed by

$$C\frac{dv}{dt} = k(v - v_r)(v - v_t) - u + I \tag{2.1}$$

$$\frac{du}{dt} = a\big(b(v - v_r) - u\big) \tag{2.2}$$

where u a phenomenological recovery variable, C the membrane capacitance, v_r the resting membrane potential, v_t the instantaneous threshold potential and finally a, b and k are three abstract parameters of the model. The neuron fires an action potential when the voltage exceeds the threshold value v_{peak} and the two variables of the model reset to

$$\begin{aligned} v &\rightarrow c \\ u &\rightarrow u + d \end{aligned} \tag{2.3}$$

where c and d are two further abstract parameters. Finally, I represents any input current that can be either dendritic or synaptic. For the purpose of this optimization algorithm, we do not model any chemical synapses and the input current of each neuron can be simply described as $I = I_{spon} + I_{injected}$, to take into account a general injected current that varies in different experiments as well as the default constant current I_{spon} that leads to the spontaneous activity of the cell.

For the rest of this section we will use equations 2.1-3.3 to generate analytical solutions when needed but a similar process can be applied to the majority of the known phenomenological models.

Optimization algorithm

The design of an optimization algorithm for spiking neurons entails two main independent challenges (Geit et al. 2008). First is the definition of a function that is able to evaluate robustly the fitness of a model to real biological data, and the second is the choice of a heuristic technique that can use this function to search for the optimal solution in the space of available parameters. Starting with the latter, we used a global search method to identify areas of potentially optimal solutions and a local search method to further optimize solutions in each of these areas (Achard and Schutter 2006). This combination of global and local search provides a balance between exploration and exploitation (Eiben and Schippers 1998) and facilitates the avoidance of local maxima convergence (Geit et al. 2008).

Figure 2.5 illustrates the high-level steps of the optimization method proposed. Once the fitness function is defined based on available experimental data, an evolutionary strategy called

covariance matrix adaptation (CMA-ES) (Hansen and Ostermeier 2001) is used to find areas of interest in the large and continuous parameter space. This method is an optimized evolutionary algorithm (EA) where the mutations represent real perturbations taken from a normal distribution, adapted to the local fitness landscape. Thus, this method is particularly suitable for ill-conditioned fitness functions, such as the multi-objective function described later in this section.

The best unique solutions of the EA are stored in a pool that divides the parameter space into grid cells, where each cell can contain up to one solution. This pool is updated after each generation according to the following algorithm

function UpdatePool(S)
if Pool $<$ PoolSize **then**
  Add S to Pool
else if $S_{score} <$ worst(Pool)$_{score}$ **then**
  for p **in** Pool **do**
    if $p \div$ GrSize $= S \div$ GrSize **and** $S_{score} < p_{score}$ **then**
      Replace p with S and **return**
    end if
  end for
  Replace worst(Pool) with S
end if

where S is the candidate solution, PoolSize the maximum size of the pool and GrSize a parameter that controls the size of the area enclosed by each grid cell.

After a pre-defined number of generations, or if the fitness criteria are met, the EA stops and the final potential solutions in the pool are returned. An exception is made for any solution S_i that $S_i \mod \text{GridSize} \approx 0$ and $\|S_i - S_j\| <$ GridSize for S_j being another solution. The former condition indicates that the grid cell occupied by S_i might have a neighbour with a better fitness score and the latter condition verifies this assumption. Therefore, these solutions are treated as redundant and removed from the pool.

Next, each solution in the resulting pool becomes the subject of further local optimization based on the simplex algorithm (Nelder and Mead 1965). This method, unlike faster and more efficient gradient-based alternatives (Bhalla and Bower 1993), has been shown to overcome the problem of noisy parameter spaces, and thus it is a natural choice for the purpose of this algorithm.

The final step of the process is to approximate the variations in the observed electrophysiological properties of the real cell, which can be used for more realistic multi-neuron simulations. First,

the neuron properties that are used as parameters of the model (e.g. AP threshold or resting potential) are sampled from a normal distribution $\mathcal{N}(\mu_i, \sigma_i)$ where μ_i is the value of the optimal solution, σ_i is the standard deviation of the real recordings and i the parameter. Finally, if there are more known properties that do not correspond to model parameters, the CMA-ES algorithm is used again to optimize σ_i for the rest of the parameters. This time, the fitness function has a single objective which is the minimization of the difference between the real standard deviations and the ones sampled from 1000 instances of the model.

Derivation of initial parameters and parameter space

The initial values of the neuron parameters that need to be optimized, are sampled from a uniform distribution $\mathcal{U}(a_i, b_i)$, where a_i and b_i express the logical limitations of the parameter i. Also, parameters with values that can be obtained from experimental studies (e.g. from the NeuroElectro database) are sampled from a normal distribution, with standard deviation obtained from the same source.

Whenever possible, some of the parameters of the neuron model are inferred by the rest and their values are calculated before any other step of the fitness function. This, however, depends on the equations of the chosen neuron model that can be used to infer extra relations between parameters. If a found relation holds for every possible value of the rest “free" parameters and equation variables, the deduced parameter is not used in the ES chromosome. In the opposite case, these relations impose restrictions to the parameter space but do not reduce its dimension.

Examples of such relations for the simple integrated-and-fire (IF) and the more realistic adaptive exponential IF neuron models can be found in Hertäg et al. 2012.

For the Izhikevich model given in (2.1-3.3), the parameters b and k can be derived from the equations

$$b = \frac{1}{R} + k(v_r - v_t) \tag{2.4}$$

$$I_{rheo} = \max\{b(v - v_r) - k(v - v_r)(v - v_t)\} \tag{2.5}$$

were R is the input resistance and I_{rheo} the rheobase current of the cell. These relations however, which are explained in Izhikevich 2007a, rely on the assumption that $b < 0$ and thus fall into the second category of relations described above.

Also, as shown in Section 2.3.3, the default current of the neuron I_{spon} can be derived as the difference between the model's rheobase current and the real rheobase current of the neuron I_{rheo} obtained from any known F-I curve (Figure 2.7.B).

Fitness function

This is arguably the most crucial feature of the optimization method since it defines the criteria by which the optimal solution will be determined. The function proposed here is based on the approximation of F-I and V-I relations in different initial conditions of the neuron as well as any available electrophysiological parameter values. This multi-objective nature requires a careful consideration of each of these criteria, for which a brief description is given below.

F-I curves A frequency-current (F-I) curve is used to describe relations between various amplitudes of injected current in a neural cell and the action potentials evoked as a response to this current. These relations have been used for the optimization of single-point neurons and shown to be sufficient for the reproduction of spike times in different cortical cells (Hertäg et al. 2012).

The proposed algorithm here is using F-I curves in different cases that include transient and steady state curves for different initial currents. Both categories are important capturing neuron's behaviour. Transient relations encode information regarding the initial response of a cell (such as rebound dynamics), while steady-state relations show the actual spike frequency and the overall behaviour of the cell. The fitness of the individual with respect to an F-I curve f_{FI} is given as root-mean-square difference between the experimental data points and the corresponding simulated neurons.

V-I curves Similarly with above, V-I relations are also divided into instantaneous and steady-state, and they are a valuable source of information for the behaviour of the cell. Above the spiking threshold, (dynamic) V-I curves have been shown to be a self-contained method for accurate prediction (Badel et al. 2008). Also, at currents bellow the rheobase level, they reflect the sub-threshold dynamics of the cell which are not easily approximated with F-I relations.

The V-I fitness of the individual f_{VI} can be obtained with the same methodology as above, by simulating a number of model neurons equal to the number of real data points. In some cases, depending on the neuron model that is used, sub-threshold V-I curves can be derived directly form its analytical equations (See section 2.3.3).

Fitness of scalar values The fitness level of electrophysiological properties is also an important objective of the function. Often, such properties represent crucial features of a targeted neuron that need to be emphasised in the tuning process. Additionally, in case of an insufficient amount of available F-I/V-I experimental data, these properties provide a valuable alternative for the approximation of instantaneous and steady-state dynamical phenomena.

Some of the most important properties that have been tested with this method include the resting potential of a neuron, action potential (AP) threshold, amplitude and width, after-hyperpolarization amplitude and width, cell capacitance, input resistance and adaptation ratio. The real values of these parameters can be obtained from centralized databases such as Tripathy et al. 2014, where cross-study statistics of multiple neuron recordings can be also easily extracted.

Unlike the previous cases, the fitness formula of an individual here is using directly the real statistics via a normalized Gaussian function. That is, if x_j is the value of the parameter j of an individual, the fitness of this parameter is given by

$$f_{sc}(x_j) = e^{-\frac{(x-\mu_j)^2}{2\sigma_j^2}} \tag{2.6}$$

where μ_j and σ_j are the mean and standard deviation of the real available data for the parameter j.

The value of σ_j encodes the range of accepted values and provides a good approximation of the corresponding fitness weights. Hence, the final fitness function has the form

$$f(S) = \sum_{i \in C_{FI}} w_i f_{FI} + \sum_{i \in C_{FI}} w_i f_{VI} + \sum_{j \in P_{known}} f_{sc}(x_j) \tag{2.7}$$

All weights w_i, although can be defined by the user, are set to favour steady-state and transient F-I curves over V-I curves as a default. The reason is that, in our experiments, the former two cases were found to influence more the dynamical behaviour of a neuron, and be less likely to over-fit.

Termination

If the algorithm does not return a satisfying solution, after the completion of the above process, the range of the accepted values for the known neuron properties broadens (by increasing the value of σ_j) and the process starts again.

In the opposite case, the algorithm has to overcome the final problem of over-fitting in any of the above objectives. Frequently, the targeted neuron properties are obtained from recordings from different cells and, depending on the model used, there is no guarantee that a perfect individual that matches parameters and all V-I and F-I curves exists. Since there is no obvious solution to this issue, the algorithm keeps track of all unique potential solutions via the pool described earlier in this section. Hence, after the successful termination of the process, all individuals in the pool should be visualized (for an example see Figure 2.7) and shown to the user.

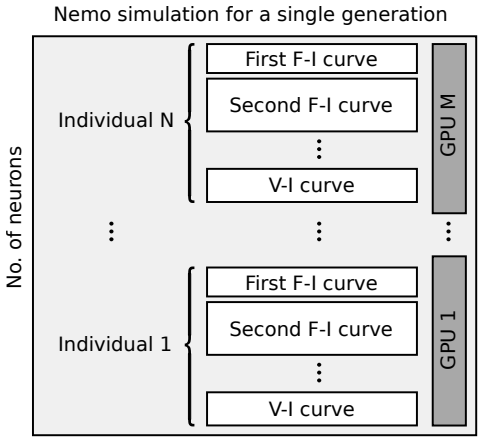

Figure 2.6: A single neural network is initialized in every generation of the ES used and it is accommodated equally in all (M) available GPUs of the system. As a result, the fitness function for each individual is calculated concurrently taking advantage of NeMo's fast GPU calculation abilities.

The toolbox

As a part of this study, a new optimization toolbox was developed, based on the above method and written in python. The most important feature of this toolbox is its high performance, which is achieved via the underlying spiking neural network simulator, NeMo (Fidjeland and Shanahan 2010). As seen before, NeMo is based on a C++/CUDA back-end and delivers a high performance when simulating large-scale neural networks on graphics processing units (GPUs).

Using this framework, the calculation of the fitness function used by the above method can be almost fully parallelized for each generation of the CMA-ES (Figure 2.6). Before the beginning of the first generation, a new NeMo simulation is initialized. The network of this simulation contains N times the neurons needed for each calculation of the fitness function, where N is the number of individuals.

In case that the available system accommodates M GPUs instead of one, the toolbox automatically generates M NeMo simulations and distributes the calculations equally.

For the implementation of the evolutionary algorithm, the python library deap (Fortin et al. 2012) was preferred, since it provides a significant number of alternative algorithms that can be also used, instead of CMA-ES, if required. Also, any local search method used in the toolbox is implemented via the standard optimization toolbox of the python library SciPy (Jones et al. 2001–2015).

One of the major aims of this toolbox is to reduce the user intervention throughout the duration of the optimization process. As shown in Figure 2.5, the only requirement of the method is the

location and extraction of the F-I and V-I relations that will be used by the fitness function. Following the same principle, the toolbox interfaces with NeuroElectro (Tripathy et al. 2014), an online database of experimentally found electrophysiological properties, that uses text mining to extract information from the published literature and thus updates on a daily basis. When the user initializes an instance of the toolbox and provides the name of the targeted neuron, every available statistic for this neuron will be downloaded, parsed and finally used during the optimization process.

The first finalized version of the toolbox will be released in `http://nemosim.sourceforge.net`.

2.3.3 Evaluation

Thalamocortical relay neuron

Dynamically, thalamocortical (TC) relay cells constitute an interesting category of spiking neurons since they integrate two spiking patterns with different dynamical behaviours. When the cell receives enough hyperpolarization, the existence of low-threshold activated Ca^{2+} current can cause a transient depolarization and, as a result, strong bursting activity, while at less hyperpolarized membrane potentials these neurons produce regular tonic spikes (Jahnsen and Llinas 1984; Zhan et al. 1999). Both these modes act as mechanisms to relay information that originates from the senses and other sub-cortical structures and is directed to the cortex. A unique characteristic that is shared among all TC relay cells is that the activation of the Ca^{2+} burst has a nearly “all-or-none" appearance (Sherman and Guillery 2006). Apart from this interesting behaviour, the fact that this neuron has been the subject of optimization with a different method (Izhikevich 2007a) as well as the availability of a substantial amount of data in NeuroElectro database and in Zhan et al. 1999, made it a reasonable choice for the evaluation of the proposed algorithm.

In Izhikevich 2007a, Izhikevich suggested an adjustment to the simple model for the accurate simulation of TC relay neurons. Equation 2.2 splits into two parts depending on the level of membrane potential in the neuron.

$$\frac{du}{dt} = \begin{cases} a\big(b(v-(v_r-m))-u\big) & \text{if } v \leq v_r - m \\ -au & \text{otherwise} \end{cases} \tag{2.8}$$

The new parameter m is positive in order to prohibit the activation of the Ca^{2+} current during the resting state of the neuron. When the membrane potential exceeds the threshold value

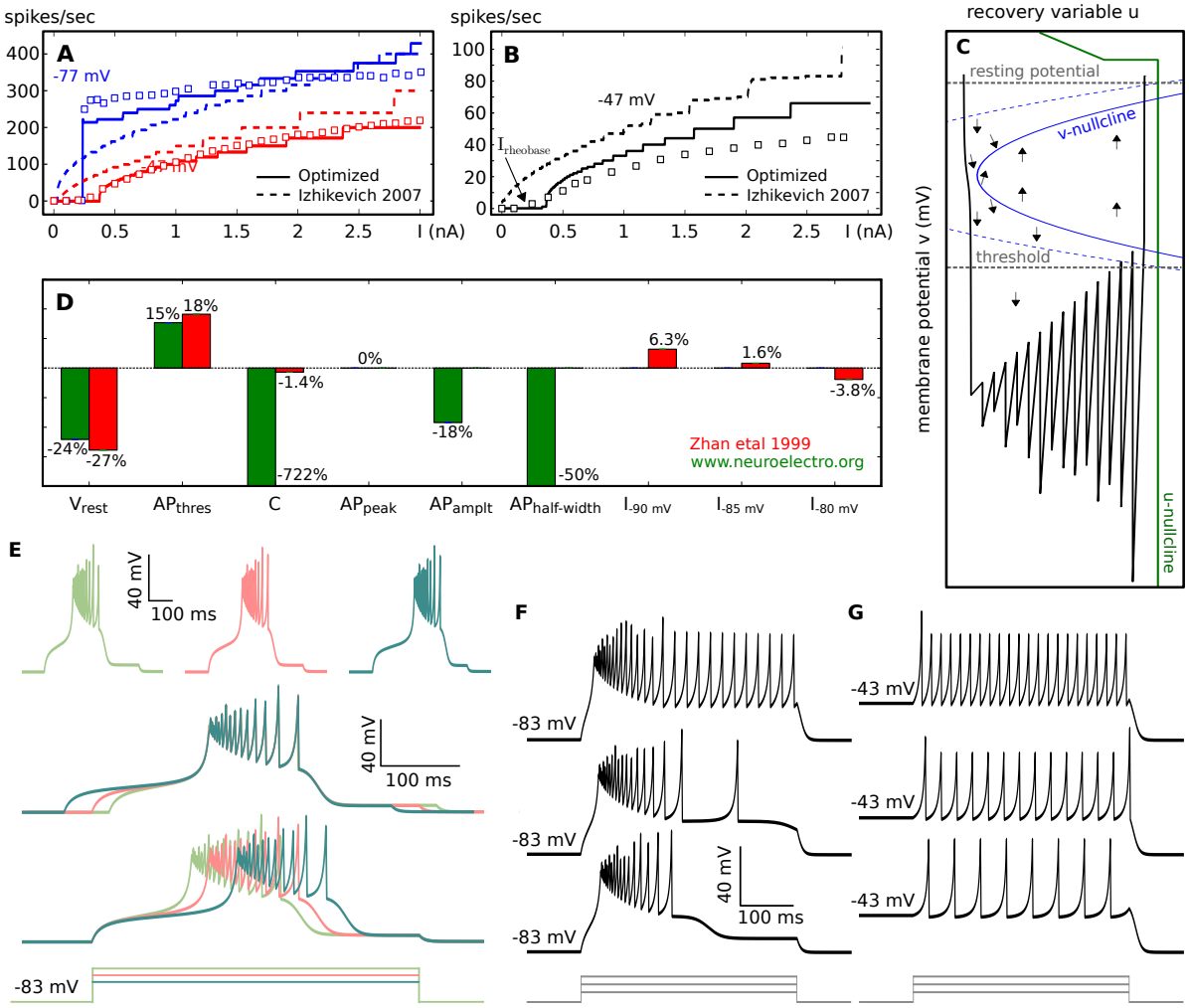

Figure 2.7: Properties of the resulting TC neuron model that arise after $400ms$ current stimulation and replicate previously obtained data in Zhan et al. 1999. **A:** Total number of spikes for current injections of different amplitudes and two different holding potentials. **B:** Firing frequency of the first 6 spikes for the same current injections. The symbols □ in A and B represent real recordings and the dashed lines represent the optimized TC model in Izhikevich 2007a. **C:** Phase plane of the TC model for the same run as in E ($486pA$). The dashed line represents the v-nullcline for zero injected current. **D:** Difference in various electrical properties of the model compared to data in NeuroElectro and (Zhan et al. 1999). **E:** Activation of the bursting mode shows the "all-or-none" nature of the Ca^{2+} activated spikes. After strong hyperpolarization, the membrane potential was stimulated with extra 240, 250 and $260pA$. The traces in the middle graph are time-shifted until the bursting pattern overlaps. The response time of the model is inversely proportional to the amplitude of the injected current. **F-G:** Response of the model for two different holding potentials. The injected currents in both cases are 486, 535.5 and $700pA$.

$v_{peak} + 0.1u$, the neuron fires a spike and the two variables of the model reset to

$$\begin{aligned} v &\rightarrow c - 0.1u \\ u &\rightarrow u + d \end{aligned} \tag{2.9}$$

With this adjustment, the purpose of the recovery variable u changes in order to capture the effects of the low-threshold Ca^{2+} current. Thus, with the proper parameter fitting, equations (2.1), (2.8) and (2.9) are able to reproduce firing traces of TC neurons in both modes (Izhikevich 2007a). However, it is not clear to what extent this model could be used to populate a biologically plausible model of a thalamic nucleus.

Taking the above into account, a new optimization attempt of the TC neuron was made, using the algorithm and the toolbox described in Section 2.3.2. The simple model was used with the same adjustments described here, keeping only the value of parameter $m = 5mV$ from the model in Izhikevich 2007a.

To calculate I_{spon}, we assume that the membrane potential of the neuron is around the AP threshold, where the input current of the cell will be equal to the rheobase current $I = I_{rheo}$. Since $b = 0$ for large membrane potentials, the system (2.1)-(2.8) behaves as a quadratic integrate-and-fire neuron and it has two eigenvalues

$$\lambda_1 = a \tag{2.10}$$

$$\lambda_2 = \frac{k}{C}(2v - v_r - v_t) \tag{2.11}$$

The values of $\lambda_{1,2}$ are always real, hence the transition from the resting state to firing will take place via a saddle-node bifurcation (Izhikevich 2007a). By definition, a condition for the classification of a bifurcation to saddle-node is the existence of two real eigenvalues one of which must be equal to zero. Therefore, from Equation (2.11), the membrane potential close to the rheobase will have the value $v_{rheo} = \frac{v_r+v_t}{2}$. In addition, the equilibrium points of the system can be found from the intersection points of their two nullclines, by solving the system (2.1)-(2.8) for $\frac{dv}{dt} = \frac{du}{dt} = 0$. The resulting equation is

$$I(v) = k(v - v_r)(v - v_t) \tag{2.12}$$

and provides an analytical method for the calculation of all V-I relations of the neuron for voltages between $v_r - m$ and the rheobase, as well as the transient-state V-I relations below this interval. By applying the value of v_{rheo} to (2.12), we can get the rheobase current of the neuron

$$I_{rheo} = \frac{k}{4}(v_t - v_r)^2 \tag{2.13}$$

The difference in the value of the rheobase current obtained from (2.13) and the real rheobase current, that can be found in the steady-state F-I curve in Figure 2.7.B, represents the spontaneous current I_{spon} that the neuron needs to better fit the physiological recordings. However, because of the existence of this constant current, the parameters v_r and v_t do not represent the

resting and threshold potentials any more. To change that, we can merge the current I_{spon} to parameters v_r, v_t and m. This can be done if the equation

$$k(v - v_r)(v - v_t) + I = 0 \tag{2.14}$$

has two real solutions. The solution with the lowest value represents the neuron's resting potential v_r^{new} while the second solution represent the threshold potential v_t^{new}. Finally, the parameter m in equation 2.8 can be transformed to $m^{new} = v_r^{new} - v_r + m$.

The above techniques were taken into account for the calculation of the fitness function described in methodology. After 50 generations of the evolutionary strategy, 66 significantly different solutions were gathered and further optimized with a local search method. The resulting parameter values of the optimal solution are $Ispon = -100pA$, $C = 294pF$, $v_{peak} = 35mV$, $k = 1.2$, $v_r = -78.99mV$, $v_t = -38.71mV$, and $m = 2.81mV$ while the abstract parameters $a = 0.0002$, $b = 20.55$, $c = -49.22$ and $d = 21.8$.

Figure 2.7 illustrates the properties of the resulting neuron model and a comparison with real data and a previously optimized set of parameters. Although the fitness function used took into account only F-I and V-I relations as well as a few basic electrophysiological properties, our simulations with this model matched data and features of cat's TC neurons that were never explicitly programmed. For instance, in most cases, activation of Ca^{2+} current evoked almost identical bursts, indicating the "all-or-none" behaviour of the cell.

The result of the optimization algorithm could be further improved if one additional recovery variable u_2 was used along with v and u. Since u is inactive in the regular spiking mode of the neuron, the model acts as a quadratic integrate-and-fire neuron with limited dynamical behaviours. Hence, with the introduction of u_2, the model would be able to exhibit rich dynamics in both modes and it might have more realistic F-I relations. However, for the purpose of this study which was the evaluation of the proposed technique, the resulting TC model needed to be comparable with previous optimized attempts, which have used only one recovery variable (Izhikevich 2007a).

Simulation of a thalamic nucleus

For further validation of the resulting TC model, we attempted to simulate a neural ensemble, whose neuron types and connectivity follow the general rules of a thalamic nucleus. Two versions of this ensemble were created; the one using the current TC model and the second using the previous approach in (Izhikevich 2007a) that was also used in the previous section. For clarity, we will refer to these ensembles as E_1 and E_2 respectively.

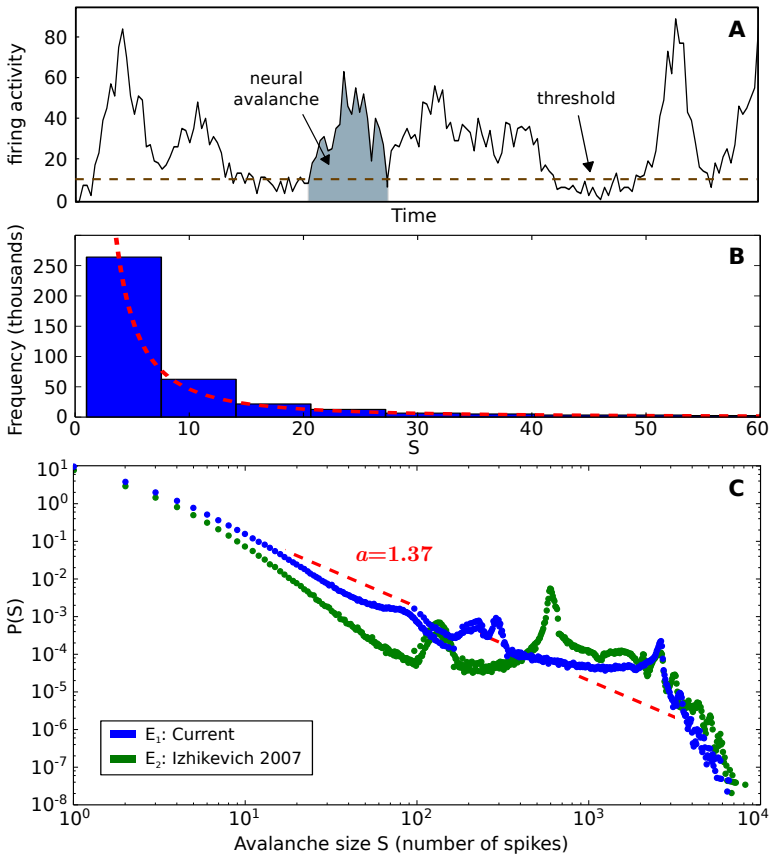

Figure 2.8: **A:** Method of avalanche size extraction. **B, C:** Histogram of 0.5M avalanches for the two simulated thalamic ensembles. The dashed line represents the estimated power-law distribution for E_1, with the best fit.

In both cases, the network comprises 800 TC relay neurons and 200 thalamic interneurons, keeping the balance that is usually found in experimental studies (Winer and Larue 1996; Sherman and Guillery 2006) and used in other computational models (Izhikevich and Edelman 2008). The synaptic input to the neurons was modelled using a typical conductance-based approach (Dayan and Abbott 2001) with default parameters for AMPA, NMDA and GABA neurotransmitters obtained from the same source. Each thalamic interneuron sends gabaergic connections to 25% of all other neurons in the group, while TC neurons have only excitatory afferents to 25% of the interneurons. The delays of all connections were randomized uniformly from 1 to 40 ms.

Furthermore, each neuron in the network was forced to spike with a rate taken from a Poisson distribution, and corresponds to 5 spikes/second, while TC neurons received an extra injected current I_{inj}, fixed at a single value. The distribution of weights, as well as the injected current I_{inj} were tuned in order to maintain a spontaneous firing rate of approximately 20 spikes/second (Wilson and Groves 1981).

Two different tuning scenarios were examined for more accurate comparison of the two TC models. First, the network connectivity and input current were kept fixed for both E_1 and E_2 and they were tuned to approximate the thalamic spontaneous firing rate. In a second experiment, connectivity remained again fixed but the injected current was tuned to make the two nuclei fire at exactly the same spontaneous frequency. To minimize the affected parameters in all cases, the inhibitory-to-excitatory weights of E_2 were normalized with respect to a ratio factor C_1/C_2, to eliminate the effect of different capacitance values to the synaptic current (see equation 2.1).

As the measure of comparison, the dynamical behaviour of E_1 and E_2 was assessed by means of the neural avalanche events in each ensemble. In biological neural systems, the size of neural avalanches over time has been found to follow a power law distribution ($P(x) \sim x^{-a}$), both in cortical slices (Beggs and Plenz 2003) and in vivo (Petermann et al. 2009), with an exponent a around 1.5 (Beggs and Plenz 2003). The degree of approximation of this distribution is sometimes assumed to indicate scale-free behaviour (Petermann et al. 2009; He 2014) of the neural system and of whether it is operating near a critical regime(Teixeira and Shanahan 2014).

The size of avalanches was measured by taking the area of neural firing activity, sampled in 1 ms bins, that exceeds the threshold of 10 spikes/ms for a number of continuously active bins (Figure 2.8.A). Figures 2.8.B and C illustrate the histograms of the avalanche sizes and the corresponding best-fit power law distribution.

In both simulated experiments, a Kolmogorov-Smirnoff (KS) test showed that, with p-values 0.26% and 0.007% respectively, the distributions of avalanche sizes in the two nuclei are different. By subtracting the final cutoff points, the result in the KS test changed to 0.42% and 0.16%, still rejecting the null hypothesis that the two samples come from the same distribution.

The next step was to run a test to see whether the two size distributions conform to a power law distribution. Due to the limited number of neurons in the system, these distributions loose accuracy towards the tail and start to bend downward, exhibiting an exponential cutoff that needs to be pruned before any fitting attempt (Figure 2.8.C).

Following the methodology in Clauset et al. 2009, the tests failed in both experiments and both models of TC neurons. However, this can be partially justified due to the rigorous nature of this test. In both simulated experiments, the KS distance between the histogram of the current model and the best-fit power law was found to be significantly smaller (in the order of 20% for the illustrated experiment) than the other approach. Finally, the distribution in Figure 2.8 could be also dramatically improved, perhaps in a degree above the requirements of the test, if the connectivity of the network was optimized by using, for instance, some form of synaptic

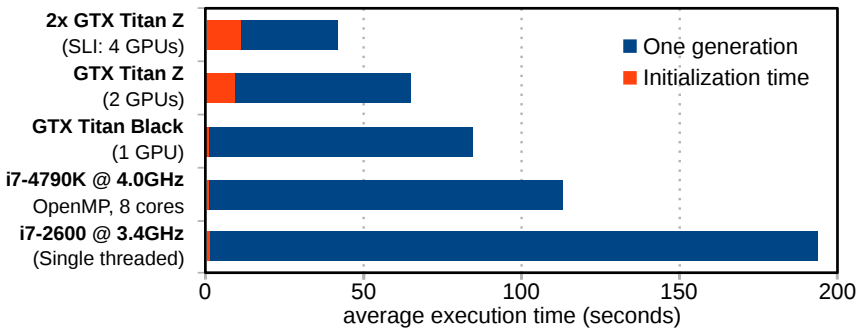

Figure 2.9: Average execution time of one generation of the CMA-ES for different hardware. As the standard deviation was always < 2 seconds, it is omitted from the graph.

plasticity (Teixeira and Shanahan 2014). Nonetheless, the results here suggest that networks using the optimized TC model in E_1 are closer to a critical state, a fact that increases the biological plausibility of the simulation.

Benchmarking

To assess the computational performance of the presented toolbox, we ran a number of simulations on different hardware platforms, optimizing the same neuron and recording the execution time of each generation. In order to calculate the fitness of each individual, the equations of 100 simulated neurons were numerically calculated for 2 seconds with 0.25 ms time step. The population of individuals was set to be 500, which corresponds to 50,000 neurons for each generation.

The average execution times are illustrated in Figure 2.9. In this figure, initialization time refers to all stages needed for the initialization of the optimization algorithm apart from the time of interaction with the online database NeuroElectro. All simulations were executed on 64bit machines with 32GB available memory and the same hard drive, while the evolutionary strategy was forced to continue for 40 generations.

The results reveal a significant speed up in GPU processing over CPU, even in the case of a high-performance state-of-the-art CPU processor with multi-threading support. This speedup ranges from 1.35 to 3.65 for the 8-threaded simulation based on the OpenMP API and from 2.31 to 6.25 for a single threaded simulation. Initialization times were negligible in all cases (< 12 seconds) with small increases in the case of multiple GPU simulations. These results indicate that there is no obvious bottleneck in our implementation and that execution time depends highly on the spiking neuron simulation platform used.

2.3.4 Concluding Remarks

The main contributions in this part of the thesis are as follows. First, the presentation of a fast optimization process that produces parameters and statistics for phenomenological neuron models which can be used for large-scale biological plausible simulations. Second, a python toolbox that implements the above process using a GPU-based high-performance spiking neural network simulator. The low requirements of this method along with the hardware acceleration allow the complete tuning process to be carried out in a manner of minutes and thus constitute the key feature of the toolbox. In addition, the initialization of this algorithm is automated, requiring a minimized user intervention. Any experimentally found neuron properties can be located in an online database and downloaded automatically.

The third and final contribution is a new model of the TC relay neuron, that is shown to fit better than a previous approach to experimental data, and to generate more realistic large-scale simulations. The detection of statistical differences in networks constructed with this new model and the previously optimized TC neuron is of high importance considering the already high accuracy of the latter.

One of the major aims of this work is to make the optimization procedure for this type of neuron models as automated and fast as possible. Nonetheless, the user of our toolbox still needs to detect a number of experimentally found F-I/V-I relations, to achieve high performance. This type of information is widely available in the literature of *in-vitro* cell recordings, either in the form of a curve or, implicitly, through other experiments. This issue can be overcome in the future, if more centralized databases for neurological data, such as NeuroElectro, arise.

We are currently extending the toolbox functionality in two ways. First, we introduce a method where the optimization includes the detection of the simplest possible model that is able to produce a good fit to the available data. In its current stage, this method starts to optimize a quadratic IF neuron as described in Section 2.3.2. If no individual can be found with a good fit, the process starts again incrementing the number of helping variables u_i as described in the last paragraph of the section 2.3.3.A. Hence, the process is likely to return a solution with a better fit, as well as the least number of variables needed.

The second extension concerns optimization at the network level. The parameter sets currently produced by the toolbox are accompanied by estimates of their variation, that can be used to produce more realistic neural ensembles. Hence, based on the foundation of Carlson et al. 2014 and the processing capabilities of NeMo, we are developing a method that can optimize the connectivity parameters between and within ensembles, as well as other important network features, based on knowledge on their behaviour in different simulation scenarios.

3 A neural model of the basal ganglia circuitry

The basal ganglia are a group of highly interconnected nuclei, believed to resolve information processing conflicts of the cerebral cortex. In this chapter, we describe the most complete neural model of the motor region of this brain structure to date, integrating available neurophysiological data from the literature. This model exhibits behaviour very similar to in vivo recordings of its biological counterpart, both in healthy and pathological conditions. In part, it was based on well-established models of various features of the BG nuclei, while a series of novel features was also introduced to complete the integration. In particular, the striatum model was partially adopted from Tomkins et al. 2013, the conductance delays between nuclei were taken from Humphries et al. 2006 and the parameters for short-term plasticity between the BG nuclei from Lindahl et al. 2013. This chapter provides justification and a full description of the mathematical models and the rest novel design choices that were made for this simulation, as well as the tuning process that followed.

3.1 The model

3.1.1 Anatomy

Canonical circuit The internal structure of the majority of the BG forms a single canonical circuit (Fig. 3.1), massively replicated in different scales. Macroscopically, it is part of a complex set of parallel loops that involve the thalamus, limbic regions and almost all major regions of the cortex including sensory, motor and associative areas (Alexander et al. 1986; Hoover and Strick 1993). However, at the level of the BG, these loops can be further broken down into parallel microscopic channels that involve the same canonical circuit and, with a small overlap, maintain the anatomical division and somatotopic organization found in the cortex (Alexander and Crutcher 1990; Humphries et al. 2006; Nambu 2011).

A widely accepted hypothesis is that these microscopic channels represent different competing "action requests" (Gurney et al. 2015) that originate from the cortex. These requests are processed by the BG circuit, which, under some conditions (Fountas and Shanahan 2014), is able to select the most salient (or urgent) potential action (Mink 1996; Redgrave et al. 1999; Humphries et al. 2006).

Along these lines, the model presented here comprises six neural populations that correspond to the four major nuclei of the biological BG and form the canonical circuit described above.

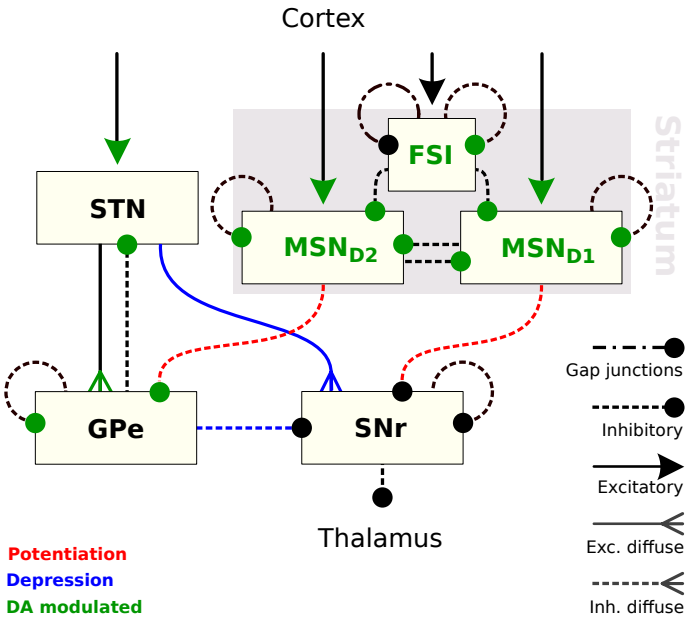

Figure 3.1: **Architecture of the system.** The BG circuit as realized in the present study. Dopamine influences both the internal behaviour of MSNs and FSIs as well as the impact of various synaptic conductances.

These include the striatum and the subthalamic nucleus (STN), the two main input structures in the BG, the external part of the globus pallidus (GPe), as well as the substantia nigra pars reticulata (SNr), one of the two output structures of the BG. Furthermore, the effect of the pars compacta part of the substantia nigra (SNc) is realized through the concentration of the neurotransmitter dopamine (DA) in the different parts of the network (green colour in Fig. 3.1).

The internal structure of the striatum has been modelled using three different groups that correspond to its three major neural populations. The first two groups constitute the two categories of medium spiny-projection neurons (MSNs), divided based on the dominant type of their dopamine receptors, which belong either to the D1- or D2-like families. Depending on their category, these neurons are either enhanced (MSN$_{D1}$) or depressed (MSN$_{D2}$) by the presence of dopamine. They have been predicted to comprise the 99% of the striatal volume (Humphries et al. 2010), a number that was also maintained here.

Finally, the remaining 1% of the striatum is occupied by fast-spiking gabaergic interneurons (FSIs) that are affected by both types of dopamine receptors and are highly interconnected with both electrical and GABAergic synapses. Despite their small concentration, FSIs have a great influence on the rest of the striatum, and it has been shown that inhibition from a single FSI

cell is able to block action potentials in large numbers of MSNs (Koós and Tepper 1999).

To estimate the number of neurons within each nucleus, we kept the same ratios of neurons found in rat BG (Oorschot 1996). The final numbers can be found in Table 3.1 and result in a total of 9586 neurons that form the BG network. The probability for a connection between two neurons P_{X-Y} depends on the pre- (X) and post-synaptic (Y) nuclei and can be found in the same table. The values of these probabilities were inferred by the same method that was used for the random model of striatum in Tomkins et al. 2013. For connections that involve only striatal neurons, the required data was obtained by the spatially embedded model in Humphries et al. 2010, while the model in Lindahl et al. 2013 was used for any other connection.

Lateral inhibition Within each nucleus in our model, there are three largely isolated subgroups that correspond to three microscopic channels of the BG circuit. As mentioned before, the BG preserves the anatomical organization of their cortical inputs, thus connections between nuclei are mainly topographic and influence only the same channel in the target nucleus. As an exception, the STN glutamatergic efferents cause diffuse excitation (Mink 1996), equally distributed across adjacent channels. In addition, evidence for local axon collaterals in GPe (Sadek et al. 2007) and SNr (Mailly et al. 2003) suggests that lateral inhibition in these structures also spans to neighbour functional subdivisions, and thus, it is also considered diffuse.

The striatum, on the other hand, has more complicated intrinsic connectivity which arises from both its enormous size and the extensively overlapping network of axon collaterals (Wilson and Groves 1980; Steiner and Tseng 2010). A large debate has been provoked regarding its connectivity structure and computational function. The "domain" theory (Wickens 1993) suggests that the striatum is divided into groups, or domains, of highly inter-connected neurons that form local winner-takes-all elements, while more recent studies show that striatal lateral connectivity is weak and sparse, and indicate that the striatal computational element should be spread across the MSN network (Koos et al. 2004; Humphries et al. 2010).

Here we use two different probability values P^{int} and P^{ext} that represent lateral connections within and between striatal channels respectively, thus allowing both views of localized and sparse connectivity to be tested. To calculate the values of these probabilities for each type of striatal local connection we generated a spatial model of two adjacent striatal microscopic channels and calculated the internal and external mean connection probabilities. Assuming that all neurons of a single channel are limited within a spherical boundary, the radius of this sphere can be found from $R = \left(\frac{3V}{4\pi}\right)^{1/3}$, where $V = \frac{N_{ch}}{84900} mm^3$ is the simulated striatal volume (since in $1mm^3$ there are $84,900$ neurons (Humphries et al. 2010)) and $N_{ch} = (N_{MSN} + N_{FSI})/3$ is the number of neurons within this sphere. For the values of N_{MSN} and N_{FSI} that are given in

Parameter	Source	Parameter	Source
$N_{MSN} = 2790000 \times 0.99/S$	O&H	$P_{Ctx-STN} = 0.03$	H&T
$N_{FSI} = 2790000 \times 0.1/S$	O&H	$P_{Ctx-MSN} = 0.084$	H&T
$N_{GPe} = 46000/S$	Oorschot 1996	$P_{Ctx-FSI} = 0.084$	**
$N_{STN} = 13600/S$	Oorschot 1996	$P_{SD1-SNr} = 0.033$	***
$N_{SNr} = 26300/S$	Oorschot 1996	$P_{SD2-GPe} = 0.033$	***
$N_{T_i} = 1000$	Assumed	$P_{STN-SNr} = 0.3$	***
$R_{GPe_A} = 0.0405$	B&D	$P_{STN-GPe} = 0.3$	***
$R_{GPe_B} = 0.85$	DeLong 1972	$P_{GPe-STN} = 0.1$	***
$R_{GPe_C} = 0.1095$	B&D	$P_{GPe-SNr} = 0.1066$	***
$R_{RB} = 0.6$	Bevan et al. 2000	$P_{GPe-GPe} = 0.1$	***
$R_{LLRS} = 0.25$	Bevan et al. 2000	$P_{SNr-SNr} = 0.1$	Assumed
$R_{NR} = 0.15$	Bevan et al. 2000	$P^{int}_{MSN-MSN} = 0.0718$	****
$S = 300$	*	$P^{ext}_{MSN-MSN} = 0.0082$	****
$P^{int}_{FSI-MSN} = 0.2925$	****	$P^{int}_{FSI-FSI} = 0.5864$	****
$P^{ext}_{FSI-MSN} = 0.0314$	****	$P^{ext}_{FSI-FSI} = 0.0092$	****

O&H Oorschot 1996; Humphries et al. 2009

B&D Bugaysen et al. 2010; DeLong 1972

H&T Humphries et al. 2010; Tomkins et al. 2013

***** Assumed to be adequate for 3 channels

****** Same as $P_{Ctx-MSN}$ Humphries et al. 2010

******* Calculated keeping the ratios from Lindahl et al. 2013

******** Calculated using probability distributions from Humphries et al. 2010

Table 3.1: **Network parameters.** N_x represents the number of neurons in each nucleus x. S is a scaling factor that determines the number of microscopic channels within the complete BG. R_x represents the ratio of each type of neuron x within the corresponding nucleus, while P_{x-y} is probability of a neuron from the nucleus x to be connected to one in y.

Table 3.1, $R = 205.8\mu m^3$.

The estimated probabilities, which are also shown in the same table, where found after the calculation of the average number of contacts within and between these two adjacent areas, using the distribution of expected number of intersections with respect to the distance between the somas of two neurons, in Humphries et al. 2010.

In addition, the striatum was shown to be asymmetric with respect to inhibition that MSN_{D1} and MSN_{D2} neurons receive, both in conductance strength and number of connections. Local

MSN collaterals have fewer and weaker connections that arrive to striatopallidal neurons than the opposite (Taverna et al. 2008; Planert et al. 2010), while FSIs also target mostly MSN_{D1} (Gittis et al. 2010) neurons. This strong inhibition of the direct pathway compensates for the over-excitement of these cells via $D1$ receptor activation, and thus brings more balance to the intrinsic activity of the striatum.

To account for the effect of the above asymmetries, the probabilities in Table 3.1 change to $P_{D2-D1} = P_{MSN-MSN} * W$, $P_{D1-D2} = P_{MSN-MSN} * (2 - W)$, $P_{FSI-D1} = P_{FSI-MSN} * W$ and $P_{FSI-D2} = P_{FSI-MSN} * (2 - W)$, where W defines the trade-off of inhibition between the direct and indirect striatal neurons. The default value used is $W = 1.5$ which is consistent with previous studies (Taverna et al. 2008; Gittis et al. 2010; Bahuguna et al. 2015). Finally, changes in maximum conductances G of collateral MSN connections were inferred from Taverna et al. 2008. For recurrent MSN_{D1} connections $G = 1.2 * G_{SD-SD}$ and for MSN_{D2} to MSN_{D1} connections $G = 0.4 * G_{SD-SD}$.

3.1.2 Mathematical models

Neuron dynamics The electrical activity of individual cells of the BG was simulated using the single-compartmental "simple model" that was proposed by Izhikevich 2003; Izhikevich 2007a. In this phenomenological model, the membrane potential v of the neuron is governed by the equation

$$C\frac{dv}{dt} = k(v - v_r)(v - v_t) - u + I + C\mathcal{N}(0, \sigma^2) \tag{3.1}$$

where I is the dendritic and synaptic current, C the membrane capacitance of the cell body, v_r the resting membrane potential, v_t the instantaneous threshold potential, k an abstract parameter and u is an abstract recovery variable with

$$\frac{du}{dt} = a\big(b(v - v_r) - u\big) \tag{3.2}$$

In this equation, a and b are two additional abstract parameters of the model. Finally, the neuron is said to fire a spike when its membrane potential exceeds the threshold value v_{peak}. In this case, the variables of the model reset to general cation currents

$$\begin{aligned} v &\to c \\ u &\to u + d \end{aligned} \tag{3.3}$$

where c and d are further abstract parameters.

If tuned properly, this model is able to display the known types of dynamical behaviour of all cortical and sub-cortical neural cells, and to quantitatively reproduce their sub-threshold, spiking, and bursting activity in response to pulses of DC current (Izhikevich 2007a). In addition, the recovery variable in (3.2) could be tuned to represent a specific mechanism of an ion channel such as the calcium-activated potassium channels in STN neurons (Hallworth et al. 2003) as will be shown in section STN model.

The equations 3.1 and 3.2 can be reduced to a simpler form, originally presented in Izhikevich 2003 and widely used, which contains only two independent parameters. However, the choice of the current extended form is considered more appropriate for this study, since the majority of the parameters and the variables here acquire biophysical meaning, which simplifies the complexity of calculations and tuning. For example, electric potentials, such as v, are represented in $mVolts$ and the input current I in $pAmperes$.

Heterogeneity of the neurons in the network is achieved by the stochastic perturbation of the capacitance C of each neuron by a small random factor, sampled from a Gaussian distribution with mean C_μ and standard deviation $0.1 \times C_\mu$. In addition, every neuron includes a general Gaussian noise factor $\mathcal{N}(0, \sigma^2)$, added to its membrane potential, with a constant standard deviation (σ in equation 3.1), which depends on the type of the neuron. This term represents the effect of external afferents that are not part of the this model and are considered stable during our simulations.

Synaptic dynamics Neurons in the network are connected with up to three different categories of synapses, depending on their position and type. A synapse can be either simple chemical, chemical plastic or electrical. The simple case of a static chemical synapse is implemented with a standard conductance-based model (Dayan and Abbott 2001) with different parameter values for different neurotransmitters and connectivity. At any given point of time t, the current of each synapse can be described with

$$I_{ij}^{s}(t) = \begin{cases} G_{ij} e^{-(t-(t_i+\lambda))/\tau_s}(E_s - v_j) & \text{if } t \geq (t_i + \lambda) \\ 0 & \text{if } t < (t_i + \lambda) \end{cases} \tag{3.4}$$

where t_i is the time of last firing of neuron i, λ is the delay of the synapse, G_{ij} is the maximum conductance of the synapse, i.e. the weight of this connection, s is the type of the synaptic receptor, E_s is the synaptic reversal potential and τ_s the synaptic decay time constant. At the arrival time $(t_i + \lambda)$, a new spike propagates to the post-synaptic neuron j, the synaptic current jumps to the value g_{ij} and finally decays exponentially with rate τ.

The effect of different pairings of neurotransmitter and postsynaptic receptor can be expressed

by means of combinations of (E_s, τ_s), with the latter representing the duration of a neurotransmitter re-uptake and dispersal. The dominant excitatory neurotransmitter in this simulation is glutamate, which corresponds to *AMPA* and *NMDA* postsynaptic receptors, while the corresponding inhibitory neurotransmitter, γ-Aminobutyric acid, is thought to bind to $GABA_A$ receptors. Following the methodology in Humphries et al. 2006, the inhibitory receptors $GABA_B$ are not explicitly simulated, since they mainly evoke intracellular signal transduction in the post-synaptic neuron instead of generating current (Bormann 1988).

Furthermore, certain types of synapses in the network are thought to be plastic (see Fig. 3.1), in order to simulate the effect of short-term facilitation and depression found in real BG connectivity (Connelly et al. 2010; Sims et al. 2008; Atherton et al. 2013), but not simulated until recently (Lindahl et al. 2013). In particular, striatal gabaergic efferents to GPe and SNr have been shown to be facilitated in periods of MSN bursts (Sims et al. 2008; Connelly et al. 2010; Kim and Kita 2013), while GPe-SNr synapses have the opposite effect (Connelly et al. 2010). The remaining SNr afferents that originate from STN have been predicted in Lindahl et al. 2013 to also be depressing, a mechanism that was later found to be regulated by $GABA_B$ receptors (Dvorzhak et al. 2013). Finally, short-term effects of plasticity have been reported to exist between more structures in the BG but in some cases without a clear facilitating or depressing pattern (e.g. GP-GP recurrent synapses (Sims et al. 2008)) and in other cases very slowly activated (e.g. GPe-STN synapses (Atherton et al. 2013)). Hence, these chemical synapses have been treated as fixed.

In the case of a plastic synapse, two extra variables, u_s^+ and x_s^-, are used to calculate the level of facilitation and depression respectively (Markram et al. 1998). Their dynamics are governed by

$$\tau_d \frac{dx_s^-}{dt} = 1 - x_s^- \tag{3.5}$$

$$\tau_f \frac{du_s^+}{dt} = U - u_s^+ \tag{3.6}$$

where τ_f and τ_d define the exponential decay time constant, and the abstract parameter $U \in [0, 1]$ controls the amount of synaptic facilitation. At the time $t = t_i + \lambda$ of a postsynaptic event, the two plasticity variables update to

$$x_s^- \leftarrow x_s^- * (1 - u_s^+) \tag{3.7}$$

$$u_s^+ \leftarrow u_s^+ + U * (1 - u_s^+) \tag{3.8}$$

with $0 < U < 1$, and the final synaptic current that arrives at the postsynaptic neuron is given

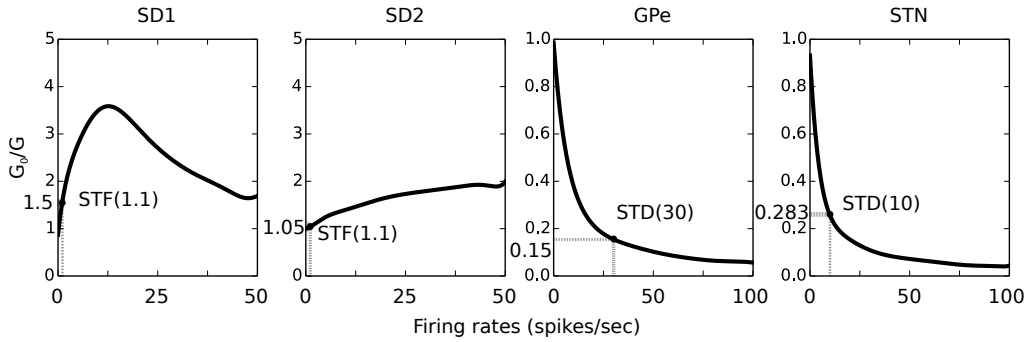

Figure 3.2: **Effect of short-term plasticity in synaptic conductances.** Ratio between steady-state conductance G and the initial value G_0 for different pre-synaptic spike frequencies, and for all plastic connections of the BG circuit.

as

$$I_{ij}^{s}(t_i + \lambda) = u_s^{+} x_s^{-} g_{ij}(E_s - v_j) \tag{3.9}$$

The values for the parameters U, τ_{rec} and τ_{fac} can be found in Lindahl et al. 2013. Although the model of plasticity used in this study was more complex than equations (3.5-3.9) , our synaptic models resulted to almost identical relations between synaptic IPSP amplitudes and spike frequencies as in Lindahl et al. 2013 (See 3.2).

Finally, when two neurons i and j of the network have a direct electrical connection, or gap junction, they both receive an extra current

$$I_{ij}^{gap} = g_{gap}(v_{gap} - v_{i/j}) \tag{3.10}$$

where g_{gap} is the conductance (weight) of the gap junction and v_{gap} represents the potential of an extra mutual compartment at the point of the interaction (Tomkins et al. 2013). This potential links the two neurons via the equation

$$\tau_{gap} \frac{dv_{gap}}{dt} = v_i + v_j - 2v_{gap} \tag{3.11}$$

and provides a force that decreases the difference between the neuron voltages with rate τ_{gap}.

All things considered, the total input I that a neuron receives via equation (3.1) has the general form

$$I = I^{ampa} + B(v)I^{nmda} + I^{gaba} + I^{gap} + I_{spon} \tag{3.12}$$

where $I^x = \sum_i I_{ij}^x$ is the sum of all synapses of type x, $B(v) = \frac{1}{1.0+0.28*e^{-0.062v}}$ is the voltage-

dependent magnesium plug in the NMDA receptors (Tomkins et al. 2013) and I_{spon} is an extra spontaneous current that is used to fit each neuron model to both *in vitro* and *in vivo* neurophysiological recordings.

Neuromodulation Neurons in the BG receive dopamine from the SNc which can affect the impact of the synaptic current of certain neurons as well as the internal dynamical behaviour of others. The neurons and synapses that are affected by dopamine are depicted in Fig. 3.1. Although the level of dopamine is considered to have a single fixed value throughout the system, we have used two variables $d_1 = d_2$ that correspond to the $D1$- and $D2$-like receptor families respectively, and influence the system differently.

To account for the dopaminergic effects, the synaptic input (3.12) as well as the neuron equations (3.1-3.2) change according to the Table 3.2.

$\mathbf{MSN}_{D1}$	$v_r \leftarrow v_r(1+\beta_1 d_1)$	$\beta_1 = 0.0289$
	$d \leftarrow d(1-\beta_2 d_1)$	$\beta_2 = 0.331$
	$I^{nmda}(1+\beta_3 d_1) + I^{ampa} + I^{gaba}$	$\beta_3 = 0.5$
$\mathbf{MSN}_{D2}$	$k \leftarrow k(1-\beta_1 d_2)$	$\beta_1 = 0.032$
	$I^{ampa}(1-\beta_2 d_2) + I^{nmda} + I^{gaba}$	$\beta_2 = 0.3$
FSI	$v_r \leftarrow v_r(1+\beta_1 d_1)$	$\beta_1 = 0.1$
	$I^{ampa} + I^{gaba}(1-\beta_2 d_2)$	$\beta_2 = 0.625$
STN	$(I^{ampa} + I^{nmda})(1-\beta_1 d_2) + I^{gaba}(1-\beta_2 d_2)$	$\beta_{1,2} = 0.5$
GPe	$(I^{ampa} + I^{nmda})(1-\beta_1 d_2) + I^{gaba}(1-\beta_2 d_2)$	$\beta_{1,2} = 0.5$

Equations and parameters are taken from Humphries et al. 2006 and Tomkins et al. 2013.

Table 3.2: **Neuron equations and synaptic input with dopamine.**

Cortical input The BG receive their main input from pyramidal glutamatergic projections from layer V of different areas of the cortex as well as the Thalamus (Steiner and Tseng 2010). Since the circuitry modelled here captures connectivity principles existing in most of the BG parallel layers (Alexander et al. 1986), the main focus of the cortical simulation lies on the oscillatory nature of these inputs rather than region-dependent characteristics. Hence, thalamic input is omitted and cortical afferents are represented by abstract isolated neural ensembles T_i,

each realized through 1000 inhomogeneous poison event generators with rate parameter

$$\lambda_i(t) = A_i cos(2\pi f_i t + \phi_i) + F_i^{spon} \tag{3.13}$$

where f_i is the frequency, A_i is the amplitude, $\phi_i \in [0, 2\pi)$ the phase and F_i^{spon} the tonic spontaneous firing rate of the oscillatory ensemble T_i. Each of these ensembles is considered to project afferent axons in a single channel (with the same index i) of the BG circuitry, without affecting the rest of the cortical activity.

Base firing rate of a tonically-active cortical ensemble is thought to have a mean value of 3 spikes/sec, equal to the tonic non-oscillating spontaneous activity $\bar{F}_i^{spon}$, while an ensemble with phasic activation oscillates with amplitude $A_i = 7$ spikes/sec and thus peaks at $F_i^{spon} + A_i = 10$ spikes/sec.

This behaviour is consistent with recordings in corticostriatal pyramidal cells of motor (Turner and DeLong 2000; Bauswein et al. 1989) and sensory (Belforte et al. 2010; Reed et al. 2010) cortices, two of the regions that are greatly involved in sending excitatory inputs to the BG.

3.1.3 Neural parameter estimation

Phenomenological spiking neuron models offer a computationally cheap and powerful method for neural simulations, whose accuracy, however, depends on the quality of fine-tuning of the model's parameters. This process can be very difficult for models that contain a large number of parameters that need to be adjusted or for real neurons with a large repertoire of behaviours that need to be replicated, and for this reason various methods have been proposed (for a review see Geit et al. 2008). To fine-tune the neurons in GPe, STN and SNr, we employed a hybrid method, presented in Fountas and Shanahan 2015 and in Chapter 2, that combines a global and a local optimization algorithm to create models that approximate the neural behaviour recorded in empirical studies. In particular, as an objective function, we took into account the major electrophysiological properties of these neurons (e.g. the action potential amplitude and width, the resting and threshold potentials, the rheobase current, etc), as well as their steady-state frequency-current (F-I) and voltage-current (V-I) relations. The resulting models closely reproduce the rich dynamical behaviour of the neurons located in the BG nuclei, as shown in detail below.

GPe model Although GPe neurons in primates have been shown to exhibit two spiking patterns (HFP and LFB neurons (DeLong 1972)), it is not yet clear whether the same classification holds for their electrophysiological properties, due to the lack of intracellular recordings in pri-

mate GPe (Bugaysen et al. 2010). This problem can be bypassed by studying the rodent globus pallidus (GP), which is believed to be homologous to the primate and human GPe (Gerfen and Wilson 1996) with retained firing patterns (Benhamou et al. 2012). In Bugaysen et al. 2010, GP neurons were examined intracellularly, in order to draw conclusions about the analogous structure in primates, and a different three-fold classification of the GPe neurons was proposed (Cooper and Stanford 2000; Bugaysen et al. 2010). In this work, we followed the same approach and we created three different models of GPe neurons that correspond to the three different types of GP neurons in Bugaysen et al. 2010.

	GPe			
Parameter	Type A	Type B	Type C	source
v_r (mV)	-50.7	-53	-54	Taken from Bugaysen et al. 2010
v_t (mV)	-42	-44	-43	Taken from Bugaysen et al. 2010
v_{peak} (mV)	38	25.0	34.5	Taken from Bugaysen et al. 2010
C_{fig} (pF)	55	68	57	Tuned manually
C_{sim} (pF)	70 ± 16.5	68 ± 16.4	65 ± 16	Optimized
a	0.29	0.0045	0.42	-"-
b	4.26	3.895	7	-"-
c (mV)	-57.4	-58.36	-52	-"-
d	110	0.353	166	-"-
k	0.06	0.943	0.099	-"-
I_{vitro} (pA)	107	52	187.5	-"-
I_{vivo} (pA)	167	64	237.5	Tuned manually
σ (mV)	3	3	3	-"-

Table 3.3: **GPe and SNr neuron parameters.**

Table 3.3 includes all intrinsic parameters and Fig. 3.3 illustrates the basic properties of the three resulting neuron models that show distinct electrophysiological characteristics and match to the literature. From a behavioural perspective, all GPe neurons have similar rheobase currents but only type B neurons are able to evoke rebound firing (Fig. 3.3.E). Furthermore, the firing rate of type B neurons increases almost linearly with increasing input rate, while types A and C peak at around 10 and 14 spikes/sec respectively.

Interestingly, the behaviour of type B neurons closely resembles the HFP cells in GPe while the other two types behave very similarly to LFB cells. Taking this into account, in this study we consider GP neurons of type B as HFP neurons found in primates and neurons of types A and C as LFB. Hence, to determine the percentage of each type of neurons in our modelled GPe, we kept the ratio of HFP:LFB found in DeLong 1972 ($N_{HFP} = 85\%$ and $N_{LFB} = 15\%$). In addition, to

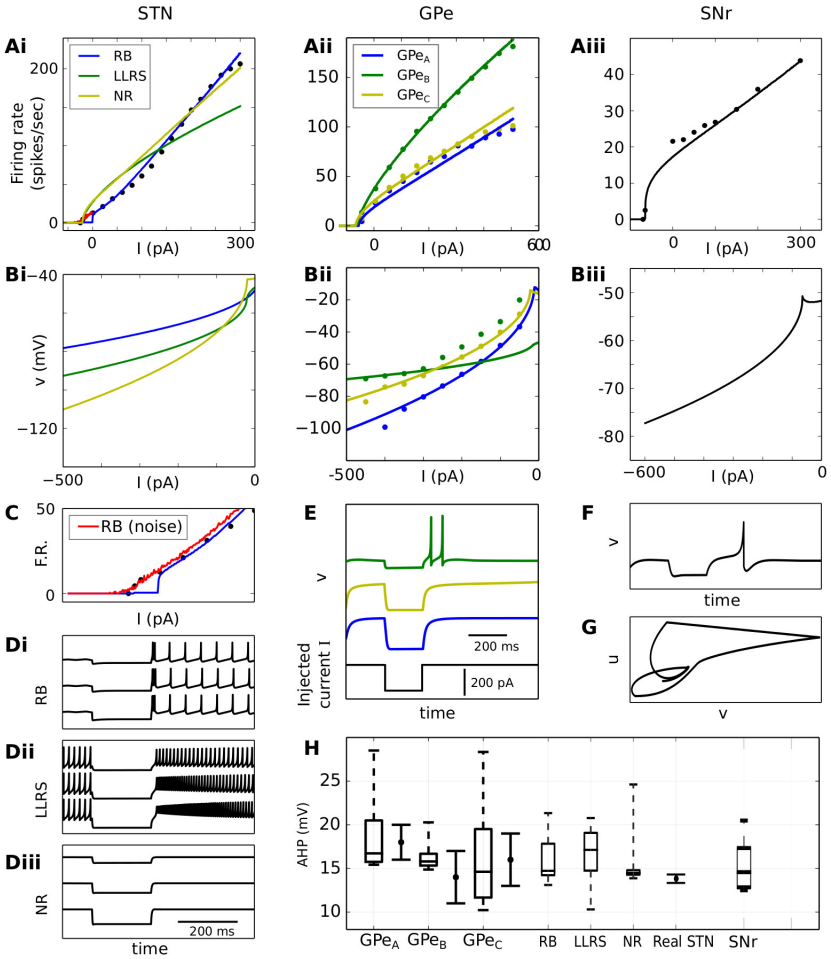

Figure 3.3: **Properties of the BG tuned neurons. A:** Steady-state F-I curves of the tuned models (solid lines). **Bi-iii:** V-I curves of the same neurons. In both cases, the coloured dots represent real *in vitro* recordings. STN: Real F-I data obtained from Hallworth et al. 2003 and V-I data provided by Daisuke Kase and Keiji Imoto via email correspondence. GPe: Real data of the three neuron types retrieved from rat slices in Bugaysen et al. 2010. SNr: Real recordings were extracted from Richards et al. 1997 and are compatible with later observed slope ($12.8 + -1.13$ spikes/sec per 100 pA) in Rohrbacher et al. 2000, while the neuron's rheobase current was taken from Atherton and Bevan 2005 and it is around -65 pA. **C:** Better fit of RB neurons to the real F-I curve is achieved by applying constant Gaussian noise with $\sigma = 1.5$ mV. **D:** Responses of STN neurons to hyperpolarizing current steps of -100, -200 and -400 pA. **E:** Responses of GPe neurons to hyperpolarizing current reveals rebound behaviour in GPe_B cells. **F:** Neuron response for hyperpolarizing current -0.6 nA matches recordings in Nakanishi et al. 1997. **G:** Phase portait of the SNr neuron in (F). **H:** Box plot of the AHP amplitudes for varying capacitance C, along with the real mean and std for each neuron type retrieved from the same study.

further break down LFB neurons into types A and C, we used an approximation based on the number of neurons examined in Bugaysen et al. 2010, where $n = 14/76$ and $n = 38/76$ for type A and C neurons respectively. The final ratios of GPe neurons are given in Table 3.1.

SNr model GABAergic SNr neurons show relatively simple, agile behaviour, that can be captured by a single set of parameters. They are able to spontaneously fire high-frequency spikes that quickly turn into bursts or silence via either excitation or inhibition respectively, by the three basic BG pathways (For review see Zhou and Lee 2011). This behaviour is facilitated by their ability to emit rebound spikes (Nakanishi et al. 1997) whose intensity changes with respect to the level of hyperpolarization. However, these cells are not able to directly influence the internal dynamics of the BG since they project only to the thalamus and dopaminergic neurons.

The majority of the electro-physiological data used for tuning the SNr neurons here were extracted from a study in rat's SNr (Richards et al. 1997) which served as the basis of our model. Thus, data from other experimental studies were selected only if consistent with the former. The parameters of the resulting model are shown in Table 3.4 and its final behaviour is illustrated in Fig. 3.3.

	SNr	
Parameter		source
v_r (mV)	-64.58	The value from Tateno and Robinson 2011 ±5
v_t (mV)	-51.8	Taken from Richards et al. 1997
v_{peak} (mV)	9.8	Calculated from Richards et al. 1997
C_{fig} (pF)	172.1	Tuned manually
C_{sim} (pF)	200 ± 44.5	Optimized
a	0.113	-"-
b	11.057	-"-
c (mV)	-62.7	-"-
d	138.4	-"-
k	0.7836	-"-
I_{vitro} (pA)	150	-"-
I_{vivo} (pA)	235	Tuned manually
σ (mV)	5	-"-

Table 3.4: **GPe and SNr neuron parameters.**

STN model Neurons in STN can be categorized according to their response after long hyperpolarization, since they exhibit three distinctively different behaviours (Bevan et al. 2000; Bevan, Magill, Hallworth, et al. 2002; Hallworth et al. 2003). The majority type of neurons elicits short rebound bursts (RB), as a response to pallidal $GABA_A$ inhibition (Bevan et al. 2000), while a quarter of the STN neurons respond with long-lasting rebound spikes (LLRS) at

lower firing rates (Bevan, Magill, Hallworth, et al. 2002). Finally, a small amount of neurons do not produce any rebound effect and thus can be called no-rebound (NR) neurons.

When depolarized above the rheobase level, STN neurons exhibit a more homogeneous behaviour, with a sigmoid F-I relation (Bevan and Wilson 1999; Hallworth et al. 2003) and they are able to fire at high firing rates of more than 100 spikes/sec (Hallworth et al. 2003). Their distinct patterns of rebound response, as well as the sigmoid shape of their F-I relation, are mainly regulated by calcium via voltage-gated calcium channels (Ca^{2+}) that activate in low thresholds (Bevan and Wilson 1999; Bevan et al. 2000; Bevan, Magill, Hallworth, et al. 2002), as well as a type of Ca^{2+}-activated K^+ ion channels (SK K_{Ca} channels) (Hallworth et al. 2003).

Our approach here was to model the three different STN types with different sets of equations and to introduce one additional recovery variable (u_2) to Izhikevich equations, as suggested in Izhikevich 2007a and Fountas and Shanahan 2015, to account for the effects of the aforementioned ionic mechanisms, without losing the basic repertoire of dynamical behaviours that are supported with the basic recovery variable $u = u_1$.

With the addition of u_2, equations (3.1- 3.3) change to

$$C\frac{dv}{dt} = k(v - v_r)(v - v_t) - u_1 - w_2 \cdot u_2 + I + C\mathcal{N}(0, \sigma^2) \tag{3.14}$$

$$\frac{du_1}{dt} = a_1\big(b_1(v - v_r) - u_1\big) \tag{3.15}$$

$$\frac{du_2}{dt} = a_2\big(Gb_2(v - v_{r2}) - u_2\big) \tag{3.16}$$

For NR neurons G is set to be equal to 1, while for RB and LLRS neurons $G = H(v_{r2} - v)$ is the heaviside step function. This makes v_{r2} to act as a threshold below which, the recovery variable u_2 activates, causing rebound responses.

Furthermore, when $v \geq v_{peak} + Uu_2$, the model variables reset to

$$v = c - Uu_2 \tag{3.17}$$

$$u_1 = u_1 + d_1 \tag{3.18}$$

$$u_2 = u_2 + d_2 \tag{3.19}$$

revealing two more mechanisms of the new recovery variable.

Besides hyperpolarization, calcium-related ion channels also activate after the rising phase of APs, influencing their shape, as well as the F-I relation of the neuron, therefore $d_2 \neq 0$. One of their effects, particularly visible during rebound bursts (Hallworth et al. 2003), is to decrease

the size of the APs. In the equations above, this effect is controlled by the term U. Since $d_2 \neq 0$, the value of u_2 can increase dramatically at high firing rates, causing the AP height to converge to a zero value. Hence, to avoid this phenomenon, we set

$$U = \frac{1}{w_1|u_2| + \frac{1}{w_1}} \tag{3.20}$$

which minimizes the impact of u_2 to the AP size when $|u_2| >> 0$.

Parameter	RB	LLRS	NR	source
$v_r(mV)$	-56.2	-56.2	-58.5	Loucif et al. 2008
$v_t(mV)$	-41.4	-50	-43.75	Beurrier et al. 1999
$v_{peak}(mV)$	15.4	15.4	15.4	Beurrier et al. 1999
$C_{sim}(pF)$	23 ± 6.4	40 ± 8.8	30 ± 8.4	Optimized
$C_{fig}(pF)$	23	40	23	-"-
a_1	0.021	0.05	0.44	-"-
b_1	4	0.2	-1.35	-"-
$c(mV)$	-47.7	-60	-52.34	-"-
d_1	17.1	1	17.65	-"-
a_2	0.123	0.001	0.32	-"-
b_2	0.015	0.3	3.13	-"-
d_2	-68.4	10	92	-"-
v_{r2} (mV)	-60	-60	-43.2	-"-
k	0.439	0.3	0.105	-"-
w_1	0.1	0.01	0.001	-"-
w_2	0	0	1	-"-
I_{vitro} (pA)	56.1	25	-1	-"-
I_{vivo} (pA)	56.1	8	-18	Tuned manually
σ (mV)	0.5	0.5	0.5	-"-

Table 3.5: **STN neuron parameters.**

Like in the case of GPe neurons, to determine the ratios of each type of neurons in our modelled STN, we used a rough approximation based on the number of neurons examined in Bevan et al. 2000. In this study, 17 out of 20 neurons were found to elicit rebound bursts, 5 of which had a long duration and thus can be considered as LLRS neurons. The final ratios of STN neurons are given in Table 3.1.

The parameters of the final optimized models are shown in Table 3.5 and their properties are illustrated in Fig. 3.3, where the strengths and weaknesses of each model are clear. While all

neurons reproduce the rebound activity of their corresponding biological counterparts, only RB neurons were successfully tuned to follow the sigmoid pattern of the STN F-I relations. However, this was adequate to prevail the behaviour of the STN nucleus, since these neurons constitute its vast majority.

All things considered, neuron optimization was conducted successfully for the purposes of this study, resulting to models with realistic dynamical behaviour and electrophysiological properties. However, for a more accurate result, that focuses on the complex dynamics of individual neurons in STN, further work is required. This would involve optimization based on broader criteria, such as the distinction between transient and steady-state F-I and V-I relations, which was however impossible here, due to the lack of consistent electrophysiological data.

3.1.4 Connectivity estimation

The transmission delays of impulses across the synapses of our system were taken from Humphries et al. 2006, and their values are shown in Table 3.6. In this section, we present the methodology we used, in the form of an algorithm, to estimate the maximum synaptic conductances G_i of the network, as well as two neural parameters (the external spontaneous current $I_{spon} = I_{vivo}$ and noise σ) based on information about the BG connectivity and firing rate taken from the literature.

The initial value of the noise factor σ needed to be increased significantly for neurons in the MSN, FSI and STN, in order to simulate the effect of the different inputs to the BG from external structures that are not modelled here (e.g. other areas of the cortex). Also, a similar increase was necessary for GPe and SNr neurons, to account for inputs from other areas of STN which might correspond to different tonically-active microscopic channels. Finally, the spontaneous current I_{vivo} was also altered for each BG nucleus, in order to approximate their basal firing rates, when all synaptic inputs are blocked.

This process consisted of the following steps, that are specialized for each afferent structure and aim to approximate results of empirical experiments.

NMDA:AMPA ratios Initially, the ratio of the two neurotransmitters used to model the glutamatergic synapses of our model needed to be determined for all excitatory synapses shown in Fig. 3.1. As discussed in Humphries et al. 2010 and Tomkins et al. 2013, it has been shown that FSI neurons receive only AMPA excitatory input from the cortex. Götz et al. Götz et al. 1997 investigated the effect of AMPA and NMDA receptors in the rest of the glutamate-based synapses of the BG and found that they both play an important role in the excitation of the BG

Connection	λ (ms)	G (nS)	G_0 (nS)	E (mV)	τ (ms)	Neurotransmitter
Ctx $\rightarrow$ MSN	10	0.6	-	0 *	6 M&T	ampa
		$\times$0.5 M	-	0 *	160 M&T	nmda
Ctx $\rightarrow$ FSI	10	0.55	-	0 M&T	6 M&T	ampa
Ctx $\rightarrow$ STN	2.5	0.388	-	0 *	2 *	ampa
		$\times$0.6 G	-	0 *	100 *	nmda
STN $\rightarrow$ SNr	1.5	14 **	49.5	0 *	2 *	ampa
		$\times$0.42 G	20.8	0 *	100 *	nmda
STN $\rightarrow$ GPe	2	1.447	-	0 *	2 *	ampa
		$\times$0.36 G	-	0 *	100 *	nmda
$SD_1 \rightarrow$ SNr	4	4.5	156.3	-80 *	5.2 C&L	gabaa
$SD_2 \rightarrow$ GPe	5	5.435	21.6	-65 L	6 L	gabaa
GPe $\rightarrow$ STN	4	0.518	-	-84 B&L	8 B&L	gabaa
GPe $\rightarrow$ SNr	3	93	603.9	-80 *	2.1 C&L	gabaa
GPe$\rightarrow$ GPe	1	0.765	-	-65 L	5 L	gabaa
SNr$\rightarrow$ SNr	1	0.2	-	-80 *	3 *	gabaa
MSN$\rightarrow$ MSN	1	0.75 K&T	-	-60 M&T	4 M&T	gabaa
FSI$\rightarrow$ FSI	1	1.1 G&T	-	-60 M&T	4 M&T	gabaa
FSI $\rightarrow$ MSN	1	3.75 T	-	-60 M&T	4 M&T	gabaa

M: Moyer et al. 2007, **G:** Götz et al. 1997, **K:** Koos et al. 2004, **T:** Tomkins et al. 2013,
B: Baufreton et al. 2005, **L:** Lindahl et al. 2013, **C:** Connelly et al. 2010
***** General value for this parameter Dayan and Abbott 2001.
****** Local optimization.
Values of G without explanation were obtained with manual optimization.

Table 3.6: **Synaptic parameters.**

neurons. To approximate the NMDA:AMPA conductance ratios, we considered the ratios of the peak current for each type of receptor, which was obtained in Götz et al. 1997 using glutamate in nucleated patches of BG cells. The final values for each ratio are given in Table 3.6. Hence, to estimate connectivity weights of the excitatory synapses we tuned only one conductance (AMPA) which was used to infer the corresponding NMDA values.

Striatum This was the first structure whose connectivity was tuned, since its activity does not depend on any other BG nuclei according to our model's architecture. The dominant striatal cell, the MSN, fires at $0.01 - 2.0$ spikes/sec in basal tonic mode and $17 - 48$ spikes/sec in

periods of high activation or bursting (Miller et al. 2008; Lindahl et al. 2013). Also, *in vivo* mouse recordings have found that the basal firing rate FSIs in the striatum is between $10-15$ spikes/sec while it increases up to $60-80$ spikes/sec during behavioral tasks (Berke et al. 2004; Berke 2008).

To tune our striatal neurons, we employed only the model of striatum, striatal afferents and internal striatal connectivity, we initially set all cortical firing rates to be 3 spikes/sec and then we changed T_1 to 10 spikes/sec to account for tonic and bursting modes respectively. The parameters that were tuned are σ_{msn}, σ_{fsi}, $G_{ctx-msn}$ and $G_{ctx-fsi}$.

STN The basal firing rate of STN is around 10 spikes/sec and increases 100% without the influence of GPe (Farries et al. 2010). In periods of high activation, STN neurons show mixed dynamical behaviour and fire at around $30-50$ spikes/sec (Schmidt et al. 2013). Hence, to tune the network properties of STN, we followed the next two steps:

1. Similarly to the previous case, we used only the model of STN and tuned parameters related to cortical afferent axons ($G_{ctx-stn}$, σ_{stn} and $P_{ctx-stn}$) in order to make it fire at around 20 spikes/sec in tonic mode (without GPe inhibition) and around 40 spikes/sec in periods of high activation.
2. We then forced GPe to fire at 30 spikes/sec (by using a poisson process instead of the neuron equations) and tuned $G_{gpe-stn}$ to make STN fire at around 10 spikes/sec.

An adequate result was achieved by setting the conductance strength of the cortico-striatal afferents, for both AMPA and NMDA receptors to 0.25 nS, decreasing the STN noise to $\sigma_{stn} = 0.5$ mV and setting $P_{ctx-stn} = 3\%$ which results to 30 spikes/sec arriving to each STN neuron in the tonic mode and 100 spikes/sec in periods of high activation.

GPe Recordings of the GPe have shown that its basal firing rate is around 30 spikes/sec (Lindahl et al. 2013). After STN lesions, GPe's activity decreases 50% (Féger and Robledo 1991) while it increases 55% without striatal inhibition and local collaterals (Celada et al. 1999). The parameters that influence the basal firing rates and connections between STN and GPe and need to be tuned are $I_{vivo-gpe}$, $G_{stn-gpe}$, $G_{msn-gpe}$, $G_{gpe-gpe}$ and σ_{gpe}. The first parameter has been already optimized in order to make each type of GPe neurons to be close to the critical state between their two firing modes (see Neural parameter estimation). Since the remaining four-dimensional parameter space is complex for hand-tuning, we employed the classical Nelder-Mead method for local search (Nelder and Mead 1965), with the following fitness function:

1. Use GPe (without the Striatum and local collaterals) and force STN to fire at 10 spikes/sec.

Return $|FR(GPe) - 46.5|$.

2. Turn the striatum and local GPe collaterals on and return $|FR(GPe) - 30|$.
3. Turn STN off and return $|FR(GPe) - 15|$.

SNr Different reports show SNr to fire at rates between $22 - 29$ spikes/sec, when the BG operate normally (STN at 10, the striatum around 1 and the GPe around 30 spikes/sec) (Zahr et al. 2004; Walters et al. 2007; Gernert et al. 2004; Lindahl et al. 2013). Also, without the influence of the GPe, SNr is shown to increase its firing rate more than 300% (Celada et al. 1999; Lindahl et al. 2013), while without STN, the firing rate is decreased 50% (Féger and Robledo 1991).

To approximate the effect of the incoming synapses to SNr, we used again the local search method described above, in the parameter space $\{I_{vivo-snr}, G_{stn-snr}, G_{snr-snr}, G_{msn-snr}\}$. The fitness function in this case includes the following steps:

1. Turn off GPe, and reduce maximum conductance of STN-SNr connections to $G_{stn-snr}/2$. Return $|FR(SNr) - 76.5|$.
2. Turn off STN and force GPe to fire at 15 spikes/sec. Return $|FR(SNr) - 12,5|$.

The two-fold reduction of STN maximum conductances was necessary to simulate the effect of the depressive STN synapses to SNr (Moran et al. 2011), since its firing rate will be increased 100% without the influence of GPe. As the final step, using the whole BG model, we hand-tuned $G_{gpe-snr}$ such that SNr fires at around 25.5 spikes/sec, which is the average value of the different findings.

Short-term plasticity The above procedure results in a static model of the BG connectivity, where the strength of all synapses remains fixed for the whole duration of a simulation. Its behaviour represents the steady-state tonic mode of the BG circuit, where synaptic conductances G have already been modulated with respect to the tonic firing rate of the pre-synaptic neuclei.

To find the initial conductance of each synapse G_0, we need to calculate the degree by which it changes in tonic mode. If $STF_X(f)$ encodes the conductance change due to short-term facilitation for a nucleus X and firing rate f, and $STD_X(f)$ the corresponding relation for depression, then the current synaptic conductance can be found as $G_0^X(f) = G^X/STF_X(f)$ or $G_0^X(f) = G^X/STD_X(f) \cdot U$ for facilitating or depressing synapses respectively. Hence, from 3.2: $STF_{SD1}(1.1) = 1.5$, $STF_{SD2}(1.1) = 1.05$, $STD_{GPe}(30) = 0.154$ and $STD_{STN}(10) = 0.283$. The final conductances G_0 are given in Table 3.6.

In conclusion, estimating connectivity between and within the BG nuclei comprises a semi-automated procedure that resulted in a model with realistic firing rates in both tonic mode and during periods of high cortical activation (Fig. 3.4.A-B). This procedure should be followed again, in case that a different number of channels or neurons within a channel is chosen.

3.2 Resulting behaviour

Our optimization process resulted in eight new spiking models of BG neurons, based on the phenomenological Izhikevich equations (Izhikevich 2003), that were integrated into a large-scale model of the BG canonical circuit. This was successfully tuned to reproduce the firing patterns observed in biological BG neurons, both measured in brain slices as well as in *in vivo* behavioural studies. Fig. 3.1 shows the internal structure of the model, with emphasis on the synaptic types between the BG nuclei. The spontaneous firing rates of all optimized types of neurons, when their synaptic input current is zero, are compared with real data in Fig. 3.4.A.

The optimization of the connectivity between BG nuclei was achieved based on two different functional scenarios that resulted in the firing rates illustrated in Fig.3.4.C, which will be termed as *tonic* and *phasic* modes throughout this document. In the tonic mode, the model received the same cortical input in all microscopic channels, which had a low mean firing rate of 3 spikes/sec and represented the default tonically-active state of the BG neurons and microscopic channels. Additionally, the phasic mode was accompanied by a higher level of stimulation in a single channel, via a fixed 10 spikes/sec-activation of the corresponding cortical ensemble (see Fig. 3.5). This enhanced cortical input was able to cause transient effects in the BG network, such as short-lasting bursts in the input structures of the circuit or transient local silence in the GPe and SNr, and represented the scenario that this part of the BG circuitry is highly engaged in a motor or cognitive task.

In both modes, the model produced behaviour which agrees well with the current literature. The phasic cortical stimulation of a single channel was enough to drop the firing rate of SNr to almost 0 spikes/sec, while activity in neighbouring channels decreased to only around 29%. This behaviour has been associated with decision making (Redgrave et al. 1999; Humphries et al. 2006; Gurney et al. 2015), since it allows the BG circuitry to selectively halt inhibition of the area in the thalamus that is targeted by the affected microscopic channel.

In additional experiments, the cortical input that the model received had an oscillatory behaviour, as described in methodology, with a mutual amplitude across the cortical spike generators of the same channel and a fixed frequency, picked randomly from 0 to 100Hz. In the case of a phasic channel, the amplitude of the oscillations was 10 spikes/sec while the amplitude in

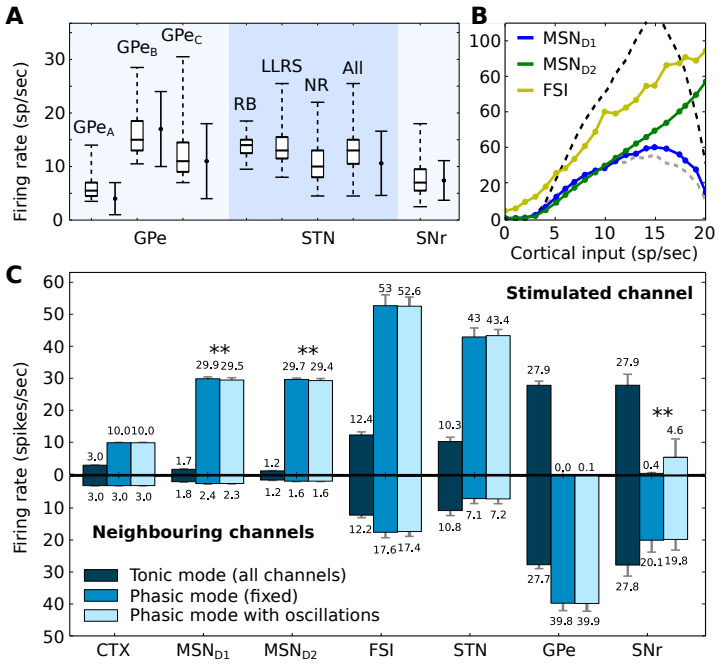

Figure 3.4: **Firing behaviour of the system. A:** The firing rates of the various neuron types when isolated. Solid error bars represent mean and standard deviation of recorded (real) spontaneous activity. Sources of data are given previously in this chapter. **B:** Cortical input-firing rate curve of striatal neurons when the complete model is in use. The dashed lines illustrate the MSN_{D1} curve for low dopamine (grey) and high dopamine (black) in the system. **C:** The average behaviour of the various neuron types when the complete model is in use. The *stimulated channel* represents the channel that received enhanced cortical input during the phasic mode, while the set of bar charts below show the average firing rates of the two *neighbouring channels*. In tonic mode, there is no discrimination between channels and the small differences in the two sets of bar charts are the result of random noise. The double asterisk (**) denotes an independent two-sample T-test with p-value $<< 0.01$.

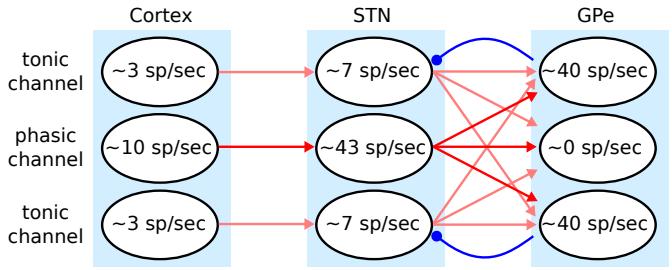

Figure 3.5: **Connectivity of the STN in the phasic mode.** The STN sends diffuse connections to the GPe that spread across all simulated neighbouring channels. The transparency of the arrows represents the firing rate of the source structure.

tonic channels was again 3 spikes/sec. Although this type of phasic input caused almost identical changes to the firing rates of the STN and GPe, compared to the initial experiments where each channel had a fixed firing rate, it had a strong influence on the activity of SNr, as well as some small influence on the striatum (see statistical tests in Fig.3.4.C). In particular, the SNr firing rate varied greatly for different cortical frequencies, between 0.13 and 23.71 spikes/sec compared to $0.07-1.25$ spikes/sec in the static case, with a standard deviation of 6.33 spikes/sec. A Spearman's rank-order correlation coefficient test between the cortical frequency and the firing rate of SNr resulted in $\rho = -0.882$ and p-value $< 10^{-40}$, indicating a nearly monotonic relationship. However, despite the fact that SNr showed such a different behaviour in the same channel, the firing rates of the neighbouring channels were indistinguishable in both cases (p-value of T-test: ~ 0.569).

Finally, when given strong cortical stimulation, the model produced symmetric activity in both groups of MSN neurons, at around 30 spikes/sec. This was a result of the fine balance between MSN_{D1} excitation, which is potentiated by dopamine, and connectivity asymmetries in local inhibition favouring MSN_{D2} neurons. Further simulations revealed the existence of a transition threshold at around 9.5 spikes/sec of cortical stimulation, above which, the firing rate of MSN_{D2} neurons exceeds MSN_{D1}, supporting the recently-proposed hypothesis of a decision threshold between the direct and indirect pathways in the striatum (Bahuguna et al. 2015).

Fig. 3.4.B illustrates this transition of the dominating neuron type, as well as the effect of dopamine in MSN_{D1} neurons that resulted in the modulation of the former. In low dopamine conditions (0%), this decision threshold shifts to around 3 spikes/sec of cortical stimulation while for high dopamine (90%), it exceeds 18 spikes/sec, an unrealistically high rate for corticostriatal neurons during behaviour (Turner and DeLong 2000).

4 The role of cortical oscillations in the basal ganglia function

4.1 Introduction

Rhythmic activity is one of the most widely-studied phenomena in the brain (Buzsaki 2006). In the mammalian cortex, oscillations in low-frequency ranges (< 100 Hz) have been associated with numerous cognitive and motor functions, that vary from feature binding (Eckhorn et al. 1988) and mental simulation (Brinkman et al. 2014) to movement preparation and execution (Leventhal et al. 2012). This cortical feature provides a fruitful framework to study neural computation and has given rise to theories that account for the control of communication between regions (Fries 2005, 2009) as well as memory formation and retrieval (Hanslmayr et al. 2012).

Oscillatory phenomena are not only prevalent in the cortex but also a prominent feature of other sub-cortical structures. In the BG, low-frequency oscillations are ubiquitous during spontaneous activity, and further enhanced in neurodegenerative disorders that affect this region, such as Parkinson's (PD) or Huntington's (HD) disease. Although the cortex and the BG are largely interconnected, both functionally and structurally, it is still unclear which elements of this rich oscillatory behaviour are generated in the cortex and processed in the BG, or vice versa.

Experimental and theoretical studies have provided initial evidence suggesting that BG activity at some specific frequency bands is driven by areas of the cortex (Litvak et al. 2011; Brittain and Brown 2014), and that those signals are not simply relayed through the BG pathways but they are rather subjected to some sort of internal processing, depending on their initial frequency (Brittain and Brown 2014). However, most of the knowledge that has been acquired so far does not emanate from studies on healthy humans, due to the inability of the most current non-invasive recording techniques to be applied in sub-cortical structures. Instead, most studies are confined either to animal models or human patients that undergo deep brain stimulation (DBS), a common surgical treatment of BG diseases, that provides the opportunity to record the spiking activity of multiple structures simultaneously.

In addition, although a substantial number of computational models have been proposed, (see Chapter 1), the topic of cortical oscillations is largely neglected by the majority of the current approaches which, depending on their level of detail, focus either on inter- or intra-nuclei interactions and locally generated rhythms.

The purpose of this chapter is to redress this imbalance and foreground the theme of cortical

oscillations by means of the biologically plausible neural model presented in Chapter 3. Using this model, we carried out an analysis on the relationship between cortical frequency, level of dopamine, locally generated oscillations and the information flow between the BG structures.

We found that the effective connectivity between the BG structures, and by extension the BG function, is completely controlled by the frequency and phase of cortical oscillations. Via this mechanism, cortical signals can be relayed, blocked or transformed depending on which BG pathway remains open in each frequency range. Furthermore, we predict that exaggerated beta band activity, a typical symptom in PD (Brown et al. 2001; Brittain and Brown 2014), originates in the subthalamic nucleus (STN) on account of single neuron dynamics of this structure, but it is entrained by the cortex. Next, the literature related to low-frequency bands is reviewed and compared against our results, and cognitive mechanisms related to each band are proposed. Finally, we point out the great impact of the phase offset between cortical oscillators to the interaction between the STN and the globus pallidus external (GPe), and its role in modulating the BG output.

Our results suggest that the BG can be viewed as the "gear box" of the cortex. Different rhythmic cortical areas are able to switch between a repertoire of available BG modes which, in turn, change the course of information flow back to and within the cortex.

4.2 Results

4.2.1 Dopaminergic modulation of intrinsically-induced beta oscillations in the GPe-STN loop

One major and well-studied feature of the BG function is the existence of strong, intrinsically-generated, oscillatory activity that originates from recurrent connections between the STN and GPe (Plenz and Kital 1999; Bevan, Magill, Terman, et al. 2002). The next step of this work was to investigate the oscillatory behaviour generated within our model, before moving to cortical oscillations, in order to assess the extent to which it agrees with the literature. To calculate the power spectra of the different BG structures we employed the multitaper method (Mitra and Pesaran 1999), applied on 1ms-binned, mean-centred and Gaussian-smoothed spike trains, which offers good frequency specificity and is able to detect low-frequency signals, better than other typical methods (Vugt et al. 2007).

Without any fluctuations of the firing rate of the input ensembles, the model was able to generate beta oscillations internally, mainly visible in STN and GPe, whose peak frequency varied depending on the activation of each channel. When the stimulation was limited at the tonic

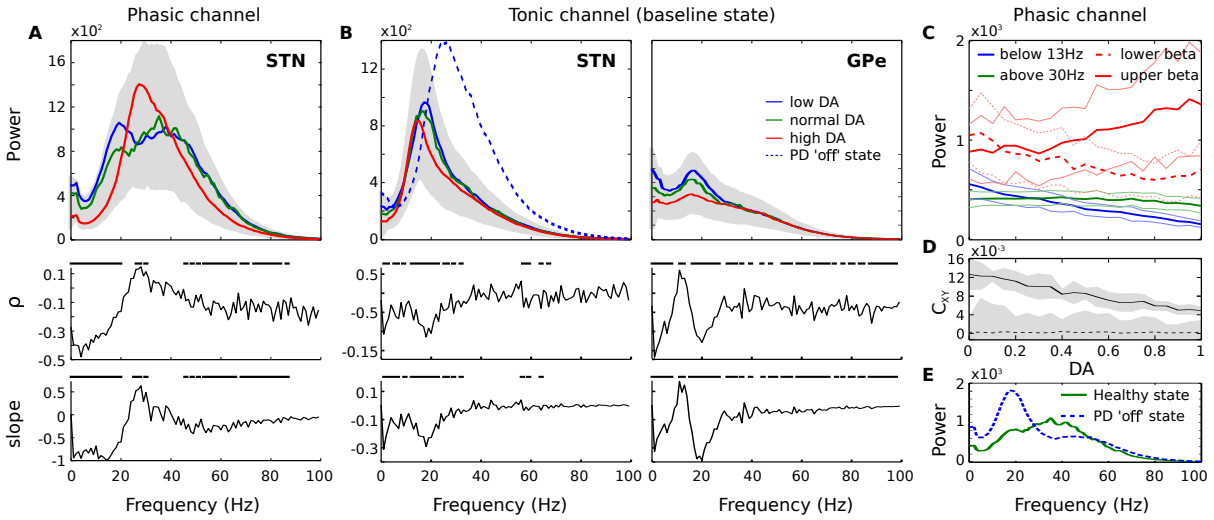

Figure 4.1: **Frequency spectrum of STN-GPe loop without oscillatory input.** Dopamine reduces lower-beta oscillations and modulates the spectrum. **A,B:** Up: Average power spectrum for different dopamine levels during the phasic (A) and tonic fixed (B) state of a single microscopic channel in the level of the STN and GPe. The light grey areas represent the standard deviation of the average power spectrum for random dopamine levels between 0 and 1 ($n = 4000$). Down: Spearman's rank correlation coefficient (ρ) and the slope of best-fit regression line between frequency power and DA levels measured in the above runs. The black lines indicate areas where p-value is less than 0.05. **C:** Mean power of the four interesting frequency bands for different plausible dopamine levels, during the phasic state of a microscopic channel in STN. **D:** Average cross-correlation between all neurons of the STN for different levels of dopamine, when BG stimulation is applied transiently (solid line), or over a long time period (dashed line), after the subtraction of the same statistic produced by surrogate data. **E:** Average power spectrum of a phasic STN channel under healthy and PD conditions. In all cases, the shaded areas or lines represent standard deviation.

levels, the STN displayed strong lower-beta oscillations with a sharp peak at $18-20$Hz while the GPe showed a weaker peak at the same frequencies (Fig. 4.1.B). An increase of the input firing rate to 10 spikes/sec, enough to cause silence in GPe and SNr, diminished the difference between areas of low frequency bands in STN, which remained, however, highly active (Fig. 4.1.A).

Furthermore, the level of dopamine in the neuron equations of the network was found to modulate these low-frequency oscillations in different ways. In a phasic STN channel, dopamine above the normal levels ($d_{1,2} > 0.3$) was able to suppress the power of oscillations lower than 20Hz (Fig. 4.1.C) and strongly amplify the upper-beta band ($23-30$Hz), resulting in a clear peak at $28-30$Hz. On the other hand, low dopamine caused an amplification of the lower-beta band, almost linearly proportional to the level of reduction, from 0% to 30%, without any significant effects on the other frequency bands.

Finally, in tonic activation of a BG channel, high levels of dopamine caused a slight shift in the

peak beta frequency in STN and abolished any indication of enhanced beta activity in GPe. As in the case of a phasic channel, these oscillatory effects were more noticeable for dopamine values significantly higher than the net concentration. This dopamine increase is expected in healthy brains, where the level of dopamine can be boosted by phasic release during behaviour (Jenkinson and Brown 2011).

Interestingly, similar oscillatory patterns have been found in clinical recordings of PD patients, during "on-" and "off-medication" periods (López-Azcárate et al. 2010). To simulate the 'off' Parkinsonian BG state more accurately, we assumed complete dopamine depletion ($d_{1,2} = 0$), as well as an increase of the cortical impact to the striatum and STN. Although PD does not influence the firing rate of the majority of biological corticostriatal neurons, low dopaminergic transmission has been shown to cause high levels of cross-correlated activity between the cortex and the striatum (Costa et al. 2006) and hyperactivity in STN (Bergman et al. 1994; Steigerwald et al. 2008). Hence, to capture this effect here, we tested two different adjustments to the model, a 20% increase of the cortical firing rate, as well as a 10% increase of the conductance of the synapses that originate from the cortical ensembles. Both simulations resulted in almost identical changes in STN behaviour, that agree well with the literature (Bergman et al. 1994; López-Azcárate et al. 2010). These comprise a substantial increase of the power of lower-beta oscillations, shown in Fig. 4.1.E, a 20% drop of low-gamma and upper-beta oscillations, and a 20% increase of the overall STN firing rate.

The excessively rhythmic behaviour of the phasic STN is particularly interesting, as its neurons remained uncoupled without the inhibition of GPe (most GPe neurons connected to a phasic STN channel remain silent), leading to the conclusion that the emergent oscillatory patterns are a result of membrane potential dynamics of the STN neurons.

In pursuit of this idea, we conducted a statistical analysis comparing the interspike intervals (ISIs) of the three simulated neuron types in STN, in order to evaluate the behaviour of its individual cells. The coefficient of variation (CV) of ISIs was used to measure irregular firings, while bursting activity was measured by means of the asynchrony index (AI), the ratio of the mode to the mean ISI (Gernert et al. 1999). Small values of AI< 1 indicate a large portion of short ISIs compared to the mean firing rate.

Fig.4.2 illustrates that, indeed, excessive beta activity observed in the Parkinsonian 'off' state is orchestrated by rhythmic bursts, produced by the rebound-bursting (RB) STN neurons. Although the rest of the neurons in the STN exhibited highly regular behaviour that did not change during the 'off' state (CV$= 8.9\% \pm 0.02$, AI$\approx 1 \pm 0.05$), the firing patterns of RB neurons were less regular (CV$= 37\% \pm 0.08$, AI$= 0.89 \pm 0.3$), and switched to rhythmic bursts (CV$= 50.2\% \pm 0.08$, AI$= 0.69 \pm 0.2$) with a clear frequency peak at 20Hz.

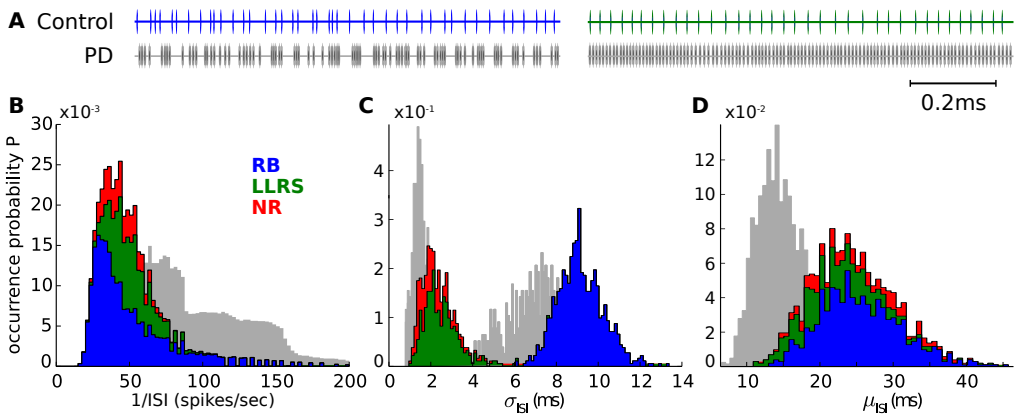

Figure 4.2: **Firing patterns of the three types of STN neurons. A**: Two recorded examples of STN neurons show irregular (left) and regular (right) firing patterns, as well as the behaviour of the same neurons during the Parkinsonian 'off' state. **B-D**: ISI distributions of STN neuron types, superimposed on stacked histograms. The shadow represents the changes in the total STN distribution during the 'off' state. LLRS: Long-lasting rebound spiking neuron, NR: No-rebound neuron.

Furthermore, we observed that tonic activation of GPe was able to drive STN neurons into a synchronous state that was sustained for approximately 400 ms, following the stimulation of the underlying BG channel. Fig. 4.1.D shows that this synchronization in phasic STN channels was influenced by dopamine, in an inversely-proportional manner. This behaviour is not surprising, since the lack of dopamine was shown to cause increases in the same frequency bands both in GPe and STN, thus facilitating synchronization. To further confirm this observation, we created a number of surrogate time series of the binned spike events of each neuron, randomly shuffled over time (Theiler et al. 1992), which destroyed any linear correlations between spikes. A comparison with the original time series produced by our model showed that there was close-to-zero correlation between synchronization and dopamine in the case of the surrogate data, in contrast to the former case, thus the null hypothesis of uncorrelated noise can be rejected.

Finally, to see if this synchronous state can be maintained when it is driven by extrinsic beta activity, we compared the STN behaviour of the above example, as opposed to the case when the simulated cortical ensembles oscillate at a upper-beta frequency ($f = 25$Hz) with a weak amplitude of $A = 6$ spikes/sec, without changing the overall cortical firing rate. As a measure of synchrony, we extracted the instantaneous phases of each STN neuron using the Hilbert transform across each mean-centred and Gaussian-smoothed spike train. The synchrony Φ was then calculated as the average of $\frac{1}{N}\sum_j^N e^{i\theta_j^H(t)}$ over time t, where N is the number of STN neurons and $\theta_j^H(t)$ represents the instantaneous Hilbert phase of the neuron j. This method was selected for its tolerance to amplitude changes (Le Van Quyen et al. 2001), since cortical oscillations at the same frequency can increase the amplitude of the STN emerging beta. After 100 simulations for different initial conditions, the static case resulted in average synchrony

$\Phi = 0.26 \pm 0.01$ in a phasic microscopic channel and 0.32 ± 0.01 in a tonic channel. This 23% increase in the tonic case was anticipated as the GPe is active and able to provide inhibitory feedback to the STN. On the other hand, although weak, cortical beta oscillations caused Φ to increase even more to 0.34 ± 0.02, while keeping the GPe silent, and therefore confirmed our initial premise.

4.2.2 Only low cortical frequencies can be maintained throughout the BG structure

When the BG model received oscillatory input from the simulated cortical ensembles, it exhibited a mixed behaviour. In this experiment, a *phasic* BG channel was stimulated by a cortical ensemble with frequency $f_1 \in (0, 80)$ Hz and amplitude $A_1 = 10$ spikes/sec, while a second neighbouring channel received input from a *tonic* ensemble with amplitude $A_1 = 3$ spikes/sec, frequency $f_2 = f_1$ and random relative phase $\phi_2 \in [0, 2\pi)$. The aim here was to explore the ability of the model's internal dynamics to filter out some frequency bands while preserving others, which would allow the discrimination between cortical frequencies that pass to the thalamus and end up back in the cortex. The metrics used for this analysis were the power of the examined frequency band in each nucleus and the coherence between the cortical inputs and the nuclei. Frequency spectra were calculated using the same methodology as before, while coherence was defined as the normalized cross-spectral density between the above sources.

In low frequencies, between 0 and 30 Hz, the oscillatory patterns of the cortical inputs were largely replicated in all BG nuclei, in both the phasic and neighbouring channels. In contrast, cortical activity at higher frequencies was preserved in the striatum but declined in subsequent structures. This is evident in Fig. 4.3.A-B, where frequency power and coherence match for most input frequencies. One clear reason for this decline is the blockage of the GPe and SNr activity in the phasic channel, that occurred at high frequencies due to striatal inhibition. However, the fact that certain frequencies also abated in STN, as well as neighbouring channels of GPe and SNr that were not silent, points to the existence of another mechanism that filters out frequency bands above 30Hz.

One candidate explanation of this effect, which was revealed here, regards the inter-channel competition that was evoked by the MSN collaterals and the multi-channel excitation from the STN. In particular, neurons of the STN that correspond to the phasic channel, were able to send EPSPs to GPe neurons of neighbouring channels, which in turn inhibited neighbouring STN neurons and cancelled out the initial oscillatory EPSPs from the cortex. Fig. 4.3.C shows that, without the influence of GPe inhibition, phasic STN neurons tended to adapt to cortical oscillations at frequencies $13-40$ Hz with a maximum effectiveness, while under normal conditions,

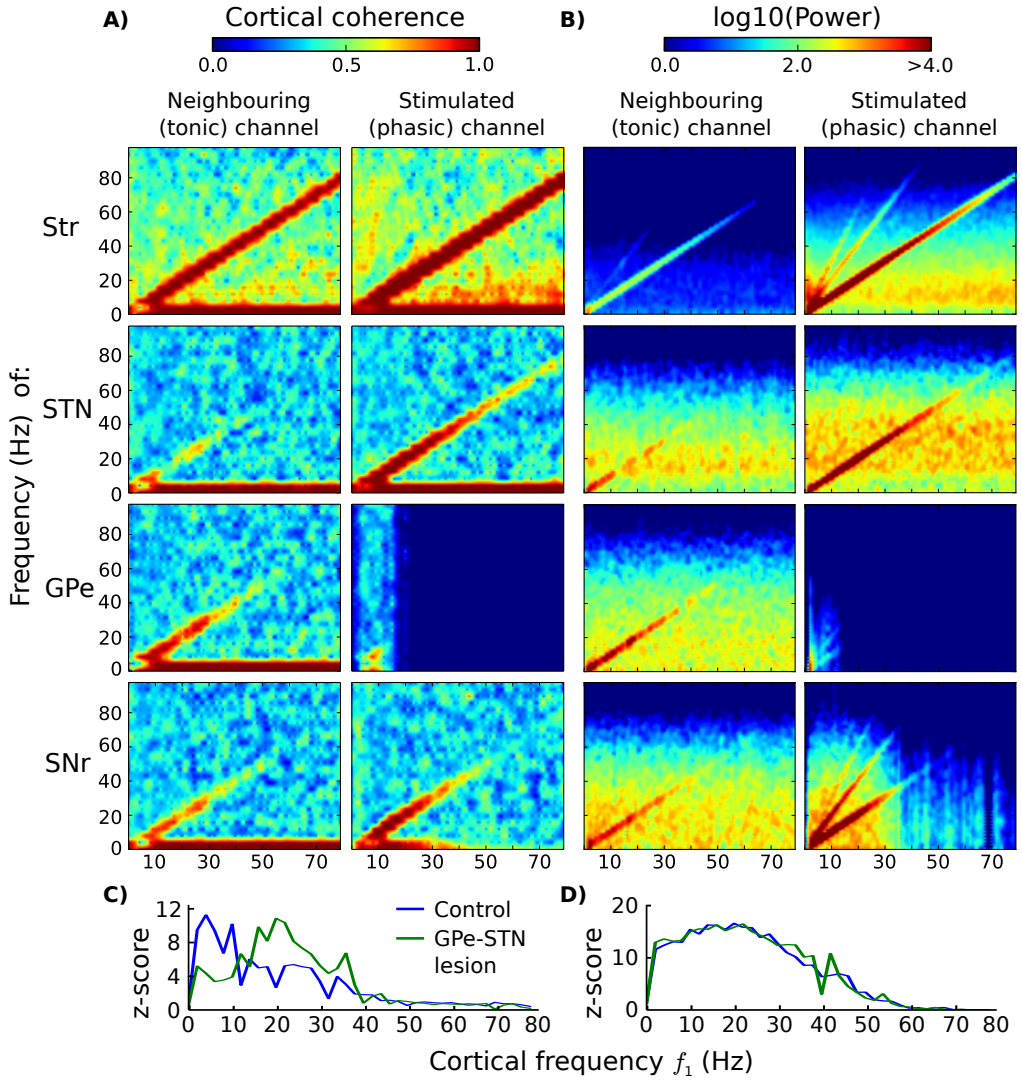

Figure 4.3: **Cortical coherence throughout the BG. A)** Cortical coherence and **B)** frequency spectrum and of the BG nuclei for different cortical frequencies f_1. A unified spectrum for all striatal populations was included (Str), since they all exhibited very similar behaviour. **C,D)** Z-score transformation of the cortical frequency f_1 in the STN power spectrum of the phasic (C) and the neighbouring (D) channels.

this frequency band shifted to $0 - 12$ Hz. Neighbouring channels were not influenced by GPe inhibition (Fig. 4.3.D). In a similar fashion, this self-cancelling mechanism affected the entire BG circuitry via STN EPSPs, and facilitated the blockage of high-frequency cortical coherence.

Furthermore, the striatum produced harmonic oscillations (mainly in MSN_{D1} neurons), at frequencies limited to the low and gamma ranges (Fig. 4.3.B). Unlike cortical oscillations, harmonics passed only to the SNr of the phasic channel via the direct pathway, which resulted in their

strong amplification. This constitutes one more BG mechanism that facilitates inhibition over excitation, and allows inhibitory BG pathways to be more tolerant to different phases than the hyper-direct pathway.

Finally, we ran the same experiments in PD conditions to evaluate its impact on the above mechanisms. The only noticeable effect was the increase of the frequency range of cortical oscillations that can be maintained throughout the BG. The maximum frequencies increased by $20\% - 40\%$ across all BG nuclei. This result was consistent for both frequency power and coherence.

4.2.3 Cortical frequency defines the effective connectivity of the BG pathways

The effective connectivity between the BG structures over a certain period of time can be measured by calculating the causal interactions between their corresponding spiking time series, using a variety of statistical methods. In this work, we used pairwise transfer entropy (TE) (Schreiber 2000), a generalization of granger causality, when the Gaussianity of the time series cannot be assumed (Barnett et al. 2009). TE between two time series X and Y at time t measures to what extent the couple $(X_{t-\tau}, Y_{t-\tau})$ is more resourceful in forecasting Y_t, than just the value of $Y_{t-\tau}$ (Wiener 1956). It is expressed as

$$T_{X \to Y} = -\sum_{t} p(x_t, x_{t-\tau}^{(k)}, y_{t-\tau}^{(l)}) \log \frac{p(x_t | x_{t-\tau}^{(k)}, y_{t-\tau}^{(l)})}{p(x_t | x_{t-\tau}^{(k)})} \tag{4.1}$$

where k, l are the lengths of the events $x_i \in X$ and $y_i \in Y$ respectively, and the time constant τ indicates the interval between the two measurements, i.e. the time delay of the information flow. The choice of τ in measuring TE between neuronal ensembles is very important and can lead to significantly different numbers , that might be influenced by the delays of different afferent connections. A reasonable choice, which was also adopted in this work, is to calculate the TE that arises on the timescale of the AP propagation via the chemical synapses between the examined ensembles.

For the generation of the time series, 10 seconds worth of data was recorded, for every frequency of cortical oscillation between 1 and 100 Hz. The amplitude of the oscillation in the examined BG channel was set to $A = 10$ spikes/sec while oscillations in neighbour channels were limited to 3 spikes/sec. The phase offset ϕ between cortical oscillations of this channel and other neighbours was randomized uniformly in every run. Finally, the spiking activity of each BG nucleus was summed for each millisecond and then low-passed using a discrete-time RC filter ($RC = 2$,

$dt = 0.1$).

Fig. 4.4.A illustrates the resulting spectrum of TEs between the cortex and the BG nuclei (first half) and for the main pathways of the BG circuit (second half). We observed a clear distinction between input frequency bands, giving rise to completely different behaviour in the model (Fig. 4.4.B). The greatest variation arose in low-frequency bands, between 4 and 30Hz, under the very conditions that are necessary to allow the relay of information via the BG.

More specifically, during stimulation at alpha frequencies, the three major BG pathways remained highly active. In the indirect pathway, striatal neurons were able to affect the behaviour of the SNr via the GPe, bypassing modulation by the STN-GPe loop and, as a result, the input-output information flow in the BG maximized. In the lower-beta band, greater information flow from the cortex allowed the STN to restore the modulation of the indirect pathway, and to maintain a higher impact than the GPe on the SNr. This balance changed again at upper-beta frequencies, where the flow of information via the STN and GPe was restricted to interactions within the STN-GPe loop, and thus the SNr behaviour was dictated by the MSN_{D1} inhibition. In gamma frequencies, a cortical information blockade turned the STN into a local-circuit component that affected the SNr only via GPe inhibition. The full indirect pathway dominated the BG behaviour and blocked cortical information flow.

Finally, below alpha, the impact of the GPe on the SNr was maximal at theta frequencies ($4 - 8$Hz), even though the information flow from excitatory sources towards the GPe abated considerably. In fact, the amount of $T_{GPe-SNr}$ was found to have increased by $84 \pm 58\%$ compared to the sum of TE towards the GPe, a fact that leads to the hypothesis that, under these conditions, some of the information that arrives to the SNr is generated within the GPe.

Fig. 4.4.C summarizes the above observations and illustrates the impact of the cortical frequencies on the activation of the three main BG pathways. This analysis was based on a heuristic method, where the values of TE between the consecutively connected nodes of a pathway were multiplied and then normalized with respect to their distribution across cortical frequencies. Interestingly, as evidenced by this figure, different frequency bands give rise to different combinations of active pathways, increasing the repertoire of potential functions that the BG are able to perform.

Furthermore, we observed that in certain low frequencies, the phase offset ϕ between the two oscillating cortical ensembles was able to change how the STN and GPe interact with their adjacent nuclei. In Fig. 4.4.D, different phase offsets between alpha oscillations were able to block, or reverse the direction of information flow between STN and GPe, which was also accompanied by a pronounced effect on the pathways that include them. This was more evident when the strong cortical signal of the phasic channel (10 spikes/sec) preceded in time the weaker (tonic) oscilla-

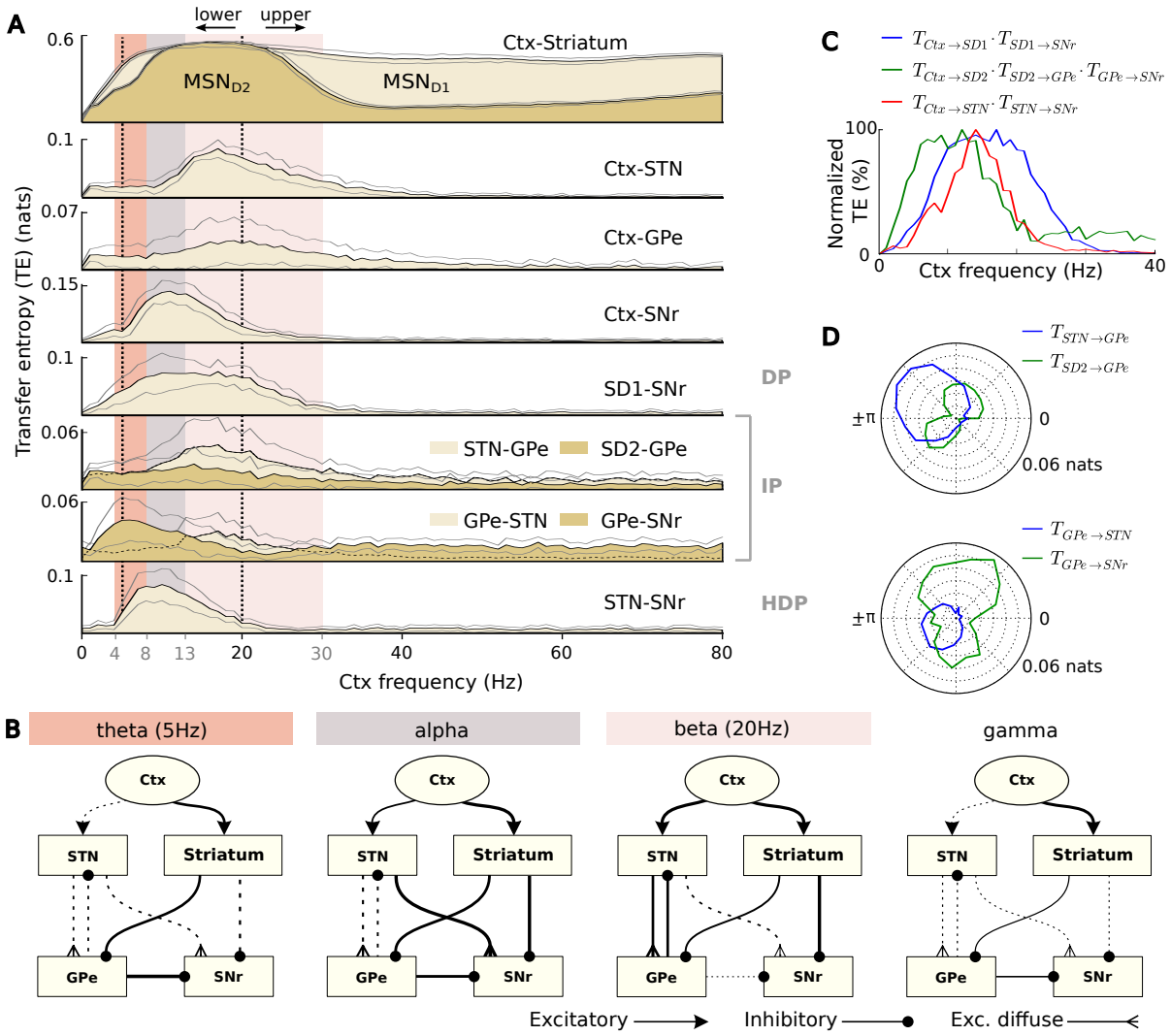

Figure 4.4: **Effective connectivity of the BG model. A:** Spectrum of TE for the connections of the BG circuit. DP, IP and HDP stand for the direct, indirect and hyper-direct pathways respectively. **B:** Resulting effective connectivity of the BG for different cortical frequency ranges. Thickness of synaptic connections represents TE (normalized across the frequency spectrum) and the solid lines show the dominating pathways. **C:** Activation of the three main BG pathways for different cortical frequencies. **D:** TE of GPe afferents versus efferents, for different phase offsets ϕ and alpha cortical rhythms. When $0 \leq \phi \leq \pi$, oscillation peaks in the phasic cortical channel precede in time oscillation peaks in the tonic channel.

tory signal of a neighbouring channel, i.e. $0 \leq \phi \leq \pi$. In this case, the flow of information was stronger towards the STN, and the activation of the hyper-direct pathway was largely modulated by the influence of GPe (Spearman's correlation between $T_{STN-GPe}$ and $T_{STN-SNr}$: $\rho = -0.72$, $p \approx 5 \times 10^{-17}$), while in the opposite case, when $-\pi \leq \phi \leq 0$, the prevailing direction of the

flow also reversed. This effect had significant ramifications for the balance between hyper-direct and indirect pathways which was found to be strongly correlated with the direction of flow between the STN and GPe (Spearman's correlation between $\frac{T_{STN-GPe}}{T_{GPe-STN}}$ and $\frac{T_{STN-SNr}}{T_{GPe-SNr}}$: $\rho = -0.44$, $p \approx 3 \times 10^{-05}$). This set of observations provides insight into the modulation mechanism of the STN-GPe loop and indicates the importance of phase-to-phase coherence in low-frequencies.

As previously, we used surrogate data testing to confirm that our observations were not a result of uncorrelated noise. After randomly shuffling the time-series of each nucleus for 1000 times, the average TE for all connections became $2.6 \times 10^{-3} \pm 8.5 \times 10^{-4}$, and it was similarly distributed across different frequencies. This value is considerably lower than the resulting TEs in Fig.4.4 and thus the null hypothesis can be rejected for any of the above results.

4.3 Discussion

The emerging oscillatory behaviour of the model was particularly interesting, since the tuning process was based only on simple firing rate rules and neuron electrophysiology, updating the maximum synaptic conductances and the internal phenomenological parameters of the individual neurons respectively. As our simulations show, the frequency of the cortical input can be maintained throughout the BG structures and dramatically changes the way that the BG circuit operates. In the rest of this section, we discuss the consistency between our results and previously published experimental data and theories, and we provide a number of testable predictions that are supported by our simulations.

4.3.1 Beta activity is locally-generated but cortically-entrained in the Parkinsonian state

Numerous associations can be made between the oscillatory behaviour of our model and experimental data both in the healthy and Parkinsonian BG. In Leventhal et al. 2012, Leventhal et al. discovered that beta power in the cortex and the BG of healthy mice changes distinctively during behaviour. They also measured coherence and correlation of frequency bands throughout the BG and found that, during their behavioural experiments, coherence was maintained at both alpha and beta frequencies but disappeared at higher frequencies. In Fig.4.3.A. we observed the same phenomenon in our modelled BG both in a stimulated channel that was driven by phasic, oscillatory cortical activity, as well as in neighbouring areas.

Within the microcircuit, recordings of PD patients and primate subjects show exaggerated beta oscillations in the STN (Bergman et al. 1998; Brown et al. 2001; Hammond et al. 2007; Brittain

and Brown 2014) that correlate with the pathological symptoms of PD (Kühn et al. 2006; Little and Brown 2014) and exhibit high local coherence (Moran et al. 2008). Although a well studied phenomenon, the literature provides conflicting evidence regarding the source of these oscillations, which are thought to either be generated internally, via the STN-GPe reciprocal coupling (Plenz and Kital 1999; Bevan, Magill, Hallworth, et al. 2002; Tachibana et al. 2011; Pavlides et al. 2012), or within other BG nuclei, such as the striatum (McCarthy et al. 2011), or in certain areas of the cerebral cortex (Hammond et al. 2007; Litvak et al. 2011).

One compelling hypothesis, presented in Brittain and Brown 2014, is that upper-beta oscillations of the motor cortex entrain beta activity generated within the BG, which however peaks in the lower-beta band, during the Parkinsonian 'off' medication state. Our results support this hypothesis and provide a potential explanation that points to the internal dynamics of the STN rebound bursting (RB) neurons as the source of these pathological oscillations.

In the simulated Parkinsonian state of a phasic channel in Fig. 4.1, our model indeed produced excessive lower-beta oscillations, enhanced by both dopamine depletion and the potentiated cortico-subthalamic projections. Despite its influence on beta amplitude, however, the lack of dopamine was not sufficient to increase the average synchronization between pairs of STN neurons, as it is found *in-vivo* (Moran et al. 2008), unless the STN activity was measured transiently, right after the halt of cortical beta oscillations (Fig. 4.1.D). To solve this problem and achieve a synchronous steady state, the model was stimulated with a weak oscillatory cortical input in upper-beta band (25 Hz), which was found able to entrain the STN neurons and increase the average instantaneous phase-synchronization Φ by 31%. The oscillatory behaviour that emerged after this modification closely resembles STN field potential recordings in the motor BG of PD patients in López-Azcárate et al. 2010, and reveals a difference between the role of lower and upper beta bands, which is consistent with the discussion in Brittain and Brown 2014.

Nevertheless, the question remains of how cortical upper-beta activity can entrain the strong lower-beta generated within the BG network. More light can be shed at the single-unit level, where the majority of the STN neurons showed a mixed rhythmic bursting behaviour, similar to recordings in Steigerwald et al. 2008, with a frequency peak at around 18 Hz (Fig. 4.2.A). In particular, we observed that, without the influence of the GPe, which is locally inhibited on phasic microscopic channels, and with excessive excitation from the cortex, the rebound-bursting STN neurons generate free and uncoupled oscillations, resulting mainly from their internal dynamics. Since they are uncoupled, these oscillations are prone to entrainment by external stimuli, insofar as those stimuli also oscillate at a compatible frequency, such as in the experiment described above.

The plausibility of the firing patterns of both the pathological and healthy simulated STN neu-

rons can be confirmed by a number of empirical studies. The positively skewed distribution of the inverse ISIs of these neurons, shown in Fig. 4.2.B, agrees well with the distribution of single neuron firing rates, recorded in the STN of healthy monkeys (Bergman et al. 1994). After a treatment with the neurotoxin MPTP, which is known to cause Parkinsonian-like symptoms (Burns et al. 1983), the distribution of firing rates shifted towards higher values and had a flattened profile, a feature that was also captured by the simulated Parkinsonian 'off' state and illustrated in the same figure. Furthermore, the ratio of burst-like neurons and the distribution of mean ISIs for each STN neuron in Fig. 4.2.D is consistent with the results of multi-electrode recordings in human PD patients in Steigerwald et al. 2008, where the power spectra of individual STN neurons were found to peak at 17.9 ± 6 Hz.

The pathological mechanism we propose here could be further investigated experimentally, with a signal-cancellation technique either at the level of the cortex (as in Joundi et al. 2012) or directly in the STN using, for instance, DBS electrodes. Our hypothesis predicts that, in highly active areas, a reduction of the influence of cortical upper-beta activity to STN neurons will also reduce the correlation between their spike trains, as they will lose their main source of entrainment, but it will leave the amplitude of lower-beta almost intact.

Moreover, the behaviour of the system in the tonic state reveals the role of the GPe in the generation and maintenance of synchrony within the STN. In Fig. 4.1.B, oscillations in STN and GPe are highly coherent at lower-beta frequencies, a relation that is inversely proportional to the amount of DA in the system. In the resting Parkinsonian state, characterized by zero dopamine, enhanced cortico-subthalamic connections and tonic cortical activation, inhibitory feedback from the GPe was able to increase the average instantaneous synchrony Φ of STN neurons by 23% and maintain it for 400 ms after the silence of GPe. This leads to further predictions regarding the interaction between the STN and GPe. First, in periods when the BG input nuclei have areas that are highly active, a subgroup of GPe neurons is expected to be silent, due to high inhibition from MSN_{D2} neurons (Fig. 3.4). These periods of silence have been observed before in the GPe (DeLong 1972), and have been linked to striatal inhibition (Kim and Kita 2013), but based on our model, they should also exhibit high correlation with STN activation. Following this vein, long periods of silence in GPe neurons lead to a halt of the only source of inhibitory feedback to the connected STN neurons. As a result, if cortical beta is cancelled out as proposed in section 4.2.2, highly active STN neurons are expected to become unable to maintain any synchronous state, and have minimum correlation (as in Fig. 4.1.D), if the duration of this activity exceeds a time threshold.

Apart from the peaks in beta band of the STN power spectrum, Lopez et al. in López-Azcárate et al. 2010 found a second area, at very high frequencies around 350 Hz, that was evidently high. This activity was shifted towards lower frequencies (250 Hz) without medication for the

Parkinsonian symptoms. Although neither case has been captured by our simulations, this was possibly due to the nature of the multitaper method used for spectral analysis, which is insensitive to weak signals at high frequencies (Vugt et al. 2007).

Finally, one more factor that might contribute to the synchronous activity within the STN is the complete BG-thalamo-cortical loop, which involves the hyper-direct BG pathway. Since the STN neurons are able to generate beta patterns spontaneously, they might also be able to to enhance beta activity throughout this loop, even in the case that GPe neurons are locally silent. This can be tested in future work, with an extended version of our model, that also incorporates neural populations corresponding to both thalamic and cortical areas.

4.3.2 Oscillations and the BG function

Beta oscillations are also prevalent in the healthy function of the BG and they are strongly associated with the motor system of the brain (Baker 2007; Leventhal et al. 2012; Engel and Fries 2010; Brittain and Brown 2014; Connolly et al. 2015). As in the Parkinsonian 'off' state (Solages et al. 2010), they show peaks in both lower and upper-beta ranges, but with a higher median frequency (Connolly et al. 2015), since lower-beta is more sensitive to suppression by dopamine (Brittain and Brown 2014). This feature was reproduced in our simulations, where dopamine was able to control the level of internally-generated lower-beta and effectively reduce it in exchange for upper-beta oscillations, in an almost linear manner (see Fig. 4.1.C). If this ability to change the peak of beta activity is confirmed experimentally, then small fluctuations in rebound-beta that are usually present after the execution of a task (Zhang et al. 2008) or after artificial modulation of dopamine (Delaville et al. 2014) could be reflected in the level of dopamine that changes due to a post-decision evaluation (Schultz et al. 1997).

With regard to their function, one theory proposes that beta oscillations are used to "signal the status quo" across brain regions (Engel and Fries 2010), both at the perceptual-cognitive and motor level, in case that its maintenance is anticipated or intended. Furthermore, a behavioural study with simultaneous, multiple recordings in healthy rats provides evidence that beta oscillations in the BG are strongly related to cue utilization (Leventhal et al. 2012), and suggests that high beta activity reflects "a post-decision stabilized state of cortical-BG networks, which normally reduces interference from alternative potential actions". These views can explain the rigidity and hypokinesia of PD patients who also exhibit abnormally exaggerated beta activity, the observed beta desynchronization in movement preparation and execution (Van Elk et al. 2010; Singh et al. 2011; Schmidt et al. 2013), as well as the beta rebound in NO-GO decisions (Zhang et al. 2008). However, it is still unclear why these oscillations have such a strong effect in maintaining the current state of the brain. One recent review suggests that beta

oscillations regulate the information capacity of the phasic channels of the loops involving the BG (Little and Brown 2014).

Here we propose that the BG is able to selectively gate information flow in these channels, via a combination of internally-generated and cortically-driven beta activities, driven by the current level of dopamine and the cortical frequency respectively. We show that, even when their amplitude is kept fixed, different cortical beta frequencies are able to completely change the information flow throughout the BG. The increased flow in low bands in Fig 4.4 is consistent with the view in Little and Brown 2014, and provides a lower bound for the information capacity during the beta regime. More specifically, towards lower beta frequencies, the communication channels of the three major BG pathways open gradually and monotonically, with the same rate but different offsets (Fig. 4.4.C). At 13 Hz, the lowest beta frequency, all three pathways have a global peak, while at the highest beta (30 Hz), they are fully blocked. Hence, the frequency of beta can be used by the cortex as a lever that adjusts the impact of the three BG pathways, and thus plays a decisive role in the generation of movement (Redgrave et al. 1999; Schmidt et al. 2013; Calabresi et al. 2014).

Apart from beta, other frequency bands also showed unique characteristics in our simulations. Alpha rhythms resulted in BG effective connectivity changes that were similar to beta, promoting all three BG pathways but with an emphasis on the indirect pathway, and with even higher input-output information flow. In experimental studies, alpha activity has been also very closely associated with beta, exhibiting desynchronization prior to movement and suppression during movement execution (Pfurtscheller and Da Silva 1999; Brittain and Brown 2014; Tzagarakis et al. 2015). However, these rhythms are considered to have a distinct function (Pfurtscheller and Da Silva 1999; Moran et al. 2008; Singh et al. 2011; Litvak et al. 2011; Tzagarakis et al. 2015) and they have been mainly associated with emotional stimuli (Brücke et al. 2007), as well as the attentional system of the brain (Jensen and Mazaheri 2010; Litvak et al. 2011; Brittain and Brown 2014). In particular, there is cumulative evidence that strong alpha power is able to inhibit task-irrelevant regions in the cortex and thus control information flow (Jensen and Mazaheri 2010; Händel et al. 2011; Brinkman et al. 2014), while it is argued that alpha desynchronization allows the formation and retrieval of new memories (Hanslmayr et al. 2012). Finally, alpha power cannot be significantly regulated by the level of dopamine (Priori et al. 2004), a fact that shows another major difference in the function of these rhythms at the level of the BG. The constant tendency of alpha to promote information flow via the indirect pathway, as observed in Fig. 4.4, agrees well with the above theories. This pathway has been shown to play a critical role in proactive inhibitory control (Zandbelt and Vink 2010; Schmidt et al. 2013) and cause movement suppression (DeLong 1990; Kravitz et al. 2010; Freeze et al. 2013) by evoking a rapid disinhibition of a subset of SNr neurons. Thus, it is likely that a local increase in

alpha power brings the affected cortical region to a stable state, where the cortico-BG-thalamic loop is active but, at the same time, restricted from accessing memory processes and with the corresponding motor responses inhibited.

The two final frequency bands under consideration are theta and gamma. The coexistence of these two bands is a well studied phenomenon in the cortex (Canolty et al. 2006), which, as opposed to alpha and beta, promotes the formation and retrieval of episodic memories via phase-amplitude entrainment between different regions (Nyhus and Curran 2010). However, in this study we assess theta and gamma separately to maintain consistency in our methodology and enable the direct comparison with other frequency bands. Cortical theta (~ 5 Hz) is involved in various cognitive processes (Cavanagh and Frank 2014) such as memory retention, novelty detection, processing of negative rewards (Van de Vijver et al. 2011) and goal maintenance (Voytek et al. 2015). Within the BG, theta is found to increase in the rat striatum during a decision-making task (Tort et al. 2008), while in humans, theta in STN increases during sensorimotor conflicts (Zavala et al. 2015). Gamma, on the other hand, is mainly associated with active information processing and feature binding (Eckhorn et al. 1988; Fries 2005, 2009). Unlike alpha and beta, it is characterized by high amplitudes during movement (Singh et al. 2011; Joundi et al. 2012) and in combination with theta, it facilitates communication between different cortical areas, thus enabling high-level cognitive control such as the simultaneous maintenance of behavioural goals (Voytek et al. 2015).

Interestingly, both gamma band and theta at 5 Hz minimized input-output information flow from the simulated cortical ensembles to the SNr and enabled only the indirect pathway without any modulation from the STN-GPe loop. This similar connectivity pattern indicates that any combination of these two rhythms, as in the aforementioned studies, will also bring the BG to the same state. Hence, our model suggests that cortical information which has been generated and processed via alpha/gamma rhythms is not able to circulate through the cortico-BG-thalamo-cortical loop, without the presence of another low-frequency band.

Furthermore, in the case of gamma, the D1 striatonigral MSNs acted as an information *sink*, receiving strong inputs from the cortex but with a minimal impact on the SNr, while theta rhythms caused GPe to fire spontaneously and dominate the behaviour of the output SNr, thus acting as an information *source*. This effect in the GPe was sensitive to the phase of theta, and it was most prominent when the phase of the stimulated (phasic) channel followed in time the phase of neighbouring-channel oscillations, particularly at an offset of $\phi \approx -\frac{\pi}{2}$.

All things considered, a picture emerges regarding the function of the BG during cognitive processing at theta/gamma rhythms. Our model's behaviour in these two bands can be viewed as a mechanism that isolates the cortex from the environment, while new information is being

processed in multiple cortical regions. In the case of a sensorimotor conflict, theta is increased in the cortex, and the GPe is 'instructed' to inhibit SNr in order for the conflict to be resolved. This behaviour is different than in the case of alpha, which boosted the circulation of information via the BG, while inhibiting relevant motor actions with the facilitation of the indirect pathway. Hence, due to the distinction between the aforementioned bands, the cortex acquires the ability to process information through a variety of streams, either by using intermediary subcortical structures, or directly, across different regions.

Although there is no direct connection between GPe and theta function, inhibition of this structure via deep brain stimulation (DBS) has been found to improve cognitive symptoms of Huntington's disease (Temel et al. 2006; Ligot et al. 2011; Beste et al. 2014), a condition that is associated with episodic memory loss (Montoya et al. 2006) and increased ectopic theta (Pignatelli et al. 2012) (for a review see Nagel et al. 2015), among other symptoms. However, further work is required to verify the above computational predictions, and to answer to the emerging questions regarding the BG function. From an experimental perspective, the role of theta in the GPe, as well as BG effective connectivity changes during behaviour, require extensive investigation. In addition, computational modelling could shed light on the possible combinations of the above mechanisms and the transient versus steady-state dynamics that emerge. Finally, an interdisciplinary investigation on how the effects of the above pathological frequencies can be cancelled out could potentially boost current research on adaptive DBS techniques (Little et al. 2013).

4.3.3 The STN-GPe circuit

The fact the GPe becomes silent during the phasic mode in our simulations does not contradict with the literature. First, this behaviour reflects to only a very small portion of GPe neurons that are associated with the microscopic channel that exhibits a phasic response. Second, the recordings of this work are conducted for two simulated seconds when the cortical input maintains a steady firing rate (either oscillatory or completely fixed). In real conditions, feedback from the BG via the thalamus, would cause changes to the cortex after some milliseconds of the initial GPe inhibition and the input that the BG receives would be modified accordingly. In fact, it has been shown in primate recordings (**Nambu:2002**; Kita et al. 2004) that GPe neurons are inhibited transiently for approximately 25 ms after cortical stimulation.

As illustrated in Fig.4.3.C, the existence of a closed loop between STN and GPe contributes to the maintenance of cortical frequencies in the alpha band, and their blockage in higher bands. Without feedback inhibition, the STN-RB neurons succumb to the cortical beta rhythms, due to their natural tendency to engage in beta activity (Fig.4.2). Then, we showed that at the same

alpha frequencies, the direction of information flow inside the STN-GPe loop changes depending on the relative phase of the stimulus versus other background oscillatory activity that influences neighbouring areas. Both these remarks highlight the strong functional connection between this internal loop and cortical low oscillations.

A closer examination of the effect of the phase offset ϕ reveals a number of modes of the STN-GPe function, able to trigger a competition between the two involved pathways (indirect/hyper-direct) over the range of possible values of ϕ. An example behaviour for alpha frequencies is illustrated in Fig. 4.5, where both the absolute magnitude and the sign of $\phi \in [-\pi, \pi)$ contribute to the outcome of this competition. While large alpha offsets always activate the indirect and suppress the hyper-direct pathway, values close to zero have the opposite result, notably when the strong input signal is preceded by background oscillation in neighbouring channels. This asymmetry cannot be observed in the direct pathway, which is not directly influenced by either STN or GPe. Thus, its TE maximises monotonically and smoothly around $\phi = 0$.

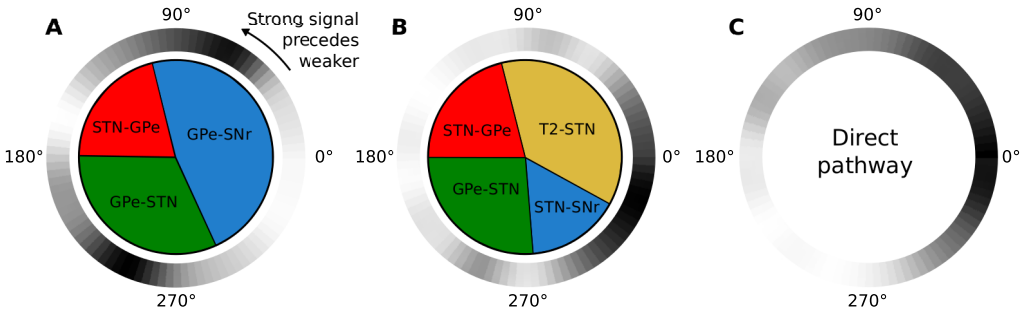

Figure 4.5: **Competition of STN-/GPe-mediated pathways triggered by cortical alpha.** Inner circle: Synaptic connection that involves (**A**) the GPe or (**B**) the STN, with the maximum TE. Outer circle: Normalized TE of the indirect (**A**), hyper-direct (**B**) and direct (**C**) pathways as defined in Fig. 4.4.

These observations lead to a hypothesis that views the impact of the STN-GPe loop as the result of two coexisting mechanisms. First, the rhythmic inhibition and excitation of the SNr by these two structures may act as a force that attempts to align the phases of different cortical low-frequency signals, in order to achieve optimal communication (Fries 2005, 2009). However, although perfect phase alignment can maximize information exchange in neural populations, optimal behavioural performance often requires more metastable dynamics (Cagnan et al. 2015). Hence, as an additional mechanism, the BG may be able to impose a veto on two conflicting signals, via the excessive activation of the indirect pathway, in case that the above process results in the wrong alignment, i.e. an amplitude difference that favours the leading signal. This veto can be released if the balance of amplitudes changes, and the leading signal increases its impact on its counterpart. This mechanism could allow the BG to function in a Hebbian fashion and

provide the right temporal conditions for the integration of anatomically distinct signals.

The credibility of this hypothesis can be further tested by the addition of neural cortical oscillators as well as a thalamic nucleus to the model presented in this study. This would allow the reverberation of the same cortical signal through the BG and reveal the conditions under which a coalition of cortical ensembles can be phase-coupled via the influence of the STN-GPe circuit.

All in all, the great variability of responses observed during our simulations highlights the extensive repertoire of BG functions. These cannot be completely captured by the analysis of this chapter, even in the toy case of fixed dopamine and steady cortical inputs with fixed frequencies. Nevertheless, our study showed that oscillatory frequencies and phase alignments could be the means by which the cortex selects between these functions, and led to a number of predictions that can be tested in future work.

==

5 The role of bursts and pauses of neurons in the globus pallidus externa

5.1 Introduction

Traditionally, GPe neurons in primates have been thought to consist of two types with different spiking behaviour (DeLong 1972; Bugaysen et al. 2010). One type exhibits high frequency firing with spontaneous pauses (HFP), while the second evokes low frequency spikes with periods of spike bursts (LFB). However, since intracellular recordings in primate GPe cannot be obtained, it is not yet clear whether these two distinct behaviours are the outcome of electrophysiological properties, or different network connectivity (Bugaysen et al. 2010), although recent evidence indicates that both genetic (Mallet et al. 2016) and anatomical (Kim and Kita 2013) factors play a role in this distinction.

To deal with this issue, computational models of the BG circuitry often consider the rat globus pallidus (GP) as a point of reference, which is found to be homologous of the primate GPe (Gerfen and Wilson 1996). This contrivance expands significantly the range of biological data that can be used to model GPe neurons, due to the numerous extracellular recording studies with rodents that focus on this structure (Schwab et al. 2013).

Conveniently, two prominent populations of neurons have been also consistently identified in the GP of freely behaving rats, which share similar characteristics with the two primate GPe types (Mallet et al. 2008; Benhamou et al. 2012). In rat brain slices, on the other hand, conflicting evidence suggests that the distinction between GP neurons diminishes (Cooper and Stanford 2000; Mallet et al. 2012; Deister et al. 2013), thus reinforcing the view of important network-level variations that have a great impact in spiking behaviour.

Bugaysen et al. 2010 performed analysis on intracellular parameters and firing patterns of GP *in vitro* cells and discovered three clusters of statistically different cellular properties. These three distinct neural groups exhibited differences in their voltage-current and frequency current relations, as well as after-hyperpolarization, spontaneous firing rates and action potential adaptation ratios, among others. The combination of two of these groups into a single super-group allowed a better twofold classification of the GP neurons, and exposed differences in a higher number of cellular properties.

This chapter is focused on the investigation of how these two antithetical behaviours emerge in the GPe, and what role they play in regulating the BG function. The main tool of this

study is the neural model of the BG circuitry, which was presented in Chapter 3. Following the methodology in Bugaysen et al. 2010, the neurons that compose the GPe nucleus in this model have been fine-tuned to correspond to the three types of GP neurons found in this experimental study.

The fidelity of spiking neurons in imitating the dynamical behaviour of biological cells offers a rich ground for studying the dynamical differences between these neuron models, both as a part of a network in simulated *in vivo* conditions, and as isolated systems. Nonetheless, simple phenomenological models are often inadequate for explaining the cause of the neuron's underlying behaviour, which might be a result of intracellular ionic mechanisms. Hence, in addition to the above network model of single-unit spiking neurons, an ionic-based multicompartmental model of the GPe, based on the equations by Hodgkin and Huxley 1952, was employed as a part of the current investigation.

5.2 Modelling cortical input

In order to simulate *in vivo* healthy conditions in the primate GPe, the complete model of the BG circuitry has been employed. A significant difference between the experiments in the previous chapters and the current methodology stems from the current need to investigate how this area would behave within a fully operational brain, instead of under ideal oscillatory conditions. This would allow us to compare the behaviour of the resulting computational model with data from healthy monkeys (DeLong 1972; Bugaysen et al. 2010; Benhamou et al. 2012) and animal models of Parkinson's disease (McConnell et al. 2012).

Hence, to model cortical stimulation to the BG input structures, a new approach was followed. The cortex is again represented by three neural ensembles of 1000 neurons each with uncorrelated firing rates. However, instead of the simple oscillatory pattern described with equation (3.13), the activity in each cortical channel is governed by a more complex spike train generator. In particular, the spike events of each neuron i in each cortical ensemble are drawn from a doubly stochastic Poisson process (Cox process), as in the algorithm presented in Krumin and Shoham 2009. This is a Poisson process where the parameter λ_i is also a stochastic process. An important property of Cox processes is that they have the ability to preserve the correlation structure of the nested process λ_i (Krumin and Shoham 2009), which in this case is also called stochastic intensity function.

In this model, the stochastic intensity function follows a reflected Gaussian random walk. That is,

$$\lambda_i(t) \sim \mathcal{N}(\lambda_i(t-1) - \beta, \sigma) \tag{5.1}$$

where $\beta \geq 0$. If $\lambda_i(t) < 0$, then $\lambda_i(t) = -\lambda_i(t)$ to satisfy the reflection property.

The parameter β denotes the asymmetric tendency of this random walk towards low values, which was selected to avoid extended periods of high local activity that are seldom present in the cortex. The resulting firing rates follow a half-normal distribution, as illustrated by the histogram of Fig. 5.2.C. The parameters σ and β were tuned to be consistent with behavioural recordings of corticostriatal neurons in primates (Turner and DeLong 2000), and the cortical firing rate restrictions described in Chapter 3. This process resulted in the values $\sigma = 0.5$ and $\beta = 0.05$.

One major advantage of this approach is that the generated time series are highly correlated across neural units of the same ensemble, while, due to the Markov property, any time correlation is destroyed.

5.3 Results

5.3.1 High-frequency GPe neurons produce pauses caused by over-excitation

Although the original study by Bugaysen et al. 2010 showed that the three types of GPe neurons that emerged (A, B and C) exhibit different dynamical behaviours, our resulting models can be better classified into only two dynamically distinct subgroups that have significant statistical differences. The firing patterns of these two groups agree well with the two categories of neurons found in the primate GPe. Fig. 5.1 illustrates the basic properties of the three tuned neuron models that show distinct electrophysiological characteristics. Neurons of type B (GPe_B) can fire at high frequency rates, with short action potential duration (AP_{dur}) and fast action potential after-hyperpolarization (AHP). As a response to hyperpolarizing current, they generate rebound firings whose number increases with the intensity of the hyperpolarization. By contrast, neurons of types A (GPe_A) and C (GPe_C) are limited to lower firing rates with very long AP_{dur}. They do not produce any rebound effect but they have similar AHP amplitudes to GPe_B neurons.

The dynamical behaviour of the three GPe neuron types was more extensively compared by means of the corresponding (v, u) phase plane trajectories. A sample of 50 vectors (v_i, u_i) was drawn for each neuron type in a single point of the phase plane, after random perturbations of the neuron capacitance $C_i \sim N(C, 20\text{pF})$, and a two-sided T-test was applied to all pairs of neuron types. This procedure was repeated for 1000 randomly selected points in the phase plane, in order to examine statistical differences in neuronal behaviour for different initial conditions. The resulting mean p value of the test between A and B types was 0.00102, with 0.2% of the p values above 0.01, between A and C types: 0.03195 with 10.4% of the p values above 0.01 and

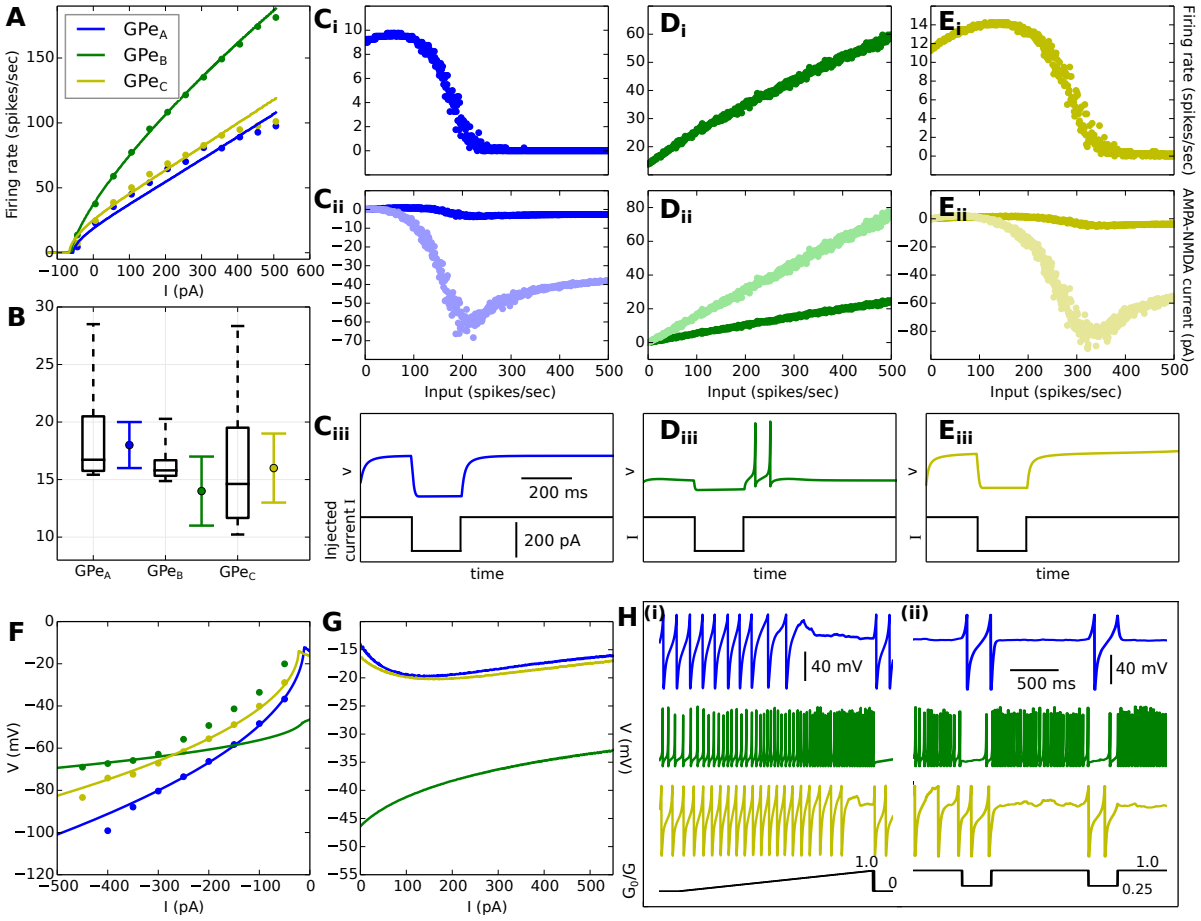

Figure 5.1: **Properties of GPe neurons. A:** F-I curves of the three tuned GPe models (solid lines). The coloured dots represent real data of the corresponding GP neuron types retrieved from rat slices in Bugaysen et al. 2010. **B:** Box plot of the AHP amplitudes for varying capacitance C, along with the real mean and std for each neuron type retrieved from the same study. **Ci-Ei, Cii-Eii:** The relation of the excitatory presynaptic event frequency with (i) the firing rate and (ii) the conductance of individual excitatory channels, averaged for 2 seconds. **Ciii-Eiii:** Responses of GPe neurons to hyperpolarizing current reveals rebound behaviour in GPe_B cells. **F,G:** V-I curves of the same neurons. Again, the coloured dots represent real *in vitro* data retrieved from the same study. **Hi-ii:** Responses of GPe neurons to 150 spikes/sec excitatory input for varying maximum conductances G_{AMPA} and G_{NMDA}. In (ii), neurons also receive a weak negative current $I_{spon} = -34$pA.

between B and C types: 0.00014 with again 0.2% of the p values above 0.01. Hence, for almost any initial condition we can reject the null hypothesis that the trajectories of GPe_B neurons are identical to other GPe neurons, while this is not always the case between GPe_A and GPe_C neurons.

Furthermore, GPe_A and GPe_C neurons also differed from GPe_B with regard to the firing patterns produced under synaptic stimulation. Whereas GPe_B neurons always fire in tonic patterns, directly proportional to the input intensity, strong activation of EPSCs in GPe_A or GPe_C neurons results in irregular firing rates or silence (see Fig. 5.1.H). This behaviour is reminiscent of neural accommodation, an effect that has been frequently observed in a small percentage of GPe cells *in vitro* (Kita and Kitai 1991; Cooper and Stanford 2000; Steiner and Tseng 2010). In the case of our model, it is caused by the conductance-based nature of the glutamatergic chemical synapses. The slow depolarization of these neurons at the initial stage of action potentials (APs) can be easily prevented by the long-lasting NMDA receptor-evoked currents, that have an inhibitory effect for positive membrane potentials, as shown in Fig. 5.1.Ci-ii and Ei-ii.

Interestingly, the two categories of firing patterns, observed in GPe_B and $GPe_{A/C}$ neurons respectively, closely resemble the aforementioned behaviour found in primates, and thus further investigation is required to identify potential conditions that might be important for the expression of this behaviour.

5.3.2 Bursting and pauses in GPe can be modulated by STN depression

In Kim and Kita 2013, it was proposed that the generation of pauses in HFP neurons is, in part, a result of the enhanced inhibition during periods of MSN bursts, which is further facilitated by short-term plasticity in these synapses. Since increased striatal activity has been repeatedly correlated to the STN, the other major input structure of GPe, during cognitive tasks (Leventhal et al. 2012; Schmidt et al. 2013), it is likely that MSN bursts are accompanied by a similar behaviour in STN neurons that project to the same GPe channel. STN-GPe synapses have been found to exhibit short-term plasticity in periods of high-activation which initially is expressed with facilitation, taken over by depression after the first few spikes (Hanson and Jaeger 2002). Hence, although not included in the basic version of our model, since it is still not well understood, plasticity of these neurons might also contribute to the behaviour in GPe.

Exploring this idea, our simulations showed that both pauses and low-frequency bursts in GPe neurons might also be significantly enhanced by STN short-term depression. In Fig. 5.1.Hii, we provided a fixed inhibitory current to the three modelled GPe types, as well as enough excitatory synaptic input to cause silence to GPe_A and GPe_C neurons. Under these conditions,

a 75% depression of the excitatory conductances for small intervals was enough to generate pauses in GPe_B neurons and to break the silence of the rest. This amount of depression would be reasonable for extended periods of phasic STN activity, where the firing rate of STN neurons can be close to 40 spikes/sec (see Fig. 3.1 and STN-SNr depression in Effect of short-term plasticity in synaptic conductances). Further results that support our view of STN depression, based on simulations of the complete BG model, can be found in the next session.

The fact that GPe_A and GPe_C showed similar dynamics contradicts, in part, with the results in Bugaysen et al. 2010, where irregular firing patterns were found only in GPe_A neurons. However, since GPe_C neurons have shorter APs, it is possible that they might have displayed the same effect if tested for higher injected currents, which would be consistent with our model's behaviour. Following the same intuition, the authors of this study combined the parameters of GPe_A and GPe_C into a single super-group and discovered that the statistical differences between these neurons and GPe_C increased.

5.3.3 GPe bursts and pauses emerge in normal BG function and depend on cortical behaviour

To further examine the impact of this mechanism under normal BG conditions, we stimulated the model with random input, using the method described in section 5.2, that resembles the rich behaviour of the active cortex. An example of random cortical activity and the response of the model can be seen in Fig. 5.2.A. Although we used the same 3-channel configuration of the model that was defined in Chapter 3, here the activity of each channel is statistically identical. Nevertheless, a single microscopic channel was arbitrarily selected, while the data produced by the other two channels were isolated from the current analysis and treated as neighbouring activity. An example of the firing patterns produced during 2 seconds of simulated time can be seen in the raster plot of the same figure. The fluctuations of the stochastic intensity function of the selected channel, as well as the instantaneous firing rate of the corresponding BG output, is represented in black, in contrast with the rest of the neighbouring channels that appear in grey.

The first result of this simulation was the confirmation that the GPe neurons show the same anticipated firing behaviour *in vivo* conditions, that was analysed in the previous section. During a 30-minute simulated period, GPe_B neurons showed two different modes, being either active close to their average firing rate (~ 30 spikes/sec) or completely silent. For a detailed distribution of their firing rates, see Fig 5.2.B. These periods of pauses comprised the 1.77% of their overall activity and had a mean duration of 54^{+73}_{-16} ms. In addition, GPe_A and GPe_C neurons also exhibited two modes. They remained silent, for the majority of the simulation time, with some interruptions of activity in low firing rates. Overall, the bursting period comprised the 4.56% of

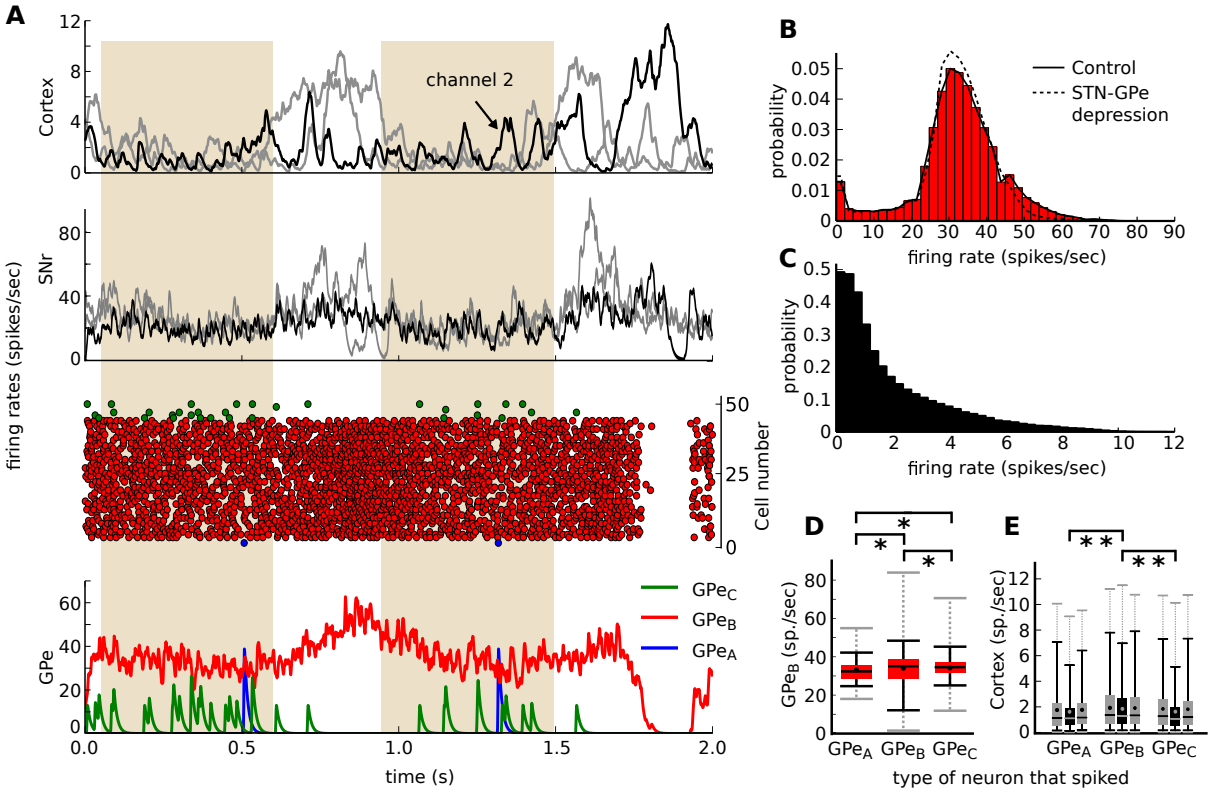

Figure 5.2: **Response of GPe neurons for random cortical input. A:** Input, driven by a Gaussian random walk $\sim \mathcal{N}(-0.05, 0.5)$, causes low-frequency bursts in GPe$_A$ and GPe$_C$ neurons and pauses in GPe$_B$ neurons. Notice that the dominance of channel 2 in the level of the cortex results in disinhibition of the thalamus by the SNr. **B:** Probability distribution of GPe$_B$ firing rates and **C:** cortical firing rates in any channel. **D:** Firing rate of GPe$_B$ neurons when GPe$_{A-C}$ neurons spike. The box plots indicate 25th/75th and 2nd/98th percentiles and the grey doted line min/max values. GPe$_A$ and GPe$_C$ fire only when the firing rate of GPe$_B$ is around its mean value. **E:** Firing rate of the cortex (grey colour neighbouring channels, black colour current channel) when GPe$_{A-C}$ neurons spike. Sample for B-E was calculated from 30 minutes worth of random input. Only GPe recordings in channel 2 are illustrated here. The single asterisk (*) denotes statistically different means (Z-tests with $p << 0.01$). In E, the mean values of each channel were examined individually and the double asterisk denotes statistical difference in all three pairs.

the GPe_A activity and the 44.91% for GPe_C neurons. Approximately, 66% of the GPe_A spikes occurred simultaneously with Gpe_C spikes (simulation timestep 0.01 ms), while there was no significant correlation between pauses and bursts.

The next step was to test the impact of MSN-GPe facilitation and STN-GPe depression, as discussed in the previous section. For the first case, we replaced the plastic inhibitory chemical synapses that arrive at the GPe with static, and used the reference value of the synaptic conductance $G_{MSN-GPe}$ found during connectivity tuning, while for the glutamatergic synapses from STN, we used (3.9) with the same parameters as in STN-SNr synapses. Without MSN-GPe facilitation, we observed a 41.73% reduction of pauses in GPe_B neurons (control significantly different, K-S p-score: 0.0543). With the addition of STN-GPe depression, the periods of bursts in GPe_C neurons were increased by 10.11% (control significantly different, K-S p-score: 0.0108), and the peak for type GPe_B neurons around their average firing rate became sharper, as shown in Fig 5.2.B.

Furthermore, we found that, as a general rule, GPe_A and GPe_C neurons release spikes only when the firing rate of GPe_B neurons is close to its average value. This window of activity, indicated with the shadowed regions in Fig. 5.2.A, has a similar mean value for both GPe_A and GPe_C neurons, but it is significantly wider in the latter case. Fig. 5.2.D illustrates a statistical sample that confirms the above observation. This behaviour is an expected consequence of the mechanism observed in Fig. 5.1 to limit action potentials via NMDA inhibition, and it is caused by a combination of all synaptic inputs that arrive at these neurons. Given the almost linear input-frequency relationship of GPe_B neurons, shown in Fig. 5.1.Di, that allows these neurons to reflect the level of activation of GPe afferents, it is also possible that GPe_A and GPe_C neurons release spikes only during specific firing regimes in preceding regions of the BG pathways.

Indeed, this relationship seems to originate from the cortex, where the distinction between the correlation of the latter with the different GPe types is less clear. While $GPe_{A/C}$ neurons showed a tendency to fire in periods when the overall cortical firing rate was close to the tonic level (3 spikes/sec), GPe_B activity was more tolerant to the variability of cortical spikes that arrive in neighbouring microscopic channels. Fig. 5.2.E illustrates that GPe_B firings required statistically higher cortical activity to fire, although the sample distribution in all cases had a similar width. In contrast, the activity of any of the three cortical ensembles connected to the different BG channels was found statistically indistinguishable when GPe_A or GPe_C neurons fire, a fact which strengthens the view that, in the network level, these two types compose a single part of the same mechanism.

In addition, GPe_B pauses occurred while the current microscopic channel received intense bursts of spikes from the cortex and the firing rate of the two neighbouring channels were below tonic

levels. More specifically, the cortical mean firing rate of the ensemble connected to the same channel was $6.54^{+8.3}_{-5}$, while the neighbouring ensembles fired at $1.86^{+2.4}_{-0.6}$ (samples significantly different, K-S p-score $<< 0.01$).

Finally, when GPe neurons located within a single microscopic channel fire, the activity of this channel in the level of the cortex is typically weaker than its neighbouring areas. Since only the same channel is able to evoke striatal inhibition to GPe, this is again an expected behaviour. However, as shown in Fig. 5.2.E, this relationship was not completely symmetric, although both cortical channels where driven by the same Poisson rule. The sample for this figure was produced from a 30-minute simulation of the model with a single random synaptic and neuron configuration. A repetition of the experiment with different random connections showed similar asymmetries but not necessarily in the same channel. This points to the specific random wiring as the source of this error and indicates its great impact, that cannot be regulated without the application of long-term plasticity.

5.3.4 GPe silence can be caused by local neural accommodation in (post-) synaptic sites

The long periods of silence that have been observed in some GPe neurons of our model are caused by an effect which is similar to neural accommodation. The latter is a phenomenon caused by desynchronization of the ionic processes that orchestrate an action potential. The contribution of the various ionic channels in this phenomenon is difficult to be analyzed with simple point-neuron models such as the equations (3.1-3.3). These models are phenomenological approximations of the membrane potential of real cells, and do not explicitly simulate individual ionic currents, in contrast to the equations by Hodgkin and Huxley 1952. However, the $\text{GPe}_{A/C}$ neurons of this study were able to capture electrophysiological and behavioural features of the corresponding biological types found in Bugaysen et al. 2010, that are likely to be a result of complex ion interactions (Fig. 5.1-5.2). This implies that the optimization process that was employed here might have converged to a combination of parameters for the model's equations that accounts for a similar behaviour without the existence of such an ionic mechanism. On the other hand, as this behaviour was not part of the objective function used for optimization, it could very well be a side-effect of the mathematical equations used.

To shed light on this issue, we tested how well our findings can be replicated using a multicompartmental model of a GPe dendritic branch, based on the ionic equations by Hodgkin and Huxley 1952. The simulated branch has a diameter of $1\mu m$, specific membrane resistivity $Ra = 1.47\Omega m^2$, specific membrane capacitance $C_M = 0.024F/m^2$, and specific axial resistivity $R_A = 1.74$. These basic electrical and morphological properties of the GPe cells were optimized

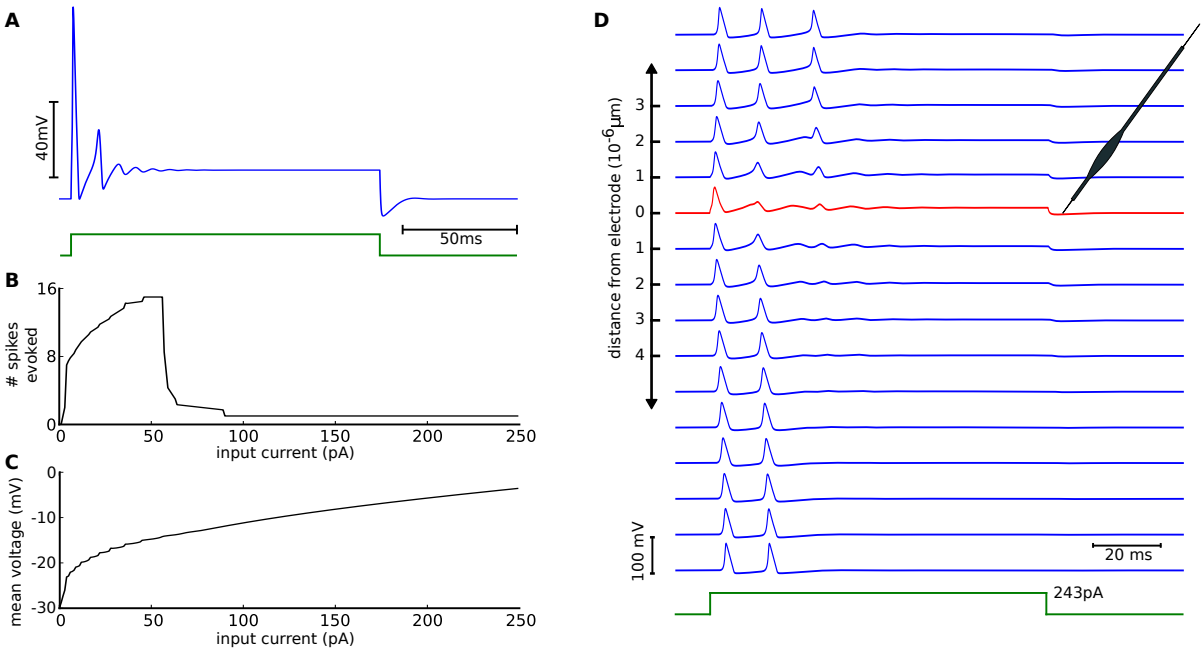

Figure 5.3: **Accommodation in dendritic spikes using the Hodgkin-Huxley model A:** Neural accommodation in a single compartment. **B:** Frequency-current (F-I) and **C:** voltage-current (V-I) relation of the model in (A). **D:** Propagation of dendritic spike in a model with 16 compartments of equal distance.

in Hanson et al. 2004 and used in Günay et al. 2008; Hendrickson et al. 2011. The resulting behaviour is illustrated in Fig. 5.3.

As this model indicates, the silence observed in $\mathrm{GPe}_{A/C}$ neurons of our BG model can be largely reproduced based on ionic channels and the morphology of GPe dendrites. In particular, the local F-I relation of the multicompartmental neuron in Fig. 5.3B follows a significantly similar trajectory to the input-current relation of the models shown in Fig. 5.1Ci and 5.1Ei. This silence is caused by excessive excitation in the stimulating area of the dendrite, which prevents any depolarization to propagate to the rest of the dendrite (Fig. 5.3D). As a result, although locally the membrane potential of the dendrite exhibits neural accommodation, this effect is undetectable even in areas that are located within a very short distance from the stimulation point ($> 10^{-5}m$).

Additionally, as illustrated in Fig. 5.4C, our simulations show that successful action potentials generated before the area affected by neural accommodation might not be able to surpass this local spike veto and, therefore, their propagation fails. This increases significantly the likelihood of a neuron to remain silent for long time intervals in case that the blocked synaptic site is located in a central dendritic hub.

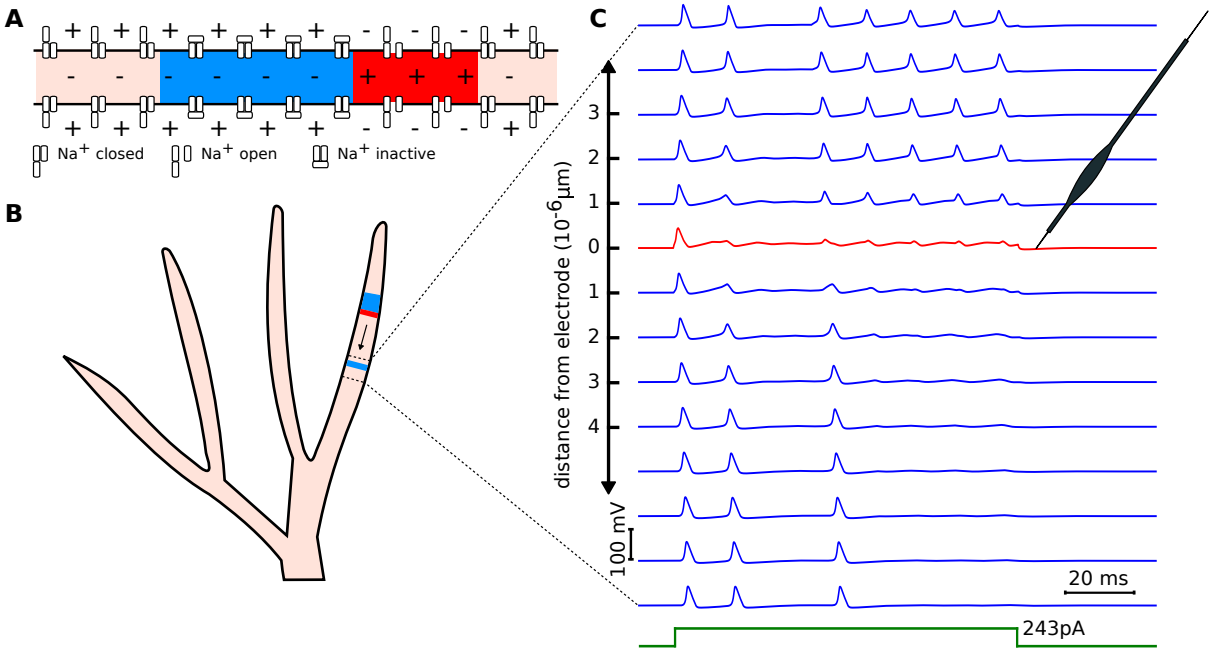

Figure 5.4: **Neural accommodation in GPe dendrites A:** Na^+ channels normally block back-propagation during action potential propagation. **B:** Illustration of an action potential blockage in an artistic representation of a part of a GPe dendrite. **C:** The same effect simulated in a model with 16 compartments of equal distance.

5.4 Discussion

5.4.1 The role of GPe bursts and pauses in BG behaviour

In this chapter we performed an analysis on the activity of the GPe neurons in our BG model. The two distinct *in vivo* behaviours, observed in primate GPe neurons (DeLong 1972) and rat's GP (Benhamou et al. 2012), emerged after tuning Izhikevich neurons to behave as GP cells recorded *in vitro* in Bugaysen et al. 2010. Short-term plasticity and cortical activity were both found to modulate this behaviour, although the role of the former was not decisive. In particular, pauses in GPe_B neurons occurred in periods of high activity in pre-synaptic cortical neurons, combined with low activity in neighbouring cortical channels. Low frequency bursts, on the other hand, were expressed by $GPe_{A/C}$ neurons and were evoked during low overall cortical activity, especially when the instantaneous firing rate of GPe_B neurons of the same channel was within a small range around its average value (~ 30 spikes/sec).

The cross-correlation between LFB spikes and the firing rate of HFP neurons could be tested in existing *in vivo* recordings, such as in DeLong 1972; Bugaysen et al. 2010 or Benhamou et al. 2012. A potential confirmation of the patterns we observed here would offer new insights into

the role of the GPe cells in the BG function and increase the validity of the remaining predictions made with our model. However, even if these predictions were validated, their impact to the normal function of the BG is still unclear. Since the LFB and HFP dichotomy is largely retained in different types of mammals, including rats and primates (Gerfen and Wilson 1996), it is highly likely that it constitutes a fundamental mechanism underlying the functional role of GPe.

An initial aid in understanding this mechanism is offered by the genetic distinction between cells that exhibit LFBs and HFPs. It has been recently found that the LFB behaviour, which is captured with $GPe_{A/C}$ neurons here, is largely expressed by Arkypallidal cells in GP (Mallet et al. 2016). These cells are anatomically unique, as they send inhibitory projections back to the MSN neurons in the striatum (Gittis et al. 2014), instead of the STN and SNr, like the majority of GPe neurons. Through this pathway, Mallet et al. 2016 shown that Arkypallidal neurons are able to block any striatal activation that corresponds to the generation of a new imminent action, and thus cause a STOP response in behavioural tasks.

Following the same line of reasoning, we argue that the function of LFB neurons may extend beyond cancelling imminent actions, to more cases in decision making. Our results suggest that, without the presence of salient cues, LFB neurons fall into an almost silent regime caused by excess excitation by STN. However, cortical signals that disturb the balance between STN excitation and striatal inhibition to GPe are able to stop this veto and evoke bursting responses by these neurons (Fig.5.2). In fact, since strong cortical signals cause the short-term facilitation of the MSN-GPe synapses (Sims et al. 2008), an imbalance of this sort could be theoretically maintained until the effect of plasticity decays. Hence, the inhibitory feedback from LFB neurons provides a good candidate to modulate this over-excitation and restore MSN baseline activity.

This view agrees well with the two-step model of action suppression in Mallet et al. 2016. Although our simulations show that LFB neurons fire in response to some input disturbances, they are completely suppressed during strong cortical input. This mechanism can provide to the STN-SNr pathway a temporal lead to initiate a fast pause process, before GPe-STN inhibition regulates STN activity and the indirect pathway engages in a more selective cancellation.

A more thorough theoretical investigation is required in order to understand this mechanism. However, the current BG model does not capture the connectivity differences between GPe neuron types, since the input pathways to these neurons and their lateral connections are still partially unknown (Humphries 2014; Mallet et al. 2016).

On the other hand, the connectivity of HFP neurons, which comprise the remaining $\sim 75\%$ of the GPe, is richer but their main function seems more straightforward. These neurons send their strongest topographic projections back to the STN, but they also project to the outputs of the BG, thalamus and amygdala (Mastro et al. 2014). Hence, they are able to regulate over-activity

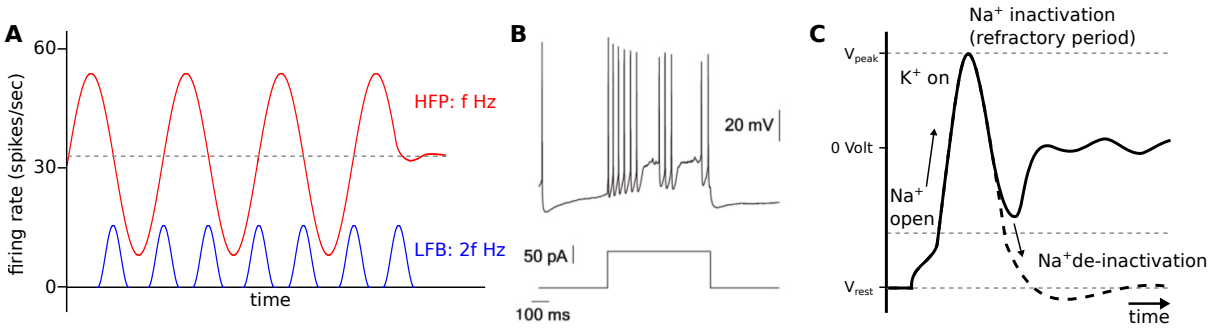

Figure 5.5: **Pauses in GPe neurons. A:** Illustration of the hypothesis of harmonics amplification by LFB neurons. Oscillatory activity in the cortex drives HFP neurons and evokes bursts in LFB neurons only around tonic levels. **B:** *In-vivo* recording of a real GP neuron that exhibits accommodation. Figure taken from Bugaysen et al. 2010. **C:** Accommodation in dendritic spikes. Strong synaptic input keeps the membrane potential close to zero, while Na^+ channel inactivation prevents the neuron from firing again.

of the STN via this feedback loop, and mediate the BG indirect pathway by providing inhibition to the SNr.

Pathologically, one plausible impact of the imbalance of the LFB inputs is the disturbance of the oscillations in the BG. Due to their narrow window of activation, these neurons create resonances that amplify higher-level harmonic frequencies in the pathways that involve the GPe. This concept is illustrated with a theoretical example in Fig. 5.5A.

Enhanced harmonic frequencies are present during application of deep brain stimulation (DBS) in GPe (McConnell et al. 2012), in GPi (Singh et al. 2011), and at resting Parkinsonian tremor frequencies in the cortex (Raethjen et al. 2009). A coherence analysis in the later study showed non-parallel time courses for the basic and first harmonic frequencies, which points to the existence of different origins for these two oscillations. A similar effect was also observed in the current BG model, where harmonics of cortical oscillations were significantly strengthened at low frequencies in the BG nuclei without any signs of cortical coherence (see Fig. 4.3).

5.4.2 Is the silence of LFB neurons biologically plausible?

The extended periods of silence in the LFB neurons of our model were evoked due to their selective nature, which allows spikes to occur only during a particular range of instantaneous firing rates in excitatory afferents (Fig. 5.2D-E). Below this range, neurons succumb to striatal inhibition, while for stronger excitation they exhibit neural accommodation. The main drawback of this mechanism is that it relies on inhibition caused by NMDA currents, when the membrane potential of these neurons exceeds the NMDA reversal potential. This is not a common effect

in biological neurons and arises, in part, from the single-point nature of simple spiking neuron models, where synaptic dynamics directly couple with neuron's soma, as discussed in Humphries, Lepora, et al. 2009.

However, we argue that, instead of a limitation of point models, this effect here could capture an existing biological process. Unlike the MSN neurons in the above study, the long and thin dendrites of GPe neurons have high concentrations of fast voltage-gated sodium (Na^+) channels at the sites of glutaminergic synaptic inputs (Hanson et al. 2004). This clustering was shown to create favourable conditions for spike initiation, and it was found to evoke dendritic spikes at these sites, even in response to weak input. Hence, it is possible that, during depolarization, the slowly decaying glutamatergic synaptic receptors at these sites, such as NMDA or namely NMDA and metabotropic receptor 1 (mGluR1), can cause inhibition to the neuron's membrane potential, when the latter is higher than the local equilibrium potential. In particular, after a successful action potential, strong and long-lasting synaptic currents can maintain depolarization above the threshold value, below which the Na^+ channels reset to their open state (de-inactivation), thus leaving the neuron unable to initiate a new spike (Fig.5.3C).

The literature offers a considerable amount of evidence that supports this hypothesis. The ability of a neural cell to adjust its action potential threshold above the level of a constant stimulus is referred to as neural accommodation. Accommodation is believed to be caused by the combination of a premature rise of the Na^+ inactivation process and an increase on the level of potassium conductance, which raise the equilibrium of the membrane potential and make the cell unable to fire (Hodgkin and Huxley 1952).

Within the GPe, a subset of neurons have been found to express strong neural accommodation, both *in-vitro* (Nambu and Llinas 1994), and in anaesthetized animals (Kita and Kitai 1991). In addition, a study on guinea pig brain slices showed that strong accommodation is closely related to the type of GP neurons that exhibit silence and low-frequency bursts (Nambu and Llinas 1994).

Furthermore, inputs from the STN are closely linked to this phenomenon. Short-term exposure to strong glutamatergic inputs can provide a long-lasting boost to the generation of neural accommodation in GPe neurons. In particular, *in-vitro* stimulation of STN axons in rats revealed that repetitive activation of their synapses generates a state of continuous depolarization to GPe neurons, which can last for several seconds (Kaneda et al. 2007). This increase, when combined with slow NMDA currents, could bring the membrane potential of these neurons closer to NMDA equilibrioum potential, or above the threshold where Na^+ inactivation ends.

Despite those facts, however, the majority of GPe neurons do not exhibit long periods of silence. One plausible explanation for this is the fact that dendritic spikes cannot be initiated in all GPe

neurons. This has been attributed to the strong variation of channel conductance densities, the same reason that these neurons exhibit high heterogeneity of dynamical behaviour (Günay et al. 2008) and input integration (Edgerton et al. 2010).

Even if the above prediction is verified, a remaining question is whether neural accommodation in a synaptic site can influence spike propagation to an extend that allows it to block spikes in the neuron's soma. GP neurons with strong accommodation have been found to stay unresponsive to STN stimulation (Kita and Kitai 1991), indicating that this question deserves further investigation. A possible explanation can be found in the same mechanism that the neurons normally use to prevent back-propagation of action potentials, namely Na^+ inactivation (Fig.5.4A). Since these voltage-gated receptors are disabled during their inactivation state, they cannot contribute to neither active nor passive conduction (Fig.5.4B). As a result, the only available means for excitatory signal propagation is calcium-based channels, which require however high voltage activation and they are more uniformly distributed across GPe dendrites (Hanson and Smith 2002).

Moreover, the mechanism observed in the $GPe_{A/C}$ requires these neurons to produce wide APs that are long enough to be subject of inhibition by glutamatergic currents (Fig. 5.2). Such widths are significantly longer than observations in real GPe neurons in Bugaysen et al. 2010. However, the stimulation in this study was based on post-synaptic current injection, and the response of the neuron was captured at the level of the soma. Both these factors contribute to the recording of sharper spikes and sub-threshold behaviour that is not directly coupled to synaptic receptors. In contrast, dendritic spikes, which are evoked by synaptic stimulation, have been shown to be longer than 30 ms in cortical pyramidal neurons *in-vitro* (Larkum et al. 2007), and thus they are consistent with the our $GPe_{A/C}$ models. The same neurons produced somatic spikes that were shorter than 3ms.

It is also illustrated that, *in vivo*, primate LFB neurons of the GPe exhibit sub-threshold oscillations closer to their AP overshot period (Bugaysen et al. 2010; Benhamou et al. 2012) (Fig. 5.5B). This is also in line with the behaviour in Fig. 5.1.H and indicates that an analogous blocking mechanism to the hypothesized dendritic accommodation might be present across the GPe neurons membrane including their somas. Finally, $GPe_{A/C}$ neurons follow the same tendency of having longer somatic AP widths than GPe_B, which may be greater than 1.5ms (Kita and Kitai 1991).

Computationally, the above issue can be overcome, and the same silence can be observed in neurons with shorter AP widths, if the STN-GPe glutamatergic synapses have a reversal potential lower than the typical value of 0 volts which was assumed here. In biological neurons, the variability of equilibrium potentials can be attributed to the existence of different concentrations

of voltage-gated ionic channels, a feature of GPe neurons that was explored inGünay et al. 2008.

All things considered, the models of the present study gave rise to a number of interesting predictions regarding the neurons in the GPe, that could be tested in future work. The most fundamental predictions indicate that the blockade of slow glutamate receptors in this nucleus, namely NMDA and mGluR1, can reduce accommodation and increase responsiveness to STN stimulation *in-vitro*, as well as reduce the silence of LFB neurons *in-vivo*. Additionally, we predict that pauses in HFP neurons occur when the salience of a cortical afferent signal exceeds a threshold. This mechanism could potentially inhibit neibouring microscopic channels throughout the BG-thalamo-cortical loop, in order to further boost the dominance of the most salience channel, forming a winner-takes-all device (Redgrave et al. 1999).

A possible future direction for the network model of the GPe is the optimization of its connectivity, in order to to be consistent with the recently identified circuitry of 3 genetically distinct neuron types in Gittis et al. 2014. These neuron types have been suspected to map directly onto the LFB/HFP dichotomy (Mallet et al. 2016). According to this theory, the arkypallidal GPe neurons correspond to LFBs and receive stronger inputs, while HFP neurons send stronger inhibitory signals back to the STN.

Nevado-Holgado et al. 2014 used genetic algorithms to optimize a rate-based model of the BG, and identify the GPe effective connectivity that fits to electrophysiological recordings from rat models of PD, taken from Mallet et al. 2008. This approach can be followed again, using the large-scale neural model of the BG circuit described in Chapter 3, and used to approximate the structural connectivity of the healthy GPe. Our model could be then employed to study the observations in Gittis et al. 2014, according to which the two main GPe neuron types partition into a synchronised and a desynchronised subset respectively during low-frequency cortical oscillations.

6 Assessing selectivity in the basal ganglia

In previous chapters, we presented a neural model of the basic BG circuit, built in a bottom-up fashion, which was used to make predictions regarding the low-level behaviour of this brain structure. This model was validated by means of a comparison with the firing rate relations of the real BG nuclei, as well as the oscillatory behaviour of the whole structure, both in healthy and pathological conditions. Hence, having established the required level of biological realism, the next step is to employ this model to investigate fundamental properties of biological cognition, such as decision making.

6.1 Introduction

The physical location of the BG, as well as their broad bidirectional connectivity with major cortical areas, the limbic system and the thalamus, place the this brain structure in a key position to modulate the flow of information between the cortex and the body. Despite the great diversity of inputs and outputs, the human BG consist of the same repeating internal circuitry (Alexander et al. 1986) which is also largely retained in most vertebrate species (Reiner et al. 1998; Stephenson-Jones et al. 2011). This strictly topographic organization on different scales suggests that through this structure, some common modulatory operations are applied to functionally different channels of information flow.

In the microscopic scale, the BG circuitry can be broken down into a massive number o parallel loops (or channels) which, as suggested, represent different competing information signals or "action requests" (Humphries et al. 2006; Gurney et al. 2015). According to this popular theory, the BG circuit is able to process those requests and finally select the most salient (or urgent) potential action, via the direct BG pathway, while providing inhibition to the rest competing channels via the indirect pathway (Mink 1996; Redgrave et al. 1999).

An increasing amount of neurophysiological evidence implicates the BG to selection of voluntary motor actions and provides indirect verification of this hypothesis (Friend and Kravitz 2014). Kravitz et al. 2010 showed that the excess activation of the direct BG pathway in freely behaving mice, via stimulation of MSN_{D1} neurons in the striatum, increases movement, while the stimulation of the indirect pathway made the same animals to freeze. In addition, although both pathways are required for healthy action selection and were found to contribute equally to the initiation of actions in Cui et al. 2013, the indirect pathway is suppressed during the execution of actions or action sequences (Jin et al. 2014), presumably because any behavioural conflicts

have already been resolved during movement (Friend and Kravitz 2014).

Low-frequency brain oscillations have been widely implicated in both the function of the BG (Brittain and Brown 2014) and the process of decision making (Zhang et al. 2008; Siegel et al. 2011; Brinkman et al. 2014). Oscillations in the cortex mediate the processing of new information (Fries 2009), the dynamic formation of neural ensembles that represent different actions and the suppression of other task-irrelevant regions (Siegel et al. 2009; Buschman et al. 2012). The are also found to encode uncertainty and influence the exploration-exploitation trade-off (Cavanagh et al. 2011). In addition, there is a substantial number of studies focusing on low-frequency oscillations in the BG, as changes of this activity are connected with a number of disorders such as PD or HD.

But are these phenomena related? Evidence suggests that oscillations in some certain bands in the striatum and STN, the input structures of the BG, are driven by cortical regions (Tseng et al. 2001; Mahon et al. 2006; Litvak et al. 2011; Kim and Kita 2013). Taking this into account, in Chapter 4 we explored the impact of cortical rhythmic activity on the BG function and we found that the former can completely shape which areas of the BG circuit are active. Yet, the connection between the BG, cortical oscillations and decision making still remains relatively unexplored.

In this chapter we attempt to narrow this gap by investigating whether cortical oscillations could influence the ability of the BG to act as a selection device. To achieve this, we initially defined a number of metrics that enable the assessment of the effectiveness of possible selection mechanisms. Using the biologically plausible neural model of the BG circuitry defined in Chapter 3, we then carried out an analysis of the relationship between cortical frequencies, dopamine concentration and BG selectivity.

We found that the frequency and phase difference between oscillatory cortical areas, the level of dopamine in the system and the examined time scale, all have a very important impact to the ability of our model to select. Our simulations resulted in a canonical profile of selectivity in the BG, which we termed selectivity portraits, that can be largely maintained in simplified versions of the model.

Using these portraits, we show that although the BG circuit can robustly and sequentially perform selection tasks, the strongly-active cortical areas instruct the mode of this selection via their oscillatory activity. Some frequency ranges promote the exploitation of actions of which the outcome is known, others promote the exploration of new actions with high uncertainty, while others simply deactivate the selection mechanism. Finally, we identified a selection cycle with a period of around 200 ms, which was used to assess the biological plausibility of the most popular architectures in cognitive science.

Our results agree well with experimental observations, provide new justifications and insights into oscillatory phenomena related to decision making and reaffirm the role of the BG as the selection centre of the brain.

6.2 Metrics

6.2.1 Selectivity

The view of the BG as the action selection device implies that their performance on this aspect could be evaluated based on measurable criteria, such as signal distinction. The further suggestion that the salience of an action is encoded in the local level of activity in the striatum and STN, which is directly affected by cortical input, can serve as the basis of this evaluation. Tomkins et al. 2013 defined selectivity in the BG as the ability of a neural mechanism to robustly distinguish competing signals. Although this definition is sufficient, the main focus of this study was confined to the difference between transient and steady-state effects, and it produced metrics that can not be applied in a more general case, such as the BG model of the current study.

Our aim here is to create a metric that is aligned with the features of our model but it also remains general enough to be used in other studies. The first step of this attempt is to find a method to measure the *distinctiveness* of a single selected channel. This can be defined as the ability of a channel to receive distinctively less inhibition than any other channel or, more specifically, the degree to which the following conditions are fulfilled: (a) The firing rate of the selected channel in the level of the SNr is close to zero, which is required in order to revoke inhibition in the thalamus, and (b) no other channel is far below tonic levels. These two conditions can be written as

$$a_j = 1 - \frac{F_j}{\max\{F_{tonic}, F_j\}}, \qquad b_j = \frac{\min F_{i\neq j}}{\max\{F_{tonic}, \min F_{i\neq j}\}} \tag{6.1}$$

where j is the examined channel, F_i is the SNr firing rate of a channel i and F_{tonic} is the tonic firing rate of the SNr ($\sim$ 25 spikes/sec). Since both denominators in (6.1) are upper-bounded by the value of the corresponding numerator, the product $\bar{D}_j = a_j b_j$ will always take values between $[0, 1]$ and reflects the requested measure. The special case of $F_j = \min F_{i\neq j} = F_{tonic}/2$ results in $\bar{D}_j = \frac{1}{4}$ and represents the baseline below which the channel j is indistinguishable. To

normalize $\bar{D}_j$, so the baseline lies in 0, the final *distinctiveness* $\mathcal{D}_j$ of a channel j is given as

$$\mathcal{D}_j = \begin{cases} \frac{1}{3}(4\bar{D}_j - 1) & \text{if } \bar{D}_j > \frac{1}{4} \\ 4\bar{D}_j - 1 & \text{otherwise} \end{cases}, \qquad -1 \leq \mathcal{D}_j \leq 1 \tag{6.2}$$

A graphical illustration of the above can be found in Fig. 6.1A. Using this metric we can now measure a number of properties of the BG selection mechanism. First, the *effectiveness* of the BG in selecting the most salient cortical input can be defined as

$$\mathcal{E} = \mathcal{D}_k, \quad -1 <= \mathcal{E} <= 1 \tag{6.3}$$

where k is the index of the most salient channel, i.e. the channel with the highest firing rate at the level of the cortex.

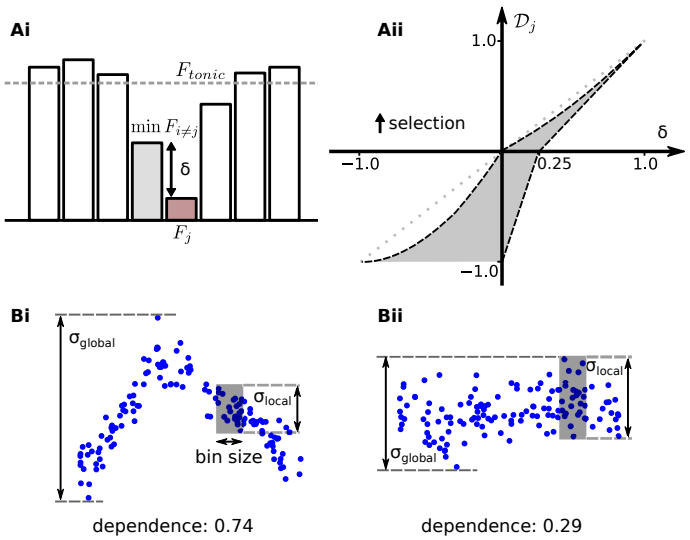

Figure 6.1: **Metrics for distinctiveness and dependence. Ai:** A multi-channel example of SNr firing rates used to illustrate the concept of distinctiveness of the channel j. **Aii:** Space of possible values for $\mathcal{D}_j$ for any difference δ between j and the least-inhibited alternative channel. Note that the line $\mathcal{D}_j = \delta$ is an upper bound to the possible values of $\mathcal{D}_j$ in this space. **B:** Example calculation of dependence.

Furthermore, the degree of *selectivity* of the BG reflects to their ability to select *any* channel regardless of its salience and can be defined as

$$\mathcal{S} = \max_j \mathcal{D}_j, \quad -1 <= \mathcal{S} <= 1 \tag{6.4}$$

Finally, one more useful property that can be measured using $\mathcal{D}_j$ is to what extent the BG is

selecting, or exploring, alternative actions. This is given as

$$exploration = \max_{j \neq k} \mathcal{D}_j, \quad -1 <= exploration <= 1 \tag{6.5}$$

and is defined as the level of exploratory behaviour of the BG mechanism, or simply *exploration*. To compare this metric with terminology commonly found in the literature, the value of effectiveness in the BG can be considered here as the level of *exploitativeness*, since the high salience of the leading microscopic channel arises from a previously learnt behaviour. Hence, selectivity can be then thought of as the union of exploration and exploitation.

To conclude, $\mathcal{D}_j$ can be used to measure various features of a neural-based action selection mechanism with minimal adjustments. The only requirements are first, a local measurement of the instantaneous firing rate in the output area of a neural structure, and second, a prior knowledge of the average tonic firing rate in the same area. In case that the latter cannot be obtained, the difference δ between the selected channel and the least-inhibited neighbouring area (Fig. 6.1Aii) provides a good approximation of distinctiveness, especially when $\delta > \frac{1}{4}$, and thus it can be used instead.

Transient versus steady-state

An event processed by a selection mechanism can have both a transient and a steady-state effect on a dynamical system such as the brain. Our BG model exhibited rich transient phenomena during the first $500ms$ after the injection of a stimulus, as well as a different post-transient steady state that was maintained indefinitely. To distinguish between these two modes, the *transient* distinctiveness of a salient channel is defined as the maximum degree by which this channel received less inhibition than any other neighbouring channel for a fixed short interval, after the generation of the salient signal. That is

$$\max_t \mathcal{D}_j^{[t-100ms,t]} \tag{6.6}$$

where $T + 100ms < t < T + 500ms$ and T denotes the point on time that the stimulation was applied. The *steady-state* distinctiveness, on the other hand, can be measured taking into account the post-transient stable firing rates in the level of the SNr.

6.2.2 Dependence

Selectivity can be affected by various parameters of the model or the current stimulus. Some of these parameters can play a decisive role in determining the model's performance. The degree

by which the BG selectivity depends on the value of a single parameter of the model can be measured by comparing the local versus the global variation of the resulting $\mathcal{D}_j$ for a number of simulation runs with random initial conditions.

For instance, in the case that selectivity is highly dependent on the value of a parameter, a significantly large sample of randomized simulation runs will result in diverse local mean values and small local standard deviations, compared to the standard deviation of the complete sample. An illustration of this concept is shown in Fig. 6.1Bi-ii.

This metric was used here to examine the effect of the phase offset φ between two oscillatory cortical inputs. In this case, local areas can be found by dividing the range of possible values for this parameter $R = [0, 2\pi)$ into a number of bins $R_i = \{x/x \in [a, a + dx), 2\pi \cdot a = i \cdot dx\}$, where dx is the length of each bin. Additionally, if σ_i is the standard deviation of selectivity values within the bin R_i and σ_{global} the global standard deviation in R, the *dependence* of the BG selectivity to φ can be defined as

$$dependence = 1 - \frac{\bar{\sigma}_i}{\sigma_{global}}, \quad 0 <= dependence <= 1 \tag{6.7}$$

For the analysis of this study we have used 30 local areas (bins) to calculate dependence, a number which was found to provide adequate and robust results.

6.3 A reduced version of the basal ganglia model

For the experiments conducted for the most part of this chapter, the full neural model described in Chapter 3 was used. However, this model contains a rather high number of parameters that might influence its behaviour and the resulting measurements of selectivity. In order to narrow down this space and establish the most important BG features for selectivity we defined an additional, simplified version of this neural model with significantly less differences between nuclei. This simplified model was then utilized for these experiments and the results were compared against the original model. The architecture of this model is shown in Fig. 6.2.

In this simulation, the striatum is modelled using only 600 D1-like and 600 D2-like MSNs with the FSIs and gap junctions being neglected due to their small number. The rest neuron groups consist of the STN, GPe and SNr, which were modeled using a single parameter, set as well as a fixed number of 150 neurons for each group. The values for all neuron parameters can be found in Table 6.1. The synapses between neurons in this model do not exhibit short-term plasticity. They include AMPA, NMDA and GABA types and they are governed by the equation 3.4. They have fixed reversal potentials E equal to 0, 0 and -80 for each neurotransmitter respectively,

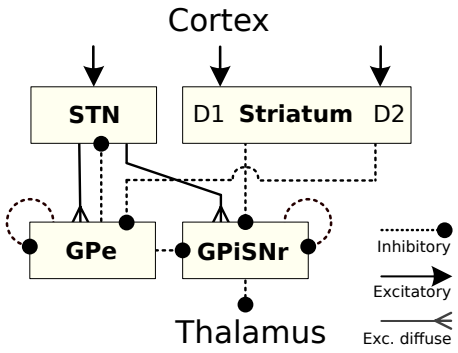

Figure 6.2: **Simplified version of the basal ganglia model.**

$\tau_{AMPA} = 2ms$, $\tau_{NMDA} = 100ms$ and $\tau_{gaba} = 3ms$, as well as a maximum conductance $g = 1nS$ for all connections in the system. In addition, no optimization was conducted to fit the firing rates of the model to the corresponding biological nuclei, as in the Section 3.1.4. Instead, the probability for each neuron of a source nucleus to be connected to a neuron in the target nucleus was always set to 0.25. Finally, the cortical input towards the three microscopic channels of this model remained the same as in Section 3.1.2, in order to enable a more direct comparison with the full version of the BG model.

6.4 Selectivity portraits

Following the methodology described in Section 6.2, we conducted a series of simulations where the BG circuitry was called to resolve a conflict between two salient potential actions. To simulate this scenario, the BG model received strong cortical input in two out of their three microscopic channels, governed by the equations described in Section 3.1.2, and background noise of 3 spikes/sec in the third channel. These two strong inputs were oscillatory, with a single fixed frequency $f = f_1 = f_2$, but different amplitudes $A_1 < A_2$. Since the firing rate of the cortical ensembles that generate these inputs represents the salience of each action, the second cortical input was always considered the most salient one or, in other words, "the right choice".

To investigate the relation between dopamine, cortical oscillations and the efficiency of the BG as a selection mechanism, we varied the frequency f of the two cortical ensembles, the phase offset φ between them, and the level of dopamine $d = d_1 = d_2$ in the system. An overview of the resulting BG behaviour can be seen in Fig. 6.3.

The coloured scatter plots of this figure illustrate the tendency of the model to select the most salient signal (effectiveness), or the alternative, less-salient signal (exploration) for any possible combination of dopamine and cortical frequency. Finally, the plots right below indicate

Parameter	MSN*	STN***	GPe****	SNr****
a	0.01	0.005	0.05	0.05
b	-20	88.33	2.5	3
$c(mV)$	-55	-65.0	-60	-65
d	91	500.0	70	200
$v_r(mV)$	-80	-61.0	-55.1	-55.8
$v_t(mV)$	-29.7	-64.035	-54.7	-55.2
$v_{peak}(mV)$	40	20.0**	15	20.0
$C_m(pF)$	15.2	333.33	40	80
k	1	13.33	0.706	1.731
d_1	0.3**	-	-	-
d_2	0.3**	0.3**	0.3**	-

Table 6.1: **Neural parameters in the simplified basal ganglia model. *** Parameters taken from Humphries, Lepora, et al. 2009 **** Parameters taken from Humphries et al. 2006 ***** Parameters derived from Michmizos and Nikita 2011 ****** Parameters derived from Lindahl et al. 2013

the ability of the system to select any signal, as well as the degree by which φ affects these measurements, across the same frequency spectrum. Since these figures can expose the critical conditions that affect the selection mechanism under examination, we termed them "*selectivity portraits*" of the model.

In the next paragraphs, we present a number of observations which were largely based on this figure, and we outline the most important testable predictions that emerged, regarding the function of the BG in the brain.

6.4.1 The combination of dopamine concentration and cortical frequency defines BG effectiveness and exploration

Fig. 6.3 clearly indicates that both the frequency of the two oscillatory inputs as well as the level of dopamine in the system play a crucial role in the ability of the BG to select. The responses of the model for various values of these two parameters revealed three main areas of interest in the frequency spectrum with completely different behaviour. The first area includes low-frequency oscillations, with a borderline at $f = 15$Hz, the second area corresponds to beta oscillations ($13 < f < 30$Hz) and the third area includes all greater frequencies.

In all cases, dopamine exhibited distinct patterns with which it regulated effectiveness and exploration. These patterns were completely different during the initial transient phase as opposed

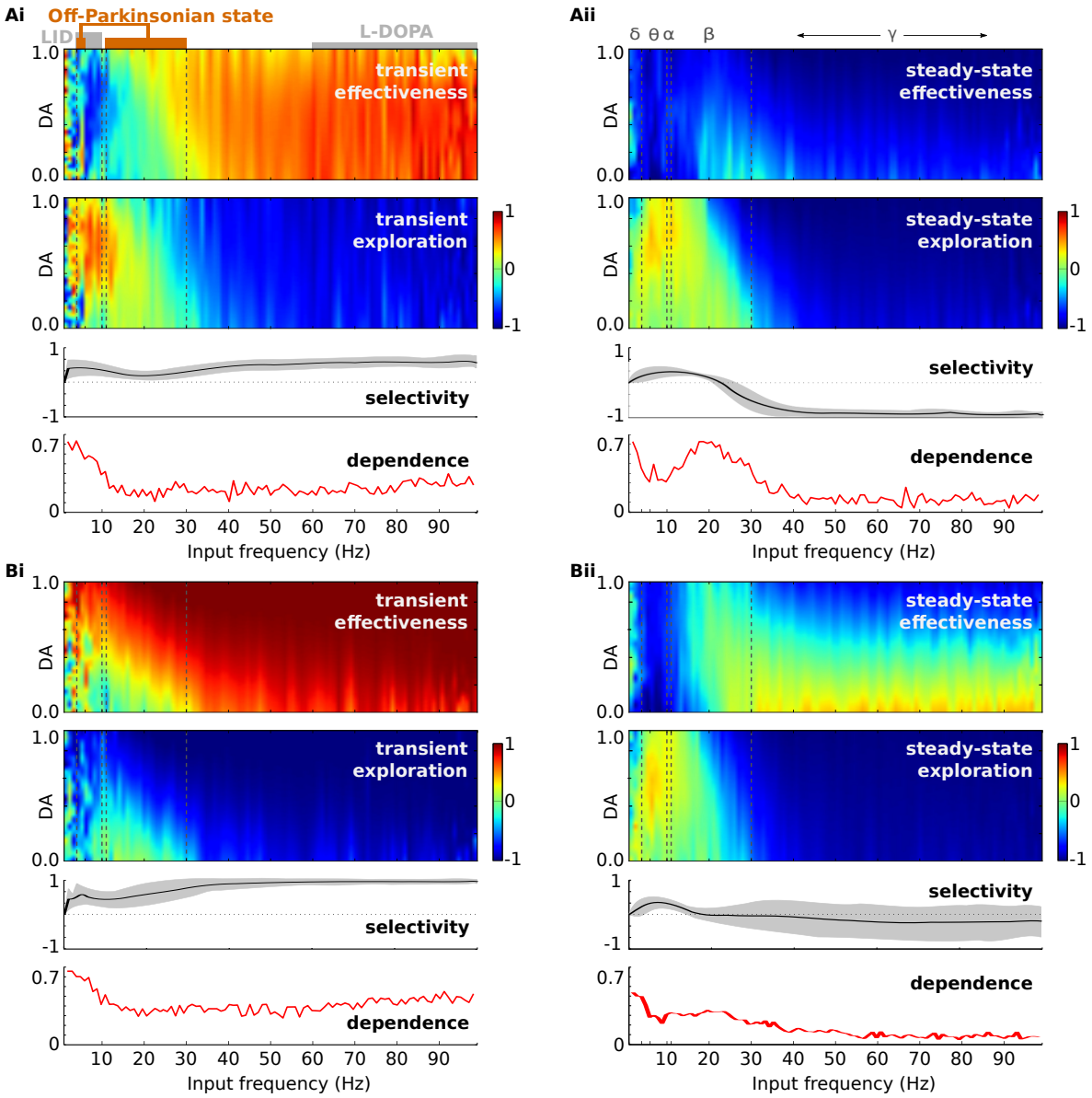

Figure 6.3: **Selectivity portraits of the basal ganglia model.** Effectiveness (scatter plot up), exploration (scatter plot down), selectivity (black curve) and dependence on the phase offset φ (red curve) when two inputs oscillate with amplitudes $A_1 = 7.5, A_2 = 10$ spikes/sec in (**A**) and $A_1 = 5, A_2 = 10$ spikes/sec in (**B**), in order to simulate strong and weak competition respectively. Cortical input to the third channel has a fixed baseline firing rate of 3 spikes/sec. Effectiveness is calculated for each combination of dopamine levels d and input frequencies f. The colour bars represent the mean of a sample of 200 runs (for each point) with random $\varphi \in [0, 2\pi)$. Selectivity curves represent the mean (black line) and standard deviation gray area for all φ and d, across frequency spectrum. Dependence was calculated for $d = 0.3$.

to the final steady-state BG response, while they were further modified depending on whether the competition was strong or week. As a result, the model generated four unique selectivity portraits when it dealt with each of the above cases.

More specifically, we found that, in our model, dopamine concentration affects selectivity only in particular frequency ranges, where its role is to either trigger or block the selection process. Notably, decisions triggered by dopamine promoted exploration over exploitation in the majority of the simulated scenarios. An exception is the case of a strong initial lead in the salience of the one of the competing channels before the level of the BG, showed in Fig. 6.3Bi. As the dominance of this channel is clear, an increased level of dopamine triggers the selection of this instead of the alternative choice. However, even if the most salient channel has already been selected transiently, this selection can be maintained over time only if dopamine decreases (Fig. 6.3Bii).

From the perspective of the cortical behaviour, low-frequency oscillations also promoted the selection of the least salient channel. This was achieved via the level of dopamine, which determined whether a selection will be made or delayed. With this type of input, the BG model became completely unable to maintain the first choice after an initial short transient.

On the other hand, beta oscillations minimized the influence of dopamine and brought the system in a neutral state, where both effectiveness and exploration are in the borderline value 0. Once more, this effect was halted in the presence of a strong difference between the two inputs.

Finally, gamma oscillations can clearly facilitate BG effectiveness. Transiently, selectivity maximized and the most salient channel was selected for any frequency, phase offset and dopamine level. In steady-state, gamma oscillations continued to support the same decision, but only if the channel remained highly salient and the level of dopamine dropped below tonic levels.

In order to ascertain the validity of these results and rule out the possibility that other stochastic parameters of the model had an important impact, we examined the variance of these measures when the examined parameters were fixed. Specifically, we ran 100 experiments where, each time, the level of dopamine, the input frequency and the phase offset φ were kept fixed to a random value within the biologically realistic limits but all other statistically defined entities in the model were randomised. These included the synaptic indexes, neural parameter perturbations and neuron types within a nucleus among others. This process was repeated 500 times giving in total 500 random points in the selectivity portraits that can be used for this analysis.

As a result, the three selectivity metrics presented Fig. 6.3 were almost identical between runs. A Shapiro-Wilk's test (Shapiro and Wilk 1965; Razali and Wah 2011) showed that the vast majority of these data points were approximately normally distributed, with an average p value $p = 0.56 \pm 0.36$ that could not reject the null hypothesis of normality. The resulting standard

deviations in each point were on average 0.114 ± 0.035 for effectiveness and 0.053 ± 0.032 for exploration.

The magnitude of this variation was very small compared to the differences in the selectivity process, and it was also comparable to the standard deviation of the normalized firing rates in the 3 channels of the SNr ($0.072(\pm 0.057) \times 25$ spikes/sec). Since these values are the only parameters of $\bar{D}_j$, our results indicate that there is no hidden correlation in the system, and the fluctuations of the standard deviation in selectivity plots of Fig. 6.3 were caused by dopamine and φ.

6.4.2 The BG can almost always select the most salient action transiently

During the simulations that produced the selectivity portraits, the BG model exhibited a significantly more aggressive selectivity transiently, at the first 500 ms after the presentation of the stimulus, as opposed to its steady-state behaviour. This is an expected range of reaction times in psychophysical choice tasks. It is consistent with oscillatory changes in the BG (Jenkinson and Brown 2011) and sensorimotor cortex (Leventhal et al. 2012) during animal decision making tasks, as well as choice reaction times in mental chronometry studies in humans (Heitz and Engle 2007; Heitz 2014; Woods et al. 2015). However, the equation (6.6) that has been used to produce the selectivity portraits of the current model, does not fully address the dynamic changes of selectivity. A further comparison with experimental studies, such as the above, requires information regarding the onset and duration of the emerging transient peaks, as well as any rebound effects. The average response of our model for the four major examined frequency ranges is presented in Fig. 6.4.

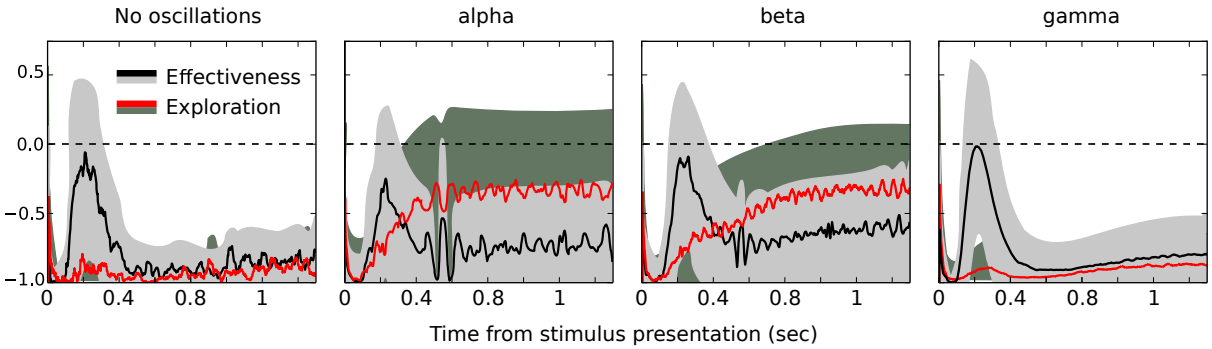

Figure 6.4: **Transient changes in selectivity.** Two competing cortical inputs oscillate with amplitudes 7.5 / 10 spikes/sec respectively. The two coloured curves represent mean value for any level of dopamine and offset φ, and the two coloured areas smoothed standard deviation.

As in the previous section, the large variations at some frequency ranges of this figure come from

the different values of phase offset φ and the level of dopamine. For instance, beta frequencies cause positive effectiveness only when dopamine is greater than 0.8. Since successful selection cannot occur for $\mathcal{D}_j < 0$, we consider the BG as able to select only in scenarios where a significant portion of our experiments had a selectivity peak above this baseline.

Right after the presentation of the stimulus the BG model did not produce any selection response for a short period with fixed duration. Instead, the firing rate in all SNr channels was high, indicating an initial STOP phase. This phase had a very similar duration of 85 ± 67 ms on average, in all frequency ranges. Next, a transient increase in effectiveness that peaked at 133 ± 155 ms on average, accompanied the initial STOP phase. Although this increase had also a similar onset at all frequencies, its exact duration and the rebound activity varied significantly between the four frequency ranges (Average duration without oscillations: 81 ± 62 ms, in alpha oscillations: $42. \pm 59$ ms, beta: 28 ± 46 ms and gamma: 70 ± 63 ms). Hence, our results indicate that cortical frequency does not influence the reaction time of the BG, although different frequency ranges cause different types of reactions.

Furthermore, the model was not able to maintain effectiveness above the baseline after the first 500 ms. An exception to this rule was the case of alpha oscillations, where effectiveness had a second sharp rebound spike, with a surprisingly similar duration and onset among runs. Indeed, in some trials at these frequencies, selectivity was stronger in this second peak. This bimodal distribution of maximum selectivity between trials could reflect to a similar pattern in behavioural tasks. The latencies of the two peaks in our simulations are consistent with the bimodal distribution of reaction times in distinct cue choice tasks with rats (Leventhal et al. 2012). However, the mechanism that caused this second selectivity peak is not yet fully understood, thus further investigation is required in order to establish its biological importance.

6.4.3 Cortical oscillations with low frequencies are required for selection change

The steady-state patterns of BG selectivity are also worth closer examination. Their function can be plausibly linked to a number of cognitive operations related to action selection. These include the ability of the BG to maintain a selection, for example during postural activities (Jenkinson and Brown 2011), to easily switch the current selection to an alternative cue, or the level of general alertness.

In Fig.6.3, it is shown that the most critical areas that affect effectiveness and exploration are mainly located in low frequencies while gamma oscillations have no discernible effect. In fact, Fig. 6.4 shows that gamma frequencies have virtually the same effect on selectivity as no

oscillations.

To shed more light into the steady-state behaviour of the BG after the presentation of two competing stimuli, Fig.6.5 illustrates the firing rate of the BG output nucleus, the SNr, during that period and for the complete examined frequency spectrum.

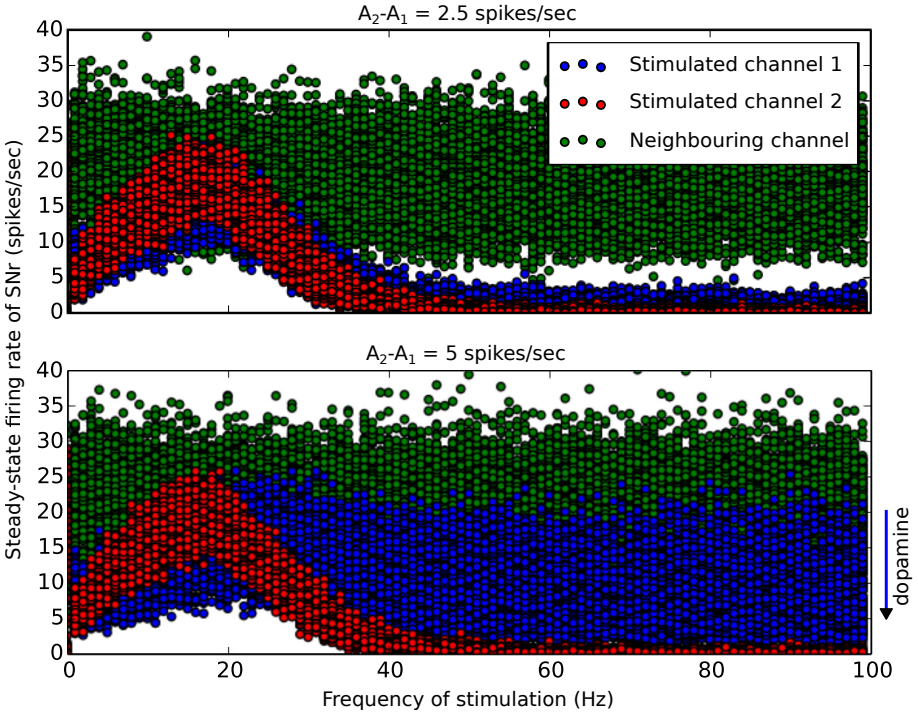

Figure 6.5: **Inhibition of the SNr microscopic channels. Up:** Firing rates of the three simulated microscopic channels in SNr, for various stimulation frequencies when two channels are stimulated with maximum amplitudes $A_1 = 7.5$ and $A_2 = 10$ spikes/sec respectively. **Down:** The same figure but for $A_1 = 5$ and $A_2 = 10$ spikes/sec. Activity in channel 1 is reversely proportional to the level of dopamine in the system.

At low oscillations, and particularly at alpha frequencies, the firing rate of the selected microscopic channel was always close to the firing rate of tonic areas of this nucleus (25 spikes/sec). When the difference between the competing signals was low, this gave a clear advantage to the less salient channel which, under some conditions, could be directly selected. However, when the competition was less ambiguous, the advantage of the less salient channel diminished. In fact, during cortical oscillations at 20 Hz, the two salient channels were treated equally. They were both inhibited to around 50% of their default tonic state and, as a result, both channels remained ready for immediate deployment.

This specific beta frequency was of particular importance, since it manifested a critical state in the model. Higher cortical frequencies favoured the most salient channel and, on average,

they significantly increased its distinctiveness, while low frequencies below 20 Hz had the exact opposite effect.

Finally, gamma oscillations also showed an interesting effect. In experiments with low ambiguity between competing channels and for low levels of dopamine, a selection of the highest salient channel could be maintained. However, under high ambiguity, or when dopamine increased, both channels remained inhibited, i.e. selected. This mechanism, which presumably allows information to flow via the cortico-BG-thalamic loop, might keep both information channels active until more evidence is accumulated. Cortical gamma synchronization has been widely associated with active information processing and feature binding (Eckhorn et al. 1988; Fries 2009; Colgin et al. 2009). Hence, the multi-selection mechanism we observed here might also contribute to these cognitive functions, by promoting integration of multiple information channels and thus allowing coalitions of neural ensembles to be formed.

6.4.4 Selectivity portraits are largely maintained in simplified versions of the BG model but not in the minimal model

The BG model that has been developed in this thesis has an increased degree of complication. Although its behaviour is similar to its biological counterpart, it is not clear yet whether our results depend on specific modelling features and how robust they are for small perturbations. Here we address this by providing a classification of the individual features of the model according to their impact on selectivity portraits. To do this, we ran the same simulations shown in Fig. 6.3 but for each set of data points created, a single parameter of the model was changed. When necessary, the connectivity optimization presented in Section 3.1.4 was repeated, to bring the firing rates of the BG nuclei back to their biologically realistic ranges. The result of this classification is illustrated on Fig. 6.6.

The model variations that were chosen to be shown here are the ones that showed the highest differences in either effectiveness or exploration. To maintain consistency with the previous figures, we ran simulations for both sets of amplitudes $A_1 = 7.5, A_2 = 10$ and $A_1 = 5, A_2 = 10$ spikes/sec. In all cases, the feature of the model that clearly had the strongest impact on selectivity was the existence of plasticity in the chemical synapses. When plasticity was off, the conductance strength of the affected synapses was reverted back to the initial static state described in Section 3.1.4, where the connectivity of the model was tuned to represent the steady-state baseline activity of the BG nuclei. This synaptic stationarity reduced dramatically the ability of the model to make selections at any frequency, and completely impaired its ability to maintain selection for longer than 500 ms. See the black selectivity curves in Fig. 6.6A and B. In contrast, the lack of lateral connectivity in the striatum had a significant positive effect

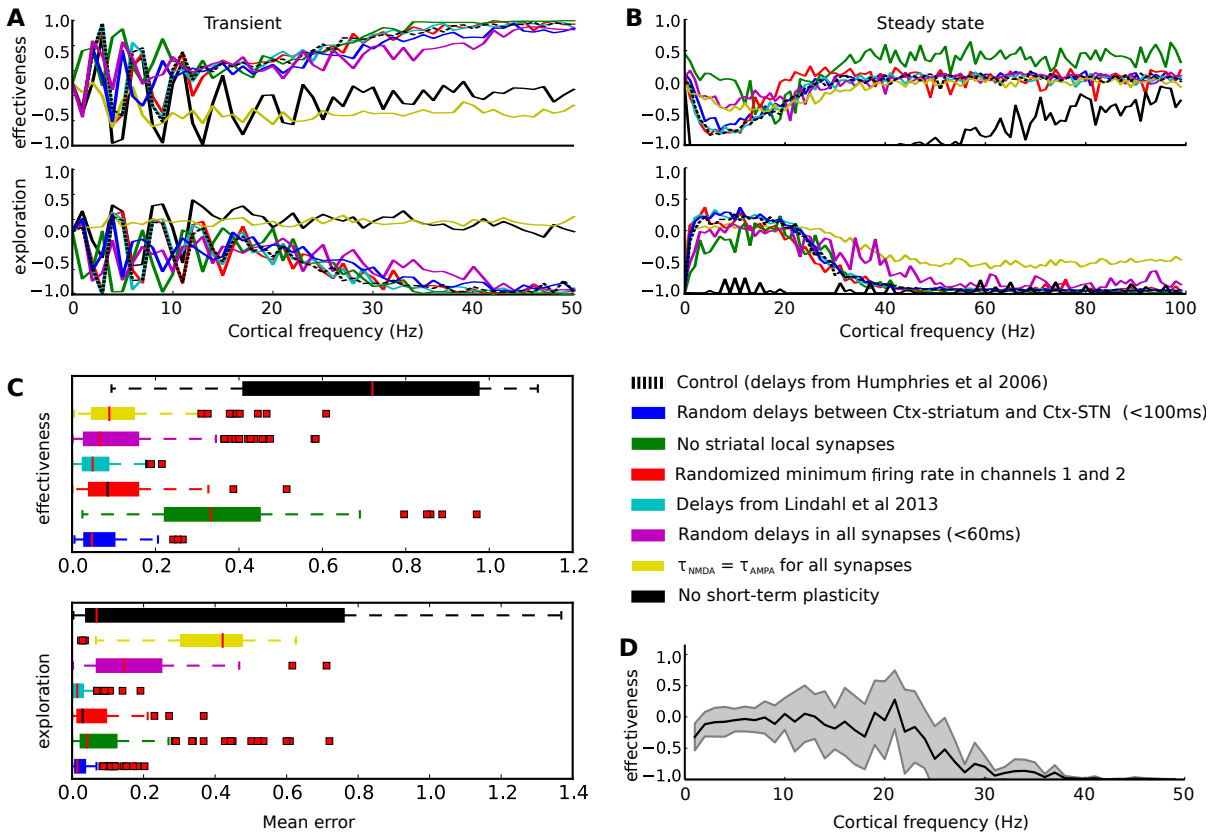

Figure 6.6: **Comparison of selectivity portraits of reduced versions of the BG model. A:** Transient effectiveness and exploration for various cortical frequencies and zero phase offset between two cortical input signals, for different versions of the BG model where a single key feature has changed. The difference between the amplitudes of these signals is 2.5 spikes/sec. **B:** The same figures but steady-state effectiveness and exploration. **C:** Box plot of the mean error between the selectivity behaviour of the default BG model and the examined reduced versions, for various initial conditions in (B). **D:** The same effectiveness figure for the minimal BG model.

in steady-state selectivity, but not transiently. Finally, the selectivity of the model underwent a similar dramatic reduction with plasticity when no NMDA receptors were used in the model ($\tau_{NMDA} = \tau_{AMPA}$), consistent both in transient and steady state.

Interestingly, variations in conductance delays in synapses between, or within, the nuclei did not play an important role in modulating the selectivity portraits. Delays were either completely randomized, maintaining a biologically plausible range, or altered in synapses where our initial choice was based on evidence with conflicts among independent studies. For example, a computational model of the BG microcircuit presented in Lindahl et al. 2013 integrated data previous studies and and concluded that the conductance delay in synapses from the STN to the GPe is on average 5 ms, for GPe-STN also 5 ms, for STN-SNr 4.5 ms, for MSN_{D1}-SNr 7ms and for

MSN_{D2}-GPe 7 ms. In the current thesis, these parameters were taken from Humphries et al. 2006 where their corresponding values are 2 ms, 4 ms, 1.5 ms 4 ms and 5 ms respectively. In addition, a second example comprised changes only in the delay of the input between the cortex and STN, which represents the extra distance that information signals have to travel to arrive to the hyper-direct BG pathway. This is an important parameter of the model, since it is not yet clear what cortical areas activate the same microscopic channels in the striatum and STN. In both examples, random variations in the synaptic delays did not cause significant variations in the selectivity portraits.

Another important observation in the comparison of this section is the effect of the phase offset φ on selectivity during low-oscillations. Fig. 6.6A and B include curves of average selectivity over various initial conditions, but with φ always being fixed at zero. We chose to show these curves in order to highlight the great impact of the phase offset at low frequencies, which remained consistent among the most versions of the model. As an exemption, when no slowly-decaying synapses are used ($\tau_{NMDA} = \tau_{AMPA}$), this effect disappears.

Finally, Fig. 6.6D illustrates that the minimal version of the BG model that is described in Section 6.3 produced a completely different behaviour. This can be attributed to a wide range of differences between the two models including the number of neurons and membrane potential dynamics. Yet, even under these simplifications, cortical oscillations at 20 Hz remained the most critical borderline in selectivity portraits that divides the frequency spectrum into two bands with antithetical behaviour (Fig. 6.3.Aii and Bii).

Taking everything into account, our results indicate the important hazards of oversimplification in computational modelling based on spiking neurons, since the latter do not always fall into the same level of biological abstraction.

6.4.5 The effect of the phase offset between low-frequency cortical inputs on selectivity portraits

So far, we showed that the combination of cortical frequency with the level of dopamine in the system defines how effective the BG circuitry is in discriminating incoming cortical information signals. Oscillators of various frequencies emerge constantly in the cortex, made by task-dependent coalitions of neural areas, or ensembles (Buschman et al. 2012; Akam and Kullmann 2010). These flexible neural populations are transiently being engaged (or coupled) and disengaged (or decoupled) in a metastable manner (Tognoli and Kelso 2014), distinguishable by their different relative phases. Evidence indicates that by staying out of phase, these ensembles maintain representations of different entities in working memory (Siegel et al. 2009).

Hence, it is likely that cortical groups that project to different microscopic channels in the level of the BG are phase-locked with a non-zero phase offset, which plays an important role in maintaining the identity of the potential action that is currently represented. Furthermore, since evidence points to the beta frequencies as the main range that mediates the formation of new ensembles (Buschman et al. 2012), it is particularly important to assess the BG behaviour in this range.

In our simulations, we found that the phase offset φ between coherent cortical signals with different amplitudes can have a strong influence on the effectiveness of the BG, at certain low frequencies, while in gamma band this effect disappears (Fig. 6.7A). Indeed, the strongest effect was clearly located in the beta range, where the BG effectiveness was significantly enhanced when the phase of the one input signal preceded in time the phase of the second, with a small offset around $\frac{\pi}{2}$.

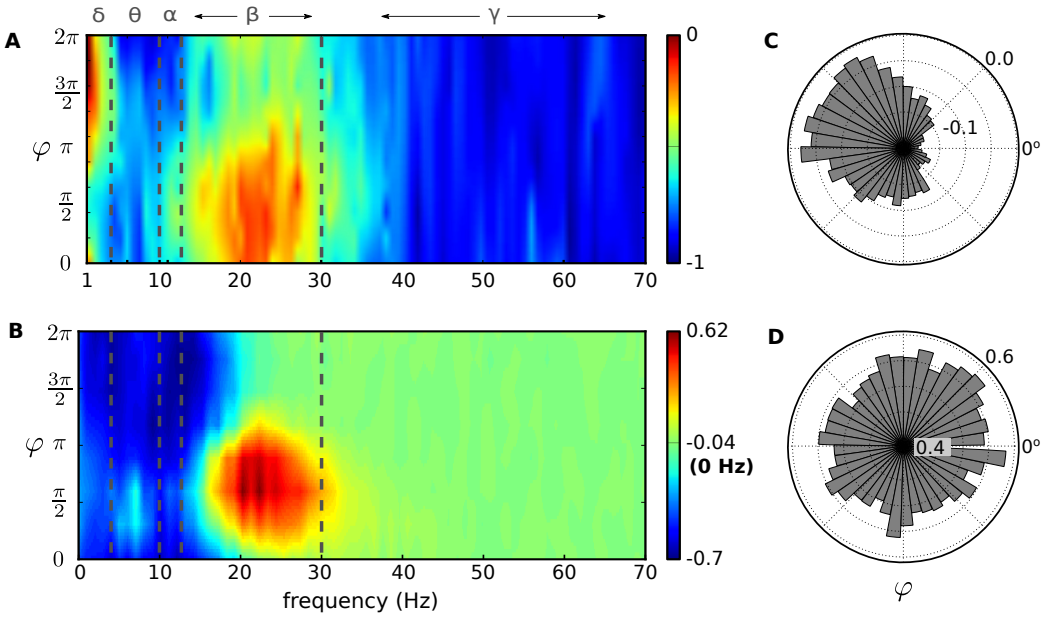

Figure 6.7: **The ubiquitous effect of the phase offset φ at beta frequencies. A:** BG effectiveness as a function of the frequency of two oscillatory cortical groups for $A_2 - A_1 = 2.5$ spikes/sec and the phase offset φ between them. **B:** The same figure for the minimal model presented in Section 6.3. **C:** BG effectiveness versus φ at theta frequencies. **D:** BG effectiveness versus φ at gamma frequencies.

Surprisingly, the sensitivity of the BG to different phase offsets during beta oscillations was largely preserved in all versions of our computational model including the minimal version described in Section 6.3. Fig. 6.7A illustrates this similarity which is even more prominent, since the two models produced different selectivity portraits, as a result of their numerous differences.

The relationship between phase and the BG function was investigated experimentally by Cagnan et al. 2015, who showed that neural synchrony increased in the Parkinsonian BG for certain phase differences between beta oscillations in STN and GPe. Fig.4.3 shows that, above the alpha range, most GPe neurons that are part of a phasic microscopic BG channel remain largely silent during this phasic process. Hence, the remaining GPe neurons are vulnerable to entrainment by weaker cortical inputs. As cortical beta oscillations were also shown to maintain coherence throughout the BG circuit, it is likely that the phase difference that Cagnan and her colleagues observed in this study reflected specific phase alignments of two competing cortical populations.

6.4.6 Selecting the most salient input does not require coherence between competitor populations.

Our results highlighted the impact of the frequency and phase of cortical ensembles that project to the BG. In order to draw conclusions regarding the phase difference between competing populations, we confined our simulations to populations of equal frequencies. However, EEG studies show that several different bands can coexist in the same or different regions of the cortex and interact with each other (Buzsáki and Draguhn 2004). Hence, to explore the dynamics of BG selectivity that emerge during a combination of two stimuli with non-equal frequencies we ran another set of simulations for frequencies $0 < f_1, f_2 < 50$ Hz and random offset φ. The resulting portraits are given in Fig. 6.8.

Despite the fact that our BG model contains various synaptic pathways that connect the two neighbouring channels, the SNr activity of each channel was immune to frequency changes in the other (Fig. 6.8B). Changes in effectiveness and exploration were both largely dominated by the frequency f_2 of the strongest input, and across the f_2 spectrum they followed a pattern similar to the portraits in Fig. 6.3. The oscillation of the weak channel was able to 'bend' this pattern only at beta frequencies, where effectiveness was enhanced.

6.5 Behavioural predictions

6.5.1 Evidence for the existence of a long selection cycle that can be used for evidence accumulation

It is assumed by a variety of models that cognitive operations in the brain require a fixed duration (Anderson et al. 1998; Stewart and Eliasmith 2009; Madl et al. 2011), which is often referred to as a cognitive cycle. Studies have implicated the BG as the central cognitive coordinator which

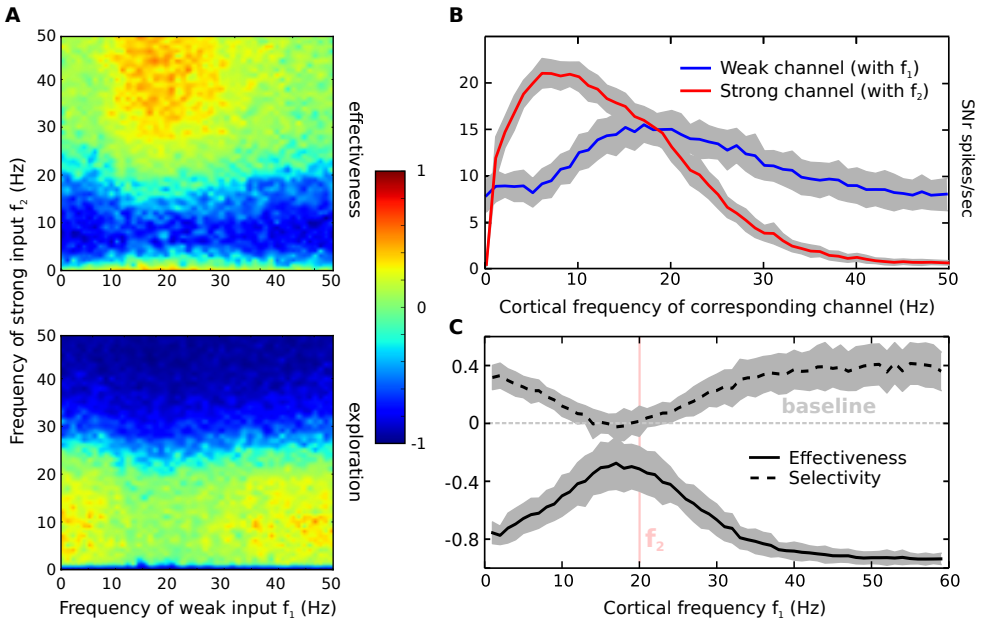

Figure 6.8: **Cortical stimulation at two non-equal frequencies. A:** Average steady-state effectiveness and exploration for all combinations of input frequencies below 50 Hz. **B:** Firing rate of the SNr in the two stimulated channels across the spectrum of the cortical frequency connected to the same channel. **C:** Average steady-state effectiveness and selectivity of the model when $f_2 = 20$ Hz.

works in a serial manner with a cycle of 50ms (Anderson et al. 2004; Stewart and Eliasmith 2009).

In order to investigate the contribution of our model to this hypothesis, we simulated a two choice task experiment, following the methodology in Tomkins et al. 2013. The BG model was stimulated with tonic input of 3 spikes/sec for 1 second in order to converge to an "inactive" steady-state where no selection is being made (Fig. 6.9). Then, a ramping increase, which lasted for 50 ms, changed the cortical firing rate of the one channel to 10 spikes/sec (*channel 2*). A second neighbouring channel received the same increase for the first 25 ms of the ramping time, but it decayed back to its tonic firing rate after another 25 ms (*channel 1*). The cortical activity in these two channels represented the urgency for two competing actions, which in the latter less-salient case was suppressed after some initial evidence accumulation.

Although the model of the striatum that has been used in this thesis is based on the neuron equations presented in Tomkins et al. 2013, we observed a consistent bimodal selectivity pattern that was different from the results in this study. Since our model does not include any feedback connections from other nuclei to the striatum, this difference can be only attributed to the asymmetric inhibition between MSN_{D1} and MSN_{D2} neurons which was examined in Section 3.1.1, but it was not taken into account in Tomkins et al. 2013.

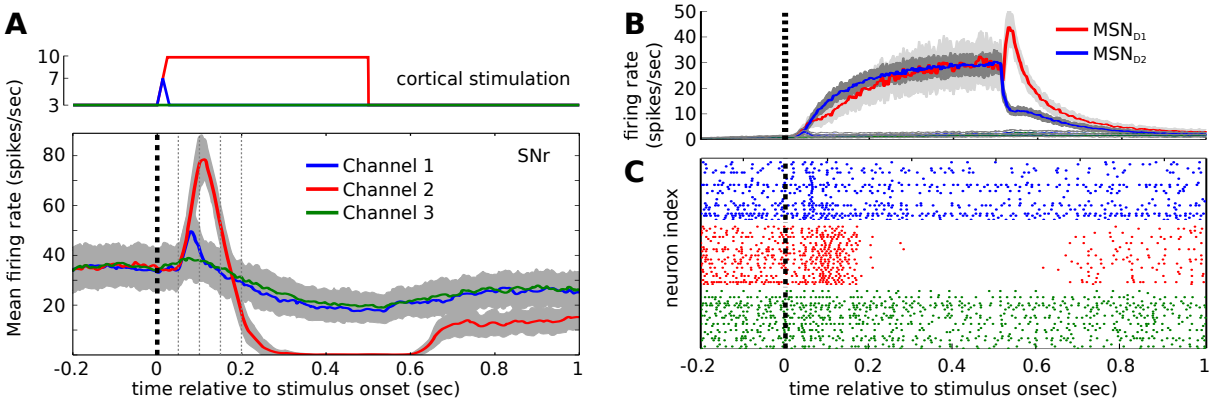

Figure 6.9: **BG output during a two-choice task. A:** Average firing rate of the 3 SNr microscopic channels and the corresponding cortical firing that caused this behaviour. **B:** The same for the two types of MSN neurons. **C:** Raster plot of the SNr during one of the runs in A and B.

The response of the SNr, the BG output nucleus, to this stimulation comprised a sequence of events. The first event occurred after 50 ms from the presentation of the stimuli in channels 1 and 2. Initially, a rapid increase in SNr firing rate was evoked, which was proportional to the intensity of the stimulus in each channel. This increase maximized after approximately 50 more ms, to be followed by a complete shut down of the selected channel, for the rest of the duration that the stimulus was presented.

The timing of this sequence of events was very similar to the experiment in Section 6.4.2 where the salience of the second action remained fixed during stimulation. This effect was shown to be robust and not influenced by the oscillatory patterns of the cortical input, therefore indicating the existence of a series of cognitive operations that take place during the selection process.

As shown in Fig. 6.9, after approximately 75 ms from the stimulation onset, channel 1 ceased to influence the outcome of the selection. But was channel 2 already selected at this particular point of time? Since the SNr does not stop its inhibitory effect to the thalamus before 200ms have passed, it is possible that a large portion of this time is used to accumulate information related to this selection. The fact that extra inhibition is provided to the phasic channels in the thalamus via the SNr, agrees well to this hypothesis.

To investigate these questions, as well as the tolerance of the time interval that is required for a successful selection, a new set of experiments was conducted. After the initial 50 ms ramp period, channel 2 received a fixed (non-oscillatory) input that had a random duration between 1 and 750 ms, while channel 1 received the same ramped input as before. In all runs, the distinctiveness D_j of the three simulated channels was recorded across time, in order to see when the maximum point of effective selection can be reached in each case. The results are presented in Fig. 6.10.

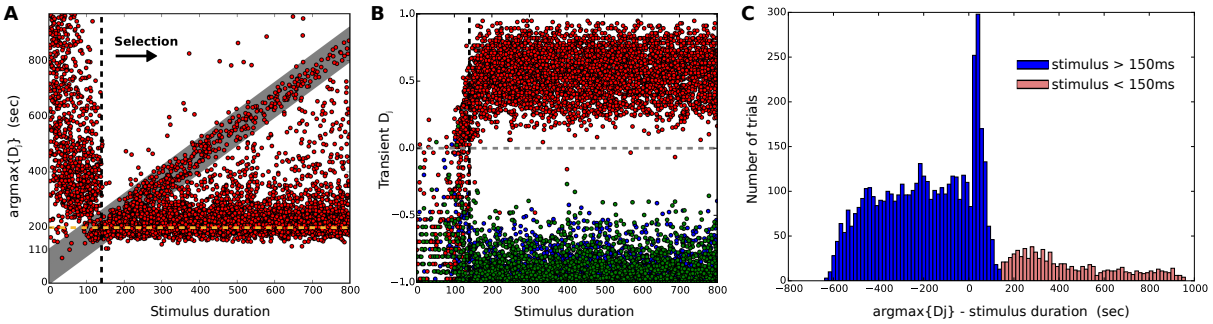

Figure 6.10: **BG response for stimulus of varying duration. A:** The point in time where BG effectiveness maximizes for a range of stimulus durations. **B:** Distinctiveness of the tree SNr channels for the same range. **C:** Histogram that shows when the maximum effectiveness was recorded with respect to the point in time that stimulation stopped.

Interestingly, we found that the BG model can discriminate between phasically and tonically-active channels only when the stimulus is presented for more than 140 ms (black dashed line in Fig. 6.10A and B). Longer stimuli are adequate to initiate this selection process, which normally lasts approximately 200 ms (yellow dashed line in Fig. 6.10A). Therefore, the inhibition of the selected channel in the level of the SNr is always preceded by excess excitation when a successful selection is performed.

This long interval, during which some information channels in the thalamus are completely shut by SNr inhibition (Fig.6.9A), could allow a mental deliberation process to be performed in the cortex, while the latter remains partly isolated from the environment. If during this process a channel looses its salience, as in the case of channel 1 in Fig. 6.9, its SNr activity will return to a neutral state, thus avoiding any interference with the final selection. Additionally, if no channel is able to maintain strong cortical activity, the process of selection will be cancelled and the excess excitation in the SNr will again prevent the inhibition of the thalamus. These features make the observed behaviour a good candidate mechanism for serial action selection.

Furthermore, the model exhibited a strong rebound effect after phasic cortical stimulation stopped. Within the range of 0 to 110 ms after stimulation, which is represented by a gray zone in Fig. 6.10A, the SNr inhibition of the most salient channel remained suspended. In fact, after approximately 50 ms the distinctiveness of the stimulated channel peaked again, as the neighbouring microscopic channels regained activity (Fig. 6.10C). This post-stimulation increase in selectivity was strongly facilitated by the rebound behaviour of the direct pathway, via excitation of MSN neurons in the striatum. As shown in Fig. 6.9B, the MSN_{d1} sub-population exhibits a sharp increase in their firing rate, which is inversely proportional to the rate of MSN_{d2} neurons of the same channel. Since MSNs do not evoke rebound spikes when stimulated in vitro (Venance and Glowinski 2003), this activity can only be due to the fast decrease of local inhibition and

the asymmetric connectivity between the two types of MSN neurons.

Although striatal lateral inhibition is crucial for the observed pattern of prolonged selectivity, it is not the only mechanism that causes rebound responses. Fig. 6.11 illustrates the response of the BG model for stimulus of various duration, when the simulated microscopic channels are connected with weak local striatal connections, to cover the possibility that these channels are physically located far from each other in the level of the striatum.

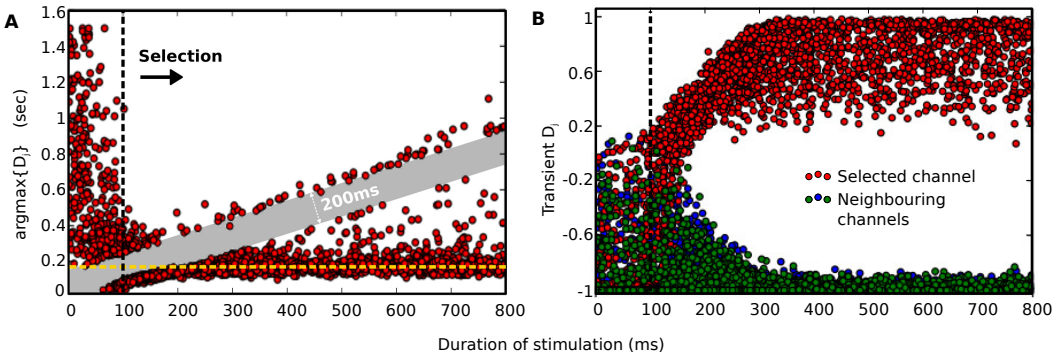

Figure 6.11: **BG response for stimulus of varying duration in non-neighbouring channels. A,B:** The same as in Fig. 6.10 in a variation of the BG model for weak striatal lateral inhibition that represents longer distance between channels.

In this case, the model required shorter presentation of the stimulus in order for a selection to be performed (around 100 ms). However, after stimulation stoped, it underwent a refractory period of approximately 200 ms (gray area in Fig. 6.11A), after which effectiveness peaked again. The fact that the duration of this period matches the initial time that the model needs to execute a selection provides additional indications of a selection cycle, which can be initiated after major changes to the input that the model receives. Although the existence of a cycle is consistent with all data presented in this section, a refractory period was not observable when strong competition took place within the striatum. A possible reason is that as the BG become more effective in distinguishing between channels, they are able to maintain a ready-to-select state, rather than initiating a new cycle, since the winning channel is already inhibiting the surrounding areas.

Finally, in order to conclude that the series of events which led to selection in our experiments constitute a cycle, the ability of the model to maintain effectiveness sequentially needs to be established. The steady-state selectivity portraits presented in Fig. 6.3 demonstrate that a single selection can not be maintained for many cycles of a duration longer than 70 ms (lower than beta frequencies), even if it is significantly more salient than an alternative choice.

Hence, to test if such a selection cycle can be repeated indefinitely, we ran an experiment where the three channels of the BG are stimulated sequentially for a fixed period T per single cycle. We

found that the BG was able to distinguish the most salient channel via excitation in the SNr when $T > 30$ms. However, the second phase of the selection process, where a selection is executed via inhibition of the corresponding SNr channel, could not be achieved when $T < 140$ms. A cycle of 200 ms was able to maintain inhibition to the SNr for approximately 50 ms. These results match with the model's behaviour in Fig. 6.11 and verify that the above selection process can be sequenced.

Cognitive architectures

Although recent cognitive models are consistent with various experimental studies, a strict definition of the timing of a cognitive cycle is a challenging task. For this reason, cognitive architectures do not currently agree on a common timing model that accounts for perception, cognition and action selection (Madl et al. 2011). As mentioned before, the BG are considered to be a fundamental element of this triad (Anderson et al. 2004), which makes the model that is described in this thesis a useful source of information for this quest. Even with an ideal design, however, a BG model is inadequate for capturing the timing of a complete cognitive cycle, since a significantly wider range of brain structures are typically involved in this process. Alternatively, the current model can be used to impose a number of biological restrictions and to establish whether the current cognitive models can be supported by the BG dynamics (Fig. 6.12A).

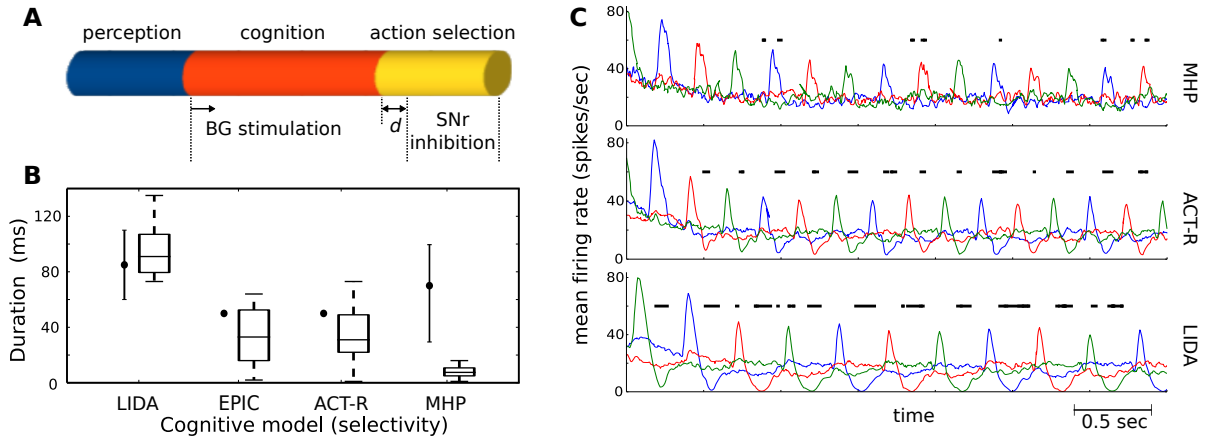

Figure 6.12: **Timing of action selection in popular cognitive architectures. A:** The three fundamental processes in a cognitive system, mapped to the activity of the BG model. The distance $d \geq 0$ to show that selection has not occurred before the onset of this process. **B:** Distribution of durations in each cycle that selectivity is above the threshold 0.22. The black dots represent expected duration while the box plots show the results of our simulations. **C:** SNr firing rates when the BG is stimulated sequentially, with timing that matches three characteristic examples of cognitive architectures. The black lines represent areas where BG selectivity is above the threshold. The three coloured curves represent different microscopic channels.

An important restriction implied by our simulations is that a cognitive cycle should be at least 200 ms, which is the time it takes for the BG to complete a selection cycle spontaneously, measured from the onset of cortical stimulation. Although it is not clear to what extend the perception process can overlap with the activation of the cortical areas that project to the BG directly, it is safe to assume that there is a minimal overlap, given the hierarchical structure of information processing in the cortex (Felleman and Van Essen 1991). Hence, if no parallelism between different cycles is assumed, our model suggests that a biologically plausible borderline range for the period of a cognitive cycle is from 200 ms to 200 ms plus the time duration required for perception. This restriction contradicts the majority of the currently proposed cognitive architectures, whose timing assumptions can be found in Madl et al. 2011 and are summarised below.

One of the most popular models examined here is called Adaptive Control of Thought-Rational model (ACT-R). Originally introduced by Anderson 1993, ACT-R is a modular and symbolic system which proposes that human knowledge comprises declarative memory chunks, and procedural rules. The brain is thought to be coordinated based on these rules via a central production unit, which was later associated with the function of the BG (Anderson et al. 2004). ACT-R assumes that the time of the human perception is approximately 85 ms, while 100 more milliseconds are required for the rest cognitive operations before selection. These intervals can be further broken down into 50 ms cycles of production rules, which correspond to information travelling through the BG-thalamo-cortical loop. Finally, since action selection is realized as a production rule cycle, it also lasts for 50 ms and, as a result, the time that remains for the BG to process input and execute a selection is 150 ms.

While this duration is shorter than the current predictions, the 50 ms cycle of ACT-R is, to some extend, consistent with our model's behaviour. Fig. 6.9 illustrates that all significant events in SNr activity that led to selection occurred in 50 ms intervals. Although the means of selection in the BG is typically hypothesized to be inhibition, excess SNr excitation discriminated the most salient microscopic channel prior to inhibition. This behaviour contradicts previous BG models and indicates that a selection is initially made in the first 100 ms, while other necessary operations take place until the selection is executed at approximately 200 ms from the stimulus onset.

A second model examined here is called Executive Process/Integrative Control (EPIC) (Meyer and Kieras 1997). The architecture and core assumptions of this model are very similar to ACT-R. The main difference in timing between these two models can be found in perception, which in EPIC is thought to last for 50 ms. Hence, the same conflict between ACT-R and our results applies also to this model.

Another influential approach was proposed by Franklin et al. 2005 and is called Learning Intelligent Distribution Agent (LIDA). LIDA is based on Bernard Baars' model of consciousness named global workspace theory, according to which, conscious cognitive content is broadcasted to all active brain processes via a globally available workspace (see the theatre metaphor in Baars 1997). LIDA assumes that perception takes 80-100 ms, the rest (unconscious) processing before action selection takes approximately 100-200 ms, while the action selection sub-process takes 60-110ms (Madl et al. 2011). The predicted timing of a cognitive cycle proposed here falls within the limits of this theory although, on average, the duration of non-perception processes is 35 ms longer than predicted.

Finally, the Model Human Processor (MHP), proposed by Card et al. 1983, is based on the same division of the mind as perceptual, cognitive and motor subsystems (or processors), which are partially coupled and have different durations. A number of studies have concluded that the cycle time for the perceptual processor in young adults is on average 100 ms with a range between 50 - 200 ms depending on the task, for the cognitive processor 70 ms with a range between 25-170 ms and for the motor processor 70 ms with a range between 30-100 ms. For a review on this topic, as well as the time changes in older adults see Jastrzembski and Charness 2007. Again, most of the range of estimated time for cognition and action selection is inconsistent with our results, which ideally require at least 140 ms for the stimulus to be projected to the BG and 60 additional milliseconds for action selection.

One issue that was not taken into account in this analysis is a potential parallelism of different cognitive cycles. Although this is a common limitation among the majority of the above models, it is known that the brain can process different tasks using some form of parallelism. Experiments with two different choice tasks performed on a single trial, have highlighted that the processing required for these tasks can overlap, but the reaction time of the second task will depend on the duration of the overlap (Telford 1931). This phenomenon, known as the psychological refractory period, is often attributed to the existence of a central bottleneck in the flow of information, that allows parallelism in perception and action execution but not during the time when the action is being selected (Pashler 1998). As shown previously in this section, our BG model could support such parallel operations which can reduce the period of a cycle down to 140 ms, the time required for stimulus presentation. Thus, given the complex dynamics of decision making which are highlighted with this paradigm, further analysis is required to assess the plausibility of the above cognitive models.

In an additional experiment, the three channels of the BG were stimulated sequentially as before, for a cycle T equal to the proposed period of each cognitive model. Stimulation was applied only in the time interval between perception and action selection, to keep consistency between the models. The response of the model was timed, in order to investigate whether it will maintain a

selection for the duration assumed by each model (Fig. 6.12A). To measure selectivity, we used the metric S which is defined in (6.4) and the model was considered to be actively selecting when $S > 0.22$. A comparison between original estimations of selection and the resulting durations that the SNr selected channel remained inhibited can be found in Fig. 6.12B.

The plausibility of LIDA was enhanced as the BG model was able to achieve the highest levels of selectivity in all trials, under these time restrictions. The timing of LIDA was also a close match, with almost all trials resulting in durations within the estimated range. Fig. 6.12C illustrates the average firing rate of the BG output during the trials and allows the comparison between models. Furthermore, the time restrictions of ACT-R and EPIC also allowed the BG model to exceed the threshold of selectivity. However, EPIC was a better match temporally, causing inhibition to the selected channel for 41 ± 28 ms, and also achieved higher selectivity scores.

On the other hand, when the BG model was stimulated with the temporal restrictions of MHP, action selection did not occur at all (Fig. 6.12C). This indicates that despite the fact that this cognitive model is able to fit to experimental data with a high degree of accuracy (Jastrzembski and Charness 2007), its underlying theory may require adjustments to be biologically consistent.

6.5.2 Low-frequency oscillations facilitate the resolution of ambiguity

Fig. 6.13 illustrates in more detail the impact of different cortical frequencies for any amplitude difference between stimuli, which represents all possible stages of a single selection. The one extreme case of $A_1 = A_2 = 10$ spikes/sec corresponds to two equally silent inputs, while the combination of $A_1 = 3$ and $A_2 = 10$ spikes/sec reflects the case that only one input has remained above the baseline. According to the selectivity portraits and this figure, at the beginning of a selection and when the correct choice is ambiguous, the BG are able to start exploring the most salient input only when the cortex does not oscillate at low frequencies, or during the combination of high beta and dopamine.

On the other hand, if a selection task requires a longer interaction with the BG, low oscillations can maintain effectiveness near the baseline (Fig. 6.13B), possibly securing extra time for evidence accumulation. Also, an increased level of dopamine in this case has the opposite effect. Interestingly, the system is unable to achieve a high effectiveness score after the initial transient period, even in the case of a clear winner. This indicates that either decision making in this case is achieved on another brain region, or that long interactions for single cognitive tasks are simply not possible. If the former hypothesis is true, low-oscillatory input to the BG could facilitate selection by maintaining a neutral state among phasically-active inputs. Finally, it is worth noting that the gamma band had the same impact with no oscillations in all simulated

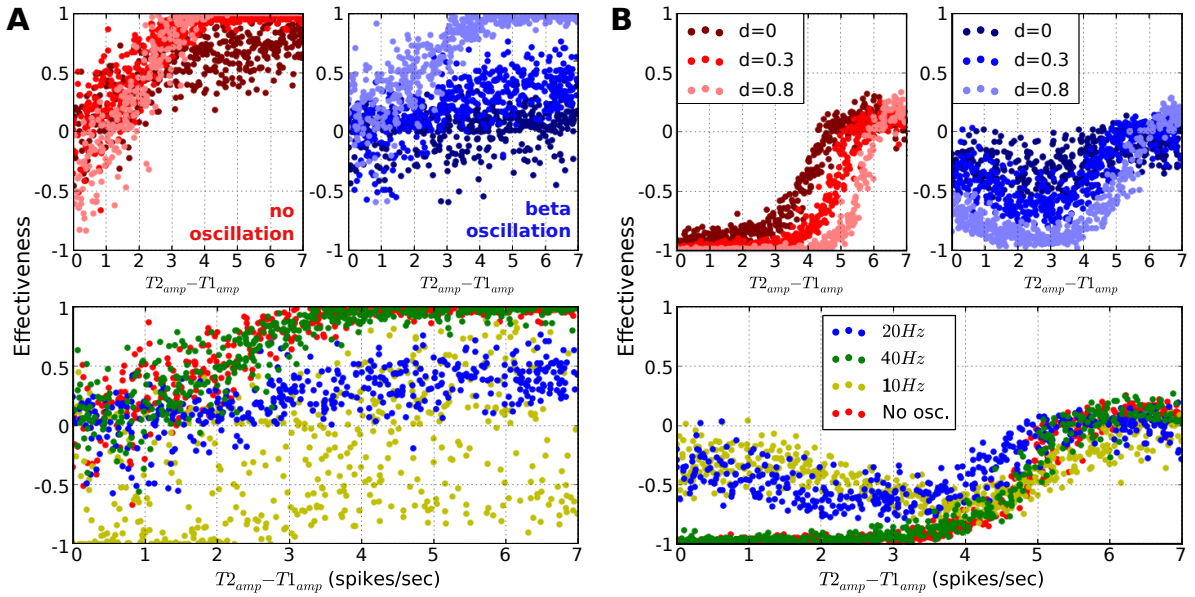

Figure 6.13: **Ambiguity effects on BG selectivity. A:** Transient effectiveness when two competing inputs have various amplitude difference, and $A_2 > A_1$. Different sets of data points represent reference cortical frequencies and dopamine levels, and are illustrated in different colours. **B:** The same as A for steady-state effectiveness.

scenarios.

All in all, the non-linear behaviour of the BG effectiveness that is illustrated in this figure, during the transition from ambiguity to certainty, shows the complexity of this circuit, when stimulated with low-frequency oscillations. However, the predictive power of our model is limited by the lack of other important brain regions, which makes difficult to draw conclusions that reflect complete behaviours.

6.6 Discussion

6.6.1 The gear box metaphor

This resulting selectivity portraits of our model constitute an interesting finding as they indicate that the cortex is actually the structure that determines whether an action selection will be performed, while the BG just execute this selection. Following the gearbox metaphor from Chapter 4, dopamine can be likened to the "*control pedals*" of action selection that either stop or initiate a decision. In the same context, the frequency of cortical oscillations acts as a *gear lever*, that instead of controlling the type and direction of thrust that the throttle provides to

an automobile, it dictates to what extent dopamine can trigger a decision, as well as what type of decision this would be.

This framework provides justification to a number of experimental findings. Cortical beta is found to increase when a postural challenge is anticipated (Androulidakis et al. 2007). Since cortical beta can bring the BG in an *neutral* state that cancels out effectiveness and exploration, it can be viewed as a frequency that causes a temporary deactivation of the action selection system when the current action needs to be maintained. In addition, the transient effects of selectivity agree well with the duration of increases in extracellular dopamine after SNc discharges *in vivo* recordings of the rat striatum in Dugast et al. 1994; Chergui et al. 1994. A single discharge increases dopamine for approximately 200 ms while an SNc burst causes an increase that lasts about $500 - 600$ ms. During this interval, our model can almost always select the most salient action (see results) and it can be significantly benefited by an increase in dopamine. However, the same selection can be maintained after this interval only if the level of dopamine decreases (Fig. 6.3Bii).

6.6.2 Psychophysical studies

Our model's predictions are also consistent with a wide range of experimental studies on mental chronometry. Although reaction times (RT) of young adults in simple tasks are in the order of $190 - 220$ ms (Laming 1968), these reactions can be simply stimulus-driven (Haggard 2008) and thus, they may bypass the action selection system of the brain. In contrast, when different responses are required depending on the class of the stimulus, choice reaction times (CRT) are found to be significantly longer, on average 500 ms in two-choice tasks (Woods et al. 2015), between $390 - 470$ ms when the subjects aim for high speed, between $450 - 610$ ms when the aim is high accuracy (Ratcliff 2002) and at a minimum of 200 ms (Heitz and Engle 2007) below which, responses are random.

By subtracting the average RT that is required by an individual to perform a simple task from the CRT of a specific choice task, we can estimate the time that is spent for the cognitive processing of the choices. This is found to vary significantly across different age groups, with an average range between $200 - 400$ ms and minimum at approximately 150 ms (Woods et al. 2015). The latency of our BG model is comparable with the lower values in the range of central processing times found in this study. This is an acceptable result given that the simulated task that was performed here constitutes arguably one of the simplest possible selection scenarios, and that the pathway of voluntary actions that involves the BG may also comprise a number of regions, as reviewed in Haggard 2008, that are not simulated here.

Furthermore, a range of studies links the duration of stimulus presentation with choice task performance in mammals. In Gold and Shadlen 2003, monkeys were presented with visual cues of varying duration, and their accuracy on a two choice task was recorded. When the stimulus was clear, their performance increased almost linearly from near-random in viewing time of 100 ms, up to 200 ms and then there was a minimal improvement. In a *GO* odor task with rats, Zariwala et al. 2013 showed that performance decreases to near random if the odor sample is presented for 100 ms or less, unless the subjects were anticipating the identity of the stimuli or the time of the response.

6.6.3 Alpha and theta oscillations act as a BG mechanism to reset selection and explore alternative actions

In the literature, there is cumulative evidence that strong alpha power is able to inhibit task-irrelevant regions in the cortex and thus control information flow (Händel et al. 2011; Buschman et al. 2012; Brinkman et al. 2014). This theory, which is known as gating by inhibition (Jensen and Mazaheri 2010), proposes that strong alpha activity is caused by GABAergic interneurons, which silence neuronal firing by providing a pulsed inhibition. Although a recent MEG study provides initial evidence that links gamma peaks to alpha troughs in the temporal cortex (Bonnefond and Jensen 2015), a number of important questions still remain unanswered. For example, it is not yet clear to what extend the phase-amplitude coupling that was observed in this study was a result of local GABAergic inhibition, or other brain regions, and whether this mechanism can operate in the same spatial scale that is required to inhibit complete neural ensembles.

Based on our simulations, we propose that alpha-induced inhibition of neural populations is mediated by the selection circuit of the BG. In particular, we found that alpha and theta cortical frequencies stop the selection of the strongest input completely and instead promote the selection of less salient areas. This exploratory behaviour was independent of amplitude difference between the two inputs, occurred transiently and remained active, even after a long exposure to the stimuli (see selectivity portrait in Fig. 6.3). In addition, the robustness of this effect to different background frequencies was established in Fig. 6.8D. When the most salient input was oscillating at alpha rhythms with frequency around 10 Hz, a second weak oscillatory input was always favoured, especially when its frequency was not in the beta range.

This view of cortical alpha is consistent with a number of experimental studies. Horschig et al. 2015 recently showed that effective connectivity from the cortex to the nucleus accumbens, a part of the striatum, increases during alpha oscillations, and reverses during theta. Also, Buschman et al. 2012 presented evidence where beta synchronization in the prefrontal cortex mediated the formation of neural ensembles that represented procedural rules, while alpha synchrony

increased in the ensembles that represented alternative rules. This led the authors to suggest that "beta-frequency synchrony selects the relevant rule ensemble, while alpha-frequency synchrony deselects a stronger, but currently irrelevant, ensemble".

While alpha importance has been already discussed, the role of theta is less clear. Interestingly, the period of a theta cycle ($150 - 250$ ms) fits well to the timing of an action selection cycle discussed in Section 6.5.1, and it is within the limits of the full cycle of the majority of the proposed cognitive models. However, in our simulations, providing strong stimulation the model for less than 140 ms did not evoke a selection unless multiple inputs were presented sequentially. Could this be an indication that cortical theta brings the BG to its extreme limit of time efficiency, below which no selection can be achieved? In behavioural experiments, theta is found to increase in the rat striatum during a decision-making task (Tort et al. 2008), while in humans, theta in STN increases during sensorimotor conflicts (Zavala et al. 2015).

6.6.4 Cortical frequency is a better predictor of the exploration-exploitation trade-off than dopamine

It has been suggested that tonic dopamine levels in the striatum encode the degree of which the brain selects the action with the most predicted outcome, over the exploration of an alternative less-safe choice, by modulating activation of the direct and indirect BG pathways (Humphries et al. 2012). Fast manipulation of the trade-off between exploration and exploitation is critical for behavioural flexibility in dynamic environments (Cohen et al. 2007). This hypothesis is supported by evidence with genetically modified mice, where increased dopamine levels resulted in selections that were less influenced by the potential cost of each choice (Beeler et al. 2010).

Here, the ratio between exploration and exploitation can be estimated via the ratio between distinctiveness of the most salient microscopic BC channel and distinctiveness of the rest active channels, that is, the ratio between effectiveness and exploration as defined in (6.3) and (6.5).

As shown in Fig. 6.3, we found that cortical rhythms play a more decisive role in this trade-off than the level of dopamine, although the combination of both cortical frequency and dopamine was crucial for the final selection. Whereas alpha and theta frequencies clearly promoted exploration over exploitation, unless uncertainty is very low, and the lack of them had the opposite effect, the level of dopamine could be largely viewed as an extra boost that triggers the selected action. In particular, during cortical beta oscillations of approximately 20 Hz, the system was in a critical state below which exploration was favoured over exploitation. However, at this very critical point and under high uncertainty, the level of dopamine was the decisive factor of the trade-off.

This complex interaction of dopamine with action selection justifies the lack of a widely accepted model, despite the fact that dopamine is evidently implicated in both exploration and exploitation (Kayser et al. 2015). On the other hand, cortical oscillations have also started to receive some attention on this topic. Cavanagh et al. 2011 found a strong correlation between theta oscillations in frontal regions and uncertainty-driven exploration. This led the authors to the hypothesis that frontal areas of the cortex take over action selection from the BG in tasks with high uncertainty. Our results however show that the BG could potentially cope the need for exploratory behaviour, in case that frontal areas 'request' it due to the detection of high uncertainty.

7 Two possible sources of Parkinsonian tremor

7.1 Introduction

In the previous chapters we showed that the BG circuitry can implement robust signal selection while the level of dopamine in the system has a crucial effect on this ability. We also showed that when dopamine is close to zero, the oscillatory activity in our neural model undergoes the same changes as observed in patients of PD, a fact that supports the biological plausibility of our methodology.

Apart from oscillatory effects, the impairment of the dopaminergic system in PD is accompanied by a substantial variety of devastating psychiatric, cognitive and motor symptoms including depression, psychosis and hallucinations (Chaudhuri and Schapira 2009), dementia, attention deficit and impairment of habitual control (Redgrave et al. 2010), as well as muscle rigidity, bradykinesia and tremor typically in a frequency between 4-6 Hz (Jankovic 2008) respectively. For a full review of non-motor symptoms in PD see Chaudhuri et al. 2014. Finally, as expected, PD has also an important impact on the process of action selection, with a characteristic loss of risk evaluation abilities (Kobayakawa et al. 2008) and a tendency to re-select motor programs that have been recently utilized (Helmich et al. 2009).

Despite this great variety of symptoms, the vast majority of current treatments and ongoing research focuses on the mechanisms of motor symptoms, such as tremor or rigidity, partly because they are more consistent and easier to measure (Chaudhuri and Schapira 2009).

A wide range of theories have been proposed in order to assess how tremor emerges in these conditions and identify the locus where it is generated. These theories implicate the thalamus (Llinas 1988; Magnin et al. 2000), the STN-GPe loop in the BG (Terman et al. 2002), the complete BG-thalamo-cortical circuit (Lenz et al. 1993) or the combination of both the BG and the cerebello-thalamo-cortical loop (Cagnan et al. 2014; Rubchinsky et al. 2007).

In this chapter we explore whether Parkinsonian tremor could be, in part, a result of the deterioration of the BG contribution to action selection. Under this hypothesis, PD tremor is viewed as the sequential alternation of the motor action selected by the BG circuit. Using our neural model described in Chapter 3, an extension of this model that accounts for the complete BG-thalamo-cortical loop and a more abstract mathematical approach, we present two possible sources of this pathological activity and we show that both can be supported computationally.

In the first proposal, PD tremor is realized based on the activity in a single microscopic BG

channel and, in particular, via the interactions between cortical input and STN at beta frequencies (*single-channelled model*). In the second proposal, the generation of tremor requires the rhythmic interaction between two channels, with theta frequencies and particular phase offsets (*two-channelled model*). We further show that this activity can be minimized with the application of the two most typical treatments of parkinsonian motor symptoms, the increase of dopamine concentration and DBS.

These mechanisms do not contradict with each other. Instead, they could coexist and harmonize together, in order to produce an enhanced tremor-like effect. A wide range of extensions can be proposed for this work, a number of which is summarized in the final conclusions of this thesis.

7.2 Methods

7.2.1 The full cortico-BG loop

The main pathway that connects the BG back to the cortex contains thalamic regions, that receive inhibition from the SNr and they send feedback excitation directly to the cortex. This creates a loop via which, the BG output controls the amount of excitation that the cortex receives. According to the action selection hypothesis (Redgrave et al. 1999), this loop is used by the BG to select the cortical regions that will maintain a high activation while this activation reflects the salience of the corresponding action.

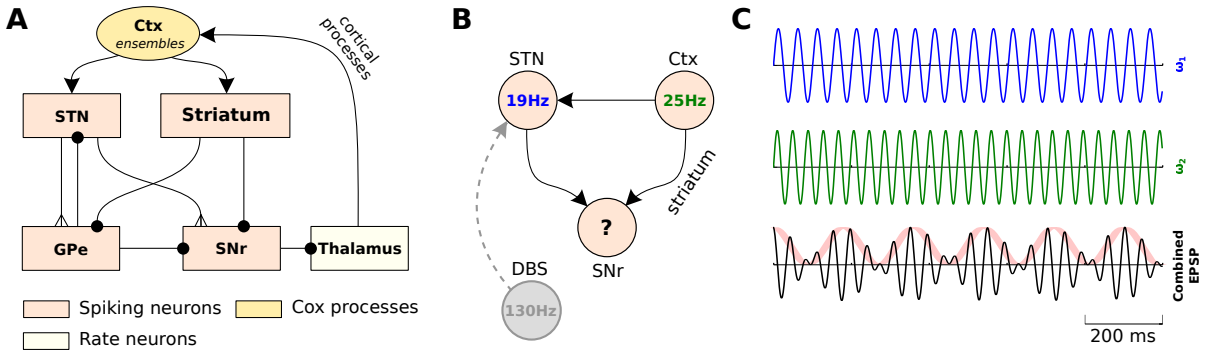

Figure 7.1: **Model architecture and visualization of the single-channelled hypothesis. A:** Schema of the complete BG-thalamo-cortical loop including rate-based and spiking-based neurons, as well as stochastic processes. **B:** Hypothetical model that shows the coupling between structures that generate oscillations. **C:** The predictive dynamics of the proposed mechanism in (B) realized with one Kuramoto oscillator for each structure. The three fast waves represent the phases of the three oscillators and the red slow wave shows the theta frequency that emerges from this interaction.

However, it is not yet clear whether the cortical neurons that are connected and stimulate a

microscopic channel in the BG are the same neurons that receive input back from the thalamus (Sherman and Guillery 2013). Therefore, more importantly, it is not clear to what extent the initial cortical frequency that was projected to the BG input structures can be influenced by BG oscillations.

This problem needs to be either resolved or bypassed in order to model the bidirectional interactions between the BG and the cortex. Within the computational framework of this thesis, this is approached by connecting the BG output with the simulated cortical ensembles via a number of rate-based neurons, which represent all intermediate structures that this signal travels through (Fig. 7.1).

In particular, the current architecture integrates the neural BG model described in Chapter 3 with three groups of doubly stochastic Poisson processes (Cox process), defined as in the section 5.2. Each group contains 1000 processes and corresponds to a neural ensemble of 1000 neurons that is connected to the BG microscopic channel i and oscillates at a fixed frequency f_i. To achieve this, the lambda parameters of all processes within a group have a common value λ_i, which follows the equation

$$\lambda_i(t) = A_i\big(1 + cos(2\pi t f_i + \phi_i)\big) \tag{7.1}$$

Here, A_i represents the oscillation amplitude that reflects the salience of this ensemble and $\phi_i \in [0, 2\pi)$ its absolute phase. To allow the BG circuit to control all saliences in a closed-loop fashion, this amplitude is connected to the channel i with the equations

$$A_i = F_{base}^{ctx} + E_i \tag{7.2}$$

and

$$\frac{dE_i}{dt} = \frac{E_i}{\tau_{ctx}} \tag{7.3}$$

where F_{base}^{X} denotes the baseline spontaneous firing rate of the structure X, E_i is the extra (task-dependent) excitation in the current ensemble and τ_{ctx} is the decay time of E_i. The SNr output can influence the excitation of the cortex when

$$E_i < \frac{\max\{-F_{base}^{ctx}, F_{base}^{snr} - F_i^{snr}\}}{F_{base}^{snr}} E_{max} \tag{7.4}$$

in which case the value on the right side of the inequality (7.4) is assigned to E_i. Here, F_i^X is the average firing rate of the current microscopic channel i in structure X and E_{max} is the maximum increase in cortical firing rate during a salient episode. Finally, if (7.4) is not true, E_i converges to 0.

In this study, we set $F_{base}^{ctx} = 3$ spikes/sec and $F_{base}^{ctx} + E_{max} = 10$ spikes/sec to be the minimum and maximum firing rates of the cortical ensembles respectively. Therefore, when the firing rate of an SNr channel is in the baseline, the corresponding cortical ensemble will have a firing rate of 3 spikes/sec. When a channel is selected, it will fire at 10 spikes/sec and when the firing rate of SNr increases beyond the baseline, the cortex will approach a silent mode. Finally a delay $d_{snr-ctx}$ is introduced to model the latency before information arrives back to the cortex. This includes synaptic delays from the SNr to the thalamus, from the thalamus to cortical areas and from the thalamic targets in the cortex to the corresponding initial ensembles. After experimentation, we set the default value $d_{snr-ctx} = 50$ ms in our simulations, but the model also exhibited similar oscillatory behaviour for values $d_{snr-ctx} = 200, 70, 30$ or 20 ms.

The benefit of this hybrid approach over a fully spiking model is twofold. First, it allows the BG to interact with cortical channels in real time while ensuring that the main cortical frequency f_i^{ctx}, which is under examination, will not shift during the simulation. Second, the complete knowledge of the connectivity pattern between the thalamus and the cortical ensembles that activate the BG is not necessary, as the only parameter that is influenced by this is $d_{snr-ctx}$. On the other hand, the main disadvantage is that information signals encoded in individual spike trains cannot be tracked outside of the BG circuit. This level of analysis is not, however, within the scope of the current study.

Modelling motor output

To model the final action that will be executed we need to transform the output of the BG model into a command. To do this, we inherit an interpretation of the BG output from Humphries et al. 2012, according to which, activity of the BG in the level of the SNr can be viewed as a probability distribution function of the prospective actions. Hence, to make the final selection we randomly draw a sample where each channel j has probability to be selected

$$P_j = \frac{F_{base}^{SNr} - F_j^{SNr}}{F_{base}^{SNr}} \tag{7.5}$$

A selection is repeated every 200 ms which is the time of a selection cycle found in Chapter 6.

7.2.2 The oscillator model

Our simulations with our neural model of the BG show that a type of STN neurons behave like oscillators which are coupled only implicitly via cortical input (Fig.7.1B). To simulate this interaction we used a simple oscillator model proposed by Kuramoto 1984, a mathematical

abstraction that has been commonly applied to explore the dynamics of neural synchronization (Shanahan 2010b; Cabral et al. 2014). In a system of N Kuramoto oscillators, the phase θ_i of oscillator i is governed by

$$\frac{d\theta_i}{dt} = \omega_i + \frac{1}{N}\sum_{j=1}^{N} K_{i,j} \sin\left(\theta_j - \theta_i - \alpha\right) \tag{7.6}$$

where ω_i is the natural frequency of the oscillator, α is a constant phase lag and $K_{i,j}$ is the coupling strength from oscillator j to oscillator i. Our model's topology comprised 100 oscillators that represent a cortical ensemble and are coupled with $K_{ctx} = 0.5$ and have the tendency to oscillate on average at $\omega_{ctx} = 20$ Hz. In addition, 50 more oscillators constitute neurons in the STN, their natural frequency is $\omega_{stn} = 25$ Hz and they are coupled with the first group with strength $K_{ctx-stn} = 1$. Finally, a readout neuron is connected with both cortical and STN populations, with weights 1 and -1 respectively, in order to capture excitation and inhibition to the SNr via the direct and hyper-direct pathways.

7.2.3 Modelling deep brain stimulation

Deep brain stimulation (DBS) is a standard invasive technique used to treat tremor in PD. Typically, either the thalamus or STN is stimulated with extra pulsatile current. To have a significant effect in the STN, the frequency of these pulses needs to be greater than 100 Hz with an optimal performance at approximately 130 Hz (Moro et al. 2002).

In this work, the impact of DBS in the STN is modelled by means of an extra rhythmic unit in the network that sends an pulsatile amount of voltage to all simulated neurons of the STN via a synapse. This amount is added to the membrane potential v after every event. Its amplitude during one simulation timestep can be calculated by taking into account the width of a pulse in a typical DBS device and the actual voltage amplitude (60μs and 3 V respectively in Moro et al. 2002). This simple technique allows us to test various scenarios, such as DBS with low-frequency pulses or feedback (Little et al. 2013).

Finally, in the oscillator model, DBS is realized via an extra Kuramoto oscillator with frequency $\omega_{dbs} = 130$ Hz, that is coupled directly to the STN population.

7.3 The single-channelled model

It is shown that oscillatory activity in the Parkinsonian BG at certain frequency bands is largely driven by the cortex (Litvak et al. 2011; Brittain and Brown 2014). However, despite the metastable formation of different oscillatory ensembles in the cortex and the fast changes of the dominant frequency bands, PD tremor is characterized by limited frequency tolerance (Brittain et al. 2015), which is uncorrelated with the cognitive state of the patient. This consistency in frequency, along with the strong therapeutic abilities of DBS when applied in the BG nuclei, point to the intrinsic interactions between these nuclei as a likely source of this type of tremor.

Studies with organotypic cultures have shown that STN and GPe have, indeed, an intrinsic tendency towards rhythmic activity under low dopamine conditions (Plenz and Kital 1999), without though exhibiting the same frequencies found in Parkinsonian BG. In Chapter 4 we showed that this exaggerated activity in the beta range and it can be generated locally, via a subset of STN neurons that evoke rhythmic bursts under dopamine depletion (Fig.4.1.D and Fig.4.2). However, it relies on cortical input to become synchronous, as the STN lacks strong lateral connectivity. Furthermore, this entrainment by cortical oscillations is problematic since the latter activity peaks in slightly higher beta frequencies.

Here we test the hypothesis that the interaction between low STN beta and high cortical beta can generate tremor-frequency oscillations in the SNr, which can then be transformed into sequential and repetitive motor actions. This concept is depicted in Fig.7.1B and C.

Another prediction that was made in Chapter 3 states that the majority of GPe neurons, connected with a phasically active area of the BG circuit, should be silent (Fig. 3.4). This can be used by the current investigation to simplify the BG circuit down to the parts that are involved in a phasic reaction. This simplified network can be viewed in Fig.7.1B and includes only the direct and hyper-direct BG pathways. By simulating this circuit using the modelling approaches discussed in methodology, we can acquire an estimation of the impact of this frequency mismatch between the two active pathways.

7.3.1 Experiment with coupled oscillators

Initially, the mechanism described by the single-channelled hypothesis was replicated using the network of Kuramoto oscillators presented in section 7.2.2. As expected, the readout neuron that represents the EPSP which arrives to the SNr from the two oscillating pathways produced oscillations with tremor-like frequencies, similar to Fig. 7.1C. Indeed, we found that the power of 5 Hz oscillations was almost linearly proportional to the level of average instantaneous synchrony

between the STN oscillators and it increased significantly even for small levels of synchrony (Fig. 7.3A).

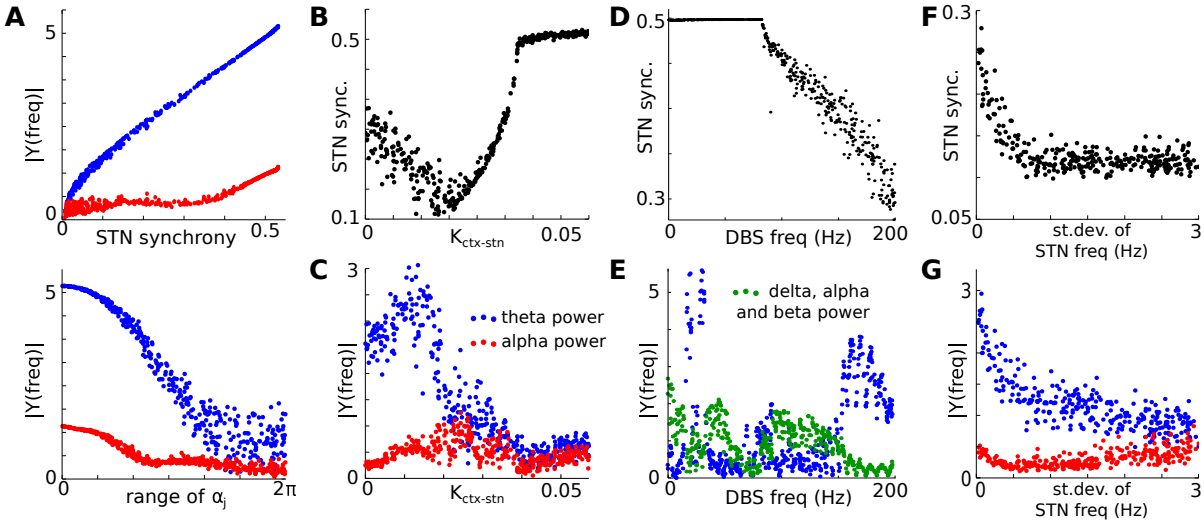

Figure 7.2: **Behaviour of an phasic BG channel in PD realized with a network of coupled Kuramoto oscillators. A:** The power of alpha and tremor-like (theta) frequencies in the spectrum of the readout neuron (SNr) for different levels of synchronization in the STN (up), as well as different ranges of random phase lags α_j (down). **B:** Synchrony in the STN for different coupling strengths. **C:** SNr alpha/theta frequencies for different coupling strengths. **D:** Synchrony in the STN for different DBS frequencies. **E:** SNr theta oscillations compared to the rest slow oscillations for different DBS frequencies. **F,G:** Synchrony in the STN (F) and SNr alpha/theta frequencies (G) under small perturbations of the natural frequency of STN.

Synchronization between oscillators was achieved with two approaches. For all data points in Fig. 7.3A, the coupling strength between oscillators in the cortex and STN was kept fixed for each oscillator at $K_{ctx-stn} \sim \mathcal{N}(0.5, 1)$ while the STN phase lags α_j varied between 0 and 2π. In contrast, the data points in Fig. 7.3B and C were produced for varying $K_{ctx-stn}$ between 0 and 4 and fixed $\alpha_j \sim \mathcal{U}(0, \pi)$. These changes in coupling strength represent different salience levels that might be caused either by increased cortico-subthalamic conductances or by increased cortical firing rate.

Under these conditions, we found that our model produces maximum tremor-like frequencies when $K_{ctx-stn} \approx 1.5$ and that it stops this activity for values greater than 2.5, although synchrony continues to increase until $K_{ctx-stn} \approx 3.5$. Between these values, due to the strong impact of the cortical oscillators on STN, the frequency of the later shifts towards 20 Hz and thus the effect that causes theta stops.

Effect of DBS and levodopa treatments

If intrinsic low-beta oscillations in the pathological STN are necessary for the generation of tremor, a disturbance of this activity should lead to detectable motor improvements. DBS in STN causes such a disturbance by forcing all local neurons to spike at very fast frequencies and thus braking their natural frequency.

To investigate whether this hypothesis can be verified with the Kuramoto model, the effect of DBS was simulated with a single extra oscillator connected to the STN. The impact of the possible parameter values for this oscillators, namely frequency ω_{dbs} and coupling strength $K_{dbs,stn}$, was explored. After a brute-force search, we found that the value $K_{dbs,stn} = 0.015$ maximizes the ability of the DBS oscillator to reduce tremor-like activity in the SNr readout.

One significant limitation of this approach of modelling the effect of DBS is that it can only be accurate in high frequencies. Real DBS devices provide a pulse wave with a very short width of approximately $60\mu S$ and a very large amplitude of around 3 Volts (Moro et al. 2002). In contrast, the oscillators in our model are constantly coupled and provide a force that drives the STN frequency towards ω_{dbs}. Fig. 7.3D verifies this limitation and shows that DBS evokes a constant synchronous state for $\omega_{dbs} < 90Hz$. However, synchrony in the STN falls for faster DBS frequencies, and the system exhibits behaviour that resembles the effect of the real DBS treatment.

As illustrated by Fig. 7.3E, the impact of the DBS oscillator under these conditions was to inhibit tremor-like (theta) activity over any other slow oscillations at the level of the SNr input. This was evident only in the range of approximately $\omega_{dbs} \in (95Hz, 150Hz)$, which is consistent with the frequencies used in real DBS electrodes (Moro et al. 2002; Eusebio et al. 2008) stimulating the STN.

Furthermore, motor symptoms of PD have been also commonly treated with chemicals that artificially restore dopamine effects in synaptic sights, such as the precursor compound levodopa. In the context of the single-channelled model, the benefit of this medication is clear as it would stop the oscillatory bursts in STN RB neurons and thus it would block STN beta. To model this effect with Kuramoto oscillators we introduce a random variation in the natural frequency of STN oscillators $\omega_{stn} \sim \mathcal{N}(19\text{Hz}, \sigma_{DA})$, where σ_{DA} is proportional to the level of activated dopamine receptors in the STN. As expected, Fig. 7.3F-G show that σ_{DA} is inversely proportional to the level of synchrony in the STN and the power of tremor-like frequencies in the SNr.

7.3.2 The thalamo-BG-cortical loop experiment

Our experiments in Chapter 4 showed that when isolated, the BG model does not reproduce the strong theta activity in the BG that indicates PD tremor, even when the cortex oscillates at beta frequencies. However, theta activity was greater in the SNr than in any other structure in the simulation, when cortical inputs had a frequency between 15 and 25Hz (Fig.4.3B), which suggests a tendency of the system towards theta rhythms. A promising way of enhancing this tendency is the simulation of the complete BG-thalamo-cortical loop, which can provide feedback activation to the same microscopic channels and thus may cause the domination of tremor-like oscillations.

This theory is, in fact, consistent with one the most recent and appealing hypotheses regarding the generation of Parkinsonian tremor called the dimmer-switch model (Helmich et al. 2012). This framework was initially based on correlations between functional magnetic resonance imaging and tremor recordings and predicts that whereas the BG network is the locus where the frequency of the tremor is generated, the thalamocortical circuit controls the amplitude of the tremor oscillation via the cerebellum.

To explore the potential of this small tendency towards tremor that was observed in our initial BG model, we employed the extended neural model described in section 7.2.1 and we ran a series of simulations where $f_1 = f_2 = 25$ Hz, dopamine was disabled and the cortico-striatal and cortico-subthalamic connections were strengthened, to model the 'off' medication Parkinsonian state. Finally, to trigger the selection of a single channel, we kept the oscillation amplitudes A_1, A_3 of the cortical ensembles connected to channels 1 and 3 respectively fixed for the first 1000 ms of the simulation. This disabled competition for channel 2 which was always selected by the system. The resulting oscillatory patterns in the level of the SNr are illustrated in Fig.7.3.

In all cases, slow frequencies were greatly enhanced in the SNr population of the winning channel, compared to beta oscillations which the cortical ensembles were forced to perform. Indeed, a clear peak of this activity was within the theta band. By increasing the level of dopamine to normal levels, to simulate the effect of a treatment with levodopa, low-frequency activity was reduced in all microscopic channels and no selection was maintained. This was an expected reaction of the system, since dopamine was found in Chapter 6 to reduce long periods of high effectiveness.

On the other hand, the addition of the simulated electrode that provides an 130 Hz positive voltage pulse to the STN evoked a different effect. The pulse width of this electrode was tuned to be 0.005 Volts, which produces only a 10% increase to the firing rate of the STN. The main outcome was an increase of the overall power in the SNr frequency spectrum, with an extra

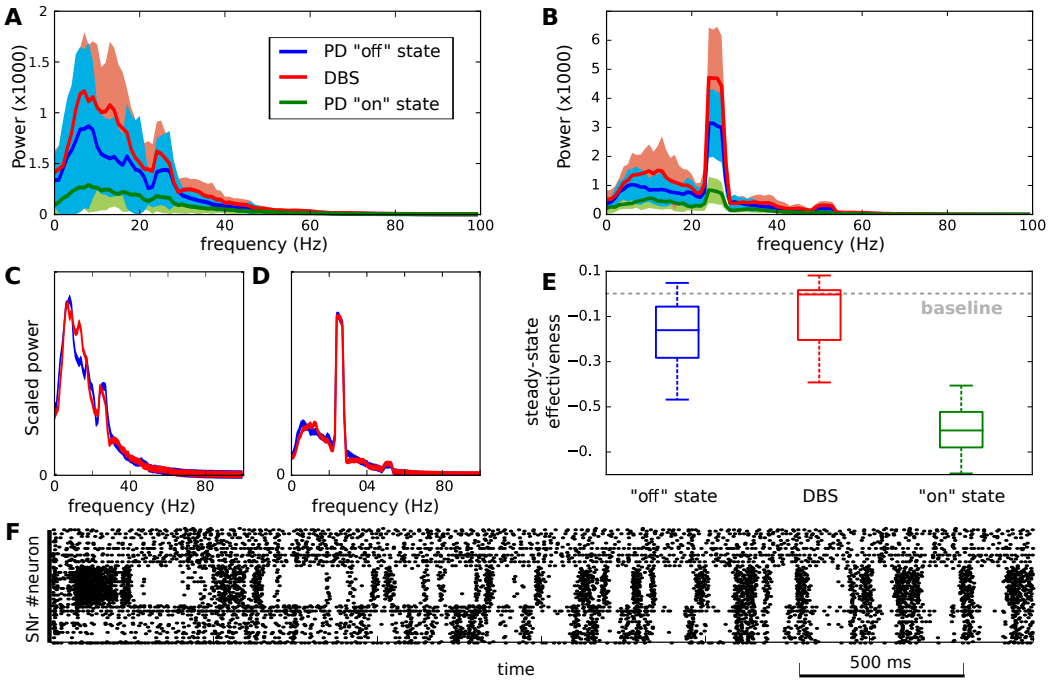

Figure 7.3: **Oscillations in the full-loop model. A:** Frequency spectrum of the SNr during the three simulated PD states in the microscopic channel that has been selected by the BG. The solid lines show average and the areas standard deviation over 50 simulations. **B:** Same as (A) in a neighbouring channel. **C,D:** The effect of DBS in (A) and (B) respectively, when the y axis is scaled to allow the comparison of relative power. **E:** Steady-state effectiveness of the BG mechanism in the same three samples. **F:** Raster plot of the SNr during the PD 'off' state.

enhancement of the STN-generated low beta band but without the expected negative effect on the theta band.

However, DBS had a positive effect to the ability of the system to select the channel that was stimulated first. Fig.7.3E illustrates that DBS improved the steady-state effectiveness recorded in the SNr, with half of the simulated experiments evoking long-lasting selection episodes above the baseline of effectiveness. This is particularly interesting as steady-state positive effectiveness could not be achieved at low frequencies with the healthy version of our BG model, according to the selectivity portraits in Fig.6.3.

Finally, we found that the parameter that plays the most substantial role in BG selectivity and the interaction between neighbouring BG channels is the baseline activation of the corresponding cortical ensembles. To produce the SNr raster plot in Fig.7.3F, F_{base}^{ctx} was increased from 3 spikes/sec to 6 spikes/sec in both channels 1 and 2. Although the channel that was stimulated first was initially selected, a gradual entrainment of the neighbouring free channel at tremor-like

theta frequencies was always evident.

7.4 The two-channelled model

The previous section was focused on a mechanism for tremor generation which is based on the interaction between the cortex and the BG in a single microscopic channel. Although our simulations produced the same tremor-like oscillations, and well-known treatments of PD were shown to reduce this activity, it is still unclear how these oscillations could be translated into sequential motor movements. Taking into account the main hypothesis that has been adopted by the current thesis, which views the BG as the locus of selection between prospective motor actions, a simple interpretation of PD tremor is the sequential alternation of the selection between different motor programs, caused by a BG malfunction.

Our BG model is consistent with this behaviour. In the section 6.5.1 of the previous chapter we found that a cortical signal can be selected, if the emitting ensembles drive the BG input structures for at least 100 ms, while the complete process of selection requires approximately 200 ms. We also found that this selection process can be partially serialized, in the sense that a number of steps of the selection process can occur in parallel. In this chapter, running the same experiment under PD conditions, we confirmed that the Parkinsonian BG can perform alternating selections effectively when both stimulation and selection time are set to 100 ms. This timing agrees well with the frequency of PD tremor (~ 5 Hz).

However, this view of tremor requires more than one competing channels to be selected sequentially, a premise that cannot be fulfilled by the current experimental setup used for the "single-channel" model. In Fig.7.3F, it was shown that, in the Parkinsonian 'off' medication state, when strong theta activity is generated in a salient BG channel, neighbouring channels become entrained and produce the same oscillatory profile with zero phase offset. Hence, as all phasic channels have the same behaviour, no single selection can be effectively made, a state that can be more associated with other PD motor symptoms such as akinesia and rigidity.

In the human brain, this spontaneous multi-channel entrainment could be avoided if strongly-active cortical ensembles become phase-locked at theta, via a mechanism outside the BG. Although uncoupled, cortical theta has been found to be strong during periods of conflict in action selection (Cohen and Donner 2013). In addition, theta phase locking has been observed between numerous brain structures during decision making, including the striatum, the STN, the hippocampus and various frontal areas of the cortex in animal models (Tort et al. 2008) and humans (Zavala et al. 2015; Voytek et al. 2015). These precise theta alignments have been shown to drive higher frequency bands in the cortex and they are thought to enable the simultaneous

maintenance of multiple prospective behaviours (Voytek et al. 2015).Finally, recordings from patients with PD have highlighted high theta coherence between the thalamus and the cortex (Sarnthein and Jeanmonod 2007).

Our simulations also highlight the need for theta phase-locking in the level of the cortex. We found that, at certain frequencies, the phase offset between different cortical sources has a great impact on the ability of the BG to select a single channel. An example for the theta band is illustrated in Fig.7.4.A and B.

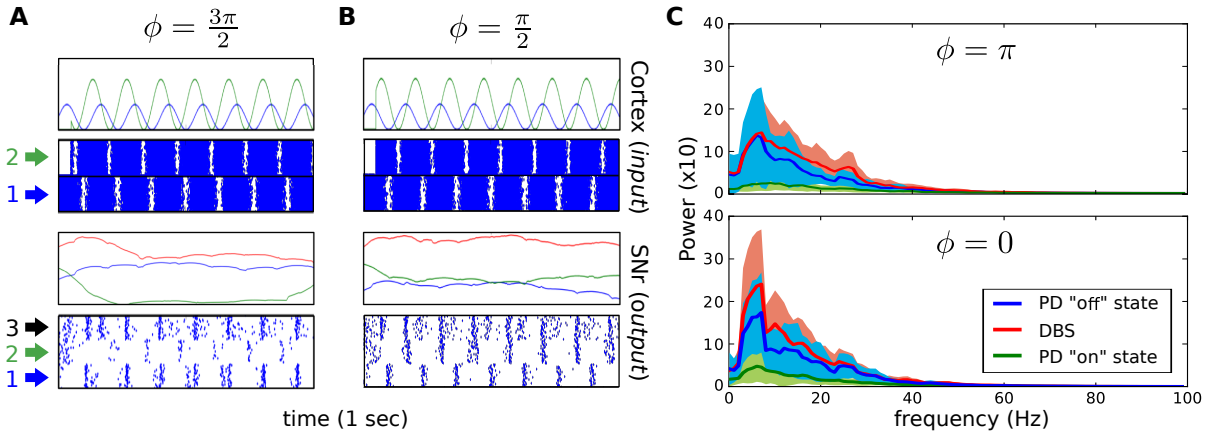

Figure 7.4: **The phase offset between two channels could cause PD tremor. A:** Effective channel selection in the minimal model of section 6.3, for cortical frequency at 5 Hz when the most salient channel precedes in time neighbouring channels. **B:** The opposite phase offset ϕ causes the sequential alternation of the selection. **C:** SNr frequency spectrum in the model of the full BG-thalamo-cortical loop. DBS can limit theta oscillations only in particular values of ϕ.

To explore how our "full-loop" system would react to an external theta phase-locking mechanism we changed equation (7.1) to

$$\lambda_i(t) = A_i\Big((1-B)\big(1+cos(2\pi t f_i^{low}+\phi_i^{low})\big)+B\big(1+cos(2\pi t f_i+\phi_i)\big)\Big) \tag{7.7}$$

in order to account for two frequencies simultaneously. Hence, we set $f_i = 25$ Hz, $f_i^{low} = 5$ Hz and $B = 0.7$, while the value of ϕ_i^{low} remained a free parameter, as it controls the phase difference between the phase-locked cortical signals. Using different values for ϕ_i^{low}, we found that the impact of DBS on inhibiting theta activity, as well as BG selectivity, changes completely for different theta phase offsets. When a large offset can be maintained between competing microscopic channels, DBS is able to enhance activity in higher frequency bands, thus minimizing the effect of theta. However, when theta oscillations are aligned between channels, DBS shows no discrimination between frequency bands.

Taking everything into account, we propose that theta activity in the BG can be initially generated by the interaction between exaggerated STN low beta and healthy cortical high beta. This activity can be phase locked via mechanisms outside the BG network, and in certain phase alignments it can cause the sequential alternation of the currently selected action, which is perceived as tremor. We call this hypothesis the “two-channelled model" since it requires the interaction between at least two BG microscopic channels that represent different motor programs. Our hypothesis could be tested in patients of PD that undergo DBS treatment, if their cortex was stimulated using non-invasive techniques, such as transcranial direct current stimulation, at the same theta frequency and an opposite phase to the current theta activity recorded by the DBS electrodes.

8 Conclusions and future directions

8.1 Summary of contributions

The contributions of the current thesis take us a step closer to understanding how action selection is realized in the mammalian brain and how it is affected by oscillatory behaviour, as well as relevant pathological conditions. They also include tools that can be used for the further investigation of these topics.

Computational tools and new methods The first main contribution of this work is a new detailed neural model of the BG canonical circuit, described in Chapter 3, which can be used as the means for both producing and testing hypotheses related to the BG function. Due to the great interest in this brain region, there are a growing number of computational modelling approaches in the literature (Fig.1.2). For reviews see Schroll and Hamker 2013; Helie et al. 2013. However, to my knowledge, there has so far been no large-scale neural model of the complete BG circuitry, that integrates so many features of the BG physiology and produces biologically plausible behaviour. The current BG model was further expanded in Chapter 7 to account for interactions of the complete thalamocortical loop.

Additionally, two software tools, that facilitate the design and simulation of any SNN models, were presented. The first, brain studio (http://brain-studio.org), is a complete graphical environment that provides methods to (1) design experiments with neural networks, (2) represent experiments in a compact manner, (3) simulate large-scale networks using all available resources on a computer, (4) observe and (5) analyse simulations in real time, both locally and remotely. The second tool allows the fast parameter optimization of spiking neuron models and outputs the best fit to available electrophysiological data. This tool is based on a novel hybrid method for neural optimization. It automatically interfaces with online databases of experimental data and it requires minimal user intervention for the complete tuning process. When used with an NVIDIA graphics card, the speed performance of this tool can be further increased, as both central and graphics processing units can be employed at the same time.

Finally, a number of novel metrics were presented, which can be used to assess the ability of a neural mechanism to dynamically select between competing signals. Apart from unidimensional effectiveness, these metrics can be used to estimate the underlying trade off between exploration and exploitation.

Predictions for the healthy BG The findings presented in Chapters 4-6 made a number of direct and indirect predictions regarding the BG function that can be tested experimentally. The former category includes the effective connectivity map of the BG circuit, based on transfer entropy analysis, for the complete spectrum of cortical frequencies, as well as the transient and steady-state selectivity portraits that are produced for various initial conditions.

Interestingly, this analysis indicates that, whereas the BG can provide the locus for the selection between information channels representing actions, the cortex is the structure that determines whether a selection will be executed, and what strategy will be followed (e.g. exploration versus exploitation). This behaviour led me to propose that the BG acts as a gearbox of information processing in the cortex, whose level corresponds to the function of cortical oscillations and the throttle is reflected by the level of the neurotransmitter dopamine.

The results of this thesis also predict that, at certain frequencies, the phase offset between competing cortical inputs influences both effective connectivity and selectivity in the BG (Fountas and Shanahan 2014), a behaviour which was later found in human patients of PD (Cagnan et al. 2015).

Furthermore, a consistent duration that the BG circuit requires to maximize its effectiveness in selection was identified. This selection cycle has a period of approximately 200 ms, and can be used to estimate the duration of a complete cognitive cycle. As an application of this finding, the current model was used to assess the biological plausibility of the most popular architectures in cognitive science, some of which were found to be inconsistent with the current results.

On a lower level, it was predicted that the silence that has been observed in GPe neurons results from neural accommodation in specific post-synaptic dendritic sites, with increased concentration of fast voltage-sodium (Na^+) channels. This can be verified if the *in-vivo* blockade of slow glutamate receptors in GPe, namely NMDA and mGluR1, can reduce the silent episodes of these neurons, and increase their responsiveness to STN input. Finally, it was predicted that short pauses in high-frequency neurons occur when the salience of a cortical afferent signal exceeds a threshold. This mechanism could potentially inhibit neighbouring microscopic channels throughout the BG-thalamo-cortical loop, in order to further boost the dominance of the most salient channel, forming a winner-takes-all device (Redgrave et al. 1999). Evidence here could come from GPe recordings during a choice task, where the salience of an action can be controlled and quantified over time. If activity in both GPe and STN is recorded simultaneously, STN phasic episodes are expected to exhibit high correlation with GPe pauses.

Predictions for the pathological BG By simulating the changes of PD in the examined region, i.e. reduced dopamine concentration and enhanced cortical excitation, the effects of this

condition on the BG behaviour were explored. The conducted simulations confirm a compelling hypothesis according to which, beta oscillations of the motor cortex entrain pathological beta activity generated within the BG, which however peaks at lower frequencies than the former (Brittain and Brown 2014). The results of this thesis also provide a potential explanation that points to the dynamics of individual STN neurons as the source of these pathological oscillations.

Continuing in this vein, two potential mechanisms were identified, which could either trigger or facilitate the generation of tremor in PD and emerge in the BG model's behaviour. According to the *one-channelled model*, tremor-like theta frequencies are generated by the joint effect of STN low-beta and cortical high-beta oscillations on the output of the BG. This activity is translated into tremor through the impact of the BG to the thalamus. The *two-channelled model*, on the other hand, presupposes that two competing inputs already oscillate at theta frequencies with a large phase offset. Under these conditions, the results of the current thesis showed that both inputs can be selected sequentially, thus causing tremor via the alternation of the currently selected motor program.

8.2 Applications and future directions

8.2.1 The BG model

One of the major aims of the model presented in Chapter 3 is to be general enough to cover a wide range of modelling challenges. For this reason, the list of possible future directions has become too extensive to be detailed in this section and thus, only a number of key areas will be highlighted.

Model improvements Possible improvements of the model include the addition of the pars compacta part of substantia nigra. These neurons could govern the release and re-uptake of dopamine in the system, using the model proposed in Best et al. 2009. In addition, the dynamic changes in dopamine concentration could be combined with long-term adjustments to the conductance of the plastic cortico-striatal synapses. This can be achieved through the integration of the current system with the model of reward-modulated spiking-timing-dependent plasticity (STDP) proposed by Izhikevich 2007b. This extended version of the model of this thesis could then be used in a wider range of studies, including reinforcement learning (Chorley and Seth 2011) and time perception (Buhusi and Meck 2005).

Open Basal Ganglia An important reason for the continuous presentation of new models of this brain region in the literature is the ever-increasing growth of our knowledge of connectivity and electrophysiology. Hence, the community of BG computational modellers could be significantly benefited by an evolving and open access approach, where new data is automatically integrated to previously acquired knowledge.

The source code of the model implementation that has been employed in the current thesis was designed to require minimal reconfiguration for any changes in experimental data. Thus, it could also be used as the basis of an online platform with the above characteristics. This platform could include a database that stores related experimental data and a number of optimization scripts that automatically tune the model based on the selected data and features. These scripts could be largely based on the methods described in sections 2.3 and 3.1.4, that account for neural parameter and connectivity estimations respectively.

Finally, the user of this online platform would be able to select from a minimal spiking model of the BG circuit, such as the one described in section 6.3, up to the version that includes the most recent additions, and download a python script based on brian simulator or a node for brain studio.

8.2.2 Action selection

Validation of the impact of the phase offset on action selection It has been shown that phase-locking in the high beta band is used to distinguish between neural ensembles that represent different context-dependent stimulus-response rules in the prefrontal and anterior cingulate cortex of monkeys (Buschman et al. 2012). In this experiment, the subjects were trained to perform two different rule-based tasks. Both cues were presented simultaneously and the subjects were asked to perform only one of the two tasks per round, ignoring the second cue.

The data obtained by this experiment could be used to explore the relation between behavioural reaction times and phase offsets between the two oscillatory ensembles. The BG model predicts that certain offsets should result in different levels of effectiveness in action selection which might be reflected in longer reaction times or lower performance in the task.

Psychophysical study To confirm the predictions regarding the role of cortical oscillations in action selection a series of additional experiments could be performed in healthy humans. In the first experiment, subjects would be asked to perform a GO/NO-GO task while they receive transcranial direct current stimulation (tDCS) at various low frequencies in their motor cortex. The BG model predicts that at certain frequencies, a selection will be more difficult as the cortex

instructs the BG to activate a non-selective mode. In a second variation, the same experimental set up from Buschman et al. 2012 could be followed, along with the application of tDCS in areas of the prefrontal cortex, in order to enforce a particular frequency and phase alignment. Again, the BG model predicts that the subject's responses would be very different depending on the frequency that interferes with the formation of rule-specific ensembles.

Computational study on action selection in the metastable brain Metastability is an important property of brain dynamics that supports human cognition. It quantifies how well the brain is able to form dynamic coalitions of functional units, which cooperate and coordinate in order to process information from the outside world (Tognoli and Kelso 2014). Researchers in the computational neurodynamics group of Imperial College London have developed a mathematical model that can simulate, to some extent, this cognitive feature (Bhowmik and Shanahan 2013). This model consists of a number of spiking neuron groups that form a population of coupled oscillators and represent ensembles across the cortex. It has been used to investigate the structural requirements for maximal metastability in the brain.

Is metastability an important property for effective action selection in the central nervous system? What other dynamics emerge through the cooperation of coalitions of neural oscillators, in order to secure their selection via the competition in the BG? What is the role of long and short-term plasticity and reward-related neurotransmitters in this process? The integration of this model with the BG model described in the current thesis would result in a mathematical tool that can be used to explore these questions.

8.2.3 Cognitive architectures

Global workspace theory Global workspace is a popular theory that describes how the interplay between multiple parallel processes can generate a serial procession of conscious states. According to this theory, active brain processes operate in parallel and *compete* to gain access to a global workspace in order to *broadcast* their messages back to the rest of the active processes (Baars 1997).

The realization of the global workspace theory via metastable dynamics in the brain has been the subject of inderdeciplinary investigation (Werner 2007; Shanahan 2010a; Váša et al. 2015). The integration of the metastable oscillators model and the current BG model described before could provide valuable insights into how the underlying selection mechanism could facilitate competition and broadcast, the two necessary ingredients of global workspace theory.

Towards a biological model of re-evaluation based on inner rehearsal Shanahan 2006 presented a biologically plausible architecture that combines the concept of global workspace theory, with those of imagination and emotion. According to this proposal, affective action selection triggers a mechanism of inner rehearsal of the outcome of different prospective actions which, in turn, influences the salience of these actions.

The modelling work of this thesis, in combination with the extension discussed in the previous paragraph and a model of reward-modulated STDP (Izhikevich 2007b), provide the necessary building blocks for a low-level implementation of this architecture, using spiking neurons. The dynamical behaviour of this model could be compared with real brain recordings and provide valuable insights into how these phenomena occur in the human brain.

8.2.4 Parkinsonian tremor

Adaptive deep brain stimulation (aDBS) is a recently proposed treatment for the symptoms of PD. It has been shown to improve the effect of classical DBS on a variety of symptoms including tremor. However, the key characteristic of this technique is that the level of improvement depends largely on the feedback signal that is provided to the stimulation algorithm (Beudel and Brown 2016).

The current results indicate that one factor of tremor generation in PD is the interaction between cortical high-beta and the intrinsically-generated STN low-beta oscillations. Hence, based on this hypothesis, it was predicted that the application of oscillatory aDBS in the STN, where the feedback cancels out low-beta oscillations in the STN and it is applied only when this activity occurs, will show improvements over the classical fixed DBS. Since this technique would be based on more targeted stimulation and reduce the duration of DBS, it may also result on the improvement of related side effects, such as problems in gait and speech.

Finally, the effect of aDBS, as well as any new invasive techniques for tremor suppression, could be simulated using either the BG model of Chapter 3, or the extended model of the BG-thalamo-cortical loop in Chapter 7. This method would allow an initial evaluation of proposed surgical treatments, without animal experimentation.

Bibliography

Achard, P. and Schutter, E. D. 2006. "Complex parameter landscape for a complex neuron model." *PLoS Computational Biology* 2 (7): e94. (Cited on pages 40, 42).

Akam, T. and Kullmann, D. M. 2010. "Oscillations and filtering networks support flexible routing of information." *Neuron* 67 (2): 308–320. (Cited on page 128).

Alexander, G. E. and Crutcher, M. D. 1990. "Functional architecture of basal ganglia circuits: neural substrates of parallel processing." *Trends in neurosciences* 13 (7): 266–271. (Cited on page 56).

Alexander, G. E., DeLong, M. R., and Strick, P. L. 1986. "Parallel organization of functionally segregated circuits linking basal ganglia and cortex." *Annual review of neuroscience* 9 (1): 357–381. (Cited on pages 56, 64, 113).

Anderson, J. R. 1993. *Rules of the mind.* Psychology Press. (Cited on page 136).

Anderson, J. R., Bothell, D., Lebiere, C., and Matessa, M. 1998. "An integrated theory of list memory." *Journal of Memory and Language* 38 (4): 341–380. (Cited on page 130).

Anderson, J. R., Bothell, D., Byrne, M. D., Douglass, S., Lebiere, C., and Qin, Y. 2004. "An integrated theory of the mind." *Psychological review* 111 (4): 1036. (Cited on pages 131, 135, 136).

Androulidakis, A. G., Doyle, L. M., Yarrow, K., Litvak, V., Gilbertson, T. P., and Brown, P. 2007. "Anticipatory changes in beta synchrony in the human corticospinal system and associated improvements in task performance." *European Journal of Neuroscience* 25 (12): 3758–3765. (Cited on page 140).

Atherton, J. F. and Bevan, M. D. 2005. "Ionic mechanisms underlying autonomous action potential generation in the somata and dendrites of GABAergic substantia nigra pars reticulata neurons in vitro." *The Journal of neuroscience* 25 (36): 8272–8281. (Cited on page 67).

Atherton, J. F., Menard, A., Urbain, N., and Bevan, M. D. 2013. "Short-term depression of external globus pallidus-subthalamic nucleus synaptic transmission and implications for patterning subthalamic activity." *The Journal of Neuroscience* 33 (17): 7130–7144. (Cited on page 62).

Baars, B. J. 1997. *In the theater of consciousness: The workspace of the mind.* Oxford University Press on Demand. (Cited on pages 137, 161).

Badel, L., Lefort, S., Berger, T. K., Petersen, C. C., Gerstner, W., and Richardson, M. J. 2008. "Extracting non-linear integrate-and-fire models from experimental data using dynamic I–V curves." *Biological cybernetics* 99 (4-5): 361–370. (Cited on page 45).

Bahuguna, J., Aertsen, A., and Kumar, A. 2015. "Existence and Control of Go/No-Go Decision Transition Threshold in the Striatum." *PLoS Comput Biol* 11 (4): e1004233. (Cited on pages 20, 60, 77).

Baker, S. N. 2007. "Oscillatory interactions between sensorimotor cortex and the periphery." *Current opinion in neurobiology* 17 (6): 649–655. (Cited on page 91).

Barnett, L., Barrett, A. B., and Seth, A. K. 2009. "Granger causality and transfer entropy are equivalent for Gaussian variables." *Physical review letters* 103 (23): 238701. (Cited on page 85).

Barto, A. G. 1995. "11 Adaptive Critics and the Basal Ganglia." *Models of information processing in the basal ganglia:* 215. (Cited on page 19).

Baufreton, J., Atherton, J. F., Surmeier, D. J., and Bevan, M. D. 2005. "Enhancement of excitatory synaptic integration by GABAergic inhibition in the subthalamic nucleus." *The Journal of neuroscience* 25 (37): 8505–8517. (Cited on page 72).

Bauswein, E., Fromm, C., and Preuss, A. 1989. "Corticostriatal cells in comparison with pyramidal tract neurons: contrasting properties in the behaving monkey." *Brain research* 493 (1): 198–203. (Cited on page 65).

Beeler, J. a., Daw, N., Frazier, C. R. M., and Zhuang, X. 2010. "Tonic dopamine modulates exploitation of reward learning." *Frontiers in behavioral neuroscience* 4 (November): 170. (Cited on page 142).

Beggs, J. M. and Plenz, D. 2003. "Neuronal avalanches in neocortical circuits." *The Journal of neuroscience* 23 (35): 11167–11177. (Cited on page 53).

Beiser, D. G., Hua, S. E., and Houk, J. C. 1997. "Network models of the basal ganglia." *Current opinion in neurobiology* 7 (2): 185–190. (Cited on page 19).

Bekolay, T., Bergstra, J., Hunsberger, E., DeWolf, T., Stewart, T. C., Rasmussen, D., Choo, X., Voelker, A. R., and Eliasmith, C. 2013. "Nengo: a Python tool for building large-scale functional brain models." *Frontiers in neuroinformatics* 7. (Cited on pages 26, 29).

Belforte, J. E., Zsiros, V., Sklar, E. R., Jiang, Z., Yu, G., Li, Y., Quinlan, E. M., and Nakazawa, K. 2010. "Postnatal NMDA receptor ablation in corticolimbic interneurons confers schizophrenia-like phenotypes." *Nature neuroscience* 13 (1): 76–83. (Cited on page 65).

Benhamou, L., Bronfeld, M., Bar-Gad, I., and Cohen, D. 2012. "Globus Pallidus external segment neuron classification in freely moving rats: a comparison to primates." *PloS one* 7 (9): e45421. (Cited on pages 66, 97, 98, 107, 111).

Bergman, H., Wichmann, T., Karmon, B., and DeLong, M. 1994. "The primate subthalamic nucleus. II. Neuronal activity in the MPTP model of parkinsonism." *Journal of neurophysiology* 72 (2): 507–520. (Cited on pages 81, 90).

Bergman, H., Feingold, A., Nini, A., Raz, A., Slovin, H., Abeles, M., and Vaadia, E. 1998. "Physiological aspects of information processing in the basal ganglia of normal and parkinsonian primates." *Trends in neurosciences* 21 (1): 32–38. (Cited on page 88).

Berke, J. D. 2008. "Uncoordinated firing rate changes of striatal fast-spiking interneurons during behavioral task performance." *The Journal of Neuroscience* 28 (40): 10075–10080. (Cited on page 73).

Berke, J. D., Okatan, M., Skurski, J., and Eichenbaum, H. B. 2004. "Oscillatory entrainment of striatal neurons in freely moving rats." *Neuron* 43 (6): 883–896. (Cited on page 73).

Best, J. A., Nijhout, H. F., and Reed, M. C. 2009. "Homeostatic mechanisms in dopamine synthesis and release: a mathematical model." *Theoretical Biology and Medical Modelling* 6 (1): 21. (Cited on page 159).

Beste, C., Mückschel, M., Elben, S., Hartmann, C. J., McIntyre, C. C., Saft, C., Vesper, J., Schnitzler, A., and Wojtecki, L. 2014. "Behavioral and neurophysiological evidence for the enhancement of cognitive control under dorsal pallidal deep brain stimulation in Huntington's disease." *Brain Structure and Function:* 1–8. (Cited on page 94).

Beudel, M. and Brown, P. 2016. "Adaptive deep brain stimulation in Parkinson's disease." *Parkinsonism & related disorders* 22:S123–S126. (Cited on page 162).

Beurrier, C., Congar, P., Bioulac, B., and Hammond, C. 1999. "Subthalamic nucleus neurons switch from single-spike activity to burst-firing mode." *The Journal of neuroscience* 19 (2): 599–609. (Cited on page 70).

Bevan, M. D., Magill, P. J., Terman, D., Bolam, J. P., and Wilson, C. J. 2002. "Move to the rhythm: oscillations in the subthalamic nucleus–external globus pallidus network." *Trends in neurosciences* 25 (10): 525–531. (Cited on page 79).

Bevan, M. D. and Wilson, C. J. 1999. "Mechanisms underlying spontaneous oscillation and rhythmic firing in rat subthalamic neurons." *The Journal of neuroscience* 19 (17): 7617–7628. (Cited on page 69).

Bevan, M. D., Wilson, C. J., Bolam, J. P., and Magill, P. J. 2000. "Equilibrium potential of GABAA current and implications for rebound burst firing in rat subthalamic neurons in vitro." *Journal of Neurophysiology* 83 (5): 3169–3172. (Cited on pages 59, 68–70).

Bevan, M., Magill, P., Hallworth, N., Bolam, J., and Wilson, C. 2002. "Regulation of the timing and pattern of action potential generation in rat subthalamic neurons in vitro by GABA-A IPSPs." *Journal of neurophysiology* 87 (3): 1348–1362. (Cited on pages 68, 69, 89).

Beyeler, M., Carlson, K. D., Chou, T.-S., Dutt, N., and Krichmar, J. L. 2015. "CARLsim 3: A user-friendly and highly optimized library for the creation of neurobiologically detailed spiking neural networks." In *Neural Networks (IJCNN), 2015 International Joint Conference on,* 1–8. IEEE. (Cited on page 26).

Bhalla, U. S. and Bower, J. M. 1993. "Exploring parameter space in detailed single neuron models: simulations of the mitral and granule cells of the olfactory bulb." *Journal of Neurophysiology* 69 (6): 1948–1965. (Cited on pages 39, 43).

Bhowmik, D. and Shanahan, M. 2013. "Metastability and inter-band frequency modulation in networks of oscillating spiking neuron populations." *PloS one* 8 (4): e62234. (Cited on page 161).

Bogacz, R., Brown, E., Moehlis, J., Holmes, P., and Cohen, J. D. 2006. "The physics of optimal decision making: a formal analysis of models of performance in two-alternative forced-choice tasks." *Psychological review* 113 (4): 700. (Cited on pages 16, 18).

Bogacz, R. and Gurney, K. 2007. "The basal ganglia and cortex implement optimal decision making between alternative actions." *Neural computation* 19 (2): 442–477. (Cited on pages 18, 19).

Bonnefond, M. and Jensen, O. 2015. "Gamma Activity Coupled to Alpha Phase as a Mechanism for Top-Down Controlled Gating." *PloS one* 10 (6): e0128667. (Cited on page 141).

Booth, V. 2014. "Neuronal Model Hand-Tuning." In *Encyclopedia of Computational Neuroscience,* 1–3. Springer. (Cited on page 40).

Bormann, J. 1988. "Electrophysiology of GABA A and GABA B receptor subtypesex." *Trends in neurosciences* 11 (3): 112–116. (Cited on page 62).

Bower, J. M. and Beeman, D. 2012. *The book of GENESIS: exploring realistic neural models with the GEneral NEural SImulation System.* Springer Science & Business Media. (Cited on page 26).

Brette, R. and Goodman, D. F. 2012. "Simulating spiking neural networks on GPU." *Network: Computation in Neural Systems* 23 (4): 167–182. (Cited on pages 22, 27).

Brinkman, L., Stolk, A., Dijkerman, H. C., Lange, F. P. de, and Toni, I. 2014. "Distinct roles for alpha-and beta-band oscillations during mental simulation of goal-directed actions." *The Journal of Neuroscience* 34 (44): 14783–14792. (Cited on pages 20, 78, 92, 114, 141).

Brittain, J.-S. and Brown, P. 2014. "Oscillations and the basal ganglia: motor control and beyond." *Neuroimage* 85:637–647. (Cited on pages 20, 21, 78, 79, 88, 89, 91, 92, 114, 149, 159).

Brittain, J.-S., Cagnan, H., Mehta, A. R., Saifee, T. A., Edwards, M. J., and Brown, P. 2015. "Distinguishing the central drive to tremor in Parkinson's disease and essential tremor." *The Journal of Neuroscience* 35 (2): 795–806. (Cited on page 149).

Brown, P., Oliviero, A., Mazzone, P., Insola, A., Tonali, P., and Di Lazzaro, V. 2001. "Dopamine dependency of oscillations between subthalamic nucleus and pallidum in Parkinson's disease." *The Journal of neuroscience* 21 (3): 1033–1038. (Cited on pages 79, 88).

Brücke, C., Kupsch, A., Schneider, G.-H., Hariz, M., Nuttin, B., Kopp, U., Kempf, F., Trottenberg, T., Doyle, L., Chen, C., et al. 2007. "The subthalamic region is activated during valence-related emotional processing in patients with Parkinson's disease." *European Journal of Neuroscience* 26 (3): 767–774. (Cited on page 92).

Bugaysen, J., Bronfeld, M., Tischler, H., Bar-Gad, I., and Korngreen, A. 2010. "Electrophysiological characteristics of globus pallidus neurons." *PLoS One* 5 (8): e12001. (Cited on pages 59, 66, 67, 97–100, 102, 105, 107, 109, 111).

Buhusi, C. V. and Meck, W. H. 2005. "What makes us tick? Functional and neural mechanisms of interval timing." *Nature Reviews Neuroscience* 6 (10): 755–765. (Cited on page 159).

Burns, R. S., Chiueh, C. C., Markey, S. P., Ebert, M. H., Jacobowitz, D. M., and Kopin, I. J. 1983. "A primate model of parkinsonism: selective destruction of dopaminergic neurons in the pars compacta of the substantia nigra by N-methyl-4-phenyl-1, 2, 3, 6-tetrahydropyridine." *Proceedings of the National Academy of Sciences* 80 (14): 4546–4550. (Cited on page 90).

Buschman, T. J., Denovellis, E. L., Diogo, C., Bullock, D., and Miller, E. K. 2012. "Synchronous Oscillatory Neural Ensembles for Rules in the Prefrontal Cortex." *Neuron* 76 (4): 838–846. (Cited on pages 20, 114, 128, 129, 141, 160, 161).

Buzsaki, G. 2006. *Rhythms of the Brain.* Oxford University Press. (Cited on pages 20, 78).

Buzsáki, G. and Draguhn, A. 2004. "Neuronal oscillations in cortical networks." *Science* 304 (5679): 1926–1929. (Cited on page 130).

Cabral, J., Luckhoo, H., Woolrich, M., Joensson, M., Mohseni, H., Baker, A., Kringelbach, M. L., and Deco, G. 2014. "Exploring mechanisms of spontaneous functional connectivity in MEG: how delayed network interactions lead to structured amplitude envelopes of band-pass filtered oscillations." *Neuroimage* 90:423–435. (Cited on page 148).

Cagnan, H., Duff, E. P., and Brown, P. 2015. "The relative phases of basal ganglia activities dynamically shape effective connectivity in Parkinson's disease." *Brain* 138 (6): 1667–1678. (Cited on pages 95, 130, 158).

Cagnan, H. et al. 2014. "The nature of tremor circuits in parkinsonian and essential tremor." *Brain* 137 (12): 3223–3234. (Cited on page 144).

Calabresi, P., Picconi, B., Tozzi, A., Ghiglieri, V., and Di Filippo, M. 2014. "Direct and indirect pathways of basal ganglia: a critical reappraisal." *Nature neuroscience* 17 (8): 1022–1030. (Cited on page 92).

Cannon, R. C., Gleeson, P., Crook, S., Ganapathy, G., Marin, B., Piasini, E., and Silver, R. A. 2014. "LEMS: a language for expressing complex biological models in concise and hierarchical form and its use in underpinning NeuroML 2." *Frontiers in neuroinformatics* 8. (Cited on pages 26, 32).

Canolty, R. T., Edwards, E., Dalal, S. S., Soltani, M., Nagarajan, S. S., Kirsch, H. E., Berger, M. S., Barbaro, N. M., and Knight, R. T. 2006. "High gamma power is phase-locked to theta oscillations in human neocortex." *Science* 313 (5793): 1626–1628. (Cited on page 93).

Card, S. K., Newell, A., and Moran, T. P. 1983. "The psychology of human-computer interaction." (Cited on page 137).

Carlson, K. D., Nageswaran, J. M., Dutt, N., and Krichmar, J. L. 2014. "An efficient automated parameter tuning framework for spiking neural networks." *Frontiers in Neuroscience* 8 (10). (Cited on pages 40, 55).

Cavanagh, J. F., Figueroa, C. M., Cohen, M. X., and Frank, M. J. 2011. "Frontal theta reflects uncertainty and unexpectedness during exploration and exploitation." *Cerebral cortex:* bhr332. (Cited on pages 20, 114, 143).

Cavanagh, J. F. and Frank, M. J. 2014. "Frontal theta as a mechanism for cognitive control." *Trends in cognitive sciences* 18 (8): 414–421. (Cited on page 93).

Celada, P., Paladini, C., and Tepper, J. 1999. "GABAergic control of rat substantia nigra dopaminergic neurons: role of globus pallidus and substantia nigra pars reticulata." *Neuroscience* 89 (3): 813–825. (Cited on pages 73, 74).

Chaudhuri, K. R. and Schapira, A. H. 2009. "Non-motor symptoms of Parkinson's disease: dopaminergic pathophysiology and treatment." *The Lancet Neurology* 8 (5): 464–474. (Cited on page 144).

Chaudhuri, K. R., Tolosa, E., Schapira, A. H., and Poewe, W. 2014. *Non-motor symptoms of Parkinson's disease.* OUP Oxford. (Cited on page 144).

Chergui, K., Suaud-Chagny, M., and Gonon, F. 1994. "Nonlinear relationship between impulse flow, dopamine release and dopamine elimination in the rat brainin vivo." *Neuroscience* 62 (3): 641–645. (Cited on page 140).

Chorley, P. and Seth, A. K. 2011. "Dopamine-signaled reward predictions generated by competitive excitation and inhibition in a spiking neural network model." *Front Comput Neurosci* 5 (21.10): 3389. (Cited on page 159).

Clauset, A., Shalizi, C. R., and Newman, M. E. 2009. "Power-law distributions in empirical data." *SIAM review* 51 (4): 661–703. (Cited on page 53).

Cohen, J. D., McClure, S. M., and Yu, A. J. 2007. "Should I stay or should I go? How the human brain manages the trade-off between exploitation and exploration." *Philosophical transactions of the Royal Society of London. Series B, Biological sciences* 362 (1481): 933–42. (Cited on pages 16, 142).

Cohen, M. X. and Donner, T. H. 2013. "Midfrontal conflict-related theta-band power reflects neural oscillations that predict behavior." *Journal of Neurophysiology* 110 (12): 2752–2763. (Cited on page 154).

Colgin, L. L., Denninger, T., Fyhn, M., Hafting, T., Bonnevie, T., Jensen, O., Moser, M.-B., and Moser, E. I. 2009. "Frequency of gamma oscillations routes flow of information in the hippocampus." *Nature* 462 (7271): 353–7. (Cited on page 126).

Connelly, W. M., Schulz, J. M., Lees, G., and Reynolds, J. N. 2010. "Differential short-term plasticity at convergent inhibitory synapses to the substantia nigra pars reticulata." *The Journal of Neuroscience* 30 (44): 14854–14861. (Cited on pages 62, 72).

Connolly, A. T., Jensen, A. L., Bello, E. M., Netoff, T. I., Baker, K. B., Johnson, M. D., and Vitek, J. L. 2015. "Modulations in Oscillatory Frequency and Coupling in Globus Pallidus with Increasing Parkinsonian Severity." *The Journal of Neuroscience* 35 (15): 6231–6240. (Cited on page 91).

Cooper, A. and Stanford, I. 2000. "Electrophysiological and morphological characteristics of three subtypes of rat globus pallidus neurone in vitro." *The Journal of Physiology* 527 (2): 291–304. (Cited on pages 66, 97, 101).

Costa, R. M., Lin, S.-C., Sotnikova, T. D., Cyr, M., Gainetdinov, R. R., Caron, M. G., and Nicolelis, M. A. 2006. "Rapid alterations in corticostriatal ensemble coordination during acute dopamine-dependent motor dysfunction." *Neuron* 52 (2): 359–369. (Cited on page 81).

Cui, G., Jun, S. B., Jin, X., Pham, M. D., Vogel, S. S., Lovinger, D. M., and Costa, R. M. 2013. "Concurrent activation of striatal direct and indirect pathways during action initiation." *Nature* 494 (7436): 238–242. (Cited on page 113).

Davison, A. P., Brüderle, D., Eppler, J., Kremkow, J., Muller, E., Pecevski, D., Perrinet, L., and Yger, P. 2008. "PyNN: a common interface for neuronal network simulators." *Frontiers in neuroinformatics* 2. (Cited on pages 26, 32).

Dayan, P. and Abbott, L. F. 2001. *Theoretical neuroscience*. Cambridge, MA: MIT Press. (Cited on pages 52, 61, 72).

Deister, C. A., Dodla, R., Barraza, D., Kita, H., and Wilson, C. J. 2013. "Firing rate and pattern heterogeneity in the globus pallidus arise from a single neuronal population." *Journal of Neurophysiology* 109 (2): 497–506. eprint: `http://jn.physiology.org/content/109/2/497.full.pdf`. (Cited on page 97).

Delaville, C., Cruz, A. V., McCoy, A. J., Brazhnik, E., Avila, I., Novikov, N., and Walters, J. R. 2014. "Oscillatory activity in basal ganglia and motor cortex in an awake behaving rodent model of Parkinson's disease." *Basal ganglia* 3 (4): 221–227. (Cited on page 91).

DeLong, M. R. 1972. "Activity of basal ganglia neurons during movement." *Brain research* 40 (1): 127–135. (Cited on pages 59, 65, 66, 90, 97, 98, 107).

DeLong, M. R. 1990. "Primate models of movement disorders of basal ganglia origin." *Trends in neurosciences* 13 (7): 281–285. (Cited on page 92).

Dugast, C., Suaud-Chagny, M.-F., and Gonon, F. 1994. "Continuousin vivo monitoring of evoked dopamine release in the rat nucleus accumbens by amperometry." *Neuroscience* 62 (3): 647–654. (Cited on page 140).

Dvorzhak, A., Gertler, C., Harnack, D., and Grantyn, R. 2013. "High Frequency Stimulation of the Subthalamic Nucleus Leads to Presynaptic GABA (B)-Dependent Depression of Subthalamo-Nigral Afferents." *PloS one* 8 (12): e82191. (Cited on page 62).

Eckhorn, R., Bauer, R., Jordan, W., Brosch, M., Kruse, W., Munk, M., and Reitboeck, H. 1988. "Coherent oscillations: A mechanism of feature linking in the visual cortex?" *Biological cybernetics* 60 (2): 121–130. (Cited on pages 20, 78, 93, 126).

Edgerton, J. R., Hanson, J. E., Günay, C., and Jaeger, D. 2010. "Dendritic sodium channels regulate network integration in globus pallidus neurons: a modeling study." *The Journal of Neuroscience* 30 (45): 15146–15159. (Cited on page 111).

Eiben, A. E. and Schippers, C. 1998. "On evolutionary exploration and exploitation." *Fundamenta Informaticae* 35 (1): 35–50. (Cited on page 42).

Eichhammer, E. 2014. "QCustomPlot." `http://www.qcustomplot.com/`. (Cited on page 37).

Eliasmith, C. and Anderson, C. H. 2004. *Neural engineering: Computation, representation, and dynamics in neurobiological systems.* MIT press. (Cited on page 20).

Eliasmith, C., Stewart, T. C., Choo, X., Bekolay, T., DeWolf, T., Tang, Y., and Rasmussen, D. 2012. "A large-scale model of the functioning brain." *Science* 338 (6111): 1202–1205. (Cited on pages 21, 39).

Engel, A. K. and Fries, P. 2010. "Beta-band oscillations—signalling the status quo?" *Current opinion in neurobiology* 20 (2): 156–165. (Cited on page 91).

Eusebio, A., Chen, C. C., Lu, C. S., Lee, S. T., Tsai, C. H., Limousin, P., Hariz, M., and Brown, P. 2008. "Effects of low-frequency stimulation of the subthalamic nucleus on movement in Parkinson's disease." *Experimental neurology* 209 (1): 125–130. (Cited on page 151).

Euteneuer, F., Schaefer, F., Stuermer, R., Boucsein, W., Timmermann, L., Barbe, M. T., Ebersbach, G., Otto, J., Kessler, J., and Kalbe, E. 2009. "Dissociation of decision-making under ambiguity and decision-making under risk in patients with Parkinson's disease: a neuropsychological and psychophysiological study." *Neuropsychologia* 47 (13): 2882–2890. (Cited on page 21).

Farries, M. A., Kita, H., and Wilson, C. J. 2010. "Dynamic spike threshold and zero membrane slope conductance shape the response of subthalamic neurons to cortical input." *The Journal of Neuroscience* 30 (39): 13180–13191. (Cited on page 73).

Féger, J. and Robledo, P. 1991. "The effects of activation or inhibition of the subthalamic nucleus on the metabolic and electrophysiological activities within the pallidal complex and substantia nigra in the rat." *European Journal of Neuroscience* 3 (10): 947–952. (Cited on pages 73, 74).

Felleman, D. J. and Van Essen, D. C. 1991. "Distributed hierarchical processing in the primate cerebral cortex." *Cerebral cortex* 1 (1): 1–47. (Cited on page 136).

Fidjeland, A. K. and Shanahan, M. P. 2010. "Accelerated simulation of spiking neural networks using GPUs." In *Neural Networks (IJCNN), The 2010 International Joint Conference on,* 1–8. IEEE. (Cited on pages 22, 26, 27, 40, 47).

Fortin, F.-A., De Rainville, F.-M., Gardner, M.-A., Parizeau, M., and Gagné, C. 2012. "DEAP: Evolutionary Algorithms Made Easy." *Journal of Machine Learning Research* 13:2171–2175. (Cited on page 47).

Fountas, Z. 2011. "Spiking neural networks for human-like avatar control in a simulated environment." Master's thesis, MSc thesis, Imperial College London. (Cited on page 36).

Fountas, Z. and Shanahan, M. 2014. "Phase offset between slow oscillatory cortical inputs influences competition in a model of the basal ganglia." In *Neural Networks (IJCNN), 2014 International Joint Conference on,* 2407–2414. IEEE. (Cited on pages 39, 56, 158).

———. 2015. "GPU-based fast parameter optimization for phenomenological spiking neural models." In *2015 International Joint Conference on Neural Networks (IJCNN),* 1–8. (Cited on pages 65, 69).

Frank, M. J. 2011. "Computational models of motivated action selection in corticostriatal circuits." *Current opinion in neurobiology* 21 (3): 381–386. (Cited on page 19).

Franklin, S., Baars, B. J., Ramamurthy, U., and Ventura, M. 2005. "The role of consciousness in memory." *Brains, Minds and Media* 1 (1): 38. (Cited on page 137).

Freeze, B. S., Kravitz, A. V., Hammack, N., Berke, J. D., and Kreitzer, A. C. 2013. "Control of basal ganglia output by direct and indirect pathway projection neurons." *The Journal of Neuroscience* 33 (47): 18531–18539. (Cited on page 92).

Friedrich, P., Vella, M., Gulyás, A. I., Freund, T. F., and Káli, S. 2014. "A flexible, interactive software tool for fitting the parameters of neuronal models." *Frontiers in Neuroinformatics* 8 (63). (Cited on page 40).

Friend, D. M. and Kravitz, A. V. 2014. "Working together: Basal ganglia pathways in action selection." *Trends in Neurosciences* 37 (6): 301–303. (Cited on pages 18, 113, 114).

Fries, P. 2005. "A mechanism for cognitive dynamics: neuronal communication through neuronal coherence." *Trends in cognitive sciences* 9 (10): 474–480. (Cited on pages 20, 78, 93, 95).

Fries, P. 2009. "Neuronal gamma-band synchronization as a fundamental process in cortical computation." *Annual review of neuroscience* 32:209–224. (Cited on pages 20, 78, 93, 95, 114, 126).

Gamez, D. 2007. "Spikestream: a fast and flexible simulator of spiking neural networks." In *Artificial Neural Networks–ICANN 2007,* 360–369. Springer. (Cited on page 26).

Gamez, D., Fountas, Z., and Fidjeland, A. K. 2013. "A neurally controlled computer game avatar with humanlike behavior." *Computational Intelligence and AI in Games, IEEE Transactions on* 5 (1): 1–14. (Cited on page 39).

Geit, W. V., Schutter, E. D., and Achard, P. 2008. "Automated neuron model optimization techniques: a review." *Biological cybernetics* 99 (4-5): 241–251. (Cited on pages 25, 40, 42, 65).

"Geppetto Simulation Engine." 2016. `http://www.geppetto.org/`. (Cited on page 26).

Gerfen, C. R. and Wilson, C. J. 1996. "Chapter II: The basal ganglia." In *Integrated systems of the CNS, Part III Cerebellum, basal ganglia, olfactory system,* edited by L. Swanson, A. Bjorklund, and T. Hokfelt, 12:371–468. Handbook of Chemical Neuroanatomy. Elsevier. (Cited on pages 66, 97, 108).

Gernert, M., Fedrowitz, M., Wlaz, P., and Löscher, W. 2004. "Subregional changes in discharge rate, pattern, and drug sensitivity of putative GABAergic nigral neurons in the kindling model of epilepsy." *European Journal of Neuroscience* 20 (9): 2377–2386. (Cited on page 74).

Gernert, M., Richter, A., and Löscher, W. 1999. "In vivo extracellular electrophysiology of pallidal neurons in dystonic and nondystonic hamsters." *Journal of neuroscience research* 57 (6): 894–905. (Cited on page 81).

Gittis, A. H., Berke, J. D., Bevan, M. D., Chan, C. S., Mallet, N., Morrow, M. M., and Schmidt, R. 2014. "New roles for the external globus pallidus in basal ganglia circuits and behavior." *The Journal of Neuroscience* 34 (46): 15178–15183. (Cited on pages 108, 112).

Gittis, A. H., Nelson, A. B., Thwin, M. T., Palop, J. J., and Kreitzer, A. C. 2010. "Distinct roles of GABAergic interneurons in the regulation of striatal output pathways." *The Journal of Neuroscience* 30 (6): 2223–2234. (Cited on page 60).

Gold, J. I. and Shadlen, M. N. 2003. "The influence of behavioral context on the representation of a perceptual decision in developing oculomotor commands." *The Journal of neuroscience : the official journal of the Society for Neuroscience* 23 (2): 632–651. (Cited on page 141).

Goodman, D. and Brette, R. 2008. "Brian: a simulator for spiking neural networks in Python." *Frontiers in neuroinformatics* 2. (Cited on pages 26, 28).

Götz, T., Kraushaar, U., Geiger, J., Lübke, J., Berger, T., and Jonas, P. 1997. "Functional properties of AMPA and NMDA receptors expressed in identified types of basal ganglia neurons." *The Journal of neuroscience* 17 (1): 204–215. (Cited on pages 71, 72).

Günay, C., Edgerton, J. R., and Jaeger, D. 2008. "Channel density distributions explain spiking variability in the globus pallidus: a combined physiology and computer simulation database approach." *The Journal of Neuroscience* 28 (30): 7476–7491. (Cited on pages 106, 111, 112).

Gurney, K. N., Humphries, M. D., and Redgrave, P. 2015. "A New Framework for Cortico-Striatal Plasticity: Behavioural Theory Meets In Vitro Data at the Reinforcement-Action Interface." *PLoS biology* 13 (1): e1002034. (Cited on pages 56, 75, 113).

Gurney, K., Prescott, T. J., and Redgrave, P. 2001. "A computational model of action selection in the basal ganglia. I. A new functional anatomy." *Biological cybernetics* 84 (6): 401–410. (Cited on pages 18–20).

Haggard, P. 2005. "Conscious intention and motor cognition." *Trends in cognitive sciences* 9 (6): 290–295. (Cited on page 16).

———. 2008. "Human volition: towards a neuroscience of will." *Nature Reviews Neuroscience* 9 (12): 934–946. (Cited on pages 16–18, 140).

Hallworth, N. E., Wilson, C. J., and Bevan, M. D. 2003. "Apamin-sensitive small conductance calcium-activated potassium channels, through their selective coupling to voltage-gated calcium channels, are critical determinants of the precision, pace, and pattern of action potential generation in rat subthalamic nucleus neurons in vitro." *The Journal of neuroscience* 23 (20): 7525–7542. (Cited on pages 61, 67–69).

Hammond, C., Bergman, H., and Brown, P. 2007. "Pathological synchronization in Parkinson's disease: networks, models and treatments." *Trends in neurosciences* 30 (7): 357–364. (Cited on pages 88, 89).

Händel, B. F., Haarmeier, T., and Jensen, O. 2011. "Alpha oscillations correlate with the successful inhibition of unattended stimuli." *Journal of cognitive neuroscience* 23 (9): 2494–2502. (Cited on pages 92, 141).

Hansen, N. and Ostermeier, A. 2001. "Completely derandomized self-adaptation in evolution strategies." *Evolutionary computation* 9 (2): 159–195. (Cited on page 43).

Hanslmayr, S., Staudigl, T., and Fellner, M.-C. 2012. "Oscillatory power decreases and long-term memory: the information via desynchronization hypothesis." *Frontiers in human neuroscience* 6. (Cited on pages 20, 78, 92).

Hanson, J. E. and Jaeger, D. 2002. "Short-term plasticity shapes the response to simulated normal and parkinsonian input patterns in the globus pallidus." *The Journal of neuroscience* 22 (12): 5164–5172. (Cited on page 101).

Hanson, J. E. and Smith, Y. 2002. "Subcellular distribution of high-voltage-activated calcium channel subtypes in rat globus pallidus neurons." *Journal of Comparative Neurology* 442 (2): 89–98. (Cited on page 111).

Hanson, J. E., Smith, Y., and Jaeger, D. 2004. "Sodium channels and dendritic spike initiation at excitatory synapses in globus pallidus neurons." *The Journal of Neuroscience* 24 (2): 329–340. (Cited on pages 106, 110).

He, B. J. 2014. "Scale-free brain activity: past, present, and future." *Trends in cognitive sciences* 18 (9): 480–487. (Cited on page 53).

Healy, A. F. and Proctor, R. W. 2003. *Handbook of Psychology,* 4:734. (Cited on page 16).

Heitz, R. P. 2014. "The speed-accuracy tradeoff: History, physiology, methodology, and behavior." *Frontiers in Neuroscience,* no. 8 JUN. (Cited on page 123).

Heitz, R. P. and Engle, R. W. 2007. "Focusing the spotlight: Individual differences in visual attention control." *Journal of Experimental Psychology: General* 136 (2): 217–240. (Cited on pages 123, 140).

Helie, S., Chakravarthy, S., and Moustafa, A. A. 2013. "Exploring the cognitive and motor functions of the basal ganglia: an integrative review of computational cognitive neuroscience models." *Frontiers in computational neuroscience* 7. (Cited on pages 20, 157).

Helmich, R. C., Aarts, E., Lange, F. P. de, Bloem, B. R., and Toni, I. 2009. "Increased dependence of action selection on recent motor history in Parkinson's disease." *The Journal of Neuroscience* 29 (19): 6105–6113. (Cited on page 144).

Helmich, R. C., Hallett, M., Deuschl, G., Toni, I., and Bloem, B. R. 2012. "Cerebral causes and consequences of parkinsonian resting tremor: a tale of two circuits?" *Brain* 135 (11): 3206–3226. (Cited on page 152).

Hendrickson, E. B., Edgerton, J. R., and Jaeger, D. 2011. "The capabilities and limitations of conductance-based compartmental neuron models with reduced branched or unbranched morphologies and active dendrites." *Journal of computational neuroscience* 30 (2): 301–321. (Cited on page 106).

Hertäg, L., Hass, J., Golovko, T., and Durstewitz, D. 2012. "An approximation to the adaptive exponential integrate-and-fire neuron model allows fast and predictive fitting to physiological data." *Frontiers in computational neuroscience* 6. (Cited on pages 40, 44, 45).

Hines, M. L. and Carnevale, N. T. 1997. "The NEURON simulation environment." *Neural computation* 9 (6): 1179–1209. (Cited on page 26).

Hodgkin, A. L. and Huxley, A. F. 1952. "A quantitative description of membrane current and its application to conduction and excitation in nerve." *The Journal of physiology* 117 (4): 500–544. (Cited on pages 27, 98, 105, 110).

Hoover, J. E. and Strick, P. L. 1993. "Multiple output channels in the basal ganglia." *Science* 259 (5096): 819–821. (Cited on page 56).

Horschig, J. M., Smolders, R., Bonnefond, M., Schoffelen, J.-M., Van den Munckhof, P., Schuurman, P. R., Cools, R., Denys, D., and Jensen, O. 2015. "Directed Communication between Nucleus Accumbens and Neocortex in Humans Is Differentially Supported by Synchronization in the Theta and Alpha Band." *PloS one* 10 (9): e0138685. (Cited on page 141).

Humphries, M. D. 2014. "Slaves to the rhythm: coupling of the subthalamic nucleus–globus pallidus network in Parkinsonian oscillations." *The Journal of physiology* 592 (7): 1427–1428. (Cited on page 108).

Humphries, M. D., Khamassi, M., and Gurney, K. 2012. "Dopaminergic Control of the Exploration-Exploitation Trade-Off via the Basal Ganglia." *Frontiers in neuroscience* 6 (February): 9. (Cited on pages 142, 147).

Humphries, M. D., Lepora, N., Wood, R., and Gurney, K. 2009. "Capturing dopaminergic modulation and bimodal membrane behaviour of striatal medium spiny neurons in accurate, reduced models." *Frontiers in computational neuroscience* 3. (Cited on pages 110, 120).

Humphries, M. D., Stewart, R., and Gurney, K. N. 2006. "A physiologically plausible model of action selection and oscillatory activity in the basal ganglia." *The Journal of neuroscience* 26 (50): 12921–12942. (Cited on pages 19, 56, 62, 64, 71, 75, 113, 120, 128).

Humphries, M. D., Wood, R., and Gurney, K. 2009. "Dopamine-modulated dynamic cell assemblies generated by the GABAergic striatal microcircuit." *Neural Networks* 22 (8): 1174–1188. (Cited on pages 20, 59).

———. 2010. "Reconstructing the three-dimensional GABAergic microcircuit of the striatum." *PLoS computational biology* 6 (11): e1001011. (Cited on pages 39, 57–59, 71).

Izhikevich, E. M. et al. 2003. "Simple model of spiking neurons." *IEEE Transactions on neural networks* 14 (6): 1569–1572. (Cited on pages 27, 41, 60, 61, 75).

Izhikevich, E. M. 2007a. *Dynamical systems in neuroscience.* MIT Press, Cambridge, MA. (Cited on pages 25, 40, 41, 44, 48–51, 60, 61, 69).

———. 2007b. "Solving the distal reward problem through linkage of STDP and dopamine signaling." *Cerebral cortex* 17 (10): 2443–2452. (Cited on pages 159, 162).

Izhikevich, E. M. and Edelman, G. M. 2008. "Large-scale model of mammalian thalamocortical systems." *Proceedings of the national academy of sciences* 105 (9): 3593–3598. (Cited on pages 39, 52).

Jahnsen, H. and Llinas, R. 1984. "Electrophysiological properties of guinea-pig thalamic neurones: an in vitro study." *The Journal of physiology* 349 (1): 205–226. (Cited on page 48).

Jankovic, J. 2008. "Parkinson's disease: clinical features and diagnosis." *Journal of Neurology, Neurosurgery & Psychiatry* 79 (4): 368–376. (Cited on page 144).

Jastrzembski, T. S. and Charness, N. 2007. "The Model Human Processor and the older adult: Parameter estimation and validation within a mobile phone task." *Journal of Experimental Psychology: Applied* 13 (4): 224–248. (Cited on pages 137, 138).

Jenkinson, N. and Brown, P. 2011. "New insights into the relationship between dopamine, beta oscillations and motor function." *Trends in neurosciences* 34 (12): 611–618. (Cited on pages 81, 123, 124).

Jensen, A. R. 2006. *Clocking the mind: Mental chronometry and individual differences.* Elsevier. (Cited on page 15).

Jensen, O. and Mazaheri, A. 2010. "Shaping functional architecture by oscillatory alpha activity: gating by inhibition." *Frontiers in human neuroscience* 4. (Cited on pages 92, 141).

Jin, X., Tecuapetla, F., and Costa, R. M. 2014. "Basal ganglia subcircuits distinctively encode the parsing and concatenation of action sequences." *Nature neuroscience* 17 (3): 423–30. eprint: `NIHMS150003`. (Cited on pages 18, 113).

Jones, E., Oliphant, T., Peterson, P., et al. 2001–2015. *SciPy: Open source scientific tools for Python.* (Cited on page 47).

Joundi, R. A., Jenkinson, N., Brittain, J.-S., Aziz, T. Z., and Brown, P. 2012. "Driving oscillatory activity in the human cortex enhances motor performance." *Current Biology* 22 (5): 403–407. (Cited on pages 90, 93).

Kaneda, K., Kita, T., and Kita, H. 2007. "Repetitive activation of glutamatergic inputs evokes a long-lasting excitation in rat globus pallidus neurons in vitro." *Journal of neurophysiology* 97 (1): 121–133. (Cited on page 110).

Kayraklioglu, E., El-Ghazawi, T., and Bozkus, Z. 2015. "Accelerating Brain Simulations on Graphical Processing Units." In *Computer and Information Technology; Ubiquitous Computing and Communications; Dependable, Autonomic and Secure Computing; Pervasive Intelligence and Computing (CIT/IUCC/DASC/PICOM), 2015 IEEE International Conference on,* 556–560. IEEE. (Cited on page 26).

Kayser, A. S., Mitchell, J. M., Weinstein, D., and Frank, M. J. 2015. "Dopamine, locus of control, and the exploration-exploitation tradeoff." *Neuropsychopharmacology* 40 (2): 454–462. (Cited on page 143).

Kim, J. and Kita, H. 2013. "Short-term plasticity shapes activity pattern-dependent striatopallidal synaptic transmission." *Journal of neurophysiology* 109 (4): 932–939. (Cited on pages 21, 62, 90, 97, 101, 114).

Kita, H. and Kitai, S. 1991. "Intracellular study of rat globus pallidus neurons: membrane properties and responses to neostriatal, subthalamic and nigral stimulation." *Brain research* 564 (2): 296–305. (Cited on pages 101, 110, 111).

Kita, H., Nambu, A., Kaneda, K., Tachibana, Y., and Takada, M. 2004. "Role of ionotropic glutamatergic and GABAergic inputs on the firing activity of neurons in the external pallidum in awake monkeys." *J Neurophysiol* 92 (5): 3069–3084. (Cited on page 94).

Kobayakawa, M., Koyama, S., Mimura, M., and Kawamura, M. 2008. "Decision making in Parkinson's disease: Analysis of behavioral and physiological patterns in the Iowa gambling task." *Movement disorders* 23 (4): 547–552. (Cited on page 144).

Koós, T. and Tepper, J. M. 1999. "Inhibitory control of neostriatal projection neurons by GABAergic interneurons." *Nature neuroscience* 2 (5): 467–472. (Cited on page 58).

Koos, T., Tepper, J. M., and Wilson, C. J. 2004. "Comparison of IPSCs evoked by spiny and fast-spiking neurons in the neostriatum." *The Journal of neuroscience* 24 (36): 7916–7922. (Cited on pages 58, 72).

Kravitz, A. V., Freeze, B. S., Parker, P. R., Kay, K., Thwin, M. T., Deisseroth, K., and Kreitzer, A. C. 2010. "Regulation of parkinsonian motor behaviours by optogenetic control of basal ganglia circuitry." *Nature* 466 (7306): 622–626. (Cited on pages 92, 113).

Krumin, M. and Shoham, S. 2009. "Generation of spike trains with controlled auto-and cross-correlation functions." *Neural Computation* 21 (6): 1642–1664. (Cited on page 98).

Kühn, A. A., Kupsch, A., Schneider, G.-H., and Brown, P. 2006. "Reduction in subthalamic 8–35 Hz oscillatory activity correlates with clinical improvement in Parkinson's disease." *European Journal of Neuroscience* 23 (7): 1956–1960. (Cited on pages 21, 88).

Kuramoto, Y. 1984. *Chemical oscillations, waves, and turbulence.* Vol. 19. Springer Science & Business Media. (Cited on page 147).

Laming, D. R. J. 1968. "Information theory of choice-reaction times." (Cited on page 140).

Larkum, M. E., Waters, J., Sakmann, B., and Helmchen, F. 2007. "Dendritic spikes in apical dendrites of neocortical layer 2/3 pyramidal neurons." *The Journal of Neuroscience* 27 (34): 8999–9008. (Cited on page 111).

Le Van Quyen, M., Foucher, J., Lachaux, J.-P., Rodriguez, E., Lutz, A., Martinerie, J., and Varela, F. J. 2001. "Comparison of Hilbert transform and wavelet methods for the analysis of neuronal synchrony." *Journal of neuroscience methods* 111 (2): 83–98. (Cited on page 82).

Lenz, F., Vitek, J., and DeLong, M. 1993. "Role of the thalamus in parkinsonian tremor: evidence from studies in patients and primate models." *Stereotactic and functional neurosurgery* 60 (1-3): 94–103. (Cited on page 144).

Leventhal, D. K., Gage, G. J., Schmidt, R., Pettibone, J. R., Case, A. C., and Berke, J. D. 2012. "Basal ganglia beta oscillations accompany cue utilization." *Neuron* 73 (3): 523–536. (Cited on pages 20, 78, 88, 91, 101, 123, 124).

Li, P. and Vu, Q. D. 2013. "Identification of parameter correlations for parameter estimation in dynamic biological models." *BMC systems biology* 7 (1): 91. (Cited on page 40).

Ligot, N., Krystkowiak, P., Simonin, C., Goldman, S., Peigneux, P., Van Naemen, J., Monclus, M., Lacroix, S. F., Devos, D., Dujardin, K., et al. 2011. "External globus pallidus stimulation modulates brain connectivity in Huntington's disease." *Journal of Cerebral Blood Flow & Metabolism* 31 (1): 41–46. (Cited on page 94).

Lindahl, M., Sarvestani, I. K., Ekeberg, Ö., and Kotaleski, J. H. 2013. "Signal enhancement in the output stage of the basal ganglia by synaptic short-term plasticity in the direct, indirect, and hyperdirect pathways." *Frontiers in computational neuroscience* 7. (Cited on pages 20, 56, 58, 59, 62, 63, 72–74, 120, 127).

Little, S. and Brown, P. 2014. "The functional role of beta oscillations in Parkinson's disease." *Parkinsonism & related disorders* 20:S44–S48. (Cited on pages 21, 88, 92).

Little, S., Pogosyan, A., Neal, S., Zavala, B., Zrinzo, L., Hariz, M., Foltynie, T., Limousin, P., Ashkan, K., FitzGerald, J., et al. 2013. "Adaptive deep brain stimulation in advanced Parkinson disease." *Annals of neurology* 74 (3): 449–457. (Cited on pages 21, 94, 148).

Litvak, V., Jha, A., Eusebio, A., Oostenveld, R., Foltynie, T., Limousin, P., Zrinzo, L., Hariz, M. I., Friston, K., and Brown, P. 2011. "Resting oscillatory cortico-subthalamic connectivity in patients with Parkinson's disease." *Brain* 134 (2): 359–374. (Cited on pages 21, 78, 89, 92, 114, 149).

Llinas, R. 1988. "The intrinsic electrophysiological properties of mammalian neurons: insights into central nervous system function." *Science* 242 (4886): 1654–1664. (Cited on page 144).

López-Azcárate, J., Tainta, M., Rodríguez-Oroz, M. C., Valencia, M., González, R., Guridi, J., Iriarte, J., Obeso, J. A., Artieda, J., and Alegre, M. 2010. "Coupling between beta and high-frequency activity in the human subthalamic nucleus may be a pathophysiological mechanism in Parkinson's disease." *The Journal of neuroscience* 30 (19): 6667–6677. (Cited on pages 81, 89, 90).

Loucif, A. J., Woodhall, G. L., Sehirli, U. S., and Stanford, I. M. 2008. "Depolarisation and suppression of burst firing activity in the mouse subthalamic nucleus by dopamine D1/D5 receptor activation of a cyclic-nucleotide gated non-specific cation conductance." *Neuropharmacology* 55 (1): 94–105. (Cited on page 70).

Madl, T., Baars, B. J., and Franklin, S. 2011. "The timing of the cognitive cycle." *PloS one* 6 (4): e14803. (Cited on pages 130, 135–137).

Magnin, M., Morel, A., and Jeanmonod, D. 2000. "Single-unit analysis of the pallidum, thalamus and subthalamic nucleus in parkinsonian patients." *Neuroscience* 96 (3): 549–564. (Cited on page 144).

Mahon, S., Vautrelle, N., Pezard, L., Slaght, S. J., Deniau, J.-M., Chouvet, G., and Charpier, S. 2006. "Distinct patterns of striatal medium spiny neuron activity during the natural sleep-wake cycle." *The Journal of Neuroscience* 26 (48): 12587–95. (Cited on pages 21, 114).

Mailly, P., Charpier, S., Menetrey, A., and Deniau, J.-M. 2003. "Three-dimensional organization of the recurrent axon collateral network of the substantia nigra pars reticulata neurons in the rat." *The Journal of neuroscience* 23 (12): 5247–5257. (Cited on page 58).

Mallet, N., Micklem, B. R., Henny, P., Brown, M. T., Williams, C., Bolam, J. P., Nakamura, K. C., and Magill, P. J. 2012. "Dichotomous organization of the external globus pallidus." *Neuron* 74 (6): 1075–1086. (Cited on page 97).

Mallet, N., Pogosyan, A., Márton, L. F., Bolam, J. P., Brown, P., and Magill, P. J. 2008. "Parkinsonian Beta Oscillations in the External Globus Pallidus and Their Relationship with Subthalamic Nucleus Activity." *The Journal of Neuroscience* 28 (52): 14245–14258. (Cited on pages 97, 112).

Mallet, N. et al. 2016. "Arkypallidal Cells Send a Stop Signal to Striatum." *Neuron* 89 (2): 1–9. (Cited on pages 97, 108, 112).

Markram, H., Wang, Y., and Tsodyks, M. 1998. "Differential signaling via the same axon of neocortical pyramidal neurons." *Proceedings of the National Academy of Sciences* 95 (9): 5323–5328. (Cited on page 62).

Mastro, K. J., Bouchard, R. S., Holt, H. A. K., and Gittis, A. H. 2014. "Transgenic Mouse Lines Subdivide External Segment of the Globus Pallidus (GPe) Neurons and Reveal Distinct GPe Output Pathways." *Journal of Neuroscience* 34 (6): 2087–2099. (Cited on page 108).

McCarthy, M., Moore-Kochlacs, C., Gu, X., Boyden, E., Han, X., and Kopell, N. 2011. "Striatal origin of the pathologic beta oscillations in Parkinson's disease." *Proceedings of the National Academy of Sciences* 108 (28): 11620–11625. (Cited on page 89).

McConnell, G. C., So, R. Q., Hilliard, J. D., Lopomo, P., and Grill, W. M. 2012. "Effective deep brain stimulation suppresses low-frequency network oscillations in the basal ganglia by regularizing neural firing patterns." *The Journal of Neuroscience* 32 (45): 15657–15668. (Cited on pages 98, 109).

Meyer, D. E. and Kieras, D. E. 1997. "A computational theory of executive cognitive processes and multiple-task performance: Part I. Basic mechanisms." *Psychological review* 104 (1): 3. (Cited on page 136).

Michmizos, K. P. and Nikita, K. S. 2011. "Local field potential driven Izhikevich model predicts a subthalamic nucleus neuron activity." In *Engineering in Medicine and Biology Society, EMBC, 2011 Annual International Conference of the IEEE,* 5900–5903. IEEE. (Cited on page 120).

Miller, B. R., Walker, A. G., Shah, A. S., Barton, S. J., and Rebec, G. V. 2008. "Dysregulated information processing by medium spiny neurons in striatum of freely behaving mouse models of Huntington's disease." *Journal of neurophysiology* 100 (4): 2205–2216. (Cited on page 73).

Mink, J. W. 1996. "The basal ganglia: focused selection and inhibition of competing motor programs." *Progress in neurobiology* 50 (4): 381–425. (Cited on pages 56, 58, 113).

Mitra, P. P. and Pesaran, B. 1999. "Analysis of dynamic brain imaging data." *Biophysical journal* 76 (2): 691–708. (Cited on page 79).

Montoya, A., Pelletier, M., Menear, M., Duplessis, E., Richer, F., and Lepage, M. 2006. "Episodic memory impairment in Huntington's disease: a meta-analysis." *Neuropsychologia* 44 (10): 1984–94. (Cited on pages 21, 94).

Moran, A., Bergman, H., Israel, Z., and Bar-Gad, I. 2008. "Subthalamic nucleus functional organization revealed by parkinsonian neuronal oscillations and synchrony." *Brain* 131 (12): 3395–3409. (Cited on pages 89, 92).

Moran, A., Stein, E., Tischler, H., Belelovsky, K., and Bar-Gad, I. 2011. "Dynamic stereotypic responses of Basal Ganglia neurons to subthalamic nucleus high-frequency stimulation in the parkinsonian primate." *Frontiers in systems neuroscience* 5. (Cited on page 74).

Moro, E., Esselink, R., Xie, J., Hommel, M., Benabid, A., and Pollak, P. 2002. "The impact on Parkinson's disease of electrical parameter settings in STN stimulation." *Neurology* 59 (5): 706–713. (Cited on pages 148, 151).

Moyer, J. T., Wolf, J. A., and Finkel, L. H. 2007. "Effects of dopaminergic modulation on the integrative properties of the ventral striatal medium spiny neuron." *Journal of neurophysiology* 98 (6): 3731–3748. (Cited on page 72).

Nagel, S. J., Machado, A. G., Gale, J. T., Lobel, D. A., and Pandya, M. 2015. "Preserving cortico-striatal function: deep brain stimulation in Huntington's disease." *Frontiers in systems neuroscience* 9. (Cited on pages 21, 94).

Nakanishi, H., Tamura, A., Kawai, K., and Yamamoto, K. 1997. "Electrophysiological studies of rat substantia nigra neurons in an in vitro slice preparation after middle cerebral artery occlusion." *Neuroscience* 77 (4): 1021–1028. (Cited on pages 67, 68).

Nambu, A. and Llinas, R. 1994. "Electrophysiology of globus pallidus neurons in vitro." *Journal of neurophysiology* 72 (3): 1127–1139. (Cited on page 110).

Nambu, A. 2011. "Somatotopic organization of the primate basal ganglia." *Frontiers in Neuroanatomy* 5. (Cited on page 56).

Nelder, J. A. and Mead, R. 1965. "A simplex method for function minimization." *The computer journal* 7 (4): 308–313. (Cited on pages 43, 73).

Nevado-Holgado, A. J., Mallet, N., Magill, P. J., and Bogacz, R. 2014. "Effective connectivity of the subthalamic nucleus-globus pallidus network during Parkinsonian oscillations." *The Journal of physiology* 592 (Pt 7): 1429–55. (Cited on page 112).

Nyhus, E. and Curran, T. 2010. "Functional role of gamma and theta oscillations in episodic memory." *Neuroscience & Biobehavioral Reviews* 34 (7): 1023–1035. (Cited on page 93).

O'Connor, P., Neil, D., Liu, S.-C., Delbruck, T., and Pfeiffer, M. 2013. "Real-time classification and sensor fusion with a spiking deep belief network." *Frontiers in neuroscience* 7. (Cited on page 39).

Oorschot, D. E. 1996. "Total number of neurons in the neostriatal, pallidal, subthalamic, and substantia nigral nuclei of the rat basal ganglia: a stereological study using the cavalieri and optical disector methods." *Journal of Comparative Neurology* 366 (4): 580–599. (Cited on pages 58, 59).

Pashler, H. E. 1998. *Attention*. Psychology Press. (Cited on page 137).

Pavlides, A., John Hogan, S., and Bogacz, R. 2012. "Improved conditions for the generation of beta oscillations in the subthalamic nucleus–globus pallidus network." *European Journal of Neuroscience* 36 (2): 2229–2239. (Cited on page 89).

Petermann, T., Thiagarajan, T. C., Lebedev, M. A., Nicolelis, M. A., Chialvo, D. R., and Plenz, D. 2009. "Spontaneous cortical activity in awake monkeys composed of neuronal avalanches." *Proceedings of the National Academy of Sciences* 106 (37): 15921–15926. (Cited on page 53).

Pfurtscheller, G. and Da Silva, F. L. 1999. "Event-related EEG/MEG synchronization and desynchronization: basic principles." *Clinical neurophysiology* 110 (11): 1842–1857. (Cited on page 92).

Pignatelli, M., Lebreton, F., Cho, Y. H., and Leinekugel, X. 2012. ""Ectopic" theta oscillations and interictal activity during slow-wave state in the R6/1 mouse model of Huntington's disease." *Neurobiology of disease* 48 (3): 409–17. (Cited on page 94).

Planert, H., Szydlowski, S. N., Hjorth, J. J., Grillner, S., and Silberberg, G. 2010. "Dynamics of synaptic transmission between fast-spiking interneurons and striatal projection neurons of the direct and indirect pathways." *The Journal of Neuroscience* 30 (9): 3499–3507. (Cited on page 60).

Plenz, D. and Kital, S. T. 1999. "A basal ganglia pacemaker formed by the subthalamic nucleus and external globus pallidus." *Nature* 400 (6745): 677–682. (Cited on pages 79, 89, 149).

Prinz, A. A. 2007. "Neuronal parameter optimization." *Scholarpedia* 2 (1): 1903. (Cited on page 40).

Priori, A., Foffani, G., Pesenti, A., Tamma, F., Bianchi, A., Pellegrini, M., Locatelli, M., Moxon, K., and Villani, R. 2004. "Rhythm-specific pharmacological modulation of subthalamic activity in Parkinson's disease." *Experimental neurology* 189 (2): 369–379. (Cited on page 92).

Raethjen, J., Govindan, R., Muthuraman, M., Kopper, F., Volkmann, J., and Deuschl, G. 2009. "Cortical correlates of the basic and first harmonic frequency of Parkinsonian tremor." *Clinical Neurophysiology* 120 (10): 1866–1872. (Cited on page 109).

Ratcliff, R. 2002. "A diffusion model account of response time and accuracy in a brightness discrimination task: fitting real data and failing to fit fake but plausible data." *Psychonomic bulletin & review* 9 (2): 278–91. (Cited on page 140).

Razali, N. M. and Wah, Y. B. 2011. "Power comparisons of shapiro-wilk, kolmogorov-smirnov, lilliefors and anderson-darling tests." *Journal of Statistical Modeling and Analytics* 2 (1): 21–33. (Cited on page 122).

Redgrave, P., Prescott, T. J., and Gurney, K. 1999. "The basal ganglia: a vertebrate solution to the selection problem?" *Neuroscience* 89 (4): 1009–1023. (Cited on pages 18, 56, 75, 92, 112, 113, 145, 158).

Redgrave, P., Rodriguez, M., Smith, Y., Rodriguez-Oroz, M. C., Lehericy, S., Bergman, H., Agid, Y., DeLong, M. R., and Obeso, J. A. 2010. "Goal-directed and habitual control in the basal ganglia: implications for Parkinson's disease." *Nature Reviews Neuroscience* 11 (11): 760–772. (Cited on page 144).

Reed, J. L., Qi, H.-X., Zhou, Z., Bernard, M. R., Burish, M. J., Bonds, A., and Kaas, J. H. 2010. "Response properties of neurons in primary somatosensory cortex of owl monkeys reflect widespread spatiotemporal integration." *Journal of neurophysiology* 103 (4): 2139–2157. (Cited on page 65).

Reiner, A., Medina, L., and Veenman, C. L. 1998. "Structural and functional evolution of the basal ganglia in vertebrates." *Brain Research Reviews* 28 (3): 235–285. (Cited on page 113).

Richards, C., Shiroyama, T., and Kitai, S. 1997. "Electrophysiological and immunocytochemical characterization of GABA and dopamine neurons in the substantia nigra of the rat." *Neuroscience* 80 (2): 545–557. (Cited on pages 67, 68).

Rohrbacher, J., Ichinohe, N., and Kitai, S. 2000. "Electrophysiological characteristics of substantia nigra neurons in organotypic cultures: spontaneous and evoked activities." *Neuroscience* 97 (4): 703–714. (Cited on page 67).

Rossant, C., Goodman, D. F., Fontaine, B., Platkiewicz, J., Magnusson, A. K., and Brette, R. 2011. "Fitting neuron models to spike trains." *Frontiers in neuroscience* 5:9. (Cited on page 40).

Rubchinsky, L. L., Kuznetsov, A. S., MD, V. L. W., and Sigvardt, K. A. 2007. "Tremor." *Scholarpedia* 2:1379. (Cited on page 144).

Sadek, A. R., Magill, P. J., and Bolam, J. P. 2007. "A single-cell analysis of intrinsic connectivity in the rat globus pallidus." *The Journal of Neuroscience* 27 (24): 6352–6362. (Cited on page 58).

Sarnthein, J. and Jeanmonod, D. 2007. "High Thalamocortical Theta Coherence in Patients with Parkinson's Disease." *Journal of Neuroscience* 27 (1): 124–131. (Cited on page 155).

Schmidt, R., Leventhal, D. K., Mallet, N., Chen, F., and Berke, J. D. 2013. "Canceling actions involves a race between basal ganglia pathways." *Nature neuroscience* 16 (8): 1118–1124. (Cited on pages 73, 91, 92, 101).

Schreiber, T. 2000. "Measuring information transfer." *Physical review letters* 85 (2): 461. (Cited on page 85).

Schroll, H. and Hamker, F. H. 2013. "Computational models of basal-ganglia pathway functions: focus on functional neuroanatomy." *Frontiers in systems neuroscience* 7. (Cited on pages 20, 157).

Schultz, W., Dayan, P., and Montague, P. R. 1997. "A neural substrate of prediction and reward." *Science* 275 (5306): 1593–1599. (Cited on page 91).

Schwab, B. C., Heida, T., Zhao, Y., Marani, E., Gils, S. A. van, and Van Wezel, R. J. A. 2013. "Synchrony in Parkinson's disease: Importance of intrinsic properties of the external globus pallidus." *Frontiers in Systems Neuroscience* 7 (60). (Cited on page 97).

Seth, A. K., Prescott, T. J., and Bryson, J. J. 2011. *Modelling natural action selection.* Cambridge University Press. (Cited on page 18).

Shanahan, M. 2006. "A cognitive architecture that combines internal simulation with a global workspace." *Consciousness and cognition* 15 (2): 433–449. (Cited on page 162).

———. 2010a. *Embodiment and the inner life: Cognition and Consciousness in the Space of Possible Minds.* Oxford University Press, USA. (Cited on page 161).

———. 2010b. "Metastable chimera states in community-structured oscillator networks." *Chaos: An Interdisciplinary Journal of Nonlinear Science* 20 (1): 013108. (Cited on page 148).

Shapiro, S. S. and Wilk, M. B. 1965. "An analysis of variance test for normality (complete samples)." *Biometrika* 52 (3/4): 591–611. (Cited on page 122).

Sherman, S. M. and Guillery, R. W. 2006. *Exploring the thalamus and its role in cortical function.* MIT Press, Cambridge, MA. (Cited on pages 40, 48, 52).

Sherman, S. M. and Guillery, R. W. 2013. *Functional connections of cortical areas: a new view from the thalamus.* MIT Press. (Cited on page 146).

Siegel, M., Warden, M. R., and Miller, E. K. 2009. "Phase-dependent neuronal coding of objects in short-term memory." *Proceedings of the National Academy of Sciences* 106 (50): 21341–21346. (Cited on pages 20, 114, 128).

Siegel, M., Engel, A. K., Donner, T. H., et al. 2011. "Cortical network dynamics of perceptual decision-making in the human brain." *Frontiers in human neuroscience* 5:21. (Cited on pages 20, 114).

Sims, R. E., Woodhall, G. L., Wilson, C. L., and Stanford, I. M. 2008. "Functional characterization of GABAergic pallidopallidal and striatopallidal synapses in the rat globus pallidus in vitro." *European journal of neuroscience* 28 (12): 2401–2408. (Cited on pages 62, 108).

Singh, A., Kammermeier, S., Plate, A., Mehrkens, J. H., Ilmberger, J., and Bötzel, K. 2011. "Pattern of local field potential activity in the globus pallidus internum of dystonic patients during walking on a treadmill." *Experimental neurology* 232 (2): 162–167. (Cited on pages 91–93, 109).

Solages, C. de, Hill, B. C., Koop, M. M., Henderson, J. M., and Bronte-Stewart, H. 2010. "Bilateral symmetry and coherence of subthalamic nuclei beta band activity in Parkinson's disease." *Experimental neurology* 221 (1): 260–266. (Cited on page 91).

Song, S., Miller, K. D., and Abbott, L. F. 2000. "Competitive Hebbian learning through spike-timing-dependent synaptic plasticity." *Nature neuroscience* 3 (9): 919–926. (Cited on page 27).

Steigerwald, F., Pötter, M., Herzog, J., Pinsker, M., Kopper, F., Mehdorn, H., Deuschl, G., and Volkmann, J. 2008. "Neuronal activity of the human subthalamic nucleus in the parkinsonian and nonparkinsonian state." *Journal of neurophysiology* 100 (5): 2515–2524. (Cited on pages 81, 89, 90).

Steiner, H. and Tseng, K. Y. 2010. *Handbook of basal ganglia structure and function: a decade of progress.* Vol. 24. Academic Press. (Cited on pages 58, 64, 101).

Stephenson-Jones, M., Samuelsson, E., Ericsson, J., Robertson, B., and Grillner, S. 2011. "Evolutionary conservation of the basal ganglia as a common vertebrate mechanism for action selection." *Current Biology* 21 (13): 1081–1091. (Cited on pages 18, 113).

Stewart, T. C., Choo, X., and Eliasmith, C. 2010. "Dynamic behaviour of a spiking model of action selection in the basal ganglia." In *Proceedings of the 10th international conference on cognitive modeling,* 235–40. Citeseer. (Cited on page 20).

Stewart, T. C. and Eliasmith, C. 2009. "Spiking neurons and central executive control: The origin of the 50-millisecond cognitive cycle." In *9th International Conference on Cognitive Modelling,* 122–127. University of Manchester Manchester. (Cited on pages 130, 131).

Stimberg, M., Goodman, D. F., Benichoux, V., and Brette, R. 2014. "Equation-oriented specification of neural models for simulations." *Frontiers in neuroinformatics* 8. (Cited on page 28).

Tachibana, Y., Iwamuro, H., Kita, H., Takada, M., and Nambu, A. 2011. "Subthalamo-pallidal interactions underlying parkinsonian neuronal oscillations in the primate basal ganglia." *European Journal of Neuroscience* 34 (9): 1470–1484. (Cited on page 89).

Tateno, T. and Robinson, H. P. 2011. "The mechanism of ethanol action on midbrain dopaminergic neuron firing: a dynamic-clamp study of the role of Ih and GABAergic synaptic integration." *Journal of neurophysiology* 106 (4): 1901–1922. (Cited on page 68).

Taverna, S., Ilijic, E., and Surmeier, D. J. 2008. "Recurrent collateral connections of striatal medium spiny neurons are disrupted in models of Parkinson's disease." *The Journal of neuroscience* 28 (21): 5504–5512. (Cited on page 60).

Teixeira, F. P. P. and Shanahan, M. 2014. "Does plasticity promote criticality?" In *Neural Networks (IJCNN), 2014 International Joint Conference on,* 2383–2390. IEEE. (Cited on pages 53, 54).

Telford, C. W. 1931. "The refractory phase of voluntary and associative responses." *Journal of Experimental Psychology* 14 (1): 1. (Cited on page 137).

Temel, Y., Cao, C., Vlamings, R., Blokland, A., Ozen, H., Steinbusch, H. W. M., Michelsen, K. A., Hörsten, S. von, Schmitz, C., and Visser-Vandewalle, V. 2006. "Motor and cognitive improvement by deep brain stimulation in a transgenic rat model of Huntington's disease." *Neuroscience letters* 406 (1-2): 138–41. (Cited on page 94).

Terman, D., Rubin, J. E., Yew, A., and Wilson, C. 2002. "Activity patterns in a model for the subthalamopallidal network of the basal ganglia." *The Journal of neuroscience* 22 (7): 2963–2976. (Cited on page 144).

Theiler, J., Eubank, S., Longtin, A., Galdrikian, B., and Farmer, J. D. 1992. "Testing for nonlinearity in time series: the method of surrogate data." *Physica D: Nonlinear Phenomena* 58 (1): 77–94. (Cited on page 82).

Tognoli, E. and Kelso, J. A. S. 2014. "The Metastable Brain." *Neuron* 81 (1): 35–48. (Cited on pages 128, 161).

Tomkins, A., Vasilaki, E., Beste, C., Gurney, K., and Humphries, M. D. 2013. "Transient and steady-state selection in the striatal microcircuit." *Frontiers in computational neuroscience* 7. (Cited on pages 20, 56, 58, 59, 63, 64, 71, 72, 115, 131).

Tort, A. B., Kramer, M. A., Thorn, C., Gibson, D. J., Kubota, Y., Graybiel, A. M., and Kopell, N. J. 2008. "Dynamic cross-frequency couplings of local field potential oscillations in rat striatum and hippocampus during performance of a T-maze task." *Proceedings of the National Academy of Sciences* 105 (51): 20517–20522. (Cited on pages 93, 142, 154).

Tripathy, S. J., Savitskaya, J., Burton, S. D., Urban, N. N., and Gerkin, R. C. 2014. "NeuroElectro: a window to the world's neuron electrophysiology data." *Frontiers in neuroinformatics* 8. (Cited on pages 46, 48).

Tseng, K. Y., Kasanetz, F., Kargieman, L., Riquelme, L. a., and Murer, M. G. 2001. "Cortical slow oscillatory activity is reflected in the membrane potential and spike trains of striatal neurons in rats with chronic nigrostriatal lesions." *The Journal of neuroscience : the official journal of the Society for Neuroscience* 21 (16): 6430–6439. (Cited on pages 21, 114).

Turner, R. S. and DeLong, M. R. 2000. "Corticostriatal activity in primary motor cortex of the macaque." *The Journal of Neuroscience* 20 (18): 7096–7108. (Cited on pages 65, 77, 99).

Tzagarakis, C., West, S., and Pellizzer, G. 2015. "Brain oscillatory activity during motor preparation: effect of directional uncertainty on beta, but not alpha, frequency band." *Frontiers in neuroscience* 9. (Cited on page 92).

Van de Vijver, I., Ridderinkhof, K. R., and Cohen, M. X. 2011. "Frontal oscillatory dynamics predict feedback learning and action adjustment." *Journal of cognitive neuroscience* 23 (12): 4106–4121. (Cited on page 93).

Van Elk, M., Van Schie, H. T., Van Den Heuvel, R., and Bekkering, H. 2010. "Semantics in the motor system: motor-cortical beta oscillations reflect semantic knowledge of end-postures for object use." *Frontiers in human neuroscience* 4:8. (Cited on page 91).

Váša, F., Shanahan, M., Hellyer, P. J., Scott, G., Cabral, J., and Leech, R. 2015. "Effects of lesions on synchrony and metastability in cortical networks." *Neuroimage* 118:456–467. (Cited on page 161).

Venance, L. and Glowinski, J. 2003. "Heterogeneity of spike frequency adaptation among medium spiny neurones from the rat striatum." *Neuroscience* 122 (1): 77–92. (Cited on page 133).

Voytek, B., Kayser, A. S., Badre, D., Fegen, D., Chang, E. F., Crone, N. E., Parvizi, J., Knight, R. T., and D'Esposito, M. 2015. "Oscillatory dynamics coordinating human frontal networks in support of goal maintenance." *Nature neuroscience.* (Cited on pages 93, 154, 155).

Vugt, M. K. van, Sederberg, P. B., and Kahana, M. J. 2007. "Comparison of spectral analysis methods for characterizing brain oscillations." *Journal of neuroscience methods* 162 (1): 49–63. (Cited on pages 79, 91).

Walters, J. R., Hu, D., Itoga, C. A., Parr-Brownlie, L. C., and Bergstrom, D. A. 2007. "Phase relationships support a role for coordinated activity in the indirect pathway in organizing slow oscillations in basal ganglia output after loss of dopamine." *Neuroscience* 144 (2): 762–776. (Cited on page 74).

Werner, G. 2007. "Metastability, criticality and phase transitions in brain and its models." *Biosystems* 90 (2): 496–508. (Cited on page 161).

Wickelgren, W. A. 1977. "Speed-accuracy tradeoff and information processing dynamics." *Acta psychologica* 41 (1): 67–85. (Cited on page 16).

Wickens, J. 1993. *A theory of the striatum.* Elsevier Science Inc. (Cited on page 58).

Wiener, N. 1956. "The theory of prediction." *Modern mathematics for engineers* 1:125–139. (Cited on page 85).

Wilson, C. J. and Groves, P. M. 1980. "Fine structure and synaptic connections of the common spiny neuron of the rat neostriatum: a study employing intracellular injection of horseradish peroxidase." *Journal of Comparative Neurology* 194 (3): 599–615. (Cited on page 58).

———. 1981. "Spontaneous firing patterns of identified spiny neurons in the rat neostriatum." *Brain research* 220 (1): 67–80. (Cited on page 52).

Winer, J. A. and Larue, D. T. 1996. "Evolution of GABAergic circuitry in the mammalian medial geniculate body." *Proceedings of the National Academy of Sciences* 93 (7): 3083–3087. (Cited on page 52).

Woods, D. L., Wyma, J. M., Yund, E. W., Herron, T. J., and Reed, B. 2015. "Age-related slowing of response selection and production in a visual choice reaction time task." *Frontiers in Human Neuroscience* 9 (April): 1–12. (Cited on pages 123, 140).

Woodworth, R. S. and Schlosberg, H. 1954. *Experimental psychology.* Oxford / IBH Publishing. (Cited on page 15).

Zahr, N. M., Martin, L. P., and Waszczak, B. L. 2004. "Subthalamic nucleus lesions alter basal and dopamine agonist stimulated electrophysiological output from the rat basal ganglia." *Synapse* 54 (2): 119–128. (Cited on page 74).

Zandbelt, B. B. and Vink, M. 2010. "On the role of the striatum in response inhibition." *PloS one* 5 (11): e13848–e13848. (Cited on page 92).

Zariwala, H. A., Kepecs, A., Uchida, N., Hirokawa, J., and Mainen, Z. F. 2013. "The limits of deliberation in a perceptual decision task." *Neuron* 78 (2): 339–51. (Cited on page 141).

Zavala, B., Damera, S., Dong, J. W., Lungu, C., Brown, P., and Zaghloul, K. A. 2015. "Human Subthalamic Nucleus Theta and Beta Oscillations Entrain Neuronal Firing During Sensorimotor Conflict." *Cerebral Cortex:* bhv244. (Cited on pages 93, 142, 154).

Zhan, X., Cox, C., Rinzel, J., and Sherman, S. M. 1999. "Current clamp and modeling studies of low-threshold calcium spikes in cells of the cat's lateral geniculate nucleus." *Journal of neurophysiology* 81 (5): 2360–2373. (Cited on pages 48, 49).

Zhang, Y., Chen, Y., Bressler, S. L., and Ding, M. 2008. "Response preparation and inhibition: the role of the cortical sensorimotor beta rhythm." *Neuroscience* 156 (1): 238–246. (Cited on pages 20, 91, 114).

Zhou, F.-M. and Lee, C. R. 2011. "Intrinsic and integrative properties of substantia nigra pars reticulata neurons." *Neuroscience* 198:69–94. (Cited on page 68).